Center for Acoustical Studies
Department of Mechanical and Aerospace Engineering
North Carolina State University
Raleigh, North Carolina

EXPERIMENTAL STUDY OF AIRFOIL TRAILING-EDGE NOISE: INSTRUMENTATION, METHODOLOGY AND INITIAL RESULTS

by

MARK B. MANLEY

A thesis submitted to the Graduate Faculty of
North Carolina State University
in partial fulfillment of the
requirements for the Degree of
Master of Science

ABSTRACT

MANLEY, MARK B. Experimental Study of Airfoil Trailing-Edge Noise: Instrumentation, Methodology and Initial Results. (Under the direction of DR. THOMAS H. HODGSON.)

The mechanism of aerodynamic noise generation at the trailing edge of an airfoil is investigated. Instrumentation was designed, tested and built and digital signal analysis techniques applied to gain insight into the relationship between the dynamic pressure close to the trailing edge and the sound in the acoustic far-field. Attempts are made to verify some trailing-edge noise generation characteristics as theoretically predicted by several contemporary acousticians.

A NACA 0012 airfoil of 2.0 foot chord and 1.5 foot span was mounted in the laminar flow of the potential core of an open jet. The test was conducted in an anechoic environment thereby providing a quiet-flow test capability. Two-dimensional boundary layer flow was established over the two surfaces of the airfoil. Means were used to "trip" each boundary layer into turbulence and thereby maintain trailing edge flow conditions such as are found on full-scale aircraft wings.

Considerations are discussed which had bearing on the design of a miniature semiconductor strain-gauge pressure transducer and associated electronic amplifier circuitry. Several of the transducers were tested and then mounted in the "upper" and "lower" surfaces of the airfoil in the vicinity of the trailing edge. Signals from these near-field transducers and other far-field condenser microphones were analyzed using digital signal processing techniques. The origins of

the computer analysis functions are briefly discussed and some errors encountered in their use are covered. Instrumentation of the overall experiment is described and the results and conclusions stemming from the computer analysis are presented.

It is found that the noise detected in the far-field is comprised of the sum of many uncorrelated emissions radiating from the vicinity of the trailing edge. These emissions appear to be the result acoustic energy radiation which has been converted by the trailing-edge noise mechanism from the dynamic fluid energy of independent streamwise "strips" of the turbulent boundary layer flow. It is also found that the far-field sound power level scales on the freestream velocity "u" raised to a power of 5.3; i.e., $p^2 \propto u^{5.3}$. This is in good agreement with the theoretically predicted $u^{5.0}$.

BIOGRAPHY

Mark Bradford Manley was born in [redacted], on [redacted]. [redacted] As a member of a United States Air Force family, he has lived in many parts of the United States in addition to a three and one-half year visit to Germany. During these years he received his primary and secondary education.

In August 1972 the author enrolled in North Carolina State University as a full-time student. While an undergraduate in Electrical Engineering, he participated in the Cooperative Engineering student employment program and worked for Research Triangle Institute, Research Triangle Park, North Carolina.

Upon graduation with a Batchelor of Science degree in Electrical Engineering in 1977, the author enrolled as a full-time student in the graduate level Mechanical Engineering program at North Carolina State University and concentrated on studying acoustics and vibrations theory. He is presently completing his studies and will be entering into the field of industrial environmental consulting.

ACKNOWLEDGEMENTS

The author wishes to express his appreciation and thanks to the many people who have contributed to the completion of his graduate studies at North Carolina State University and have made his stay most enjoyable. He would like to extend special thanks and his deepest admiration to Dr. Thomas H. Hodgson, his Advisory Committee Chairman and mentor. Sincere appreciation and gratitude are also extended to the other members of his Advisory Committee: Dr. Franklin D. Hart and Dr. N. J. Rose. Very special thanks are extended to Dr. Thomas F. Brooks at NASA Langley, Hampton, Virginia, who has been most helpful in providing the materials and financing for this study under NASA Contract No. G1377.

Particular appreciation is owed to Dr. Allen C. Eberhardt and especially to Messrs. J. A. Cooke and R. L. Underwood for their invaluable stimulating and enlightening discussions covering the broad spectrum of academic subjects. The author is forever indebted to Miss Elizabeth M. Seawell for her genuine interest shown and inspiration so freely given during the course of his studies.

Finally, the author wishes to express his deepest gratitude and appreciation to his parents, Colonel Richard Earnest Manley and Zora Dean Manley, for their constant patience, encouragement, understanding and sacrifices throughout all the academic years of his life.

TABLE OF CONTENTS

TABLE OF CONTENTS (continued)

LIST OF TABLES

LIST OF FIGURES

LIST OF FIGURES (continued)

LIST OF FIGURES (continued)

LIST OF FIGURES (continued)

LIST OF FIGURES (continued)

LIST OF FIGURES (continued)

1. INTRODUCTION

The understanding of the aerodynamic noise generation phenomena has been a long sought goal of acousticians. Up until the last few years, however, most engineering attention and research has been focused on the most obvious source of aircraft noise, namely the engine. Recently, airframe component noise due to struts, flaps, wheel cavities, etc. has been studied because of its possible importance on the aircraft landing configuration.

Theoretical studies by many acousticians including Lighthill [30, 31], Curle [15], Powell [33], Ffowcs-Williams and Hall [20], Crighton [14], and most recently Howe [27] have indicated that purely aerodynamically induced noise may be generated by the interaction of turbulent air flows with rigid planar surfaces. That is to say that the surfaces themselves need not vibrate for the noise to be radiated. In particular, enhancement of the noise is predicted to occur at the trailing edges of the planar surfaces as turbulent boundary layers develop as a result of forward flight. (See Howe's review paper [27].)

For the case of turbulent flow over an infinitely large rigid flat plate, theory predicts that the pressure (force) fluctuations of the turbulent boundary layer flow generate dipole noise sources. The sound power level or p^2 level of dipole sources generally depends on the sixth power of a characteristic flow velocity "u," typically the freestream flow velocity u_∞; i.e., $p^2 = ku^6$, where k is a constant. However, because these dipole sources are reflected in the rigid surface of the plate, they give rise to quadrupole noise emissions as sensed in the acoustic far field. Typically, quadrupole noise scales on the eighth power of the velocity; i.e., $p^2 = ku^8$.

For the case of a semi-infinite rigid flat plate, the theories of both Ffowcs-Williams and Hall [20] and Howe [27] predict that the large extent of the plate can possibly cause enhancement of the sound field due to scattering at the edge. This enhancement of the quadrupole noise has been theorized to scale on the fifth power of the velocity; i.e., $p^2 = ku^5$. This makes the efficiency of the trailing-edge noise phenomena lie between that of the highly efficient monopole ($p^2 = ku^4$) and the aforementioned dipole ($p^2 = ku^6$). Thus, the extensive rigid planar wing surfaces of aircraft such as a Boeing 747 jumbo jet may actually become the dominant contributors to the overall radiated noise sensed on the ground as the large aircraft approach airport runways at low altitudes with the engines throttled back.

This purely aerodynamic nonpropulsive related noise source has been recognized as a possible lower bound or "barrier" in preventing the noise floor of future aircraft from being reduced. H. G. Morgan, Division Chief of the NASA Langley Acoustics and Noise Reduction Division has stated:

> We have made enough progress in quieting jet engines that we are nearing a point where the airflow over the airframe becomes what is actually heard on the ground. . . . We cannot quiet engines more than another 5-8 dB before we run into the new noise floor. [13]

Figure 1.1 illustrates that as engines for a given aircraft size are becoming quieter, increasingly larger aircraft and correspondingly larger planar surfaces areas are radiating ever increasing amounts of aerodynamic noise.

As part of its Federal Aviation Regulations, in 1974 the Federal Aviation Administration issued a noise standard for aircraft, FAR-36,

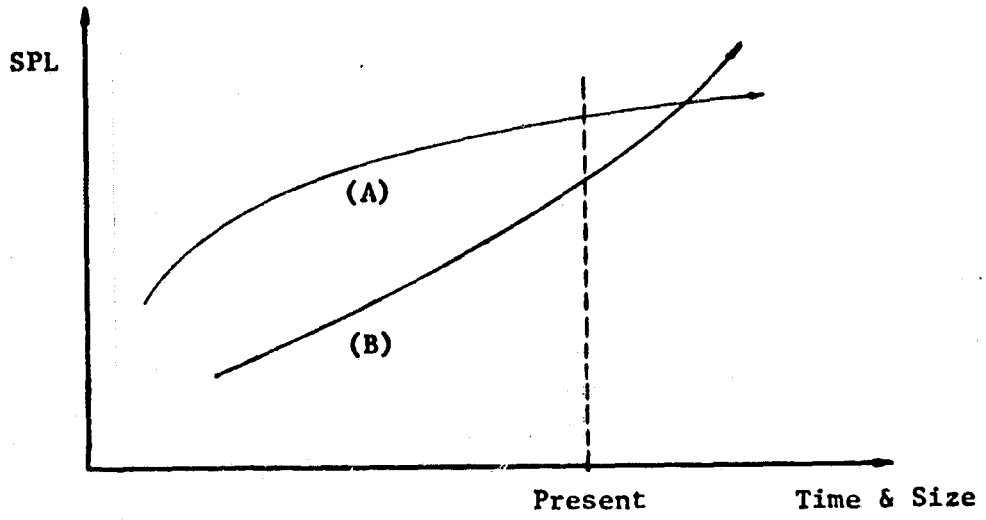

Figure 1.1 Past and future trends showing (a) decreasing engine noise for a given size aircraft due to better technology and (b) increasing aerodynamic noise due to increasing surface area

which states in part that it ". . . does not agree with those that believe the use of specific noise abatement/flight procedures . . . would, by itself, provide the necessary noise control and abatement" [18]. It is the opinion of the FAA that noise control must be undertaken at the source of the noise generation.

This has led experimentalists to attempt verification of the different facets of the proposed acoustic theories. Experimental work had been accomplished by many parties including Siddon [37], Fink [21], Healy [26], Putnam et al. [34], Hahn [22], Yu and Tam [40], and others (see Hardin's review paper [24]). The most promising theory at present appears to be Howe's "Unified Theory of Trailing Edge Noise" [27] which is a variation of Lighthill's treatise on the

subject in 1952 [30] with sweeping modifications to suit recent findings and theories.

However, only lately has extensive experimental work of laboratory quality involving the latest signal processing techniques been possible. These can be used to accurately confirm the legitimacy of Howe's or other proposed theories. It is to this end that an experimental study was initiated under Contract No. NSG 1377 for testing to be performed at the quiet flow facility located at the NASA Langley Acoustics and Noise Reduction Laboratory, Langley, Virginia. It is the purpose of this thesis to discuss the preparations for and initial findings of the first stage of testing, known as Series I tests.

A NACA 0012 airfoil was used for the tests over which turbulent boundary layers could independently develop on both surfaces. Boundary layer characteristics and flow speeds were achieved which approximated those actually encountered on the surface of full-size aircraft wings. Thus, the primary differences between model and actual wing are those of geometric scale, i.e., dimensions of chord length and trailing-edge span.

The considerations that were involved in the design of a miniature strain-gauge pressure transducer and associated electronic amplifier circuitry are discussed. Several of the pressure transducers were tested and then mounted in the upper and lower surfaces of the airfoil in the vicinity of the trailing edge. Signals from these near-field transducers and other far-field microphones were analyzed using digital signal processing techniques. The origins

of the analysis functions are briefly discussed and some errors encountered in their use are covered. Instrumentation of the overall Series I experiment is described and the results and conclusions stemming from the computer analysis are presented.

2. TEST CONFIGURATION

2.1 Airfoil

In order to generate the turbulent boundary layer at a trailing edge in a controlled manner, a symmetrical NACA 0012 airfoil was employed. It was machined from solid aluminum stock as shown in Figure 2.1. Dimensions are given in Figure 2.2 (a). Slots were machined to allow small strain gauge pressure transducers to be mounted flush with the surface. The trailing edge as manufactured had a bluntness of 0.10 inch with corners of 0.030 inch radius (see Figure 2.2 (b)) which allowed some of the pressure transducers to be mounted in very close proximity to the edge itself. (In later tests, Series II, a sharp extension was added.)

2.2 Facility and Experiment Geometry

The test was conducted in the recently-modified open-jet quiet flow anechoic test facility located at the NASA Langley Acoustics and Noise Reduction Laboratory (ANRL). Figures 2.3 and 2.4 depict the basic facility setup and define the coordinates used throughout this thesis. Also the positions of the one-half inch Brüel and Kjaer type 4133 condenser microphones are shown.

A rectangular nozzle with dimensions 1.0' W x 1.5' L was mounted on the air supply opening and was capable of airflow velocities in excess of 250 feet per second. Essentially laminar flow was achieved at exit through the use of the nozzle profile and flow straightners and silencers located upstream in the air supply tunnel. The airfoil was mounted in the potential core of the jet so that laminar flow was

Figure 2.1 Unmounted NACA 0012 airfoil with Kulite strain-gauge pressure transducers installed

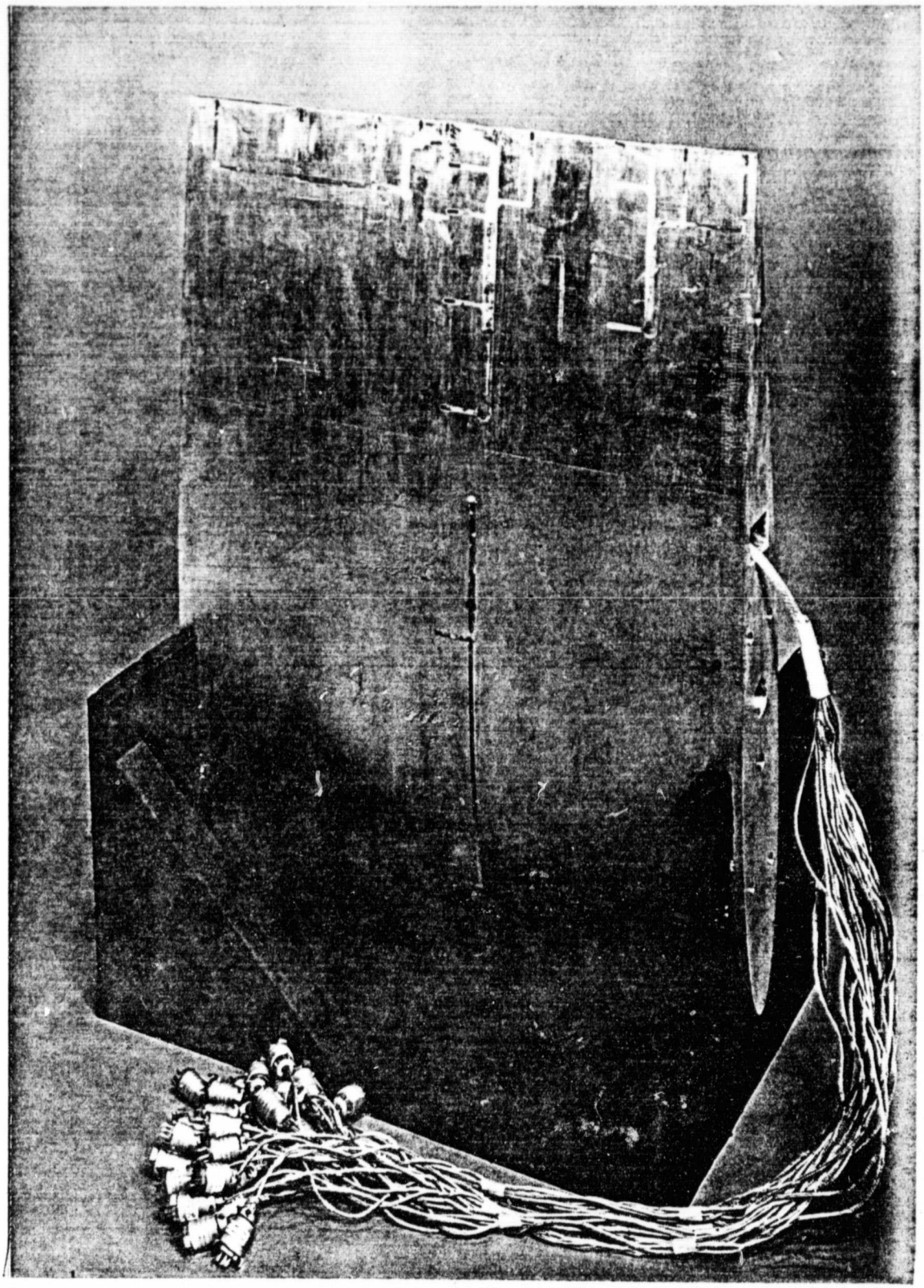

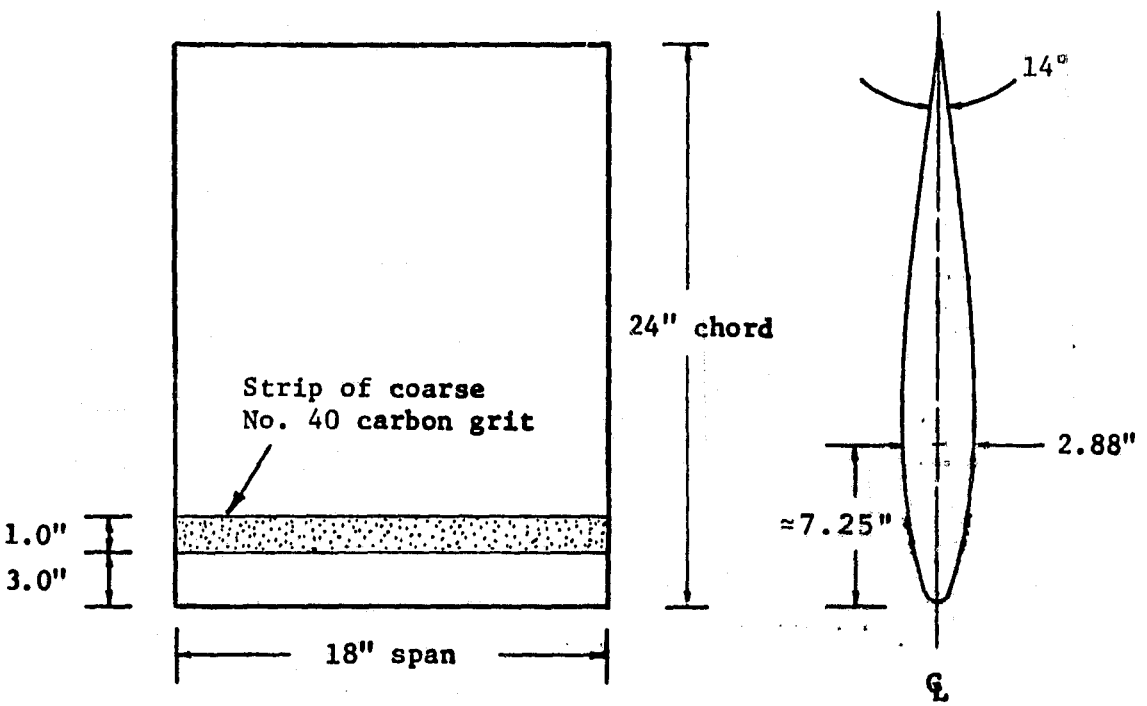

(a)

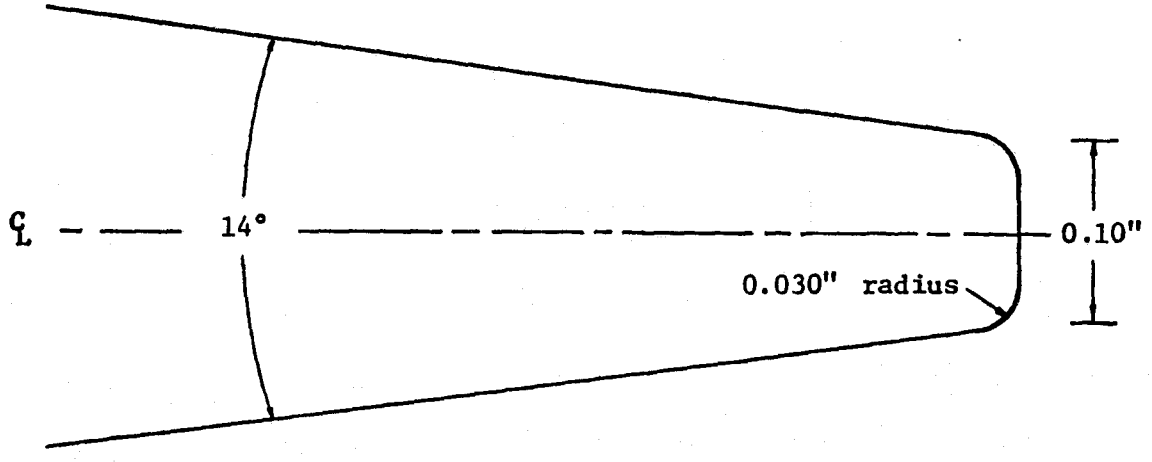

(b)

Figure 2.2 Dimensions of the unmodified NACA 0012 airfoil (general or basic configuration): (a) overall, showing boundary layer trip at 15% chord, (b) detail of trailing edge

Figure 2.3 Overall view of the experimental setup and facility as viewed from the control room door ("upper" surface of the airfoil)

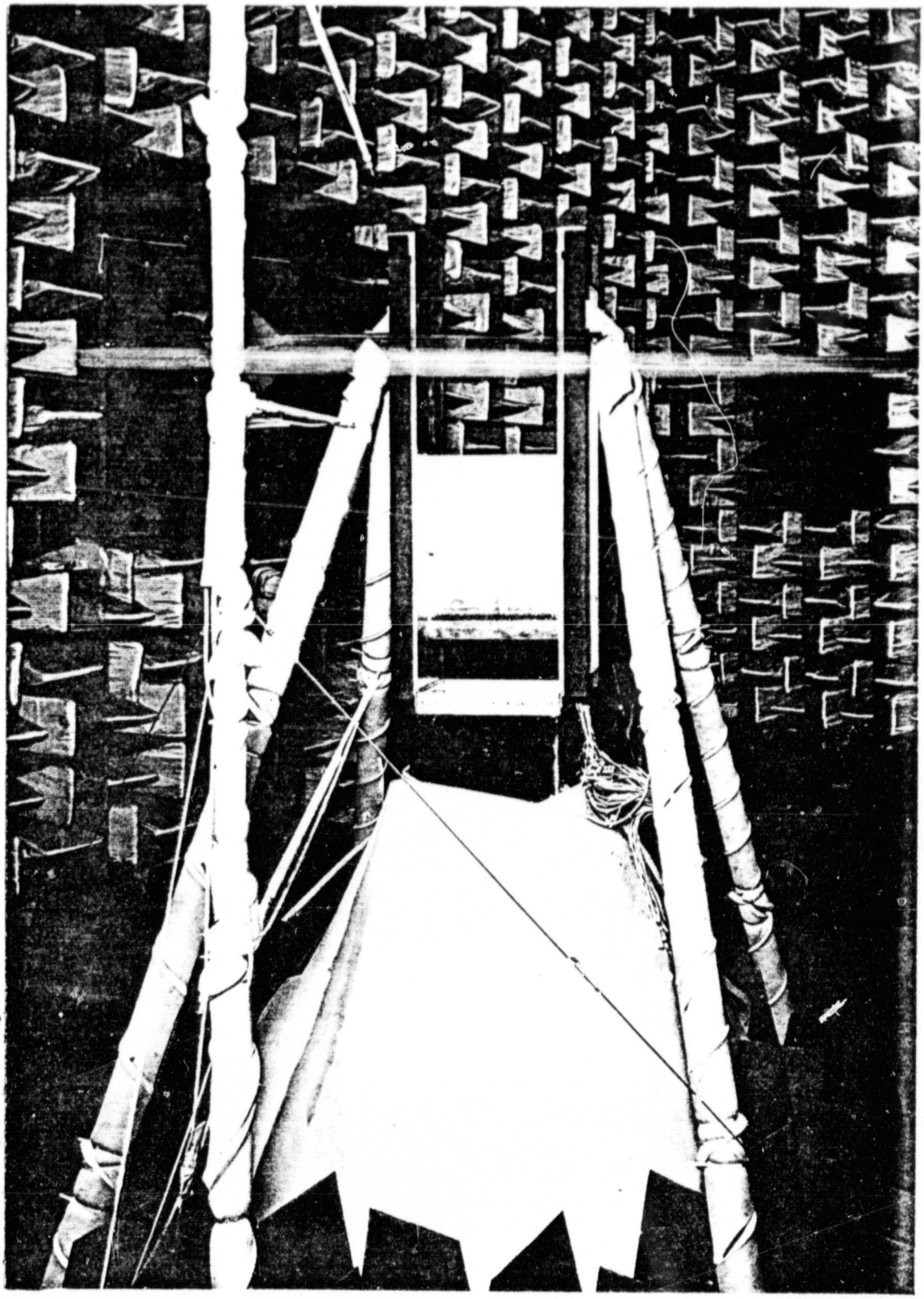

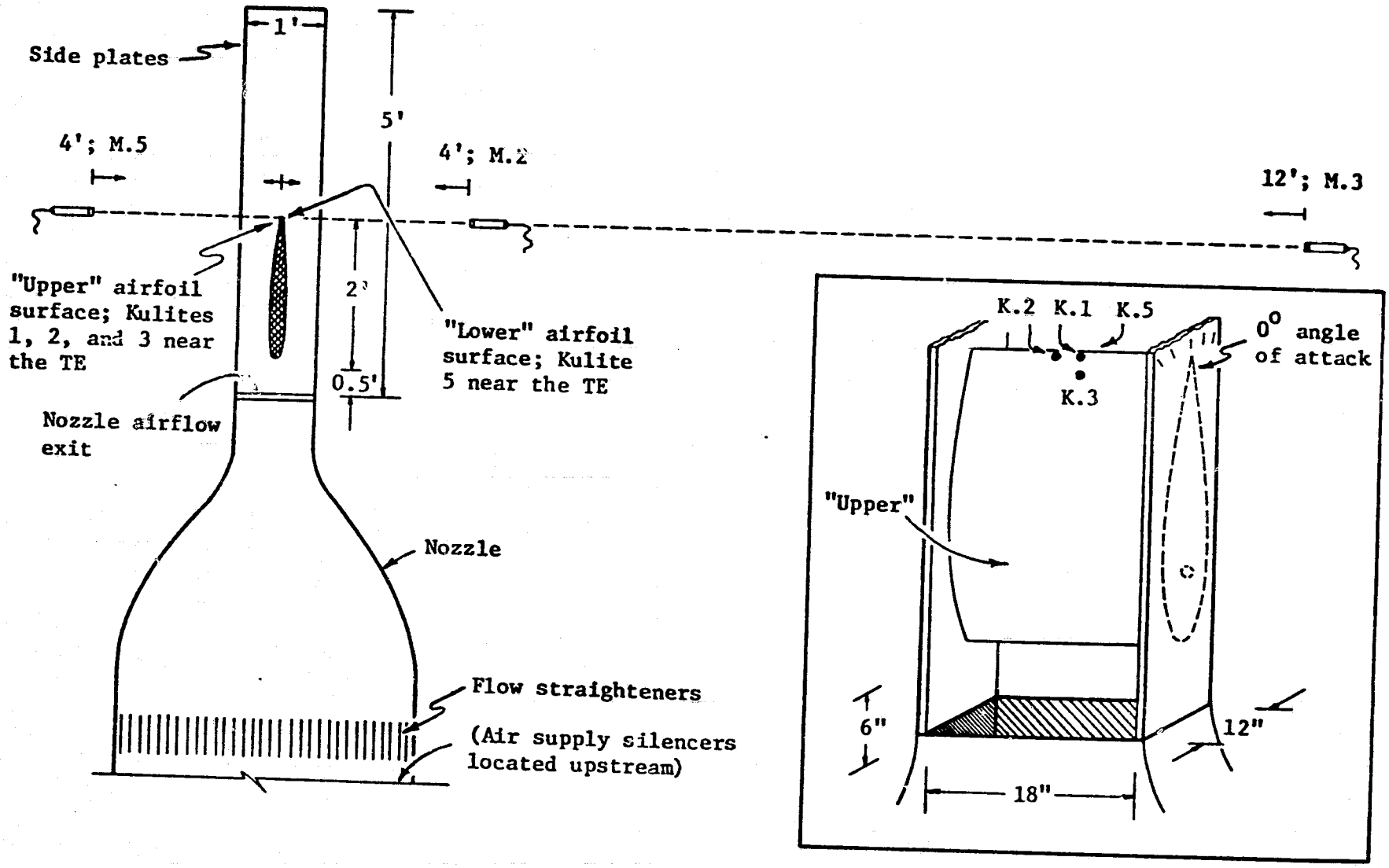

Figure 2.4 Geometry of the mounted airfoil, nozzle and sideplates with positions of Kulites and B&K type 4133 microphones shown

maintained in the freestream up to and beyond the trailing edge of the airfoil.

2.3 Flow Conditions

Two-dimensional flow was maintained over the surface of the airfoil by means of sideplates mounted on either side of the nozzle opening. The sideplates had foam attached to the rear edges outside of the main airflow to prevent detrimental edge-tone and diffraction effects from occurring (Figure 2.5).

To obtain fully-developed turbulent boundary-layer flow within such a short distance as the 24-inch chord length of the airfoil, a boundary layer "trip" was used. It consisted of a strip of coarse grit 1.0 inches wide centered at 15 percent chord as measured from the leading edge. Both upper and lower surfaces were provided with such a trip to facilitate the growth of statistically equivalent but separate turbulent boundary layers. The turbulent boundary layer characteristics then closely represented the flow characteristics over a full-scale wing.

The airfoil was tested at angles of attack equal to $\alpha = 0^{o}$, $\pm 5^{o}$, and $\pm 10^{o}$, but little dependence on α was detected so only $\alpha = 0^{o}$ results are presented.

Freestream flow velocities ranged from 50 ft/sec to 250 ft/sec. Most testing was done at a velocity of 225 ft/sec which is equivalent to 900 rpm of the air supply fan. Most results in this thesis relate to the preliminary study which was conducted using a flow velocity of 225 ft/sec.

Figure 2.5 Airfoil mounted at $\alpha = 0^{o}$ angle of attack with Kulites, sideplates, foam, nozzle opening and boundary-layer trip visible

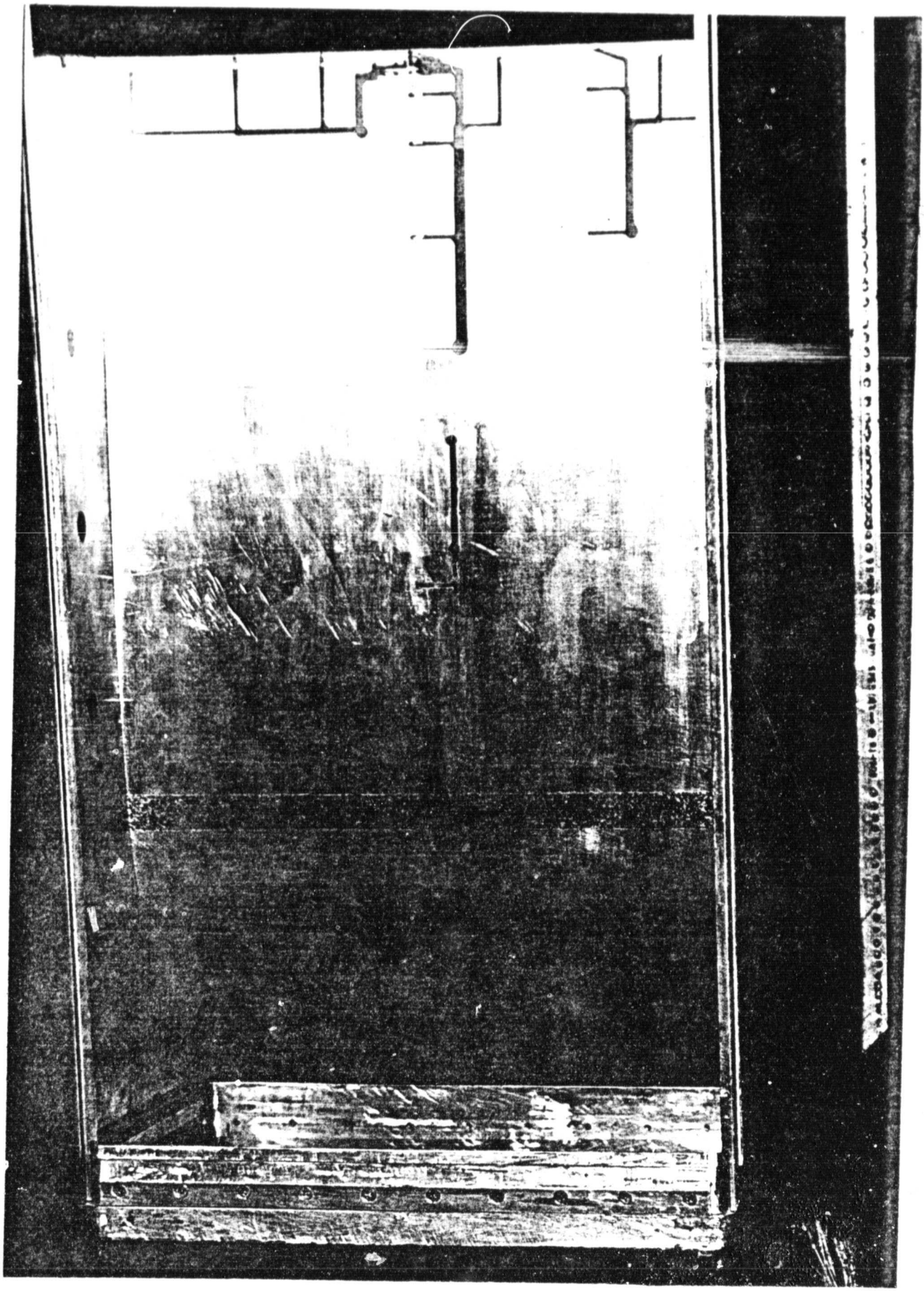

Boundary layer and airflow conditions were established using widely accepted standardized techniques. Some data parameters pertaining to the boundary layer conditions when the freestream flow velocity was 225 ft/sec are listed in Table 2.1.

Table 2.1 Initial test boundary-layer characteristics

Parameter	Value	Description
U_∞	225 ft/sec	freestream velocity
U_1	214 ft/sec	velocity at edge of B.L.
U_τ	7.01 ft/sec	friction velocity
δ	1.24 in.	boundary layer thickness
δ_1	0.154 in.	displacement thickness $\simeq \delta/8$
θ	0.162 in.	momentum thickness
R_θ	1.67×10^4	Reynolds # based on θ
R_c	2.88×10^6	Reynolds # based on chord
ν	1.56×10^{-4} ft^2/sec	kinematic viscosity

3. PRESSURE TRANSDUCER DESIGN

To sense the pressure fluctuations occurring in the turbulent boundary layer at the trailing edge of the airfoil, a very small pressure transducer or microphone was designed and flush-mounted as near the trailing edge as possible. The considerations that went into the design, calibration and installation of this transducer follow.

3.1 Design Considerations

Several competing phenomena mandated that the transducer dimensions be carefully chosen to provide the best compromise design. Of prime importance was that the transducer be small enough so that several could be clustered side-by-side on the upper and lower surfaces at the trailing edge. Kulite Semiconductor Products, Inc., of Ridgefield, New Jersey, was contacted due to their prior experience in manufacturing miniature transducer for this purpose. Manufacturing and physical limitations produced a transducer of overall outside dimensions of 0.375" L x 0.125" W x 0.045" D. This permitted a minimum center-to-center transducer diaphragm spacing of 0.125 inches (Figure 3.1).

It was desired that the flow of air over the airfoil surface be disturbed as little as possible by the transducer so that only valid boundary-layer pressure-field data would be collected. Therefore, the transducer design incorporated a pinhole opening in the upper surface which led to an internal cavity. The bottom of the cavity was formed by a diaphragm of semiconductor material on which a strain-guage sensing element was etched.

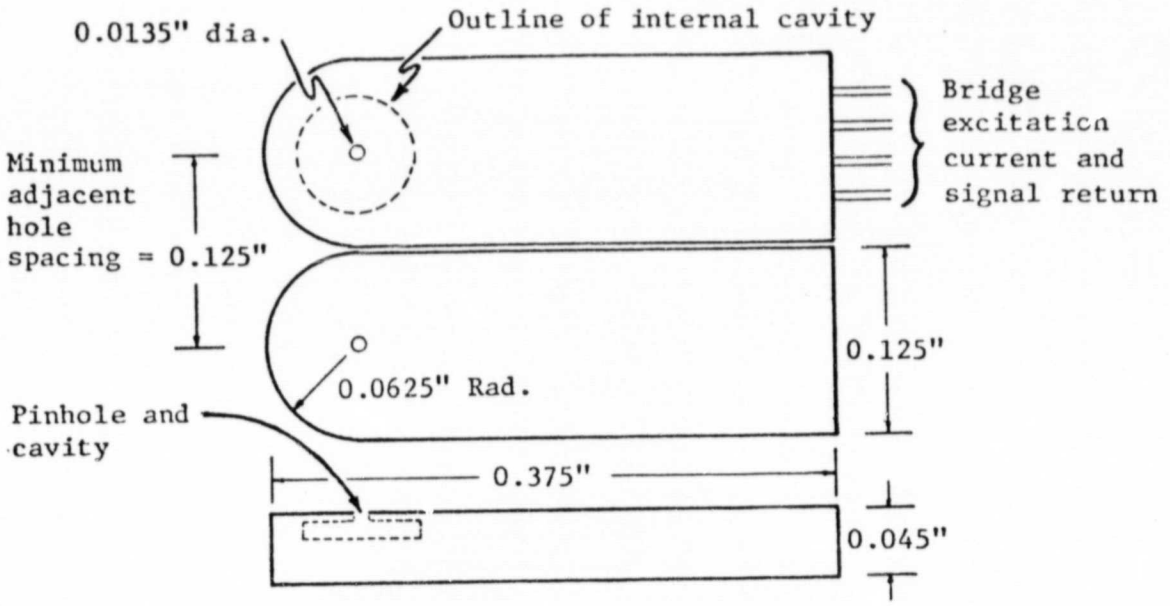

Figure 3.1 Overall outside dimensions of the Kulite strain-gauge pressure transducer

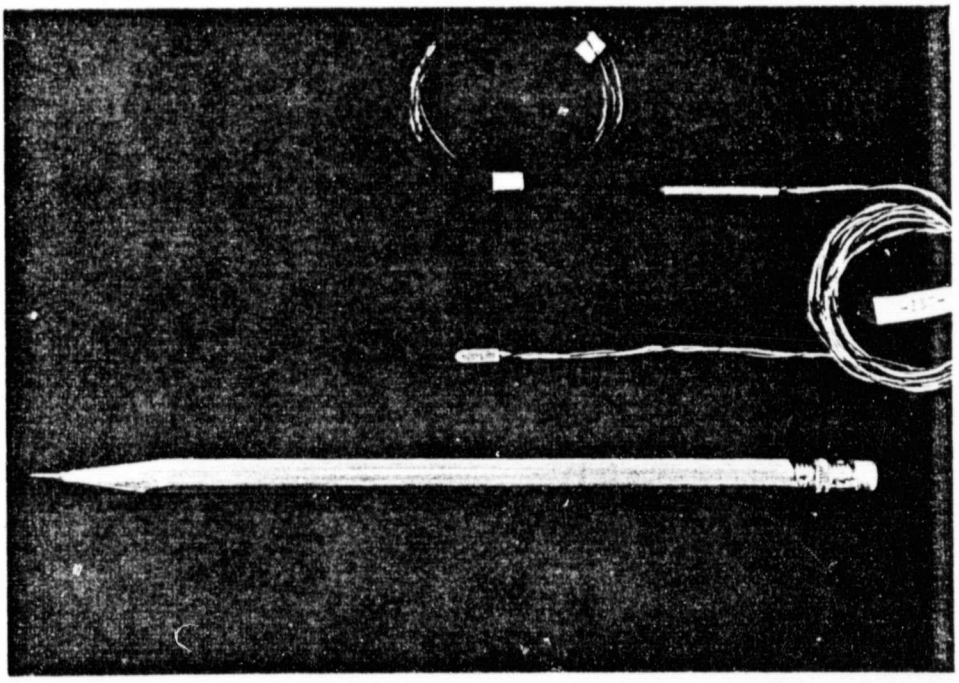

Figure 3.2 Kulite strain-gauge pressure transducer with temperature compensation module visible

It was predicted that increasing the diameter of the pinhole opening would have as a result an increasingly pronounced effect on the frequency spectrum of the naturally occurring turbulent flow at the airfoil surface. This is because the hole diameter approaches the order of dimension of the boundary layer thickness [10]. However, decreasing the hole size lowers the natural frequency of the Helmholtz resonator formed by the cavity and pinhole opening. Then the frequencies thought to exist in the extent of the pressure-spectrum become prone to resonant magnification within the transducer cavity, again causing erroneous data readings.

3.2 Parameter Calculations

Using normalized wind tunnel wall-pressure spectrum data and methods outlined by Bull and Thomas [10] the approximate upper bound of frequencies that could be measured accurately was computed. They conclude that measurements made with a pinhole microphone are prone to error for frequencies such that:

$$\frac{\omega\nu}{u_\tau u_\infty} > 0.01 \qquad (3.1)$$

where: $\nu = 1.56\ 10^{-4}$ ft^2/sec, kinematic viscosity of air;

$u_\tau = 7.01$ ft/sec, friction velocity;

$u_\infty = 225$ ft/sec, freestream velocity;

$\omega = 2\pi f$ rad/sec, radian frequency.

The resulting value for f = 16.1 kHz.

Inspection of curves presented in reference [10] suggested that for pinhole transducers, the term

$$\frac{du_T}{\nu} \simeq 50 \tag{3.2}$$

where d is the pinhole diameter. Substituting previous values for u_T and ν yielded a diameter d = 0.0135 inches.

It was necessary to place the Helmholtz frequency well above the highest frequency to be analyzed, i.e., well above 16 kHz. Thus, accompanying phase and amplitude effects on the pressure spectrum were kept to a minimum. Keeping in mind the dimensions of the basic transducer model to be modified and the range of permissible pinhole diameters, the remaining critical dimensions for a high Helmholtz frequency were obtained. Repeated calculations with the following equations were made in the selection process.

The basic Helmholtz resonant frequency equation employed [29] is given as:

$$f_o = \frac{c}{2\pi} \left[\frac{S}{(\ell+1.7a)V} \right]^{\frac{1}{2}} , \text{ Hz} \tag{3.3}$$

where: c = 13,500 in./sec, speed of sound;

$S = \pi a^2$ in.^{2}, pinhole cross-sectional area;

a = radius of the pinhole, in.;

ℓ = length of the pinhole opening, in.;

$V = \pi r^2 h$ in.^{3}, cavity volume;

h = cavity height, in.;

r = cavity or diaphragm radius, in.

The "sharpness" of the resonance or quality factor Q is given by [29]:

$$Q = 2\pi \left[\frac{(\ell+1.7a)^3 V}{s^3} \right]^{\frac{1}{2}} . \qquad (3.4)$$

The upper and lower "half-power" or -3dB frequencies for the resonant peak may be found by [7]:

$$f_2 = f_o \left(1 + \frac{1}{2Q}\right), \quad \text{Hz}, \qquad (3.5)$$

$$f_1 = f_o \left(1 - \frac{1}{2Q}\right), \quad \text{Hz}, \qquad (3.6)$$

where: $f_1 < f_o < f_2$, Hz.

By simple algebraic manipulation the -3dB bandwidth results:

$$\Delta f_{-3dB} = f_2 - f_1 = \frac{f_o}{Q} , \quad \text{Hz}. \qquad (3.7)$$

The amplification and phase effect due to the resonance is found using a transfer function quantity [9]:

$$\underset{\sim}{H}(f) = \frac{f_o^2}{(f_o^2 - f^2) - j\left[\frac{f_o f}{Q}\right]} \qquad (3.8)$$

where $\underset{\sim}{H}(f)$ is a complex function of frequency.

The finalized dimensions of the finished transducer, henceforth referred to as a "Kulite," are given in Figures 3.1-3.3. The accompanying manufacturer's specifications and computed values resulting from the above equations are given in Table 3.1.

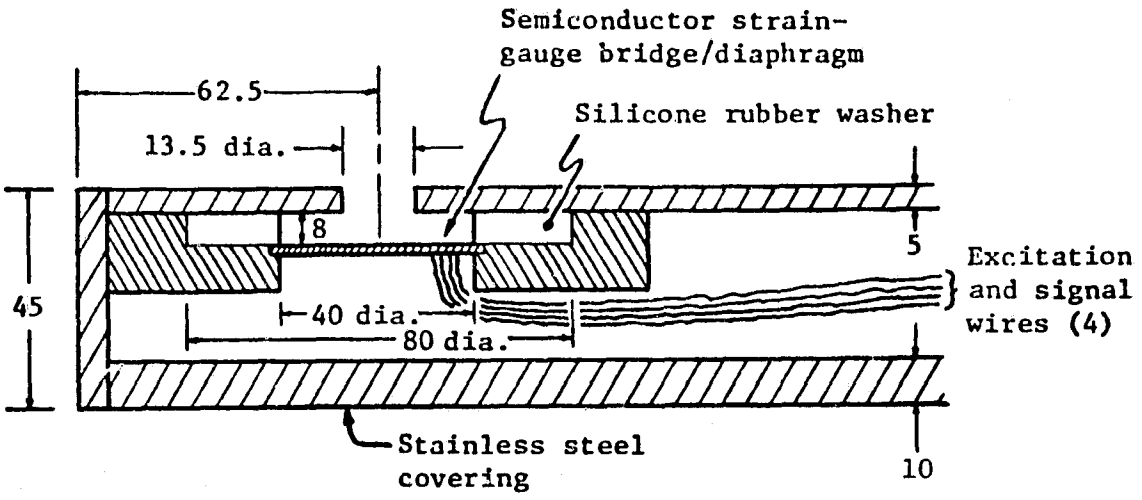

(Note: Dimensions are in thousandths of an inch)

Figure 3.3 Internal Kulite dimensions and construction details

Table 3.1 Specified and calculated Kulite performance parameters

Parameter	Value	Description
$f_{o,d}$	100	diaphragm resonant frequency
	25 mV/psi	nominal sensitivity
	15 VDC	excitation voltage
Z_o	750	electrical output impedance
	±1%/±2 psi	combined nonlinearity & hystersis in percent over the given pressure range about ambient conditions
f_o	63.2 kHz	Helmholtz resonant frequency
Q	24.6	quality factor
Δf_{-3dB}	2.57 kHz	-3dB bandwidth
f_1	61.9 kHz	lower -3dB frequency
f_2	64.5 kHz	upper -3dB frequency

Various calculated values for resonant magnification factor and phase are presented in Table 3.2 and plotted in Figure 3.4 as functions of frequency.

Table 3.2 Absolute value and phase of the resonant magnification factor for selected frequencies

Frequency, kHz	$\|H(f)\|$	$\phi(f)$, degrees
10.0	1.03	0.378
16.0	1.07	0.630
61.9, (f_1)	17.7	44.7
63.2, (f_o)	24.6	90.0
64.5, (f_2)	17.1	134.7
100.0	0.663	177.6

Standing wave effects in a cavity of such small dimensions were not considered to be at all significant.

3.3 Pressure Coupler Design and Use

The Kulites were to be mounted symmetrically on the "upper" and "lower" surfaces of the airfoil. To best match the phase, frequency response and sensitivity of symmetric Kulites to one another, an acoustic calibration pressure coupler was employed (Figure 3.5). It was constructed of steel and had cavity dimensions as shown in Figure 3.6.

The coiled tube connected to the coupler was provided to relieve static pressure build-up as the microphones were inserted. It was cut

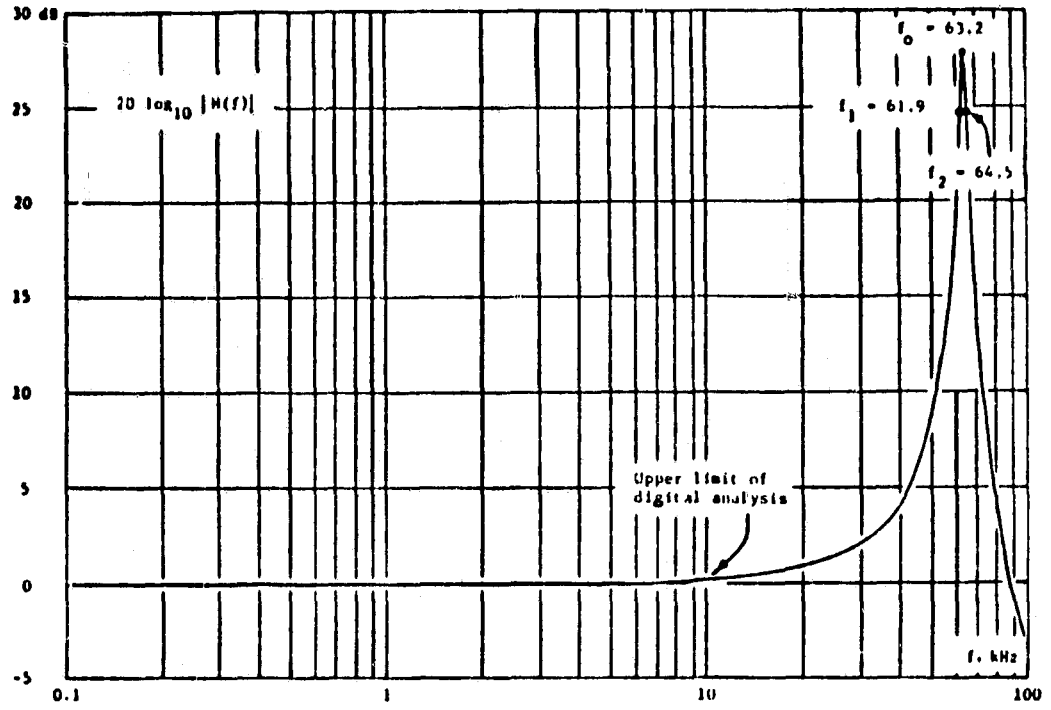

(a)

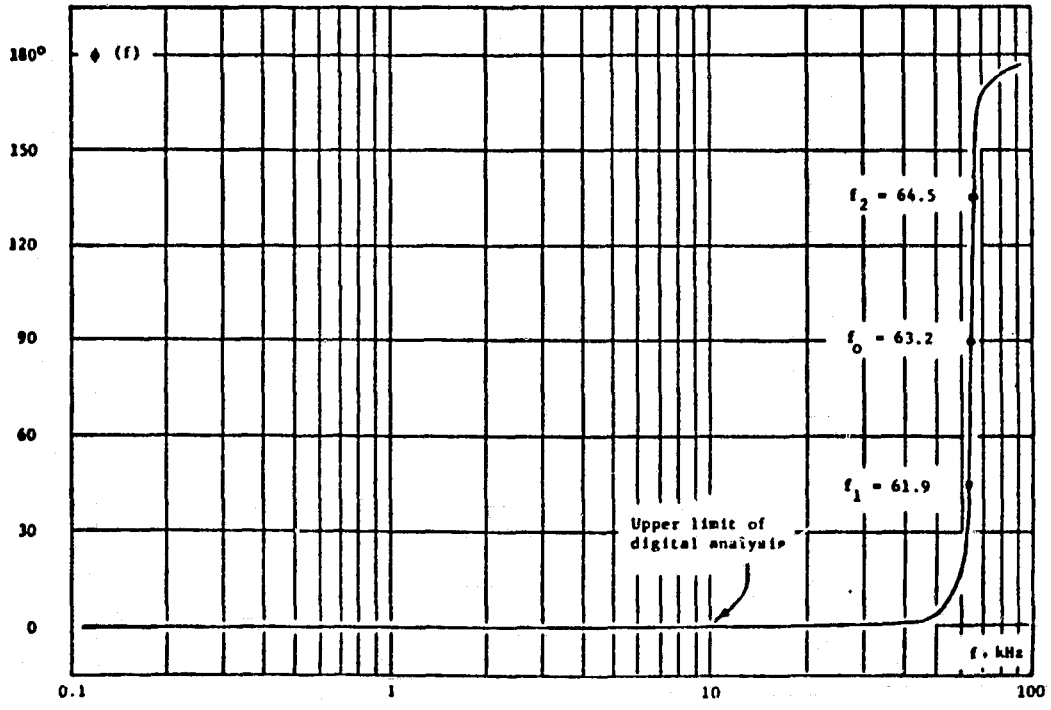

(b)

Figure 3.4 Calculated (a) magnitude and (b) phase of the magnification factor resulting from the Helmholtz resonance of the Kulite pressure transducer cavity

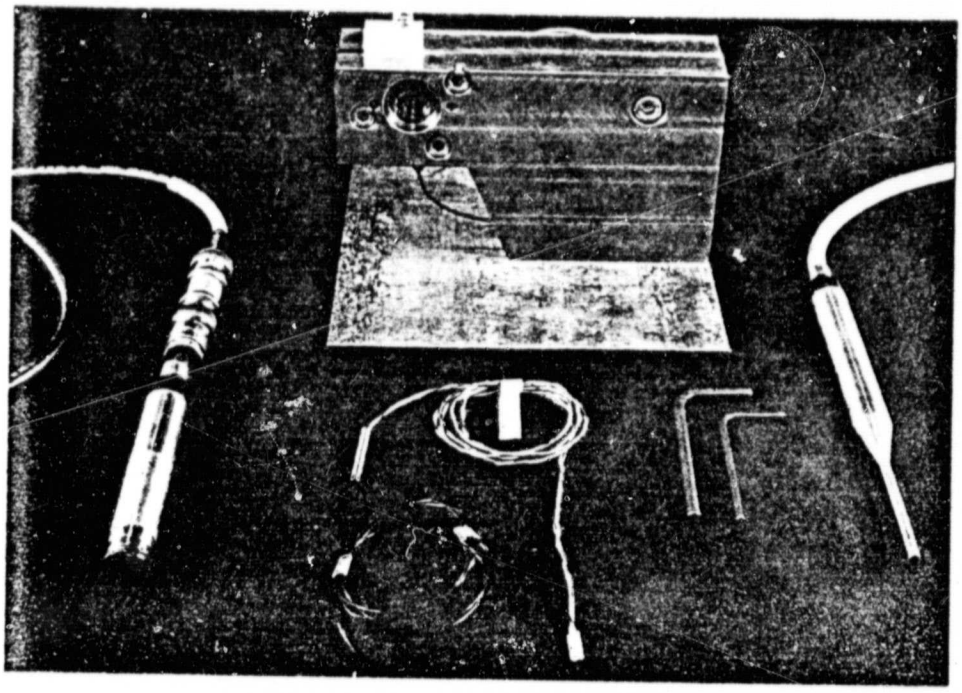

(a)

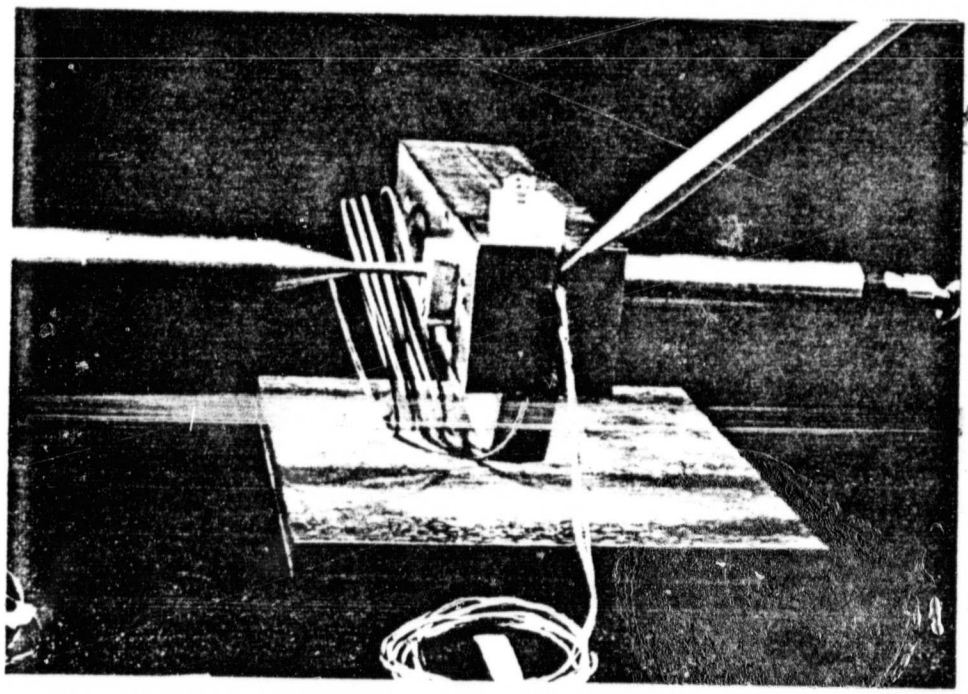

(b)

Figure 3.5 Pressure coupler components showing (a) driver, Kulite and reference microphones with cavity visible, (b) unit in operation

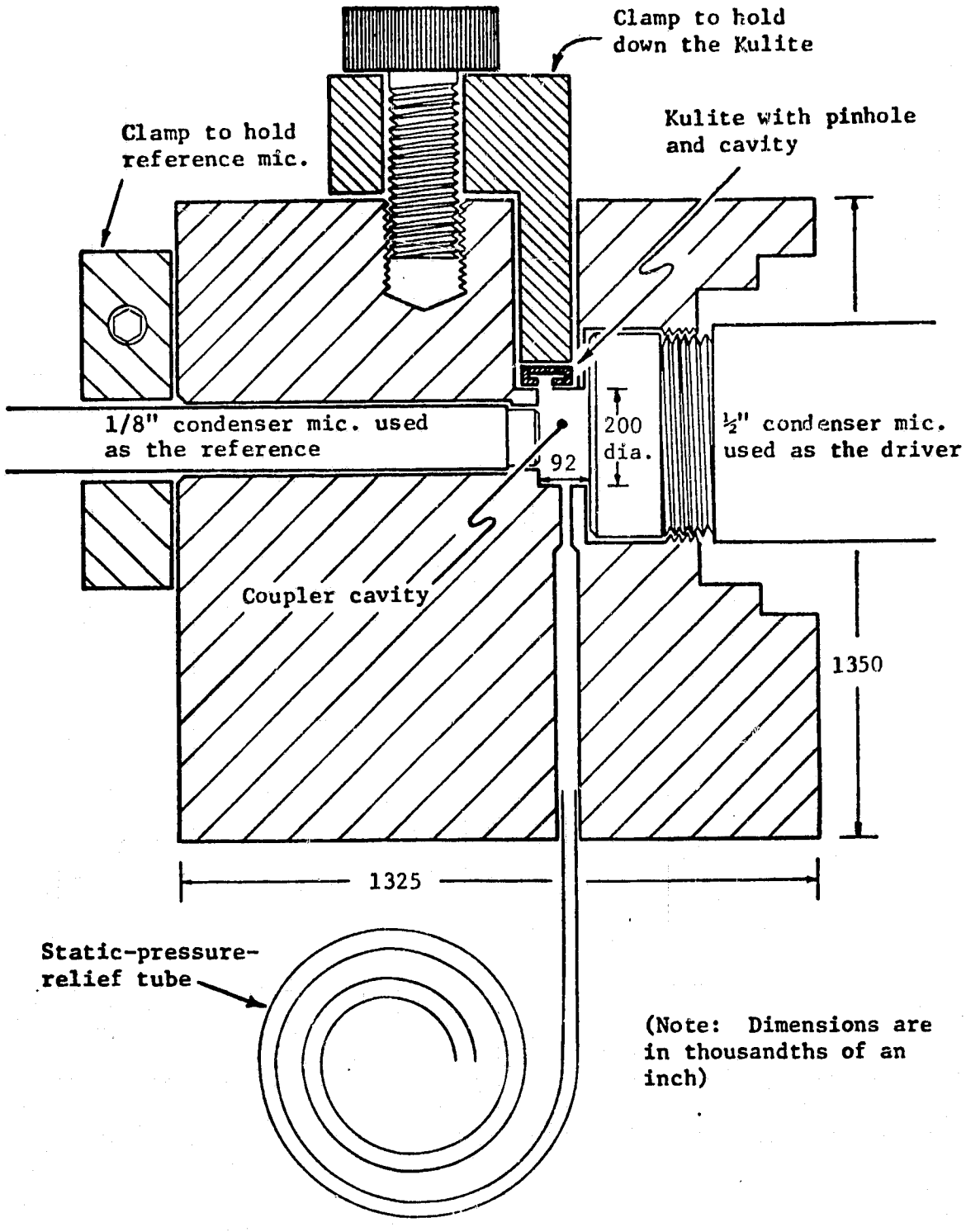

Figure 3.6 Arrangement of components and internal cavity dimensions of the Kulite pressure coupler/calibrator

long and had a small inner diameter to place any pipe resonances well below the lowest measurement frequency.

The principle of operation for a pressure coupler/calibrator is straightforward. A high quality microphone with known frequency and phase response characteristics is used as a reference. It is inserted into one side of the coupler until it reaches the internal cavity. Another microphone which may be of lesser quality is used as a driver to provide a noise source. It too is inserted into the coupler until it reaches the cavity and is facing the reference microphone. The pinhole opening of the Kulite is also provided access to the cavity. Except for the static pressure relief tube, the cavity is now sealed. The very close proximity of driver, reference and Kulite microphones together with the small volume of the cavity insure that the acoustic pressure is the same throughout when the driver emits a tone. Thus, the dynamic pressure response of the Kulite may be accurately calibrated against that of the reference microphone.

The small dimensions involved prevented standing wave resonances from becoming a problem in the frequency range of interest which was < 100 kHz.

A Brüel and Kjaer type 4134 one-half inch condenser microphone was used as the driver. It was connected to a high impedance 200 VDC power supply to provide the polarization voltage necessary for operation as a transducer. A swept-sine signal generator provided the source signal. A Brüel and Kjaer type 4138 one-eighth inch condenser microphone was used as the reference. A Brüel and Kjaer type 2619 preamplifier and type 2607 measurement amplifier connected the

reference microphone to a type 2971 phase meter. The output of the phase meter was connected to an X-Y plotter. Synchronizing the X-Y plotter to the signal generator allowed plots of phase to be obtained from 1 kHz to about 30 kHz. Figure 3.7 shows the actual measured values of the magnitude and phase lag of the Kulite pressure response as functions of frequency.

The phase and magnitude of the frequencies near Helmholtz resonance were checked utilizing the coupler, signal generator, microphone amplifier and a Tektronix model 5103N oscilloscope. Only one Kulite was measured in order to verify the accuracy of the predicted resonance. The measured f_o = 62 kHz was within ±1 kHz of the predicted 63.2 kHz and the phase was within an acceptable margin ($\phi < 1.0^o$) as observed using Lissajous figures.

It was found during calibrations that the strain-gauge sensing element in the Kulites required a considerable warm-up period before stable operation was achieved. This period was avoided during the weeks of measurement by leaving the strain-gauge excitation power supply on at all times.

3.4 Kulite Mounting Positions

The Kulites were mounted flush to the surface with epoxy. The wiring was routed through channels machined into the airfoil surface. The geometric spacing of the Kulites was based on prior knowledge of the approximate rate of falloff of the correlation of the pressure field [22]. The possible failure of the transducers was also considered so some of the spacings between pinhole centers were repeated (Figure 3.8). This redundancy also allowed a second measurement of a

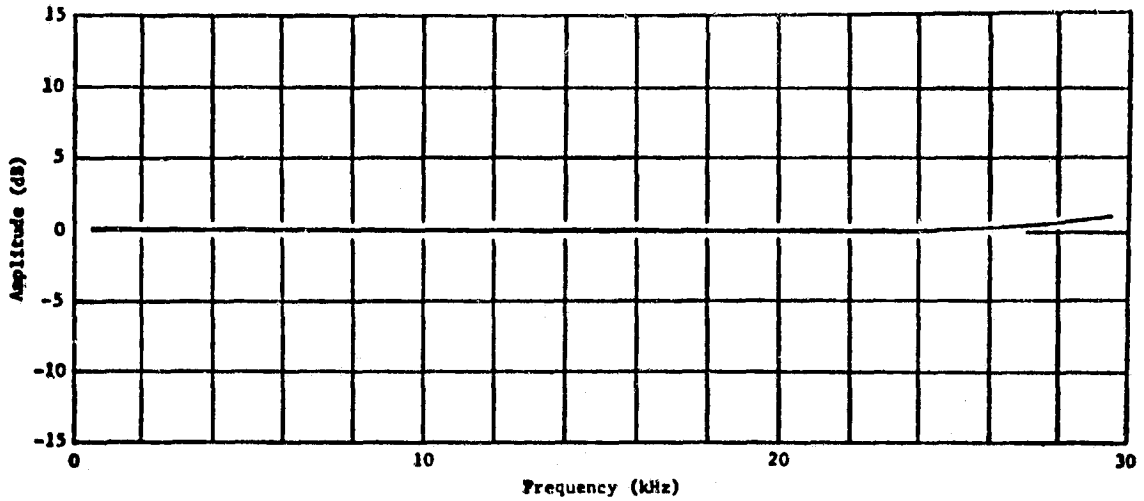

(a)

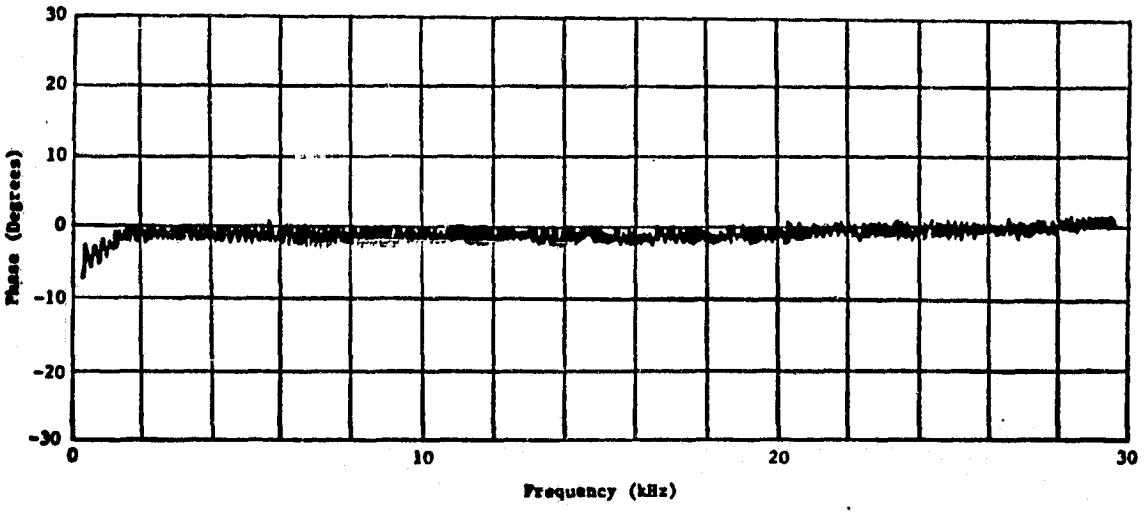

(b)

Figure 3.7 Measured values of (a) magnitude and (b) phase lag of the Kulite pressure response as functions of frequency

Figure 3.8 Detail of the upper airfoil surface and trailing edge, showing mounted Kulites and epoxy-filled grooves which accommodate wiring

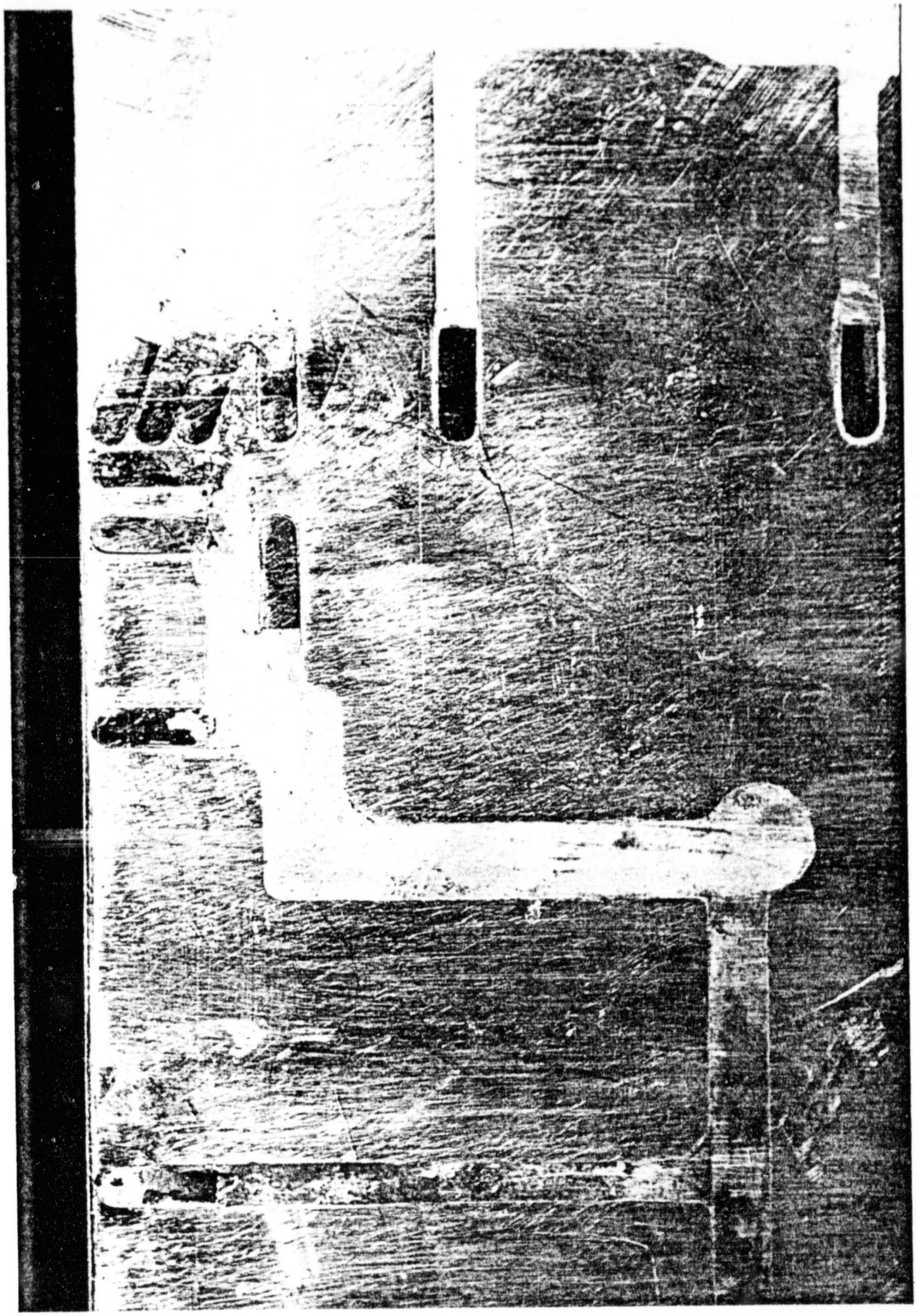

parameter to be made under similar dimensional conditions for verification purposes. Figures 3.9 and 3.10 show the positions of the Kulites as used in this initial study.

3.5 Kulite Amplifier Design

A circuit was needed to amplify the double-ended electrical signal originating at the corners of the semiconductor strain-gauge bridge network. Desirable characteristics included:

1) Low electrical noise of operation at high gain factors.
2) High common mode rejection ratio (CMRR) > 100 dB to exclude 60 Hz hum and radio frequency noise pickup.
3) Suitable gain on the order of 10^4 V/V to boost signals from a level of 25 μVrms to a voltage level compatible with most analysis instrument inputs, about 0.5 Vrms.
4) Wide bandwidth capability to prevent amplitude or phase distortions.
5) dc coupling at the input to allow the dc excited bridge to operate properly.
6) ac coupling at the output to prevent small dc voltage offsets due to the transducer from being amplified ten-thousand fold and clipping or overloading the output circuitry. These offsets may originate from barometric and/or temperature shifts acting on the bridge.

These criteria were easily and economically met by using two stages of amplification. Thus, the goals were accomplished:

1) The gain-bandwidth product for any one amplifier stage being fixed, wide bandwidths for each stage were achieved by requiring only relatively low gains. This kept amplitude and phase distortions to a minimum.

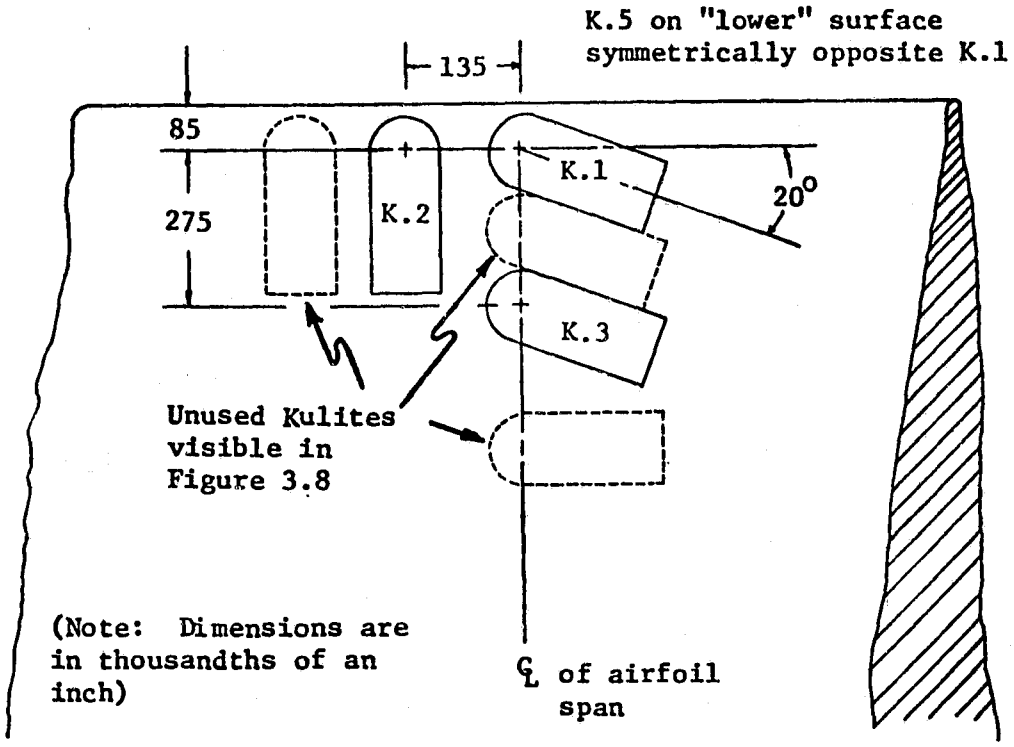

Figure 3.9 Locations of Kulites defined (upper surface shown)

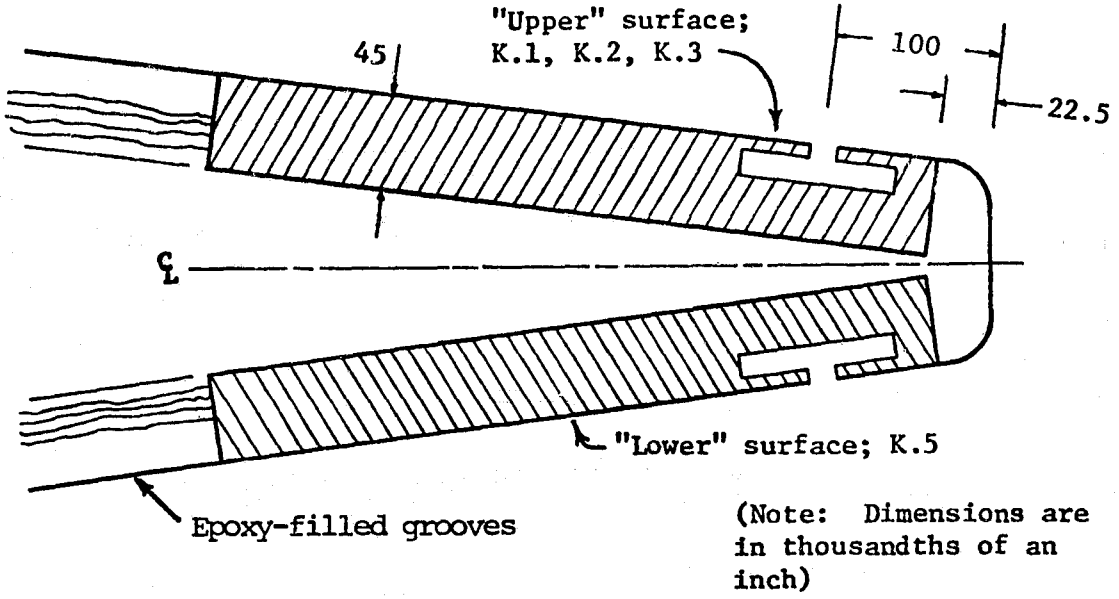

Figure 3.10 Cross-sectional detail of Kulites mounted at the trailing edge

2) The first stage was designed with a relatively low gain of 50 V/V (as compared with the overall gain of approximately 5000 V/V). This prevented small input dc offsets from overloading the output. The balanced input of the first stage operational amplifier used provided a minimum CMRR of 110 dB.

3) The two-stage design allowed the ac coupling to be placed between stages rather than at the output of the amplifier. A rather small-valued capacitor provided the coupling to the high but constant input impedance of the second stage. The low frequency cutoff achieved was ≈ 100 Hz.

A prototype circuit of the above general description was built at North Carolina State University using two operational amplifiers. The circuitry as actually used at NASA was constructed by Wyle Labs, Hampton, Virginia, and is shown schematically in Figure 3.11. Neff model 122 amplifiers operating at unity gain were connected to the outputs to provide line driving from the anechoic chamber area where the Kulite amplifiers were situated to the control room where all other amplifier circuitry was located.

Ithaco model 455 active filters operating at voltage gains of 25 to 45 dB and set for low frequency cutoffs of 100 Hz provided the remaining voltage boost required by this design. Flat frequency and linear phase response beyond the 100 kHz range of testing was achieved with this configuration.

Figure 3.11 Schematic of the power supply and one of eight first-stage amplifiers for the Kulite pressure transducers

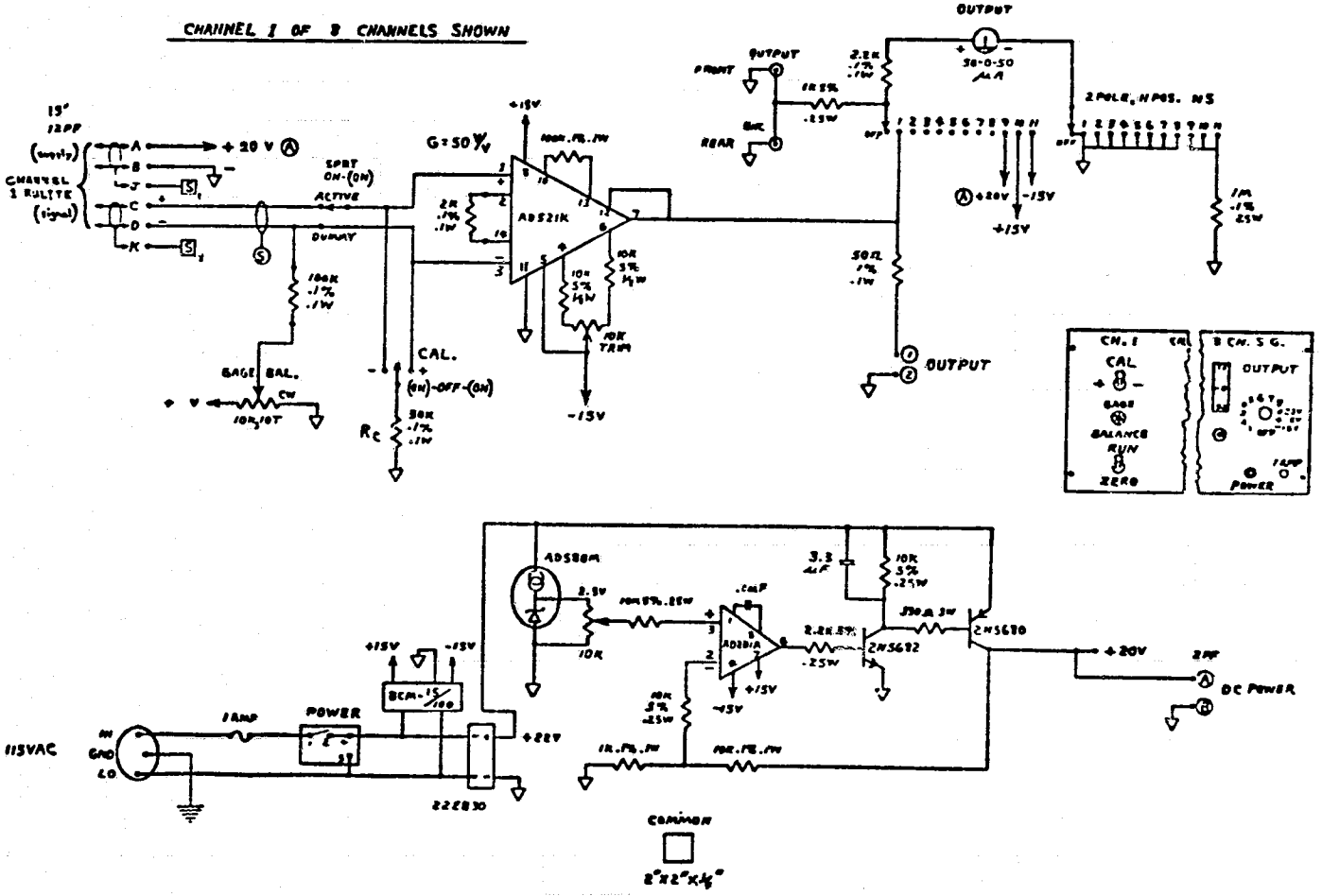
CHANNEL 1 OF 8 CHANNELS SHOWN
19' 12PP
CHANNEL 1 MULTIX
+20 V
SPST ON-(ON) ACTIVE
DUMMY
100K .1% .1W
GAGE BAL.
10K/10T
CAL.
(ON)-OFF-(ON)
Rc
50K .1% .1W
G=50 V/V
+15V
AD521K
2K .1% .1W
10K 5% 1/4W
10K TRIM
-15V
OUTPUT
FRONT
REAR
2.2K .1% .1W
1K 5% .25W
50-0-50 μA
2 POLE, N POS. NS
+20V
-15V
+15V
1M .1% .25W
50Ω .1% .1W
OUTPUT
CH. 1 CAL
GAGE BALANCE
RUN
ZERO
8 CH. S.G. OUTPUT
POWER
AD588M
3.3 μF
10K 5% .25W
.1μF
AD518A
2.2K 5%
.25W
2N5682
390Ω 1W
2N5680
+20V
2W
DC POWER
10K 5% .25W
10K
115VAC
HI
GND
LO
1 AMP
POWER
BCM-15/100
+22V
22EB30
COMMON
8"x2"x4½"

4. SIGNAL ANALYSIS FUNCTIONS

It is the purpose of this section to provide a brief review of the mathematical development and usefulness of the functions used for signal analysis in this study.

4.1 Auto-Correlation Function

Correlation as it applies to signal processing is generally understood to be a means of providing an indication of the amount and nature of the time dependency of one time signal x(t) on another y(t).

For the case where the two time signals are identical, the "auto-correlation" results. Its calculation provides an indication of the influence of "past" events on a chosen "present" event time t as a function of the time delay or lag τ between the two events. It is defined in its infinite-limit continuous form as:

$$R_{xx}(\tau) = \lim_{T \to \infty} \frac{1}{T} \int_{-T/2}^{+T/2} x(t)\, x(t+\tau)\, dt \qquad (4.1)$$

where T is the length in time over which the multiplication is carried out. Because the signal is correlated with itself, the resulting function is symmetric about $\tau = 0$. The maximum value for the auto-correlation will always occur at $\tau = 0$ which also corresponds to the mean-square value of the signal.

The auto-correlation is useful for characterizing a single signal as to its periodic versus nonperiodic content, which includes echoes, periodic pseudo-random noise, etc. [6, 35]. Examples of some characteristic auto-correlation curves may be found in the literature [2, 6, 19].

Physical limitations of data storage space and computational time prohibit infinitely long data collection; thus, finite time dependent functions are employed to provide approximate values in lieu of the exact values provided by the infinite continuous functions.

The auto-correlation may be re-defined for continuous but finite data record lengths as:

$$\hat{R}_{xx}(\tau) = \frac{1}{T} \int_{-T/2}^{+T/2} x(t)\ x(t+\tau)dt \qquad (4.2)$$

where the "^" indicates the result of many averages (Section 7.1). If, however, the auto-correlation is to be computed on a digital computer, the continuous time signal must be sampled and quantized into discrete data points (see Section 6.1). Then the straightforward computation involves the equation:

$$\hat{R}_{xx,n}(nh) = \frac{1}{(N-n)} \sum_{i=1}^{(N-n)} x(ih)\ x[(i+n)h] \qquad (4.3)$$

where: $n = 0, 1, 2, \ldots, r$.

N is the total number of data points in the sample record, nh is the incremental time displacement, $r = \tau_{max}/h$ is the maximum lag number, and h is the time interval between consecutive sample points.

In many instances information in the frequency domain is more desirable for characterizing signals since amplitude and phase as functions of frequency are obtained. These are not directly available when the same data are processed through a time function such as correlation.

4.2 Fourier Transform and Auto-Spectral Density Functions

The most common time - to - frequency domain transform function used is the forward Fourier transform. In its infinite-limit continuous form it is "double-sided" in frequency about f = 0:

$$FT\{x(t)\} = \underset{\sim}{X}(f) = \int_{-\infty}^{+\infty} x(t)\, e^{-j2\pi ft}\, dt \qquad (4.4)$$

where: $-\infty < f < +\infty$,

x(t) is some piecewise-smooth function of time and the "~" denotes a complex quantity. At times, rather than presenting a complex quantity in terms of a magnitude with phase (which is known as "phasor" notation) the quantity is separated into its real and imaginary components. The use of Euler's equation [39]:

$$e^{-j(z)} = \cos(z) - j\sin(z) \qquad (4.5)$$

where z is a general variable yields the real and imaginary components of the frequency spectrum when applied to Equation (4.4):

$$\begin{aligned} \underset{\sim}{X}(f) &= |\underset{\sim}{X}(f)|[\cos(2\pi ft) - j\sin(2\pi ft)] \\ &= |\underset{\sim}{X}(f)|\cos(2\pi ft) - j|\underset{\sim}{X}(f)|\sin(2\pi ft) \quad . \end{aligned} \qquad (4.6)$$

Fourier transformed functions are often called "spectral densities" because they show how the frequency spectra are amplitude weighted.

The finite Fourier transform for obtaining the spectral density function is defined as:

$$\hat{X}(f,T) = \int_{o}^{T} x(t)e^{-j2\pi ft}\,dt \tag{4.7}$$

where x(t) is a continuous function of time but is integrated over the finite period T. The resulting function is no longer a continuous function of frequency as in Equation (4.4) but is instead represented by discrete frequency bands of bandwidth:

$$BW = \frac{1}{T} \quad , \text{ Hz} \tag{4.8}$$

with an infinite number of bands in the positive and negative frequency axis yet symmetric about zero.

Since, as stated previously, only finite capabilities exist for collecting and analyzing the data, the function x(t) must be represented by a finite time length sample record x(ih) (Section 6.1). Thus, the period of integration T as used in Equation (4.7) is replaced by the product Nh and the discrete finite Fourier transform is given by:

$$\hat{X}_{N}(f_n,Nh) = h \sum_{i=o}^{(n-1)} x(ih)e^{\frac{-j2\pi ni}{N}} \tag{4.9}$$

where: $n = 0, 1, 2, \ldots, (N-1)$,

$$f_n = \frac{n}{Nh} \quad , \text{ the incremental frequency,} \tag{4.10}$$

x(ih) is the finite length time history of events comprised of N data points h seconds apart, and N, h, and i are as previously defined.

For actual direct computation of the spectral density on a computer, Euler's relationship, Equation (4.5) may be used on (4.9) to obtain [2, 6, 28, 32]:

$$\hat{X}_n(f_n,Nh) = h \sum_{i=o}^{(N-1)} x(ih)\cos[2\pi(\frac{ni}{N})] - jh \sum_{i=o}^{(N-1)} x(ih)\sin[2\pi(\frac{ni}{N})] \qquad (4.11)$$

where the variables are as defined previously.

4.3 Fast Fourier Transform

A much faster method of computing the discrete finite Fourier transform known as the fast Fourier transform, or FFT, was developed by Cooley and Tukey in 1965 [12] and has since been refined by other mathematicians. The FFT algorithm used during this study was developed by R. C. Singleton in 1969 [38] and has proven to be an accurate and efficient FORTRAN version of the original Cooley-Tukey FFT algorithm.

In the computer implementation of the FFT, the input data are assumed to be complex valued and hence formatted as two time series arrays--one the real part of the input data and the other the imaginary. A single real-valued time series x(ih) could be inserted into the real time series array while all points of the imaginary time series array are set to zero. A more efficient method suggested by Singleton [38] is to insert odd-numbered data points of the real-valued time series into the real array and even-numbered data points into the imaginary array. Although a sorting algorithm must be used

on the output of the FFT algorithm to yield interpretable results, storage space is halved and the computation time considerably speeded up.

4.4 Properties of Spectral Density Functions

Since spectral density functions are two-sided and symmetric about f = 0, and because negative frequencies have no physical meaning when analyzing real-life time events, the single-sided spectral density function is defined as:

$$\underset{\sim}{G}(f) = 2\,\underset{\sim}{X}(f), \qquad 0 \leq f < +\infty \ . \tag{4.12}$$

Due to the squared-quantity nature of correlation functions, the Fourier transform of the auto-correlation is a "power-like" quantity. Hence, it is termed the "auto-power spectral density" or auto-PSD and is normally converted to single-sided form so that:

$$G_{xx}(f) = 2\ FT\{R_{xx}(\tau)\} \ . \tag{4.13}$$

Note that because the auto-correlation is a real and symmetric function of time, the resulting auto-spectral density function is real and symmetric [6, 45]. Thus, the associated auto-PSD is real as indicated in Equation (4.13). This is a general result of the integral of the sine function with infinite limits, Equations (4.4) and (4.5), being equal to zero when real and even functions are transformed.

4.5 Computer Implementation of Signal Analysis Functions

This same result is obtained digitally on the computer by multiplying the complex FFT result with its complex conjugate as denoted

by the *:

$$G_{xx}(f_n, Nh) = 2\,\hat{X}_n\,(f_n, Nh)\,\hat{X}_n^{*}\,(f_n, Nh) \qquad (4.14)$$

$$= (A + jB)(A - jB)$$

$$= A^2 + B^2, \text{ real} ,$$

where A and B represent the respective real and imaginary frequency components of the complex FFT result. This yields the requisite power-like squared quantity that is obtained from the theoretical discrete finite Fourier transform of the auto-correlation.

Equation (4.13) indicates that the auto-correlation and the auto-PSD constitute a Fourier transform pair. This is known as the Weiner-Khintchine relationship [2, 32, 35] and implies that the inverse Fourier transform of the auto-PSD yields the auto-correlation:

$$R_{xx}(\tau) = \frac{1}{2\pi} \int_{-\infty}^{+\infty} \tfrac{1}{2} G_{xx}(f) e^{j2\pi f\tau}\, df \qquad (4.15)$$

or in discrete finite form [2, 6]:

$$R_{xx,n}(nh) = \frac{1}{2\pi N} \sum_{i=1}^{(N-n)} \tfrac{1}{2} G_{xx,i}(f_i, Nh)\, e^{\frac{j2\pi ni}{N}} \qquad (4.16)$$

where: $n = 0, 1, 2, \ldots, (n-1)$

and the other variables are as defined previously.

This is a very useful result as it allows the inverse FFT computer algorithm to compute correlation function values from spectral

density values. It is much quicker and more economical than the straightforward point-by-point time domain computations. It also allows the correlation to be computed on data that have been "filtered" into frequency bands of interest. This "filtering" may be accomplished by editing the frequency spectrum of the data after they have been forward transformed by the FFT. This roundabout method of computing the correlation has been called "circular correlation" and is the method used to calculate the correlation values in the program CIRCXCOR listed in Appendix 11.4 [2, 6, 32].

4.6 Cross-Correlation and Cross-Correlation Coefficient

The cross-correlation function is similar to the auto-correlation function in that two time series are compared. The cross-correlation is more general in that the two time series are of different origin--from two transducer locations, for instance. Thus, it is seen that the auto-correlation is merely a special case of the cross-correlation.

Some of the more common characteristic cross-correlation curves are similar to the auto-correlation curves of references [2, 6, 19] except that the axis of symmetry no longer lies at $\tau = 0$ but rather at some other time delay. Nor is there necessarily an axis of symmetry because real-life phenomena and measurement systems may contain extraneous noise in data channels, nonlinearities such as dispersive media, etc.

The cross-correlation is useful for detecting the propagation time delay between transducer locations, the existence of a signal

(not necessarily periodic) that is buried in noise, and the determination of transmission paths [6, 35].

The cross-correlation of two continuous real signals, x(t) and y(t), as a function of the arbitrary delay or lag time τ is defined as:

$$R_{xy}(\tau) = \lim_{T\to\infty} \frac{1}{T} \int_{-T/2}^{+T/2} x(t)\, y(t+\tau)dt \ . \tag{4.17}$$

As for the case of the auto-correlation function, physical limitations necessitate the use of finite time versions of (4.17). Therefore, the cross-correlation function is re-defined for continuous but finite data record lengths as:

$$\hat{R}_{xy}(\tau) = \frac{1}{T} \int_{-T/2}^{+T/2} x(t)\, y(t+\tau)dt \tag{4.18}$$

and in the discrete finite-time form as:

$$\hat{R}_{xy,n}(nh) = \frac{1}{N-n} \sum_{i=1}^{(N-n)} x(ih)y[(i+n)h] \tag{4.19}$$

where: $n = 0, 1, 2, \ldots, r$

and the other variables are as defined previously.

A normalized version of the cross-correlation is often more informative as to the "percent" of correlation between two signals. This is useful for comparing the results of one test with the results of another without regard as to absolute reference values or scaling of data. This normalized cross-correlation function is called

the "correlation coefficient" $\rho_{xy}(\tau)$ and its value always will lie between +1 and -1. Provided the two signals x(t) and y(t) have zero mean, $\rho_{xy}(\tau)$ may be computed using the auto-correlation functions with $\tau = 0$ [2, 6, 32]:

$$\rho_{xy}(\tau) = R_{xy}(\tau)/[R_{xx}(0)R_{yy}(0)]^{\frac{1}{2}} , \quad -1 \leq \rho_{xy} \leq +1 . \tag{4.20}$$

4.7 Cross-Spectral Density and Ordinary Coherence Functions

In the same vein as for the single-channel auto-PSD the two-channel "cross-PSD" is obtained from the cross-correlation. But because the cross-correlation is in general not an even function, the cross-PSD is usually complex:

$$\underset{\sim}{G}_{xy}(f) = 2\ FT\{R_{xy}(\tau)\} . \tag{4.21}$$

In a simplified likeness of Equation (4.14), the cross-PSD as computed from the output of the FFT is given as:

$$\hat{\underset{\sim}{G}}_{xy}(f) = 2\hat{\underset{\sim}{X}}(f)\hat{\underset{\sim}{Y}}^{*}(f) \tag{4.22}$$

where the quantities are averaged for reasons given in Section 7.1.

A normalized version of the cross-PSD that is void of any phase information is called the "ordinary coherence" or just "coherence." Maintaining the notation simplification used above with the additional stipulation that all following spectral quantities are assumed to be averaged and real or complex as necessary, the coherence is defined as a real number between 0 and 1:

$$\gamma^2_{xy}(f) = \frac{|G_{xy}(f)|^2}{G_{xx}(f)\ G_{yy}(f)} , \quad 0 \leq \gamma^2_{xy} \leq +1 . \tag{4.23}$$

Whereas the cross-correlation coefficient indicates the degree of wide-banded dependency of one signal on another for a given time lag, the coherence indicates the degree of narrow-banded frequency dependency of the two signals on one another. It is analogous to computing the cross-correlation in narrowly filtered frequency bands. Note that the theoretical coherence is nonzero only if there is some degree of fixed phase information between x(t) and y(t). Therefore, there would be no coherence ($\gamma_{xy}^2 = 0$) between two signals, whether random or periodic, if they were totally uncorrelated over a long period of time.

4.8 Partial Coherence Function

In some instances a system may exist which has multiple input signals that combine to yield a single output signal. If these inputs are partially dependent on one another, then the ordinary coherence function cannot correctly yield the amount of relationship between any one single input and the output.

Consider the hypothetical acoustic system of Figure 4.1. The two independent source mechanisms $s_1(t)$ and $s_2(t)$ partially combine with one another to yield emission signals x(t) and y(t). These emissions come from two separate locations and are sensed simultaneously by the far-field microphone as z(t). It is desired to have knowledge of the amount of contribution each of the input noise source mechanisms $s_1(t)$ and $s_2(t)$ make to the output signal z(t). Such knowledge is useful for locating the root cause of a particularly offensive sound from a machine or for determining the nature and

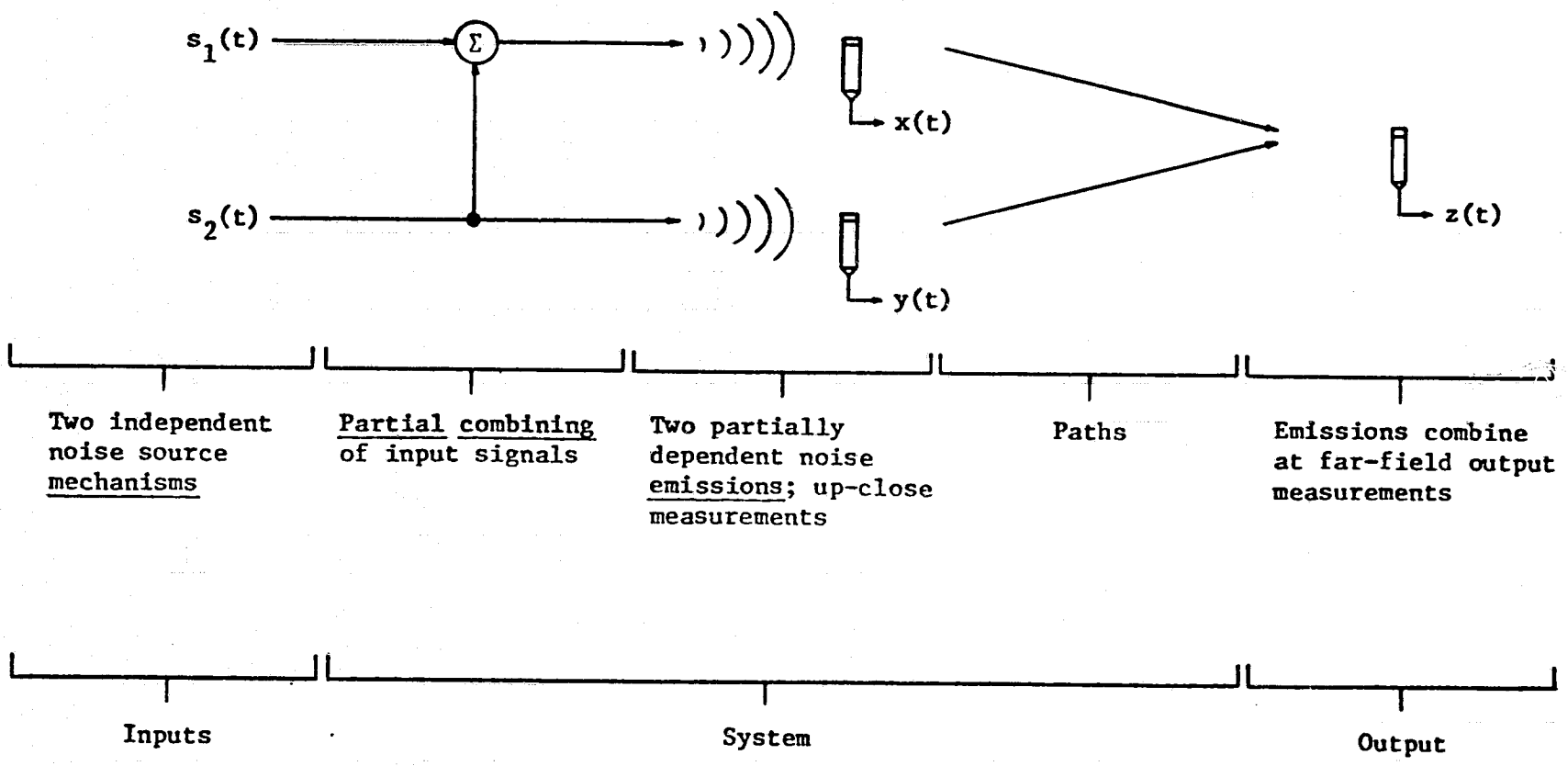

Figure 4.1 Hypothetical system demonstrating the need for analysis involving partial coherence

extent of a subtle noise source mechanism such as exists with the TE noise phenomena.

Suppose the ordinary coherence γ^2_{xy} is taken between x(t) and z(t). An appreciable amount of coherence would be indicated whether source mechanism $s_1(t)$ were responsible or not. This is due to the partial dependence of x(t) on input mechanism $s_2(t)$.

The "partial coherence" is a more advanced type of coherence function that can overcome this problem in the following manner: If the phase coherent effects of y(t) were removed from both x(t) and z(t), the correct relationship between $s_1(t)$ and z(t) could be established (Figure 4.2).

Thus, if all sound emission inputs of a system could be taken into account, then the actual degree of coherence between an acoustic source mechanism and the output sound at the far-field observer's microphone can be computed. Often, however, the capability exists for analyzing only a limited number of channels. In that case the partial coherence will yield a result that, although a better estimate than the ordinary coherence, is still not the true value of the degree of fixed-phase relationship between a noise source mechanism and the received noise output.

For a three-input/single-output system, the equations for computing the partial coherence from cross-spectral and auto-spectral values are given [3, 5, 19, 52]. They are so written as to yield the partial coherence between the input 1 and the output 4 with the phase-coherent effects of inputs 2 and 3 removed:

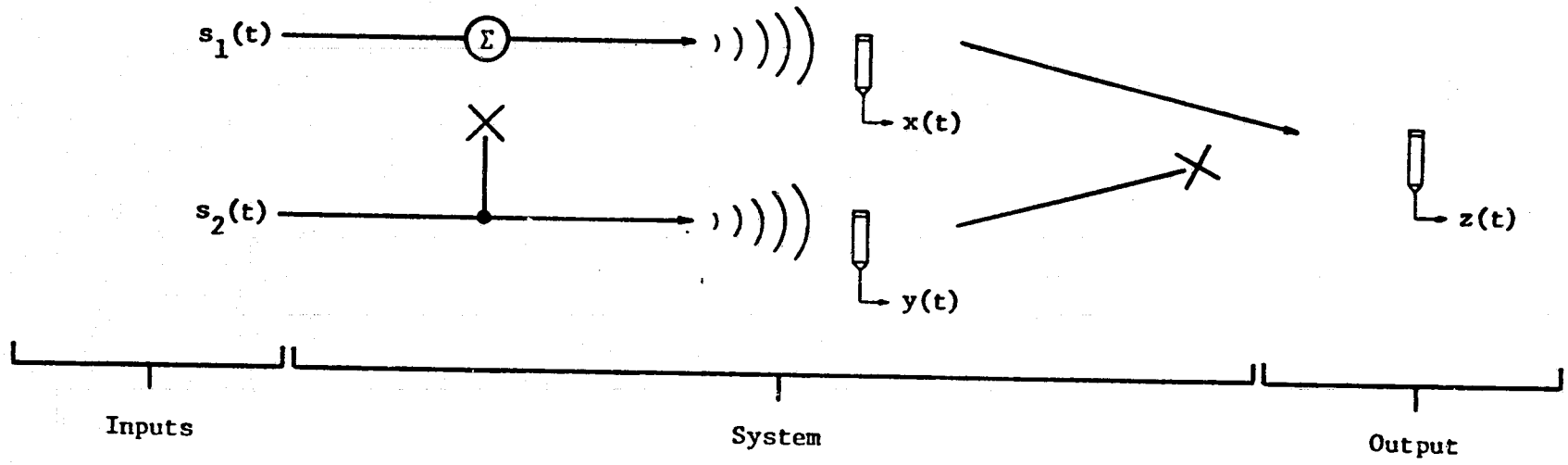

Figure 4.2 Showing the analogous physical method of obtaining the partial coherence between input $s_1(t)$ and output $z(t)$ with the effects of $s_2(t)$ removed

$$\gamma^2_{14\cdot 23} = \frac{G_{14\cdot 12}\, G_{14\cdot 12}^*}{G_{11\cdot 23}\, G_{44\cdot 23}}$$

$$= \frac{G_{14\cdot 12}\, G_{41\cdot 12}}{G_{11\cdot 23}\, G_{44\cdot 23}}$$

$$= \frac{|G_{14\cdot 12}|^2}{G_{11\cdot 23}\, G_{44\cdot 23}} \quad , \qquad 0 \leq \gamma^2_{14\cdot 23} \leq +1 \qquad (4.23)$$

where:

$$G_{14\cdot 22} = G_{14} - \frac{[G_{14}G_{11}G_{22} - G_{14}G_{12}G_{21} + G_{11}G_{12}G_{24} - G_{12}G_{24}G_{41}]}{(G_{11}G_{22} - G_{12}G_{21})}$$

$$G_{11\cdot 23} = G_{11} - \frac{[G_{12}G_{21}G_{33} - G_{13}G_{21}G_{32} + G_{13}G_{31}G_{22} - G_{12}G_{23}G_{31}]}{(G_{22}G_{33} - G_{23}G_{32})}$$

$$G_{44\cdot 23} = G_{44} - \frac{[G_{24}G_{42}G_{33} - G_{24}G_{32}G_{43} + G_{34}G_{43}G_{22} - G_{23}G_{34}G_{42}]}{(G_{22}G_{33} - G_{23}G_{32})} \quad .$$

5. DATA COLLECTION

5.1 Recording at NASA

Test run data were collected at the NASA facility using the system shown in Figure 5.1. All data were recorded on the Honeywell model 96 14-track wideband FM tape recorder. It conformed to IRIG Group I specifications and featured flat response to 40 kHz when operated at the 60 inch-per-second speed used during the tests.

A Lockheed model 417D FM tape recorder was used to bring data back to the North Carolina State University computing facility for analysis. Selected transducer combinations were dubbed from the 14 tracks available on the NASA Honeywell machine onto the 4 tracks of the North Carolina State University Lockheed machine. The Lockheed machine had been modified to give flat record/playback response from dc - 10 kHz within ±0.5 dB with some sacrifice of signal-to-noise ratio when operated at 15 inches per second. Playback response of the Honeywell machine was also dc - 10 kHz at 15 inches per second. Dubbing speed for both machines was 15 inches per second, thus dc - 40 kHz test run data response was possible after a simple 4:1 scale-up of frequency on computer analysis outputs.

5.2 Data Collection and Analysis Facility

To collect the data for digital analysis, it was necessary to:

1) Filter the played-back data in a manner compatible with FFT and digital analysis requirements.

2) Digitally sample the data at a rate compatible with FFT and digital analysis requirements.

3) Qualify the data as suitable for subsequent analysis.

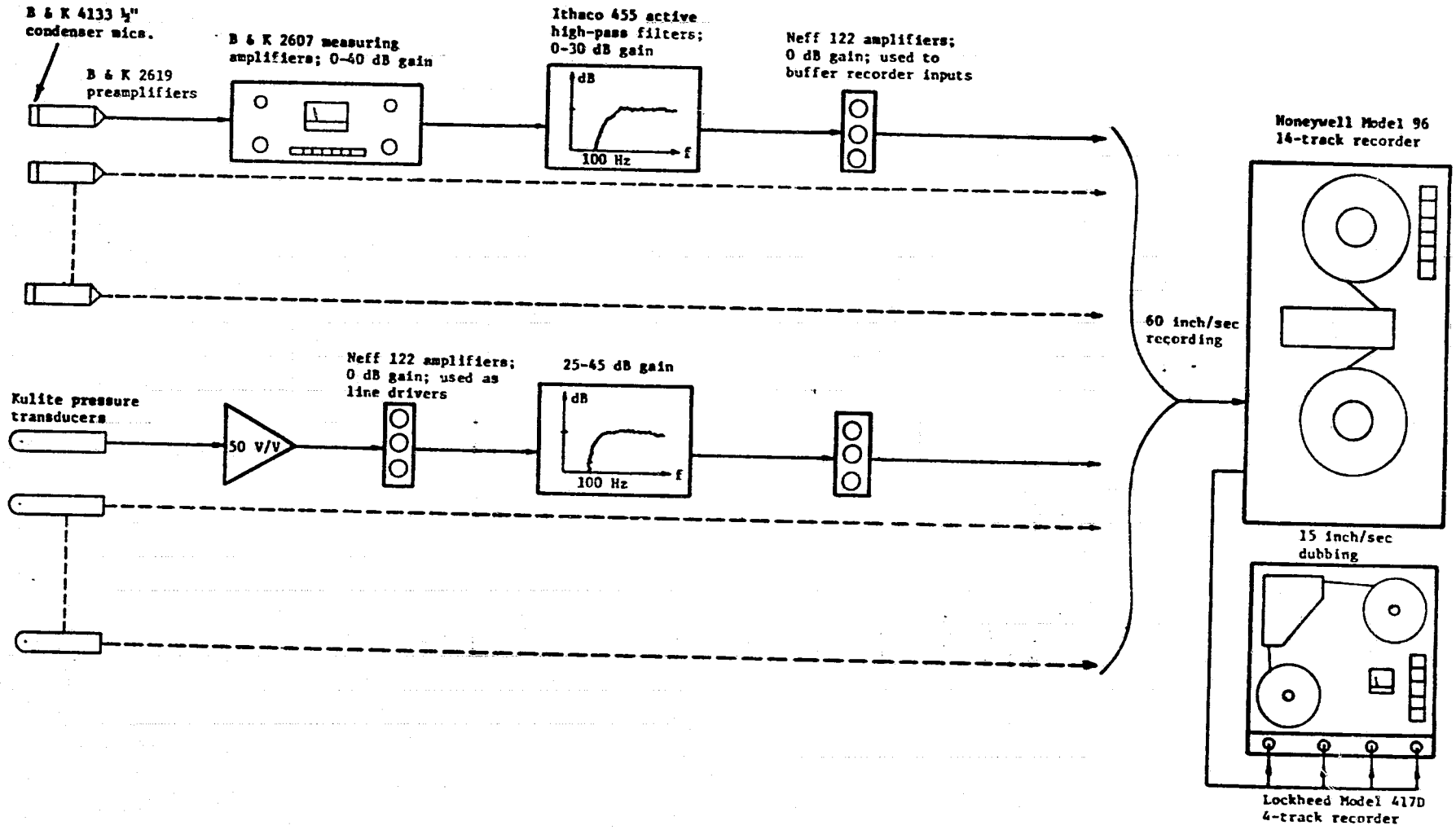

Figure 5.1 Data collection chain of equipment used at the NASA Langley ANRL facility

4) Store the data in a mass storage/retrieval system for convenient use at a later date.

The equipment used at the North Carolina State University facility for data collection and analysis is listed below:

1) Lockheed FM Tape Recorder, Model 417D, Serial No. 800.

2) Rockland Dual Hi/Lo Filter (two sets), Model 1042 F-03, Serial Nos. 1147709 and 1147710.

3) Biomotion Waveform Recorder, Model 1015, Serial No. 3139.

4) Digital Equipment Corporation PDP 11/40 Minicomputer, Serial No. WM 0106412.

5) International Business Machines System /7 and System /370 computer systems.

Figure 5.2 illustrates the system configuration of the North Carolina State University data analysis facility described below.

5.3 Digital Data Collection Procedures

Various combinations of the four available data channels were chosen to be analyzed from the dubbed Lockheed recorder data. The selected data were then played back at the North Carolina State University computing facility through the Rockland filters which were used primarily to prevent anti-aliasing when sampling (Section 6.1). A secondary function of the filters was to reject undesirable low frequency components up to 100 Hz (400 Hz in "NASA test-run time" due to the 4:1 recording speed change). The filters were also used on occasion to band-pass filter the data to verify the performance of the digital filter incorporated into the program CIRCXCOR (Appendix 11.4).

The data were then sampled by the Biomation analog-to-digital converter (ADC) which contained a 4096, 10-bit word buffer memory.

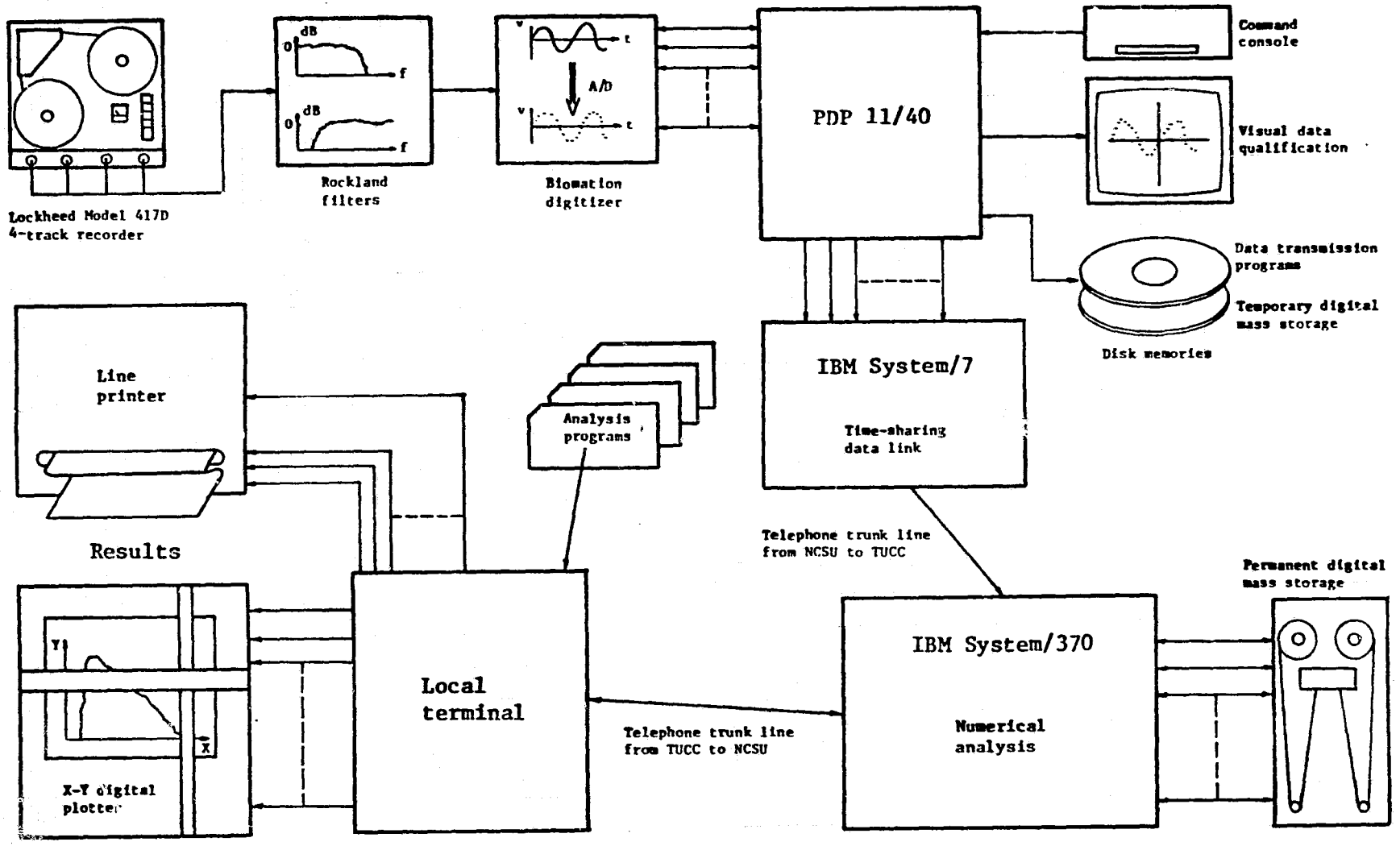

Figure 5.2 NCSU data collection, storage, and analysis facility

The waveform recorder could be set to collect one, two, or four channels of data with corresponding memory allocations of 4096, 2048, or 1024 data points (words) per channel. Individual adjustment for zero offset and input voltage scaling for each channel was available so that the maximum use of the 1024 (2^{10}) level dynamic range of the ADC in each channel could be achieved. The sampling rate was also set on the Biomation.

A command from the PDP 11/40 minicomputer operator's console initialized the sampling procedure. Then the Biomation would sample data from its selected inputs until the 4096 word buffer memory would fill. The memory contents were then transferred to a disk memory connected to the PDP 11/40. The Biomation could then fill its memory again. This process was repeated until a specified number of Biomation "dumps" were collected in the disk memory.

The data could be recalled and plotted on a video graphics display screen. This was typically employed to insure that the data were of sufficient amplitude to yield good dynamic range results when later used with the signal analysis software. It was also used to detect gross collection errors such as signal drop-outs between recorded data runs, evidence of bad electrical connections, filter settings, overloads, etc.

Additional operator console commands edited the Job Control Language (JCL) information which was then joined with the stored data dumps. The final command to the minicomputer sent out the JCL followed by the data as one large file to the IBM System/7 computer. The System/7 was used as a time-sharing data link between many on-campus

facilities at North Carolina State University and the Triangle Universities Computation Center, or "TUCC." TUCC is a large computing facility jointly operated by the three large universities in the region: North Carolina State University, Duke University, and the University of North Carolina.

When the proper conditions permitted, the System/7 computer transmitted the JCL and data to TUCC. The JCL accompanying the data then directed the IBM System/370 computer at TUCC to identify and store the data for later use.

Punched card versions of the computer programs listed in Appendices 11-2 - 11.4 were submitted to TUCC from on-campus computer terminals. These programs included the JCL which identified the proper data to be analyzed. The results of the computations were then returned on paper printouts and in plotted form.

6. DIGITAL ANALYSIS PARAMETERS

6.1 Sampling and Frequency Parameters

Analysis of data by digital means using the discrete finite forms of the functions outlined in Section 4 required sampling and conversion of the signals from analog to digital form. After storage, computer versions of the functions (Appendices 11.2 - 11.4) were utilized. The qualification of the data and the sampling requirements prior to analysis are herein discussed.

Representative segments of a signal are used for data analysis due to time and storage space restrictions. These segments are known as time histories or "sample records." The sampling of the data at time intervals "h" for a total number of sample points "N" results in a sample record period of T = Nh seconds. It is this perior which is used by the discrete finite functions of Section 4.

The resolution of the frequency bands which result from using the discrete finite Fourier transform (Equation 4.9) is then given by:

$$BW = \frac{1}{T} = \frac{1}{Nh} \quad , \quad Hz \ . \tag{6.1}$$

The Shannon Sampling Theorem [32, 35] states that at least two samples are required per period of the highest frequency of interest "f_N" contained in an analog signal if the signal is to be adequately represented by the sample record. Thus, all frequencies or Fourier harmonic components in a signal up to f_N are satisfactorily described by the samples, but those greater than f_N are not. Instead frequencies greater than f_N are mistaken for frequencies lower than f_N and are the basis for calling f_N the "Nyquist folding frequency."

To prevent this "aliasing," any frequency components in the analog data are filtered out before sampling takes place. The low-pass filter must therefore have a very sharp folloff above f_N and must minimize any alterations of the signal below f_N, thus imposing strict performance requirements. The Butterworth-type filter set used in this study had a rolloff of 48 dB/octave.

It follows from Shannon's Sampling Theorem that the sampling rate "f_s" must be at least twice that of the cutoff frequency f_N, or:

$$h = \frac{1}{f_s} \leq \frac{1}{2f_N} \quad , \quad \text{sec/sample.} \tag{6.2}$$

Thus, for the 0 - 10 kHz analysis range which was most commonly used for this study the low-pass anti-aliasing filters were set for 10 kHz and the sampling rate f_s = 20 kHz (or h = 0.05 msec). A higher sampling rate would have resulted in less chance for aliasing errors but the resulting loss of resolution would have increased any bias errors in the spectral density functions (Section 7.2). Also it was learned before any analysis took place at North Carolina State University that all discernible trailing-edge noise activity occurred below 6 kHz.

6.2 Dynamic Range

The data was digitized with a 10-bit binary analog-to-digital converter (ADC). This gave a dynamic range of ±512 levels or 1 part in 1024. Expressed in decibels the maximum signal-to-noise ratio or "S/N" possible if the total dynamic range were used is approximately [8]:

$$S/N \simeq 20 \log [2(2^{10} - 1)]$$

$$\simeq 66 \text{ dB} . \qquad (6.3)$$

The fast Fourier transform subroutine used in this study (Sections 4.3 and 11.5) had a dynamic range in excess of 100 dB [17]. The anti-aliasing filters used specified a S/N of at least 85 dB. The modified FM tape recorder employed had at best about a 45 dB S/N and was thus the limiting link in the entire data analysis chain.

6.3 Data Qualification

"Stationarity" of the data had to be justified before any finite Fourier transform functions could be computed; otherwise, results would have been in serious error [6, 11, 17]. To be classified as "weakly" stationary, the mean value or "first moment" and the auto-correlation or "joint moment" of the data (Section 4.1) should be time invariant. That is to say the data points from any given sample record should produce similar values for the auto-correlation function and overall mean as the data contained in another sample record of the same signal. If there are trends present in the mean and auto-correlation, the data is "nonstationary."

"Strongly" stationary data are such that all possible moments and joint moments are time invariant. Since it is impossible to check all moments for trends, the establishment of weak stationarity usually justifies the assumption of strong stationarity.

The data used in this study was assumed to be stationary based on knowledge of the wide-band random nature of the phenomena. Also, repeated visual checks for trends in the digital sample records were

made throughout the data collecting process using a videl graphics terminal. Figures 6.1 - 6.4 illustrate respective time and spectrum plots for representative near-field and far-field dynamic pressure signals.

6.4 Weighting Function

Because the data involved were steady-state random noise, there was an abrupt truncation of values at the beginning and end of the time series sample records. These instantaneous changes of value from zero to nonzero are viewed as dirac delta functions by the finite Fourier transform. The resulting wide-band spectra associated with dirac delta functions (sometimes called "spike spectra") add to the valid data spectra, causing errors in both spectra amplitude and shape.

To reduce these errors, a time-series weighting function was employed. Typically this weighting function has a smooth shape with tapering endpoints which are made to coincide with the endpoints of the time series. The effect of multiplying the weighting function and time series is to gradually reduce the data values to zero as the endpoints are approached. Figure 6.5 shows the use of the Hanning ($\sin^2$) function which was employed for the computer programs used in this study. More detailed information on this and other weighting functions may be found in the literature [2, 6, 11, 17, 28, 32].

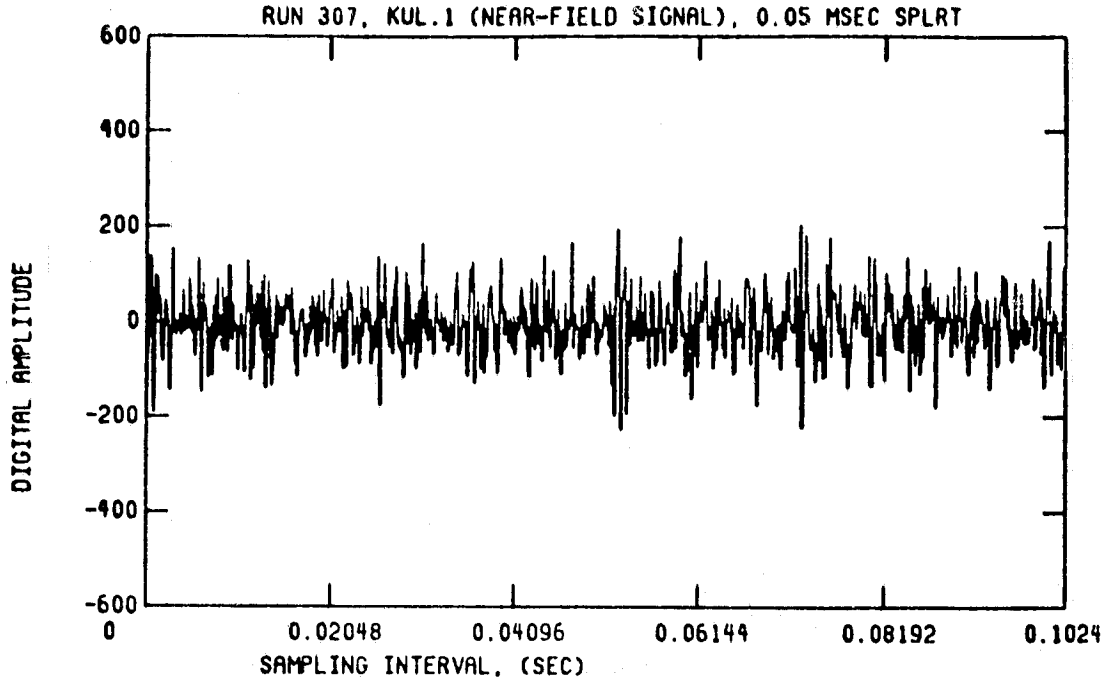

Figure 6.1 Single representative sample record of a near-field pressure signal from a TE Kulite

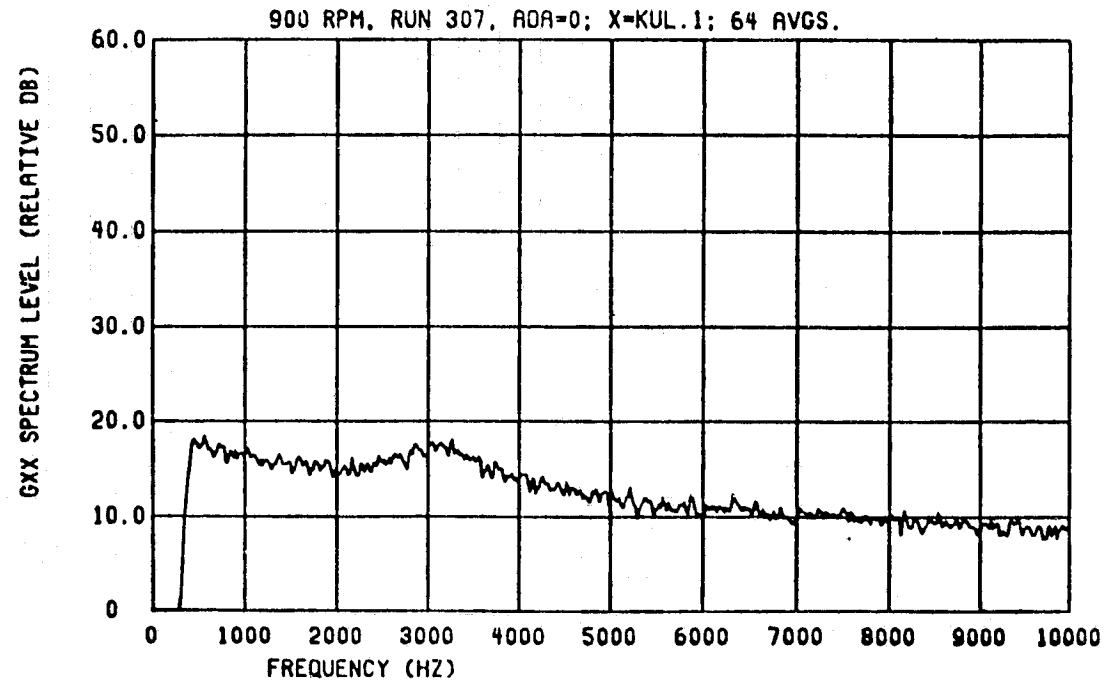

Figure 6.2 Representative auto-PSD of the near-field pressure signal of Figure 6.1 after 64 such sample records were zero-meaned, Hanned, Fourier transformed and averaged

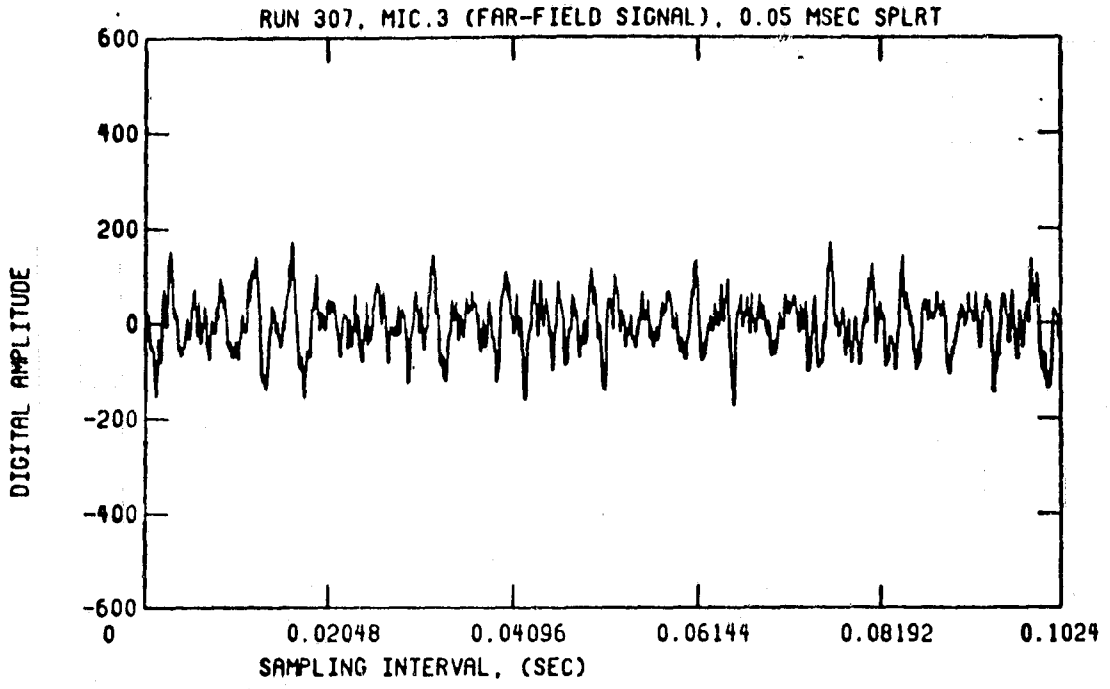

Figure 6.3 Single representative sample record of a far-field pressure signal from a B&K microphone

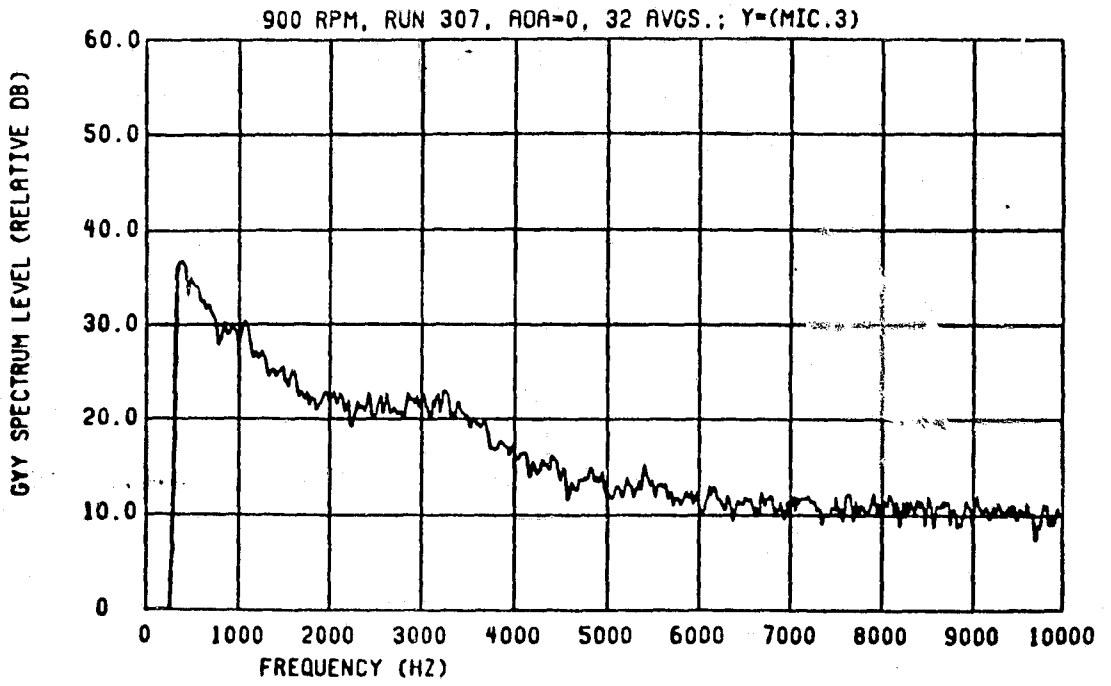

Figure 6.4 Representative auto-PSD of the far-field pressure signal of Figure 6.3 after 32 averages

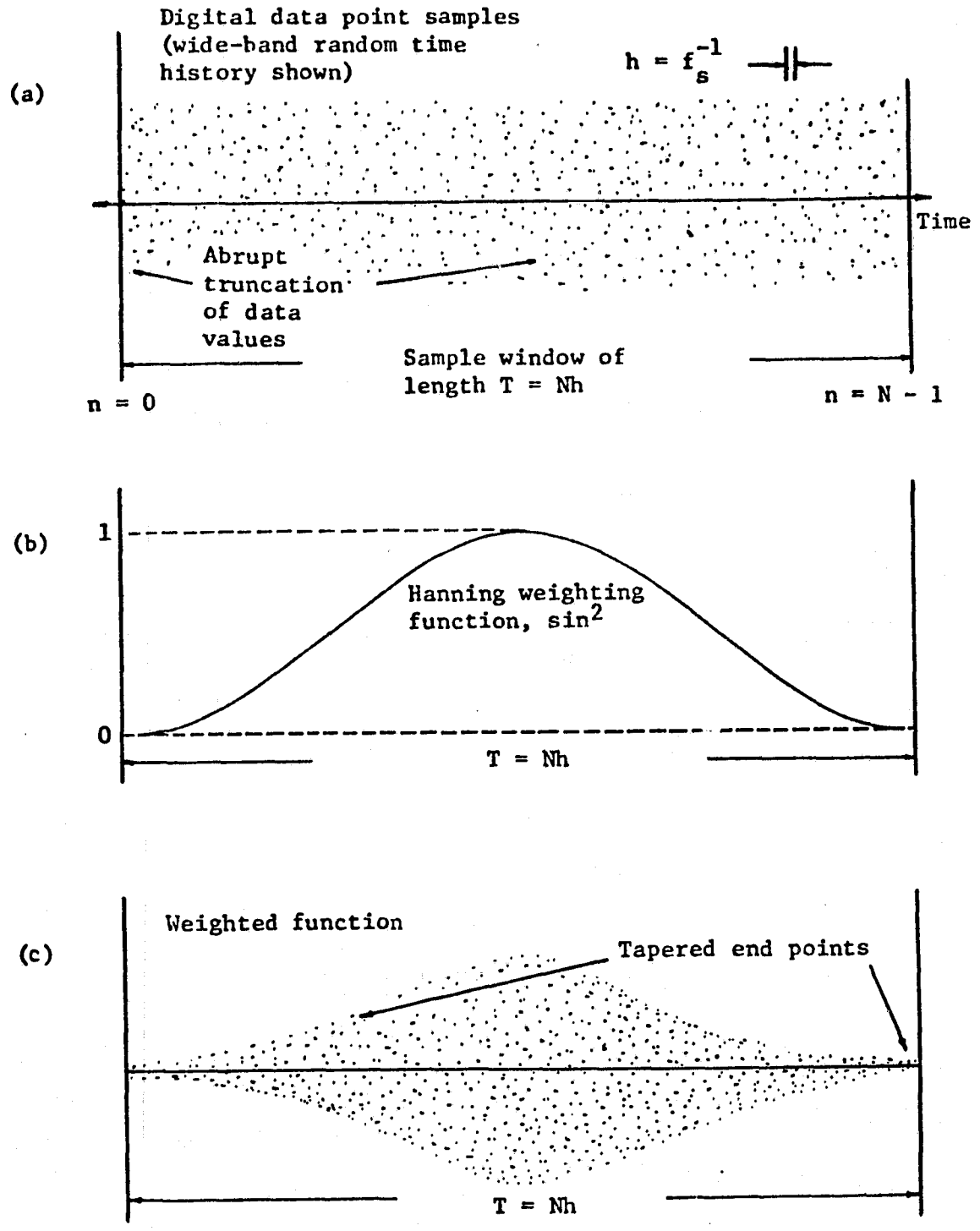

Figure 6.5 Sample record parameters and the effects of Hanning weighting

7. ERROR ANALYSIS

Statistical errors due to the use of discrete finite Fourier transform methods in signal analysis have been thoroughly reviewed and are well documented in the literature [2, 6, 28, 32]. Such errors result from the inability of a finite length time history of an event to exactly represent the statistical behavior of the event for all time. Thus, some knowledge of the extent of the error is necessary.

7.1 Random Errors in Spectral Density Functions

Spectrum ensemble averaging was used in this study to reduce the majority of statistical errors. The normalized standard (random) error as defined for the PSD functions is given in reference [6] as:

$$er = (B_e \; T_t)^{-\frac{1}{2}} \tag{7.1}$$

where: $B_e = W/T$, effective line BW, (7.2)

$T_t = T \times m$, total time period, (7.3)

m is the number of spectral ensemble averages, T is the time period of one sample record, and W is the factor relating the bandwidth of the time window weighting function employed to the bandwidth of a rectangular window. The use of the window weighting function is described in Section 6.4.

Substituting relationships (7.2) and (7.3) into Equation (7.1) yields:

$$er = (W \times m)^{-\frac{1}{2}} . \tag{7.4}$$

The error in percent is stated as 100(er). The error in dB is given by:

$$er_{dB} = 10 \log_{10} (1 \pm er) . \qquad (7.5)$$

For this study Hanning weighting was employed (W = 1.5). The number of averages taken was either m = 32 or m = 64. Substituting W = 1.5 and m = 32 into the above equations yields a worst case error of 14.4 percent or +0.59, - 0.68 dB which was marginally acceptable for the purposes of this study.

7.2 Bias Errors in Spectral Density Functions

Whereas the normalized standard error discussed above depends solely upon data acquisition and analysis parameters, the amount of "bias" error depends partially upon the nature of the data itself. Thus, it cannot be predicted before analysis.

The nature of the bias error in the PSD estimates is such that the "peakedness" of the function is reduced. Thus, sharp "peaks" in the true spectra are underestimated or reduced, and narrow "valleys" are overestimated or increased when the PSD estimate is made [6].

The broadbanded character of the trailing-edge noise phenomena reduced the bias errors to a minimum. Because the standard and bias errors are most severe for the PSD estimates on which no corrections were made [6], no attempts were made at correcting the errors in the transfer function phase as computed by the program COHERENC (Appendix 11.2).

7.3 Bias Errors in Coherence Functions

The coherence function contains another type of bias for which corrections were made. By the nature of its definition the coherence function (Equation 4.22) always has a value of unity when only one spectrum ensemble average is taken. Increasing the number of averages reduces this positive bias and yields a better estimate. The bias corrected coherence is computed from [32]:

$$\hat{\gamma}^2 = \hat{\gamma}_o^2 - \frac{(1 - \hat{\gamma}_o^2)}{2Wm} \tag{7.6}$$

where $\hat{\gamma}_o^2$ is the averaged uncorrected estimate for the coherence and W and m are as defined previously.

The degree to which the corrected value of coherence at any one frequency can be relied upon may be stated in terms of a confidence interval. For a chosen percentage of reliability this interval indicates the upper and lower limits within which the coherence must fall.

7.4 Confidence Interval for Coherence Functions

The 95 percent confidence interval for the bias-corrected coherence estimate is computed by using a method developed by Benignus as outlined in reference [32]:

$$\hat{\gamma}^2_{upper} \leq \tanh [z - b + s\,(za)] \tag{7.7}$$

$$\hat{\gamma}^2_{lower} \geq \tanh [z - b - s\,(za)] \tag{7.8}$$

where: $z = 0.5\ \ell n\ [(1 + \hat{\gamma}) / (1 - \hat{\gamma})]$,

$s = b^{\frac{1}{2}}[1 - 0.004^{(1.6\gamma^2 + 0.22)}]$,

$$b = p / [2Wm - 3p + 1],$$

$$za = 1.96,$$

p is the number of coherence function inputs, za is the one-sided 100 α percentage point of the normal distribution of the data and W and m are as defined previously. For 100 α = (100 - 95) = 5 percent, $\alpha/2$ = 0.025 and thus za = 1.96 (as found in statistics tables).

A plot of the 95 percent confidence limits as a function of the number of spectral averages and the original coherence estimate with W = 1.0 is given in Figure 7.1 [17].

7.5 Errors Due to Time Delay in Spectral Quantities

An additional error that affects all spectral quantities is the negative bias caused by signal path time delays. These delays which occur, for example, between separated transducers are best compensated for by time alignment of the data sample records prior to processing.

Where time alignment is not possible, references [4, 23, 36] give detailed information on determining the amount of the error. Basically, the PSD and coherence functions are in error by an amount:

$$\frac{\hat{G}(f)}{G(f)} \approx \frac{\hat{\gamma}^2_{xy}(f)}{\gamma^2_{xy}(f)} \approx \left(1 - \frac{\tau}{T}\right)^2 \tag{7.9}$$

where $\hat{G}(f)$ and $\hat{\gamma}^2_{xy}$ are the computed averaged estimators with no time-delay compensation, G(f) and γ^2_{xy} are the "true" values, T is the time length of one sample record, and τ is the time delay. Although these simple equations are useful for obtaining approximate amplitude corrected values of $\hat{G}(f)$ and $\hat{\gamma}^2_{xy}$, they cannot compensate for the

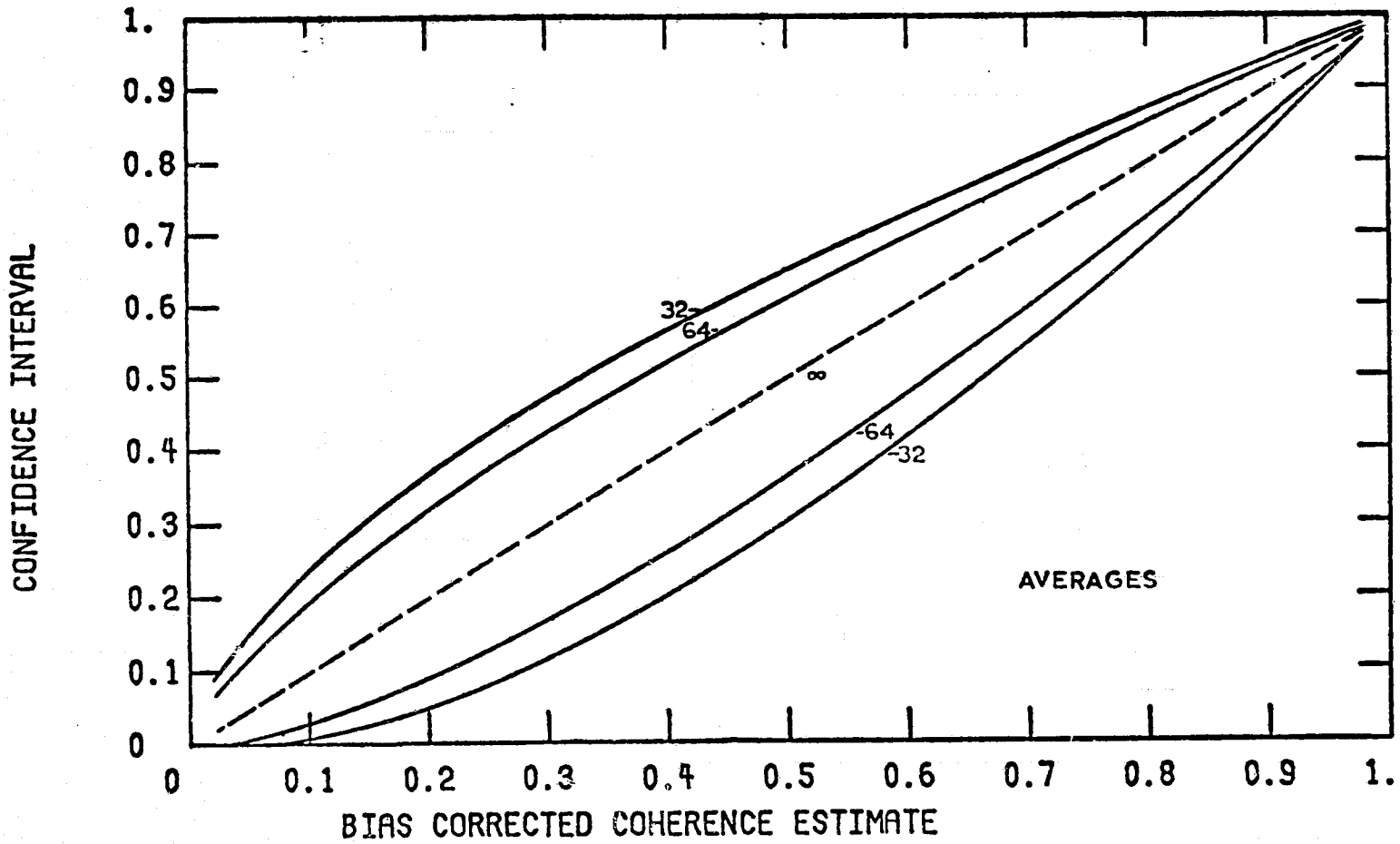

Figure 7.1 Graph to find the confidence interval for the bias-corrected coherence for m = 32 or 64 averages [17]

increase in bias and standard (random) errors discussed previously. For determining the total extent of these errors, the reader should consult the above-mentioned literature [4, 23, 36].

Another source of time-delay error arose from the refraction of the acoustic wave as it traveled through the shear layer of the open jet wind tunnel to the far-field microphone. Cross-correlation and cross-spectral measurements between a transducer at the trailing edge of the airfoil and the far-field microphone were thus potentially subject to this additional time delay (Figure 7.2, path A).

A study of this effect and the derivation of equations for obtaining correction factors has been performed by Amiet [1]. The freestream Mach number of the flow in this study did not exceed 0.20 (225 ft/sec), and the far-field measurement microphones were on a line perpendicular with the trailing edge and the air flow. Based on conclusions reached in Amiet's paper, it was determined that the acoustic pressure amplitude and phase corrections were not warranted. The amplitude corrections were less than 0.5 dB which is less than the normalized standard error.

As an example, the worst case time delay error (not including refraction effects) is computed for 12-foot distant microphone M.3 (Figure 7.2, path B).

$$\tau = \frac{d}{c} = \frac{12.0}{1125} = 10.7 \text{ msec}, \tag{7.10}$$

$$T = \frac{N}{f_s} = \frac{1024}{20{,}000} = 51.2 \text{ msec}, \tag{7.11}$$

$$(1 - \frac{\tau}{T})^2 = (1 - 10.7/51.2)^2 = 0.628 \tag{7.12}$$

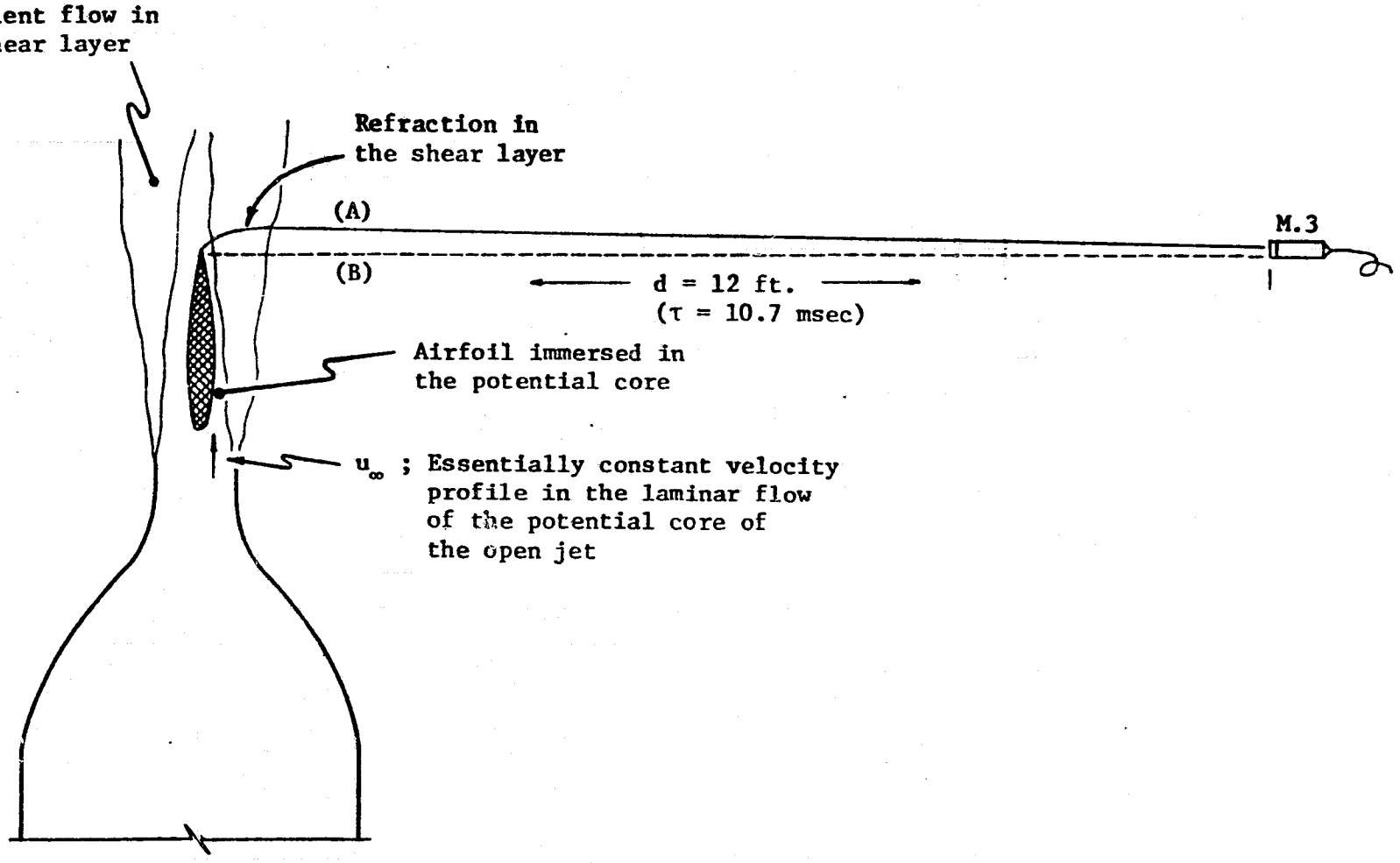

Figure 7.2 Sources of time delay errors: transducer spacing and shear-layer refraction

or expressed in decibel form:

$$10 \log_{10} (0.628) = -2.03 \text{ dB} \qquad (7.13)$$

where d is the spacing, c the speed of sound, f_s the sampling frequency, N the number of sample points per time record, and T and τ are as defined previously. The quotient τ/T indicates that the two sample records are effectively offset in time by 20.8 percent.

Time alignment by data point shifting was not employed because of the limited capabilities of the North Carolina State University analysis facility. In order to maintain the maximum frequency resolution possible out of the available fixed sample record length of 1024 points per channel, no points could be sacrificed. Shifting the data would negate the negative bias errors due to time delay, but at the expense of an accompanying increase of standard (random) errors due to the lesser number of data points to be Fourier transformed. Also, comparisons between spectral density curves would become difficult if the frequency resolution were different among curves.

8. EXPERIMENTAL RESULTS

Series I data brought back from the NASA test facility for analysis at North Carolina State University was only sufficient for a preliminary evaluation of the trailing edge noise phenomena. Subsequent analysis of data from Series II tests should yield substantially more detailed analysis results. Thus, the information presented herein primarily represents the methodology developed and the characteristics of the TE noise phenomena which were observed.

8.1 Microphone Calibration

Calibrations for the one-half inch microphones were performed using a Brüel and Kjaer type 4220 Pistonphone producing 124.0 ± 0.2 dB SPL.

Calibrations for the Kulites were performed after they were flush-mounted in the airfoil. A General Radio model 1562-A Sound Level Calibrator equipped with a seal was verified as producing 112.9 dB SPL when pressed against a flat surface. It was then pressed over each Kulite in turn to yield an in-place "flush" calibration.

All results in this thesis, however, are presented in "relative dB" meaning that the dB scale for each plot is not calibrated against any reference standard. Thus, pressure levels between plots may not be compared, but pressure level comparisons on any one spectrum plot are permissible.

8.2 Validity of Far-Field Microphone Measurements

Before analysis took place, a check was made to insure that the closest "far-field" microphones were indeed in the acoustic far-field

of the radiated TE noise. An assumption was made (which was later justified) that a line source of independent dipoles radiating wide-banded noise would have a SPL falloff with distance similar to that for a spherical wave source. Therefore a check could be made to see if Ka >>1, say 10 as a lower limit. For the 4-foot distant microphones, then a = 4 and:

$$Ka >> 1, = 10 \quad \text{say,} \tag{8.1}$$

$$K = \frac{10}{a} = \frac{10}{4} = 2.5 \text{ ft}^{-1}, \quad \text{the wavelength constant,}$$

$$f = \frac{Kc}{2\pi} = \frac{2.5(1125)}{6.28} \simeq 450 \text{ Hz.} \tag{8.2}$$

Thus, due to the high-pass filtering at 400 Hz as set on the anti-aliasing filters, all observed spectral phenomena were assumed to be valid far-field measurements.

The nearness of the 4-foot microphones to the jet did not appear to produce auto-spectra that were significantly different from those of the 12-foot distant microphone M.3. However, the noise floor of the FM tape recorder was reached in some instances, and so deviations between plots of 3-4 dB in frequencies above about 5 kHz were occasionally noticed in some auto-spectra.

8.3 Initial Checks Using a Cylindrical Rod

As an initial check on the test setup, the airfoil was removed and an 18-inch long steel rod of 0.375-inch diameter mounted in its place at the trailing edge position (Figure 8.1). The rod provided a dipole line source whose known radiation characteristics could be used to verify correct operation of the analysis system.

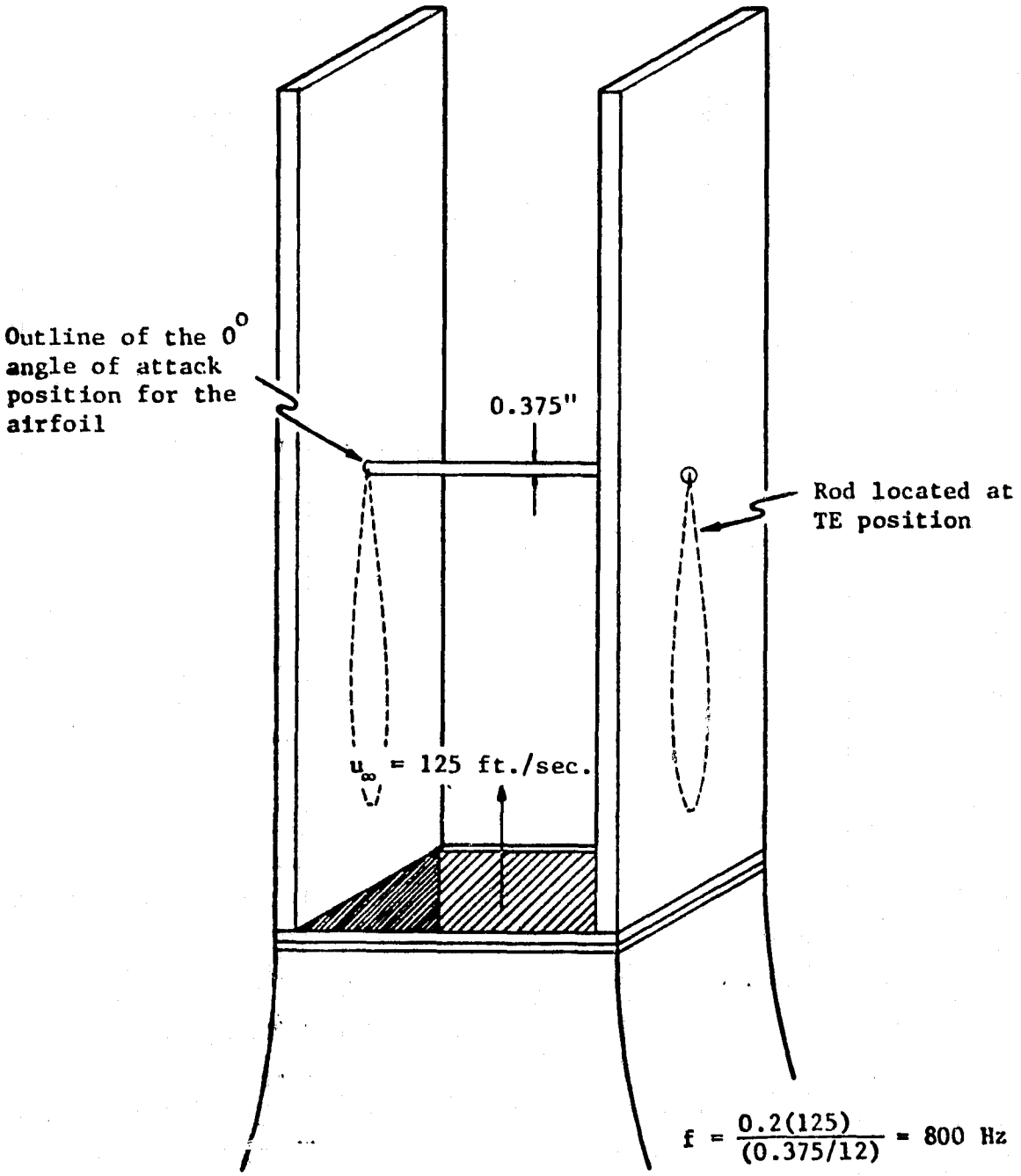

Figure 8.1 Initial check run using a rod mounted at the TE position to produce a known sound emission

For a flow rate of 125 feet per second (500 rpm), the peak frequency of the alternate vortex shedding for the rod was calculated using [25]:

$$f = \frac{Su_\infty}{d} \tag{8.3}$$

where S is the subsonic Strouhal number for a cylinder, u_∞ is the freestream velocity, and d is the rod diameter. Using the above values and a Strouhal number of 0.2, the peak frequency was calculated to be 800 Hz.

Using the two 4-foot distant microphones, M.2 and M.5, the actual auto-spectra, cross-spectrum, phase and coherence were computed by the program COHERENC (Appendix 11.2) (Figures 8.2 - 8.6). The actual peak of 780 Hz was in good agreement with the above predicted 800 Hz. The 180° dipole nature of the alternate vortex shedding is evident in the phase plot. The cross-spectrum and coherence also give evidence of the high ratio of fixed-phase common signal to uncorrelated signal present in such a phenomena.

8.4 Test Conditions

A generalized airfoil test configuration was used during the initial phases of analysis. No modifications such as the trailing edge extensions used in Series II tests were made to the basic airfoil as shown in Figure 2.2.

The airfoil was tested at angles of attack $\alpha = 0^\circ, \pm 5^\circ, \pm 10^\circ$; but for any given airflow velocity no differences could be detected in

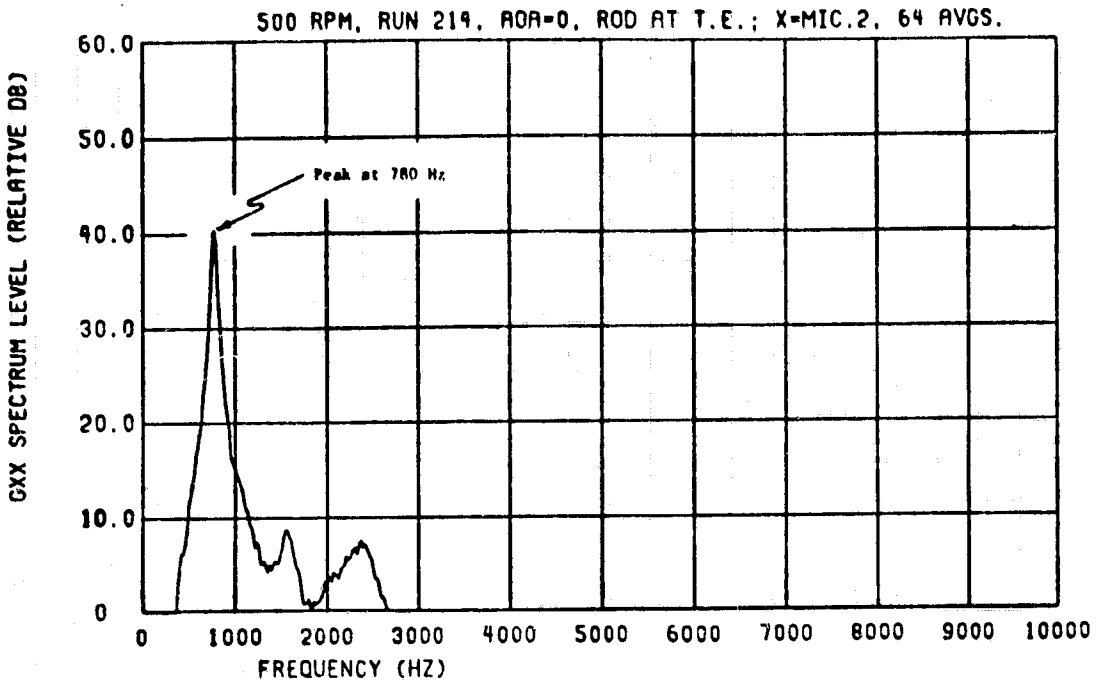

Figure 8.2 Auto-PSD of a tone generated by the 0.375 inch diameter rod mounted at the TE position as detected by M.2

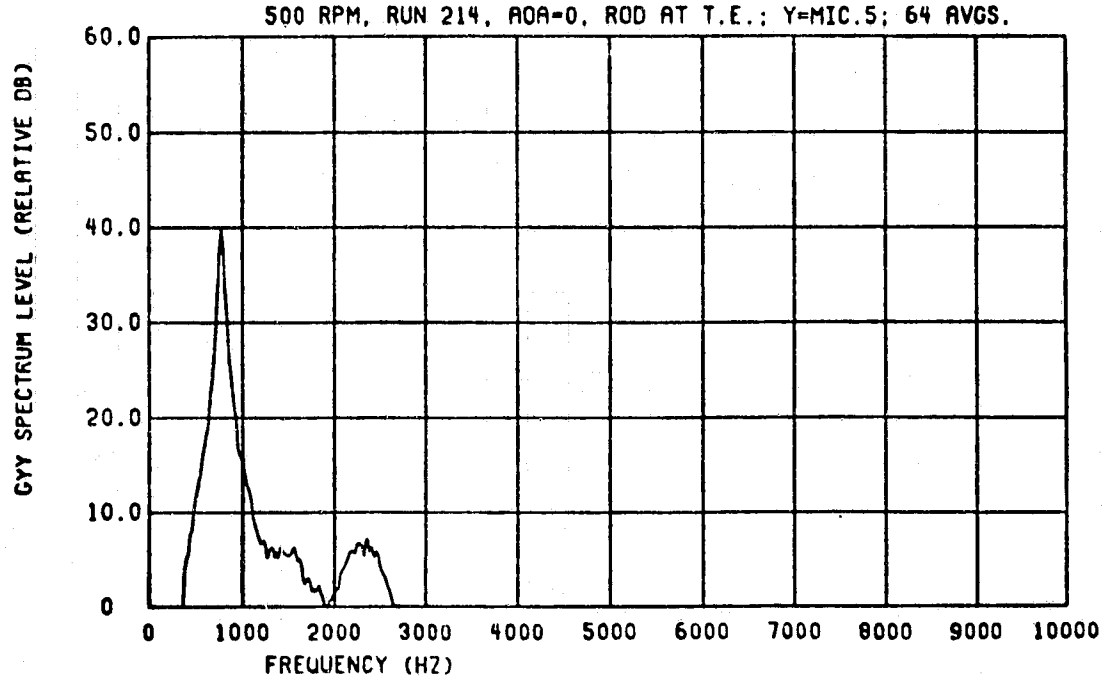

Figure 8.3 Auto-PSD of a tone generated by the 0.375 inch diameter rod mounted at the TE position as detected by M.5

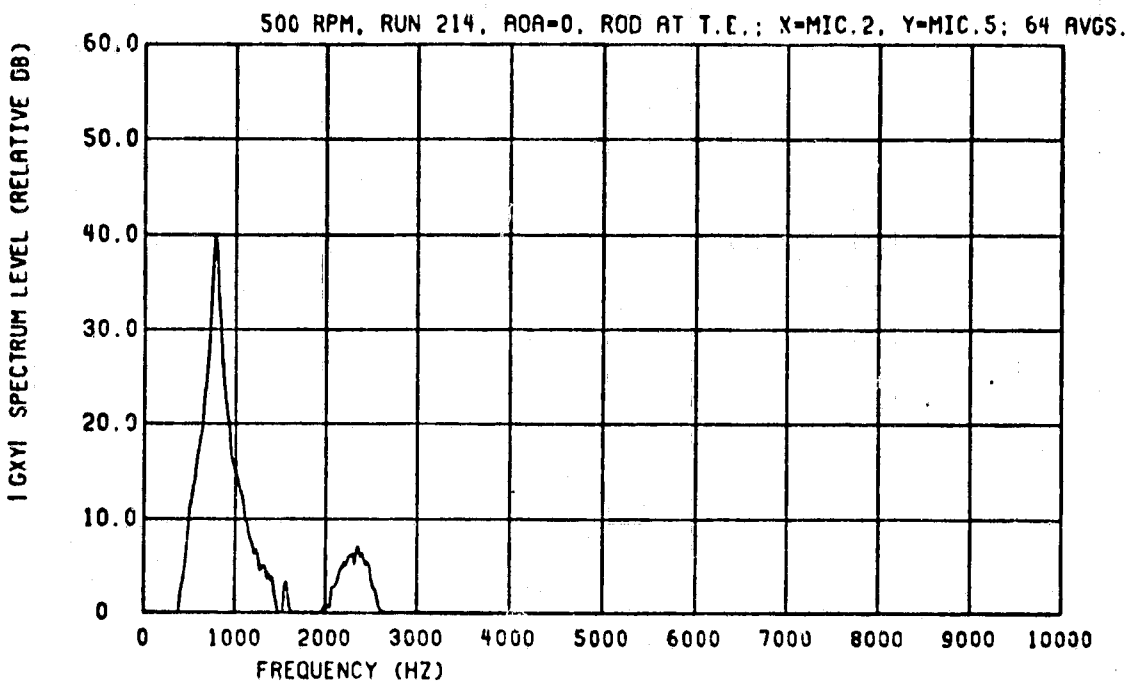

Figure 8.4 Cross-PSD of a tone generated by the 0.375 inch diameter rod mounted at the TE position as detected by M.2 and M.5

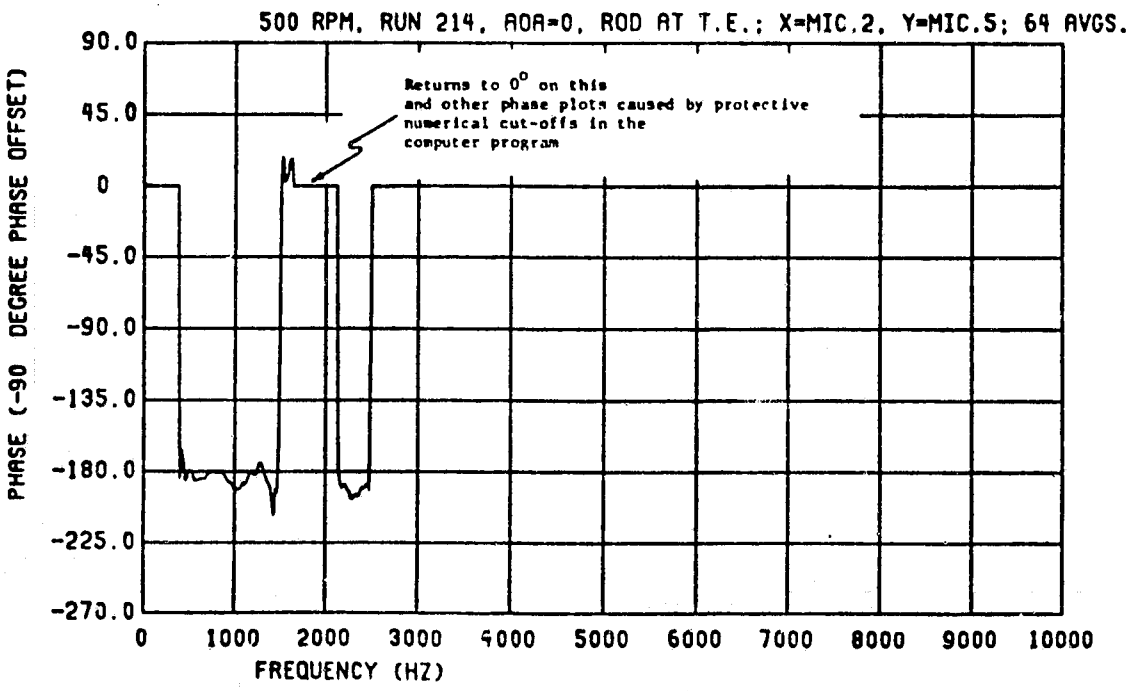

Figure 8.5 Phase between dynamic pressure field signals originating at M.2 and M.5 for the 0.375 inch diameter rod mounted at the TE position

the observable phenomena. Thus, all results reported in this section deal with the airfoil mounted at $\alpha = 0^{o}$.

Data were recorded for freestream velocities ranging from 52 to 225 feet per second. However, a single data run, Run 307, was the single most widely analyzed collection of data. It consisted of recordings of the phenomena at the highest flow rate available (225 feet per second, or 900 rpm) with the airfoil in the general test configuration. It was thought that at this freestream velocity the noise phenomena, if it existed, would be most strongly excited and therefore easily analyzed. It was assumed that the blunt leading edge radiated no noise.

8.5 Auto-Power Spectral Density Measurements

Figure 8.7 depicts the auto-spectrum of far-field microphone M.3. Immediately noticeable is the 4-5 dB hump in the 2.0 - 4.0 kHz band of frequencies. This auto-spectrum is characteristic of all far-field microphone positions for the airfoil general configuration.

The wide-banded background noise floor or BNF (the downward sloping curve without the inclusion of the hump) is due to the aerodynamic noise of the open jet and not the anechoic facility itself. Up to a frequency of about 5.0 - 6.0 kHz, the pressure level of the BNF can be predicted for the 225 foot-per-second freestream velocity by:

$$p(f) = k(f)^{-1.125} \tag{8.4}$$

where k is a constant particular to each plot. Good agreement was found among the auto-spectra of all three far-field microphones (M.2,

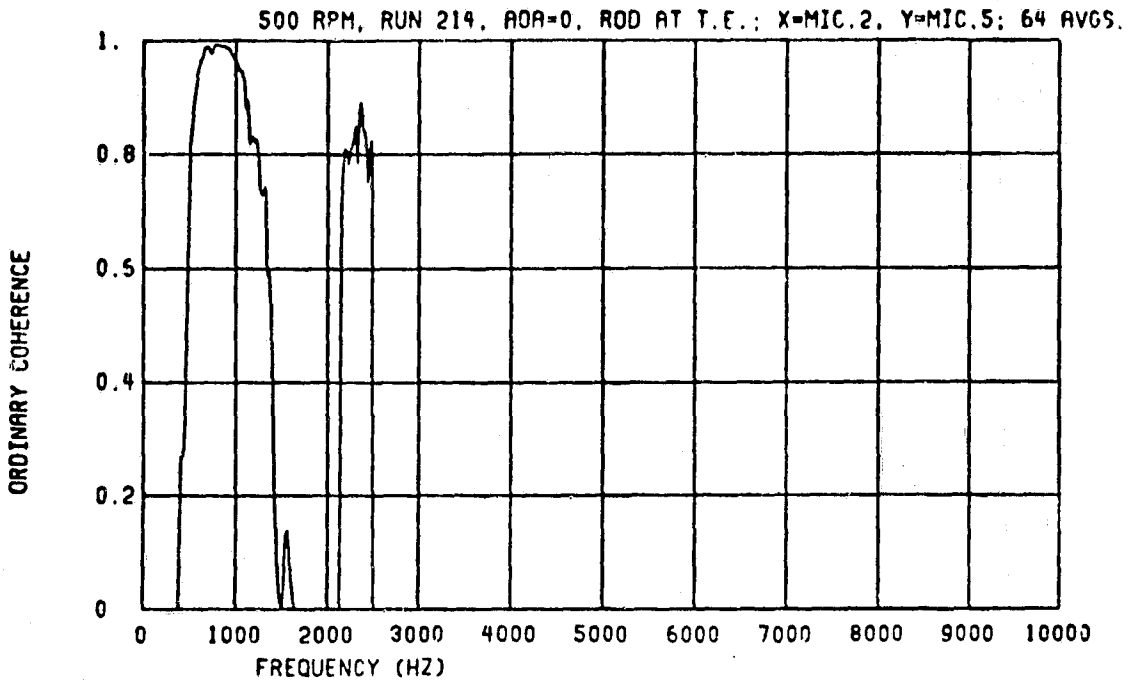

Figure 8.6 Coherence between dynamic pressure field signals originating at M.2 and M.5 for the 0.375 inch diameter rod mounted at the TE position

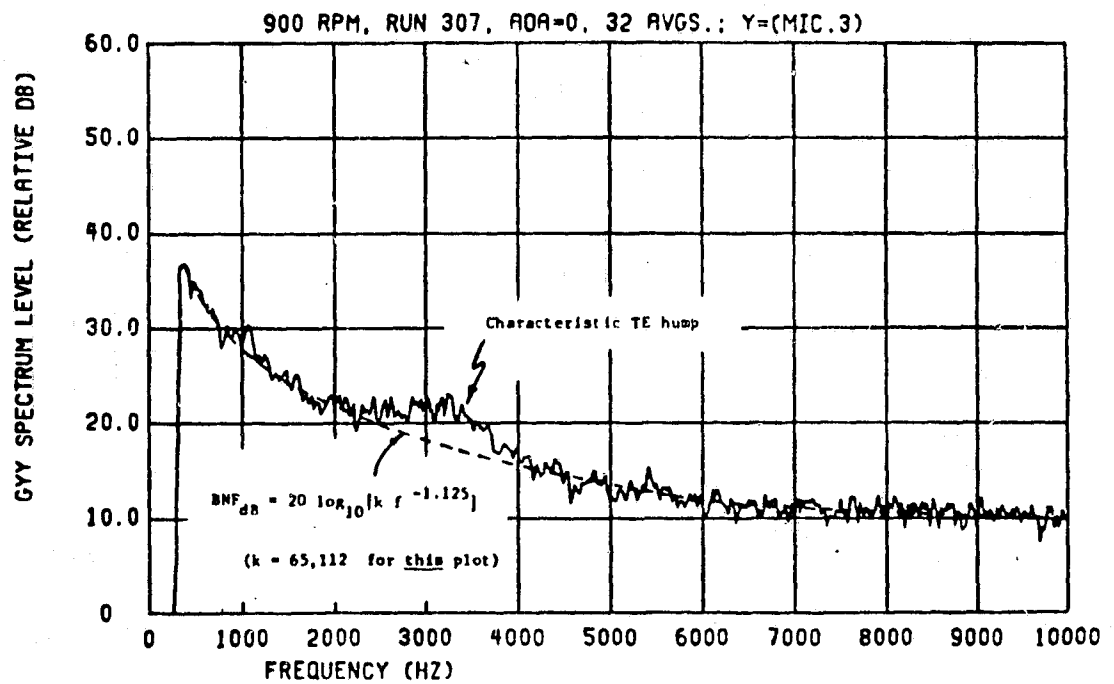

Figure 8.7 Auto-PSD of far-field dynamic pressure signal from 12-foot distant microphone M.3; also representative of 4-foot distant microphones M.2 and M.5

M.3, M.5). The flattening out of the auto-spectral curves above 5.0 - 6.0 kHz is possibly due to the TE phenomena, the noise floor of the FM recorder, or both.

The auto-spectra of the TE Kulites (K.1, K.2, K.5) also display the characteristic "hump" in the 2.0 - 4.0 kHz band of frequencies (Figure 8.8).

The auto-spectrum of the upstream Kulite (K.3) has the same flat BNF as the TE Kulites but without the hump (Figure 8.9).

A check run was made to insure that the characteristic hump observed in all far-field and TE transducer positions was due solely because of the airfoil and not because of the sideplates or nozzle. The nozzle and sideplate assembly without airfoil were tested at the same freestream velocity of 225 feet per second as the standard configuration. The far-field auto-spectra appear the same as Figure 8.7 with the same level of BNF except for the lack of a hump.

Another check was made with the airfoil held in place over the nozzle but without the sideplates. The far-field auto-PSD is virtually unchanged from the standard configuration, whereas the near-field auto-PSD of the TE Kulite shows a slightly more pronounced hump (Figures 8.10 and 8.11).

8.6 Cross-Spectral Function Measurements

To clarify the nature of the hump the coherence, cross-PSD, and averaged phase were computed for the symmetrically opposing equidistant far-field microphones M.2 and M.5. The coherence indicates a strong relationship between the pressure fields which existed at the microphones in the range of hump frequencies (Figure 8.12). When

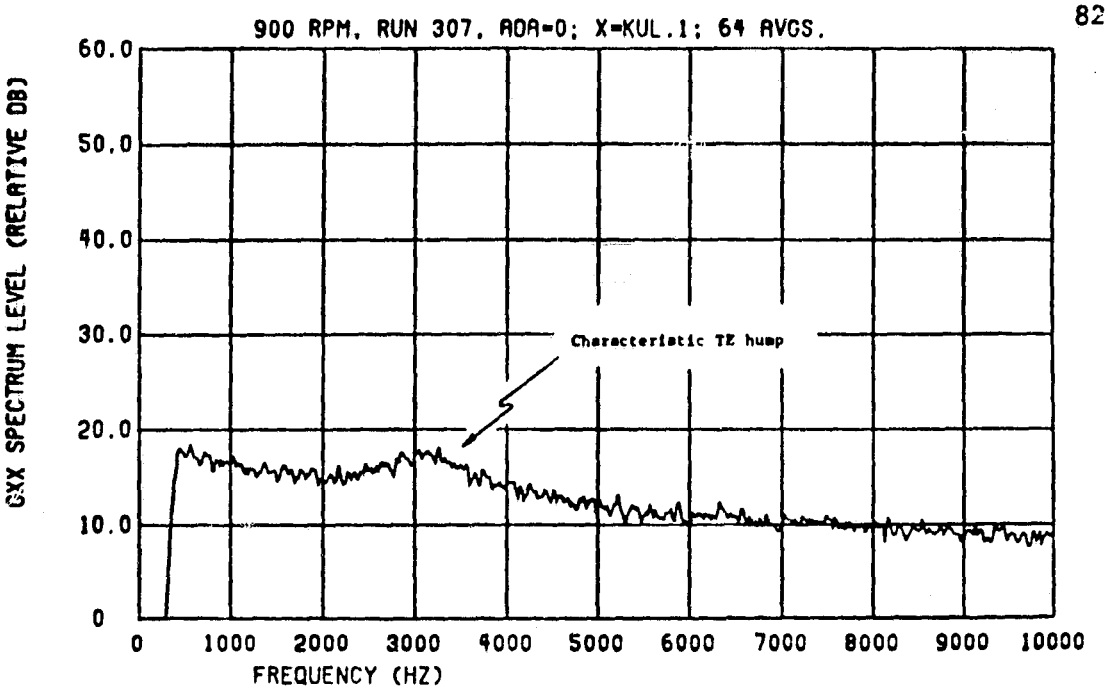

Figure 8.8 Auto-PSD of near-field dynamic pressure signal from TE Kulite K.1; also representative of signals from TE Kulites K.2 and K.5

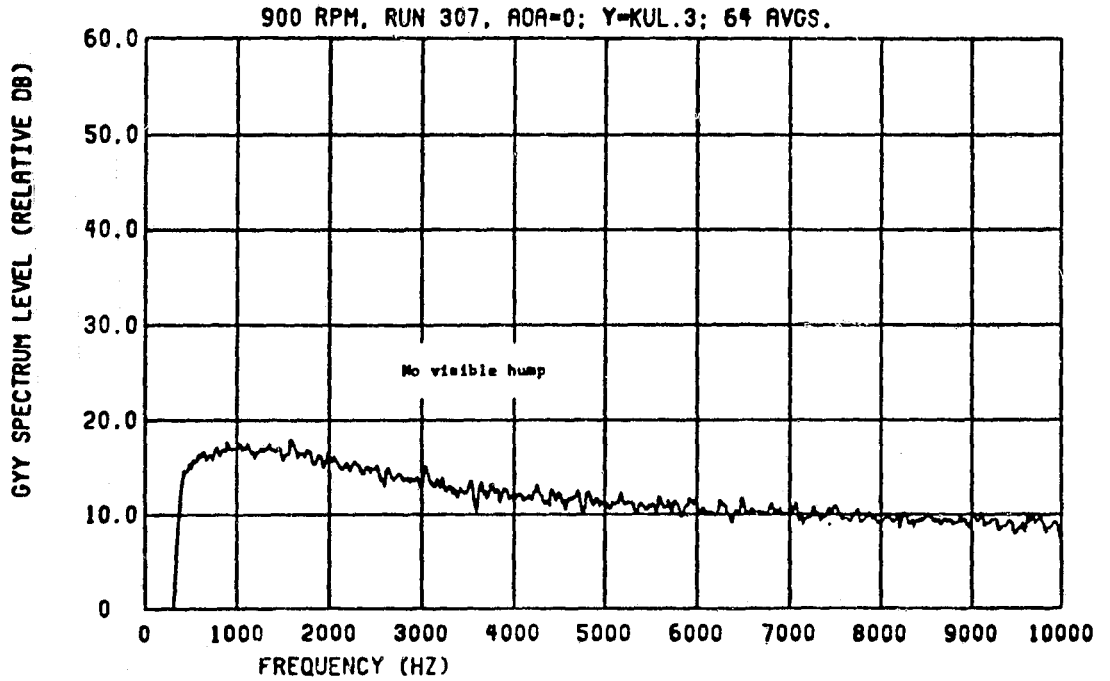

Figure 8.9 Auto-PSD of near-field dynamic pressure signal from upstream Kulite K.3

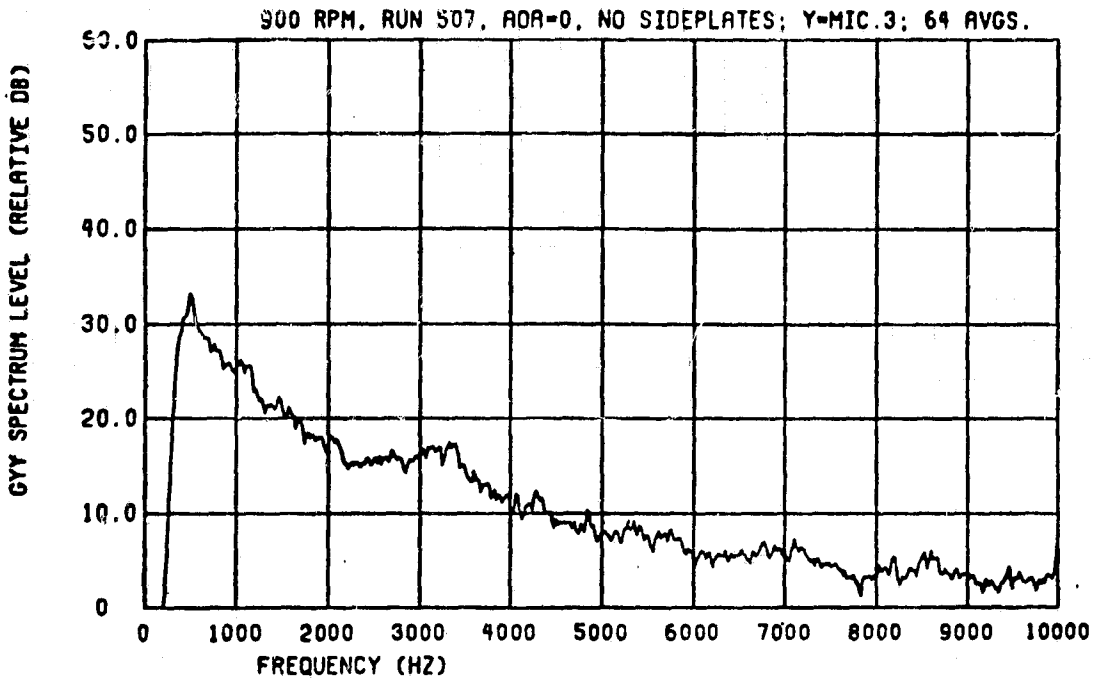

Figure 8.10 Auto-PSD of signal from M.3; no sideplates

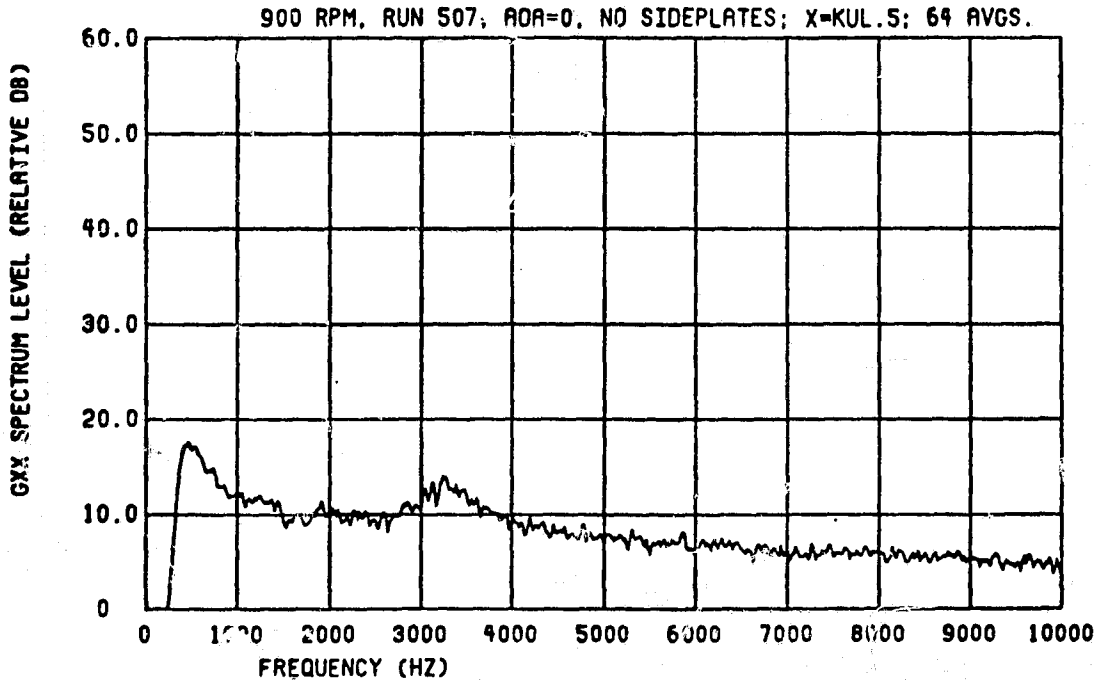

Figure 8.11 Auto-PSD of signal from TE K.5; no sideplates

C-2

coupled with the knowledge that there is no visible hump in the far-field auto-PSD spectra when the airfoil was not present nor in the upstream Kulite K.5 signal when the airfoil was present, this leads to the conclusion that the phenomena responsible must be at or near the TE.

The coherence also indicates a smaller secondary emission which extends from about 0.8 to 2.2 kHz. Both emissions average 180 degrees out-of-phase which indicates that the TE noise phenomena is "dipole-like" (Figure 8.13).

The two humps are clearly visible in the cross-PSD plot of Figure 8.14. Interesting to note are the values of the slopes on the upper frequency side of each hump. These slopes are frequency related to the pressure as was the far-field BNF and may be found by generalizing Equation (6.4):

$$p(f) = k(f)^{\beta} \tag{8.5}$$

where k is a constant particular to each test-run plot and β is the power constant or slope of the 20 log (p) curve. Values of -1.5 for the lower hump and -3.0 for the upper hump were obtained. This results in a 2:1 slope ratio for the respective upper and lower humps.

The coherence and cross-PSD curves for symmetrically opposing TE Kulites K.1 and K.5 also show signs of a double-humped phenomena (Figures 8.15 and 8.16). However, the frequency range of the lower hump has shifted downward and the phase plot, Figure 8.17, shows that the lower hump is, on the average, comprised of in-phase components, contrary to the far-field results. These may indicate a totally

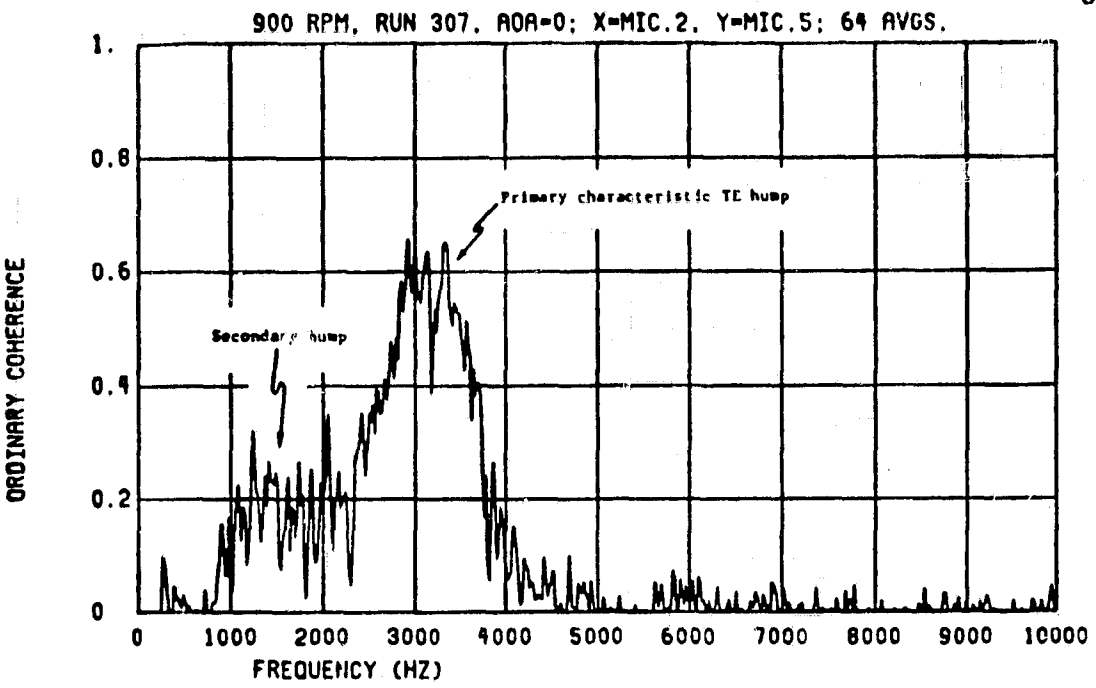

Figure 8.12 Coherence between signals from symmetrically opposing M.2 and M.5

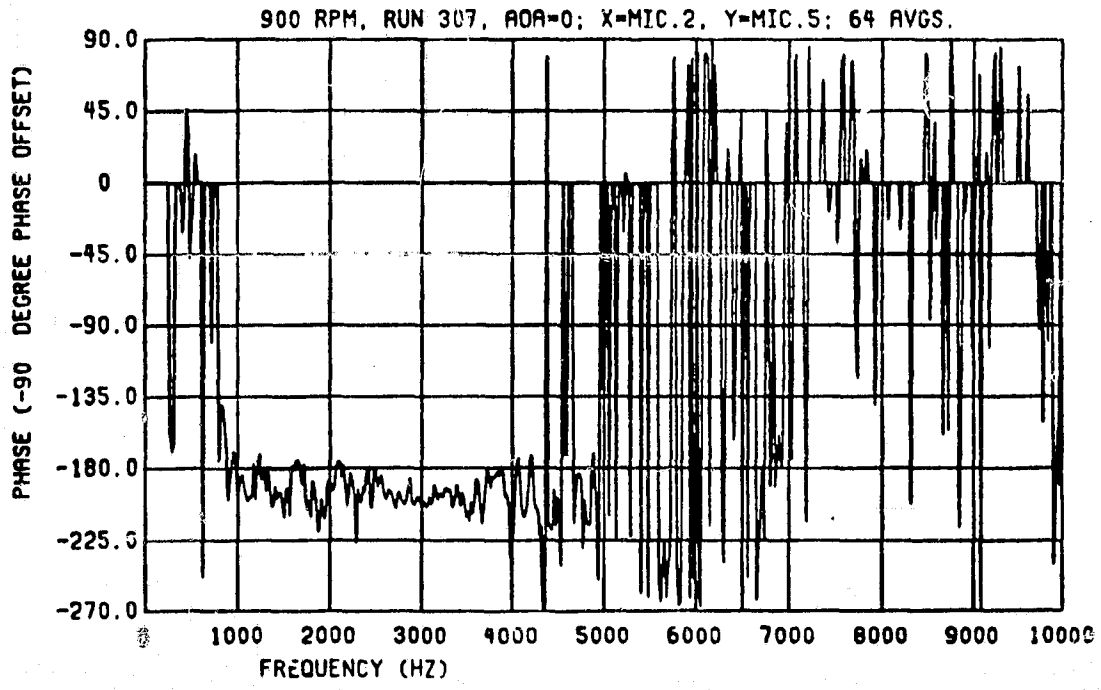

Figure 8.13 Averaged phase between signals from symmetrically opposing M.2 and M.5

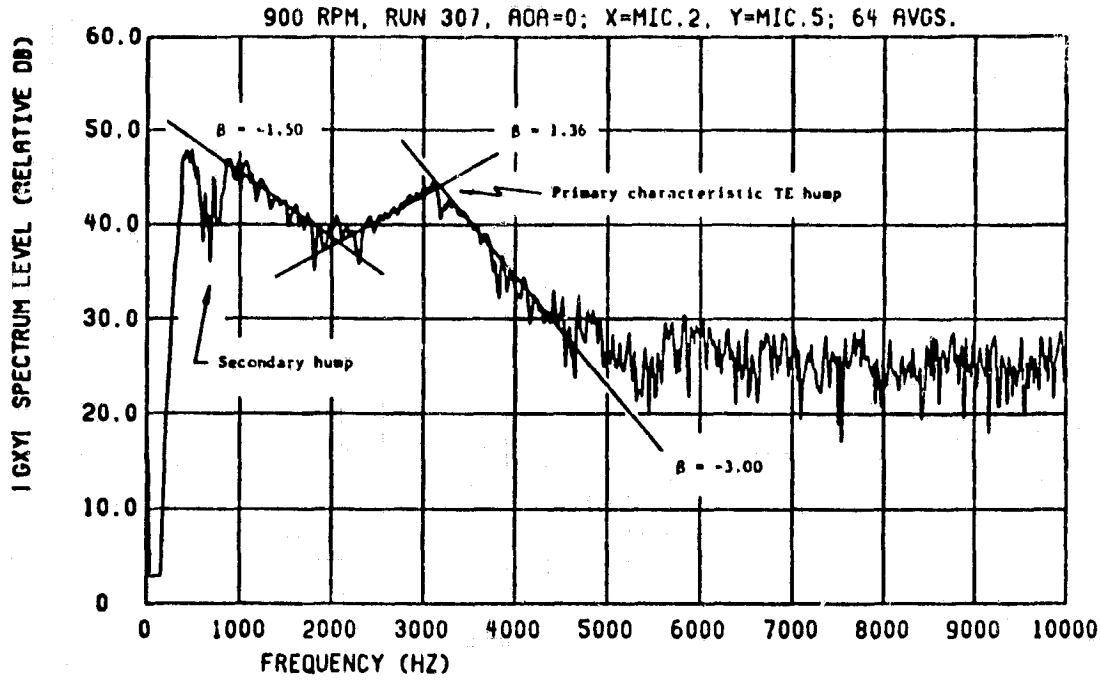

Figure 8.14 Cross-PSD between signals from symmetrically opposing M.2 and M.5

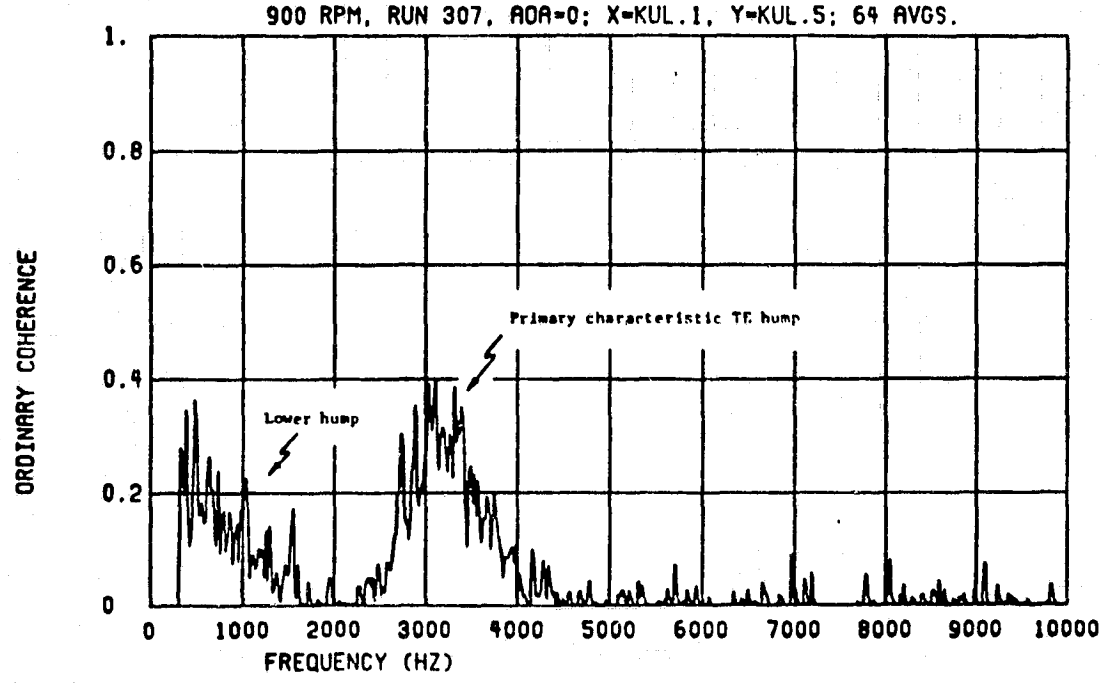

Figure 8.15 Coherence between signals from symmetrically opposing TE Kulites, K.1 and K.5

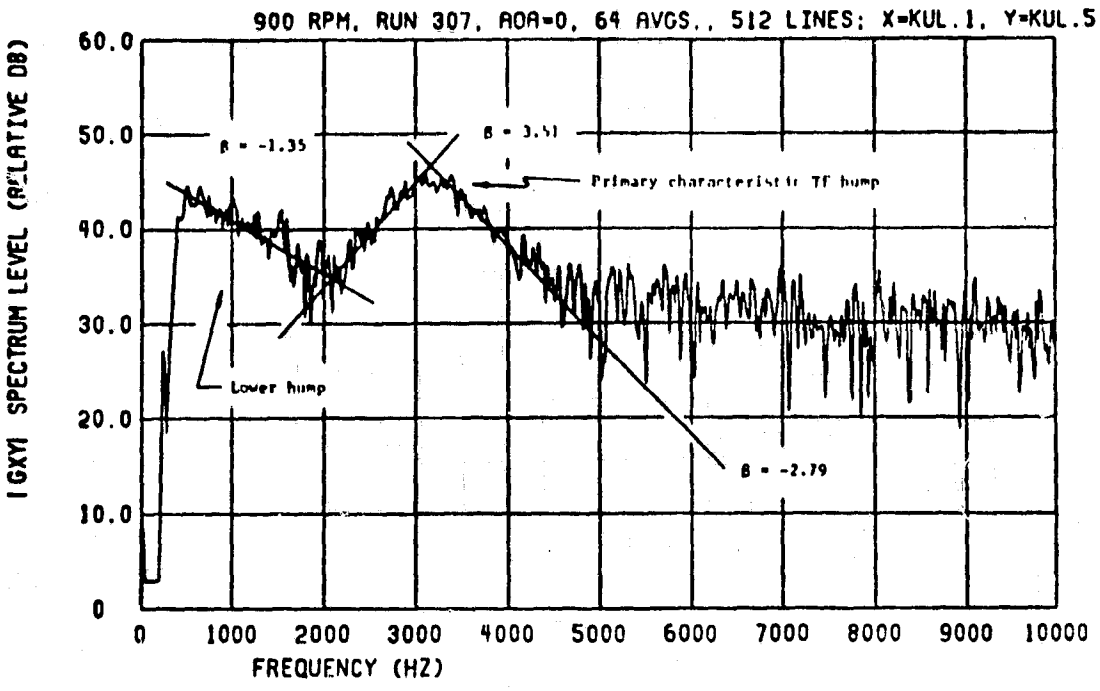

Figure 8.16 Cross-PSD between signals from symmetrically opposing TE Kulites, K.1 and K.5

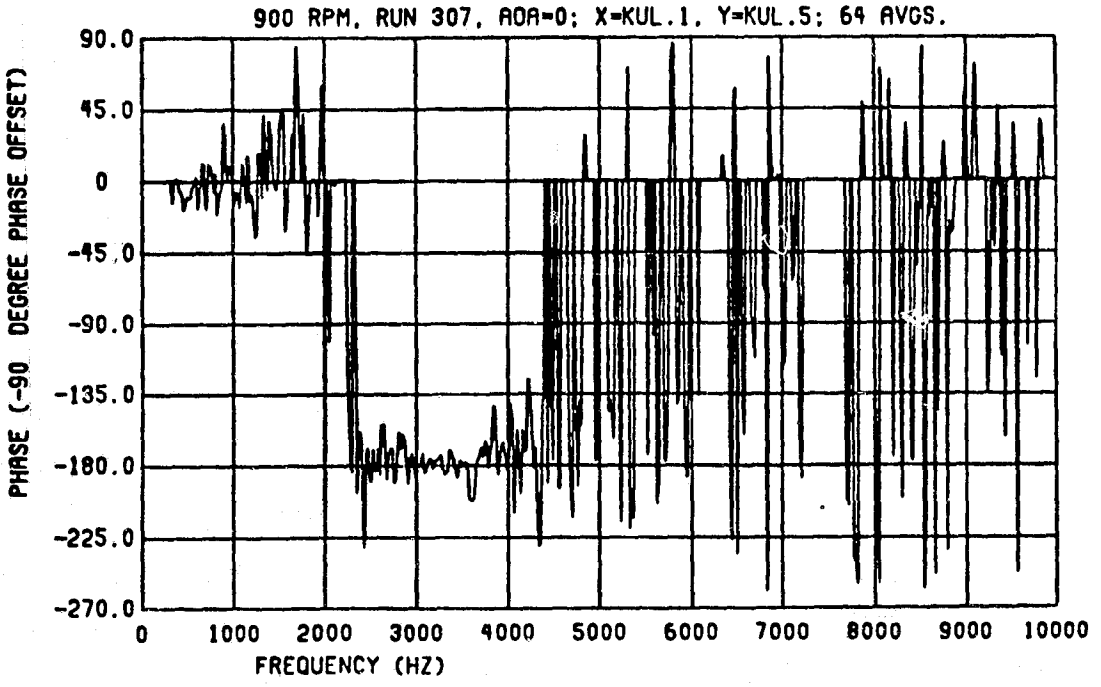

Figure 8.17 Averaged phase between signals from symmetrically opposing TE Kulites, K.1 and K.5

different type of mechanism although the fairly low coherence reveals that even in the near-field close to the TE, the lower hump mechanism on the upper surface is not very strongly related to any that may exist on the lower surface.

Again using Equation (6.5) to find the slopes β of the upper and lower frequency humps, it is learned that there is a 2:1 slope ratio for the respective upper and lower humps (Figure 8.16).

In both cases of symmetric transducer pairs, the averaged phase of the pressure-field components is random in frequencies above the characteristic primary (upper frequency) hump.

A 2.0 - 4.0 kHz cross-correlogram of the opposing TE Kulites K.1 and K.5 as computed by the program CIRCXCOR (Appendix 11.4) also exhibits the out-of-phase structure of the pressure field at the TE (Figure 8.18).

Indications of a strong relationship between the pressure fluctuations near the TE (K.1) and at a position 0.275 inches upstream (K.3) are given by the coherence in Figure 8.19. The averaged phase, Figure 8.20, exhibits the characteristics of a pure time delay. This distance-time information was used to obtain the mean convection velocity u_c of the turbulent BL air flow by employing the equation:

$$u_c = \frac{360d}{\beta} \tag{8.6}$$

where d is the transducer separation distance in feet and β is the slope of the phase in degrees/Hz. Taking $\beta = 0.0678^{o}$/Hz and d = (0.275/12) feet yielded a convection speed of 122 feet per second for u_∞ = 225 feet per second.

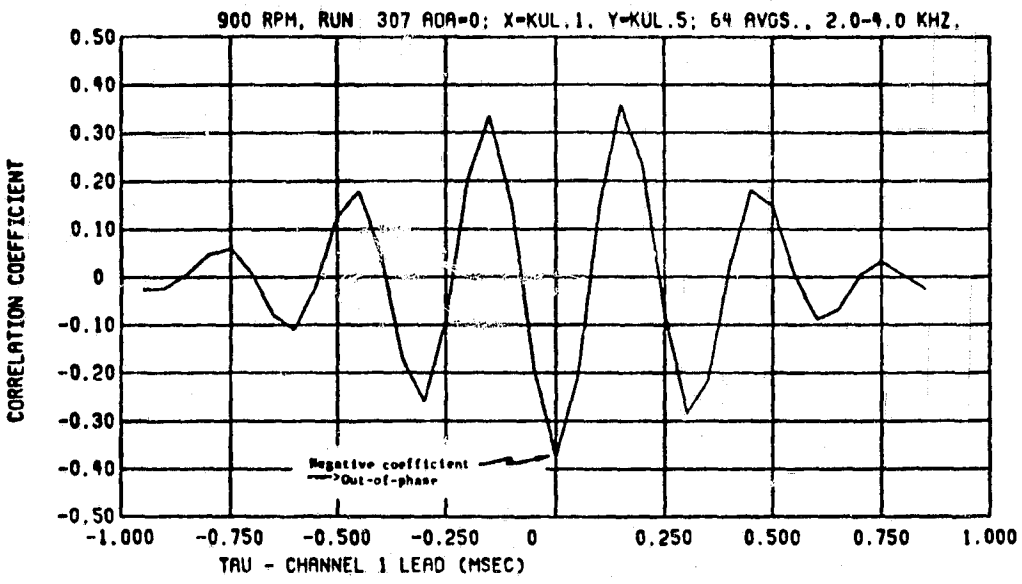

Figure 8.18 Cross-correlogram of symmetrically opposing TE Kulite K.1 and K.5 after digital band-pass filtering from 2.0-4.0 kHz

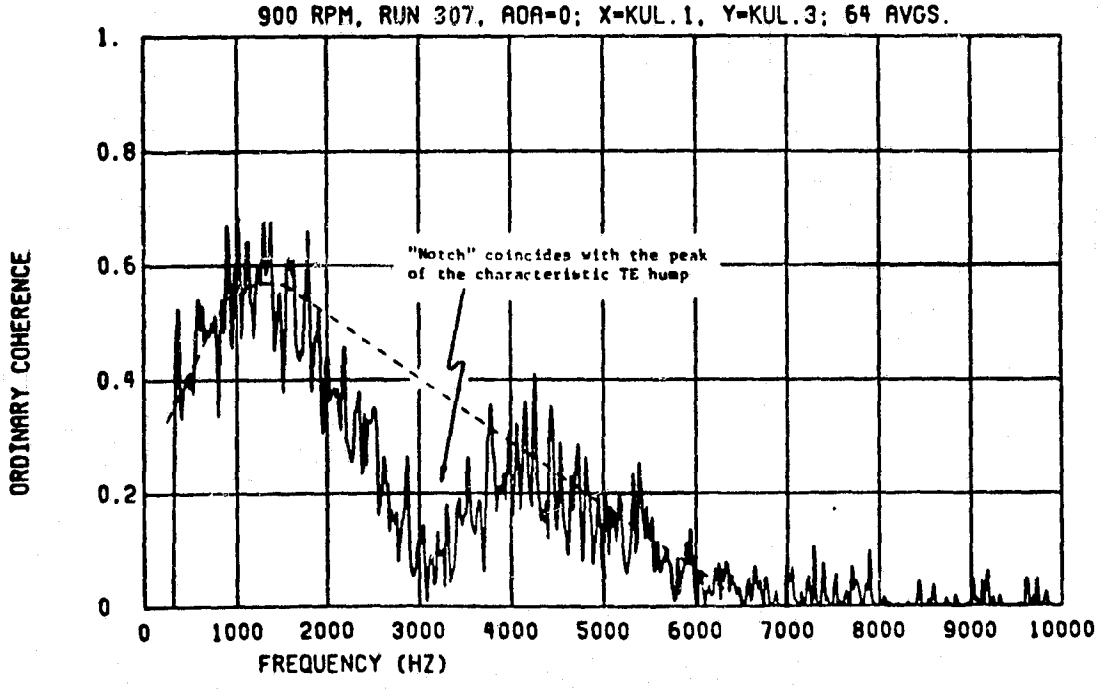

Figure 8.19 Coherence between signals from TE K.1 and upstream K.3

The amount of time τ necessary for a nonacoustic disturbance to propagate from K.3 downstream to K.1 is found using:

$$\tau = \frac{d}{u} \tag{8.7}$$

where u is some mean airflow velocity and d is as defined previously. Using d = (0.275/12) feet and u_c = 122 feet per second, a value of τ = 0.188 milliseconds is obtained for the propagation time.

The 2.0 - 4.0 kHz hump filtered cross-correlation coefficient plot for K.1 and K.3 is shown in Figure 8.21. The timing of the first large positive peak at -0.150 milliseconds agrees well with τ = 0.188 milliseconds computed above. It is likely that if finer resolution of the time delay axis were obtained (i.e., a faster sampling rate), a more accurate value approximately equal to 0.180 milliseconds could be attained, as indicated by the dashed line.

The coherence (Figure 8.19) and to a much lesser degree the cross-PSD (Figure 8.22) exhibit two strong humps in the 0.5 - 3.0 and 3.0 - 6.0 kHz bands. This contrasts with the 2.0 - 4.0 kHz auto-PSD hump seen in both near- and far-field pressure spectra (not including K.3 which exhibits no hump at all).

An interesting point to note at this time is how the center frequency of the characteristic 2-4 kHz hump mentioned above may be approximated by the use of the Strouhal relationship between the convection velocity u_c and the characteristic blunt TE dimension of 0.10 inches (see Figure 2.2) [37]. Substituting u_c = 122 feet per second, d = (0.10/12) feet and S = 0.2 into Equation (8.3) results in a frequency of 2928 Hz. No justification is given for using 0.2 as

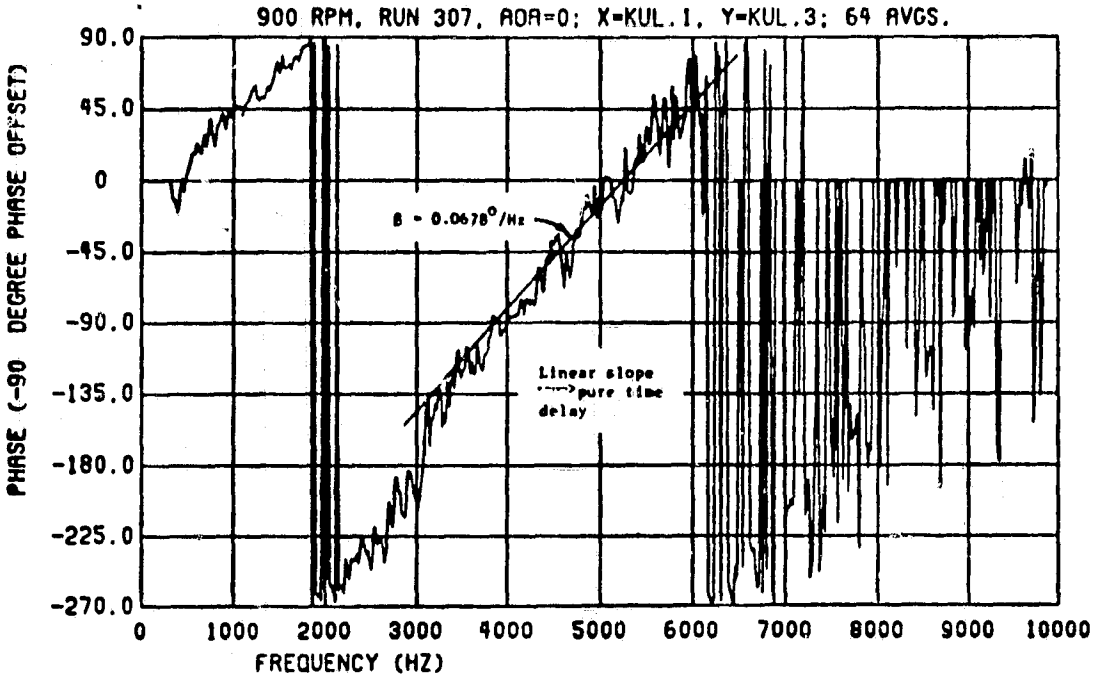

Figure 8.20 Averaged phase between signals from TE K.1 and upstream K.3

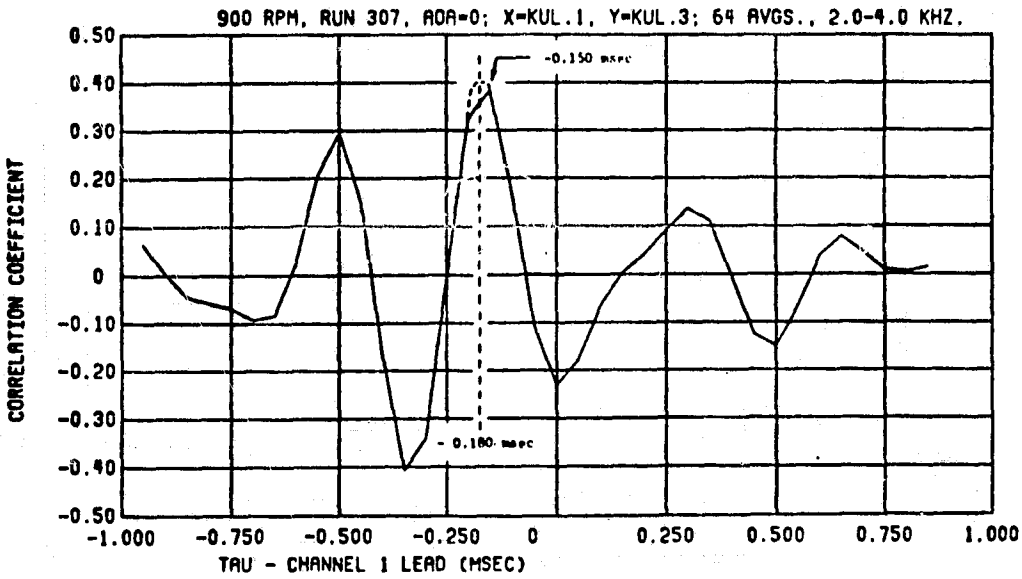

Figure 8.21 Cross-correlogram of TE K.1 and upstream K.3 after digital band-pass filtering from 2.0-4.0 kHz

the proper Strouhal number for the geometries involved other than its acceptance as a value to use for most structures under general subsonic flow conditions.

It seems likely that the suggested frequency selective Strouhal phenomena may be responsible for the "notch" in Figures 8.19 and 8.22. It also appears likely that were it not for the TE phenomena, whatever its true mechanism, the coherence would lack the "notch" and smoothly taper as denoted by the dashed line. The taper then gives evidence that the high frequency energy in a small turbulent volume of air convecting downstream dissipates much more rapidly than the low frequency energy in the volume.

Thus it is possible to explain this "notch" on the basis of frequency-related elemental volume energies. If the TE noise radiation mechanism were selectively converting the turbulent kinetic energy of an elemental volume of air to acoustic radiation energy on the basis of frequency, then that energy transformation must have come from a change in the pressure/density structure of the volume of air. Thus the pressure field of the volume as it passes over K.1 is not the same as it was when it passed over K.3, and hence the "notch" appears in the cross-spectral quantities.

Spanwise communication of the turbulence is not nearly as great as in the streamwise direction. The random phase and low coherence as shown in Figures 8.23 and 8.24 indicate the lack of any definite relationship that exists between upper surface spanwise Kulites K.1 and K.2 which are separated by 0.135 inches.

The relationship between the pressure field at TE Kulite position K.5 and 12-foot-distant M.3 on the same side is typified by Figures

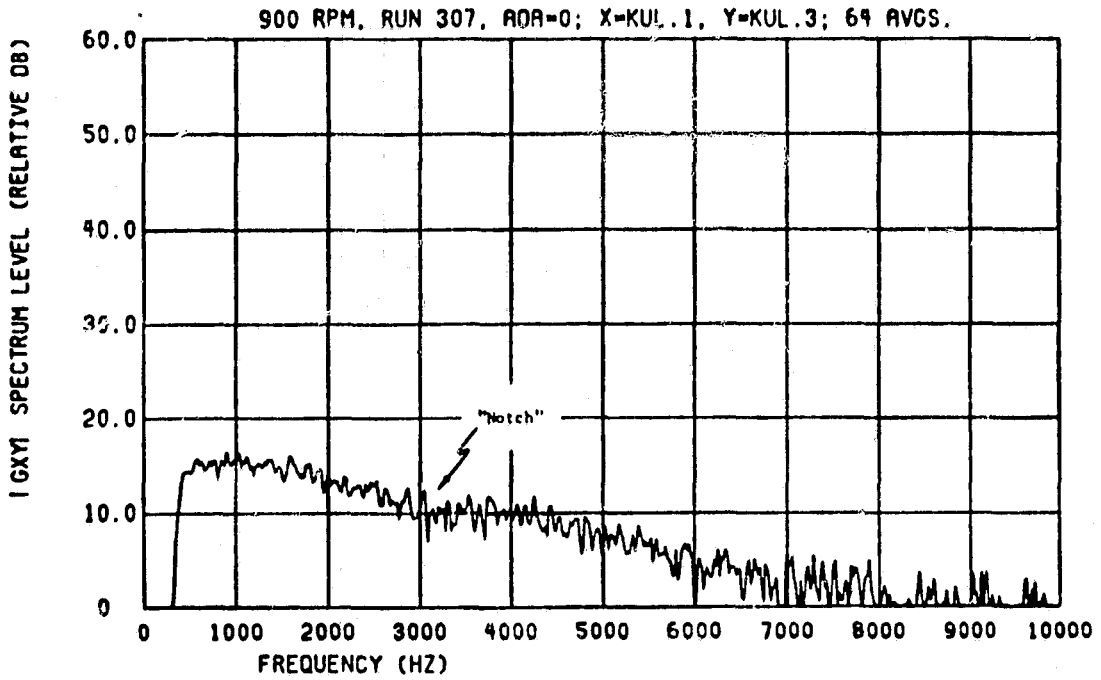

Figure 8.22 Cross-PSD between signals from TE K.1 and upstream K.3

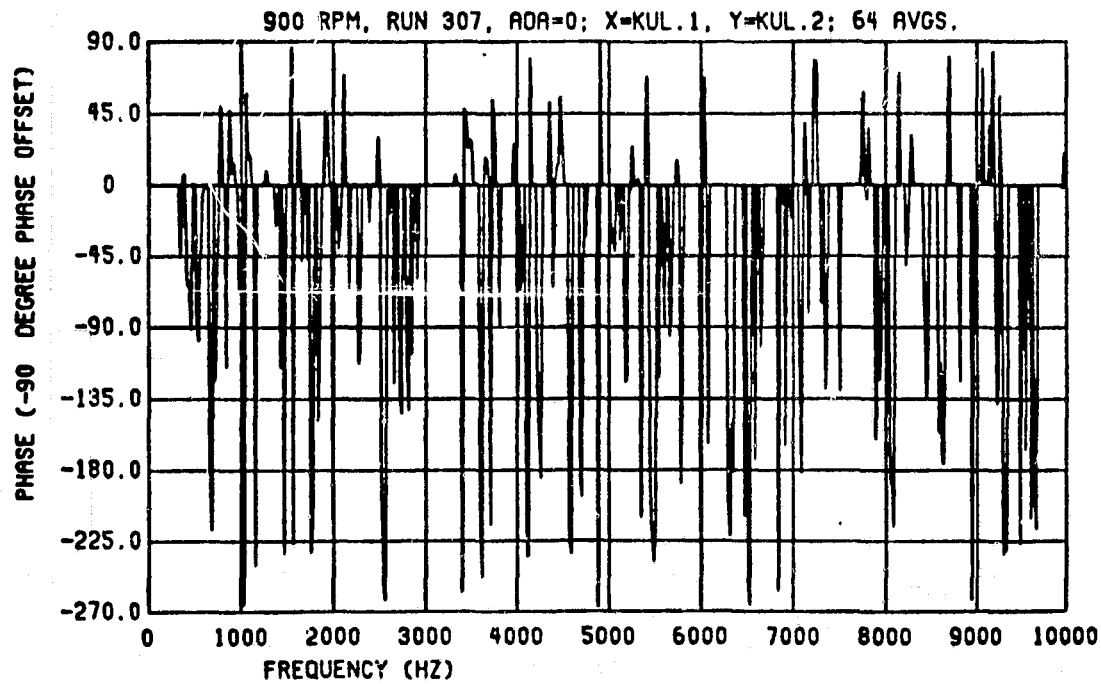

Figure 8.23 Averaged phase between signals from upper surface spanwise TE K.1 and K.2

8.25 - 8.27. Again the randomness of the phase and accompanying lack of any appreciable coherence reveal that the local near-field pressure and the far-field pressure are not intimately related. The cross-PSD plot does not yield any additional information.

A similar result was obtained for the near-field/far-field transducer pair consisting of TE K.1 and 4-foot-distant M.5 (Figures 8.28 and 8.29). The cross-correlation coefficient plot for this pair (Figure 8.30) does, however, imply that:

a) Some degree of dependency does indeed exist.

b) There is some sound which travels the required 3.55 milliseconds from the TE K.1 to the 4-foot M.5 as computed using Equation (8.7) where u is replaced by c = 1125 feet per second.

The cross-PSD plot for this pair is similar to Figure 8.27.

8.7 Detection of Near-Field/Far-Field Relationships via Subtraction Schemes

In an attempt to enhance the capability of the analysis system to establish a definite relationship between near-field Kulite and far-field microphone signals, two computational schemes were employed.

The first involved the computer subtraction of signals from Kulite pairs via the program COHERENC after appropriate amplitude scaling. The intention was to take advantage of the 180^{o} dipole-like nature of the pressure field in the 2.0 - 4.0 kHz hump frequency band and perform a point-by-point subtraction of the time data series of one TE Kulite from the time data series of its symmetrically opposite twin.

A factor to amplitude-match the two channels to be subtracted was derived from the overall rms signal level as computed via COHERENC

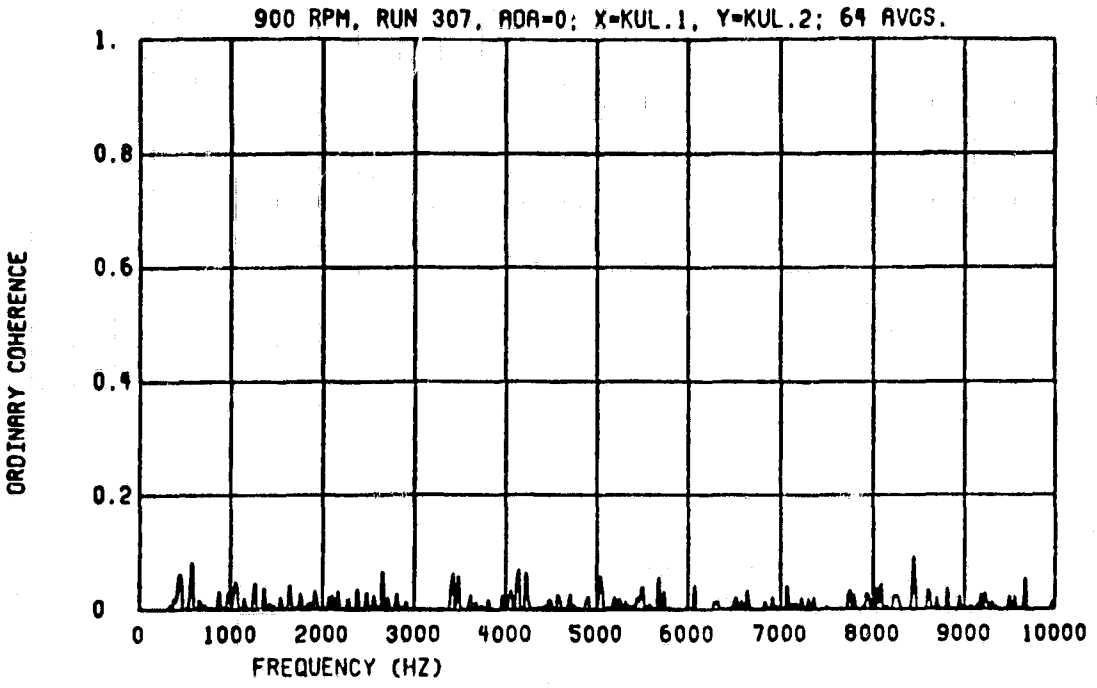

Figure 8.24 Coherence between signals from upper surface spanwise TE K.1 and K.2

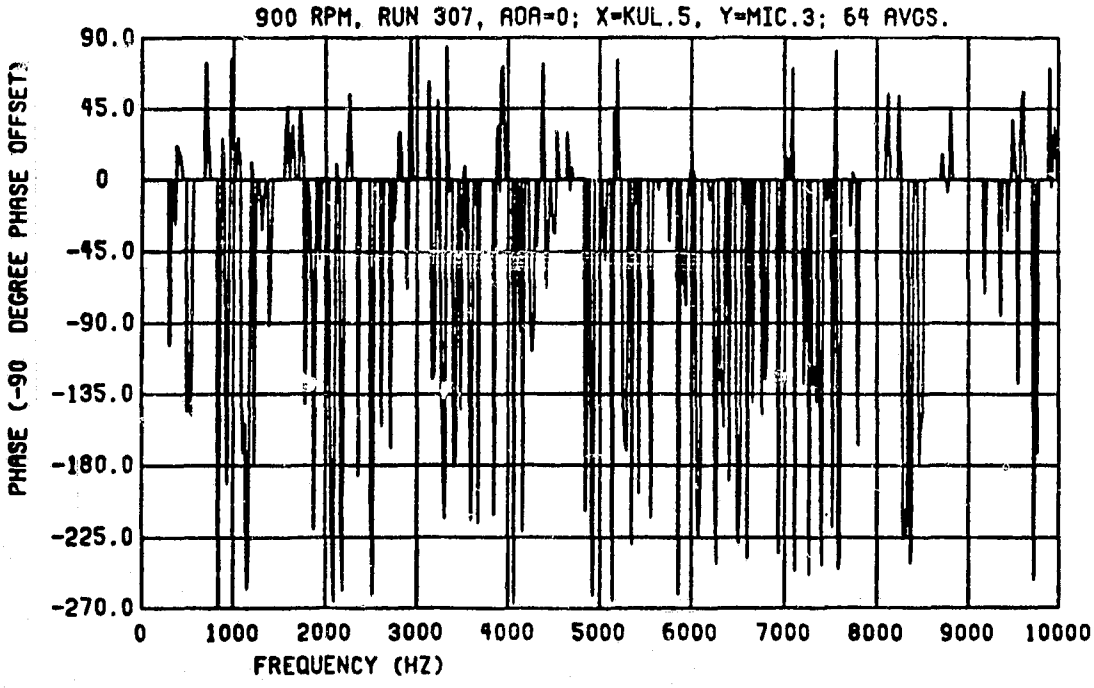

Figure 8.25 Averaged phase between signals from near-field TE K.5 and far-field M.3

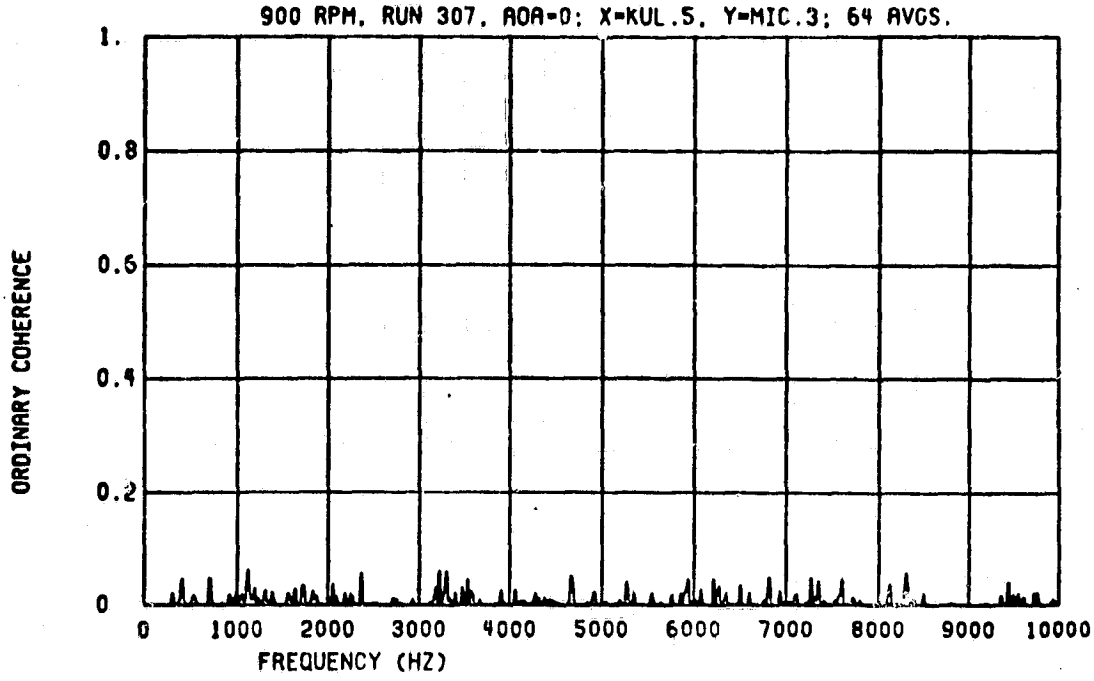

Figure 8.26 Coherence between signals from near field TE K.5 and far-field M.3

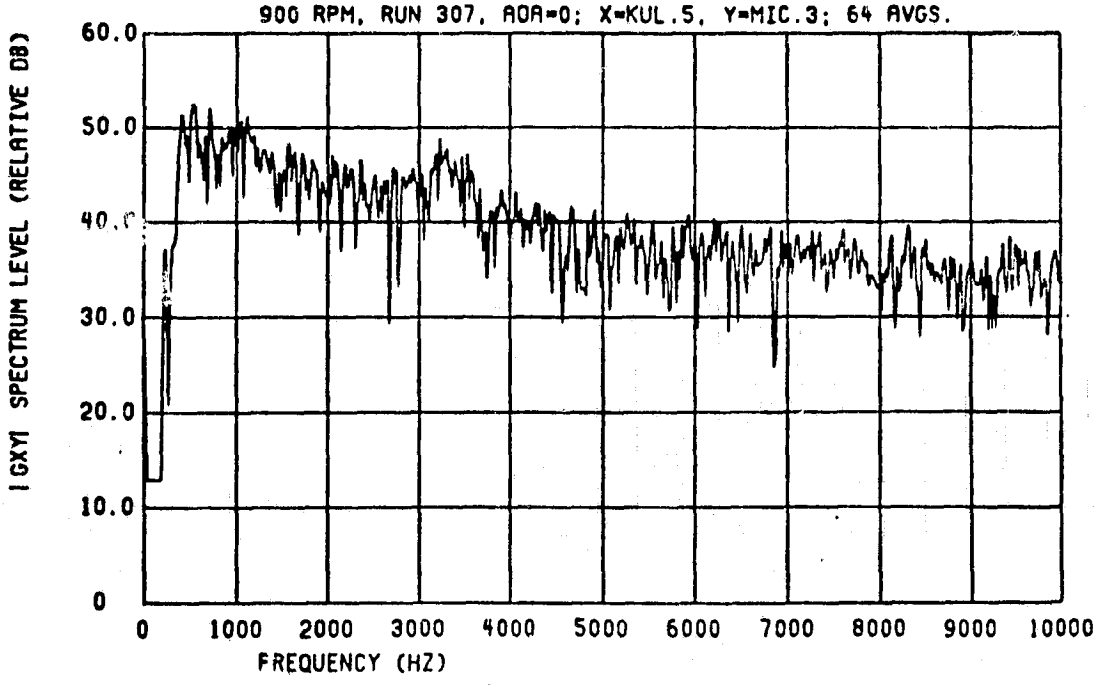

Figure 8.27 Cross-PSD between signals from near-field TE K.5 and far-field M.3

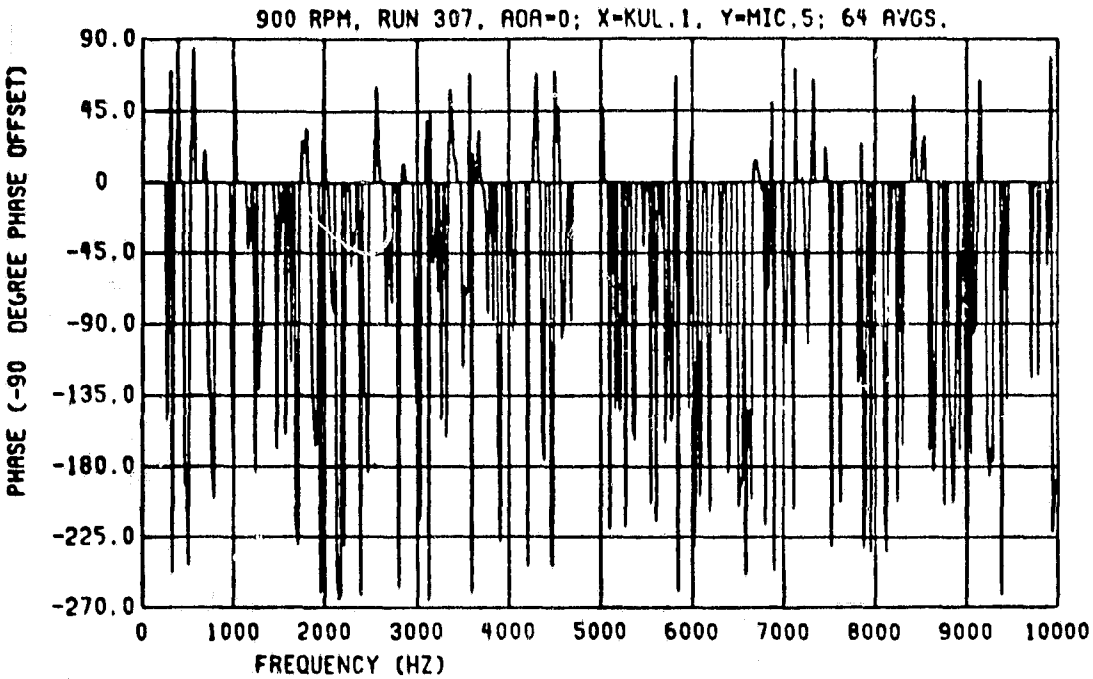

Figure 8.28 Averaged phase between signals from near-field TE K.1 and far-field M.5

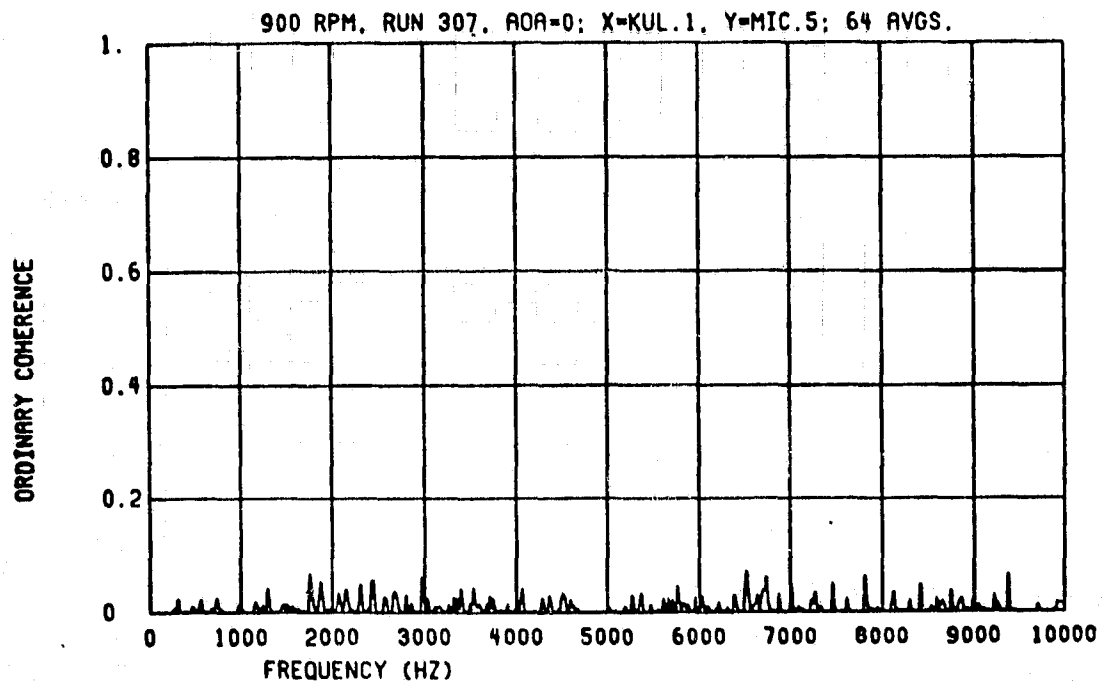

Figure 8.29 Coherence between signals from near-field TE K.1 and far-field M.5

in the 6.0 - 10.0 kHz band--i.e., those frequencies well away from the hump phenomena.

The signal information in the out-of-phase hump frequencies was predicted to double in amplitude (6 dB). The lower frequency in-phase information, which represented the insignificant life components of the pressure field, was expected to subtract out, and the higher frequency random phase information would increase by a factor of 1.414 (3 dB).

The first attempt at using this method involved K.1 and K.5 versus M.3. The results are shown in Figures 8.31 - 8.34. The auto-PSD for M.3 was identical to the general far-field spectrum given in Figure 8.7.

The characteristic hump displayed in the auto-PSD of the subtracted TE Kulites seems to be enhanced and the relative level of the pressure in the lowest frequencies appears to be reduced as compared with an unmodified TE Kulite auto-PSD such as Figure 8.8. The cross-PSD has a more pronounced hump as compared with Figure 8.27, and there seems to exist a smaller secondary hump from 1.3 - 2.3 kHz, akin to that shown by the coherence between M.2 and M.5 (Figure 8.12). However, the averaged phase is still predominantly random and the coherence still does not indicate any near-field/far-field relationship.

A second attempt at enhancing the ordinary coherence, cross-PSD, and phase functions involved not only the above-discussed Kulite subtraction, but also the subtraction of the symmetrically opposing 4-foot microphones M.2 and M.5 (Figures 8.35 - 8.38). The subtracted

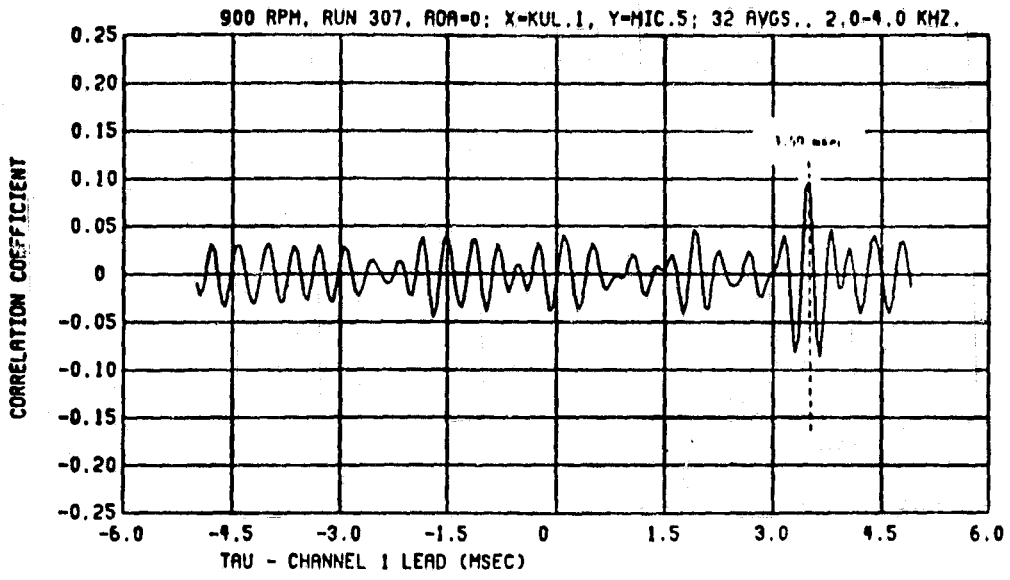

Figure 8.30 Cross-correlogram between signals from near-field TE K.1 and far-field M.5 after digital band-pass filtering from 2.0-4.0 kHz

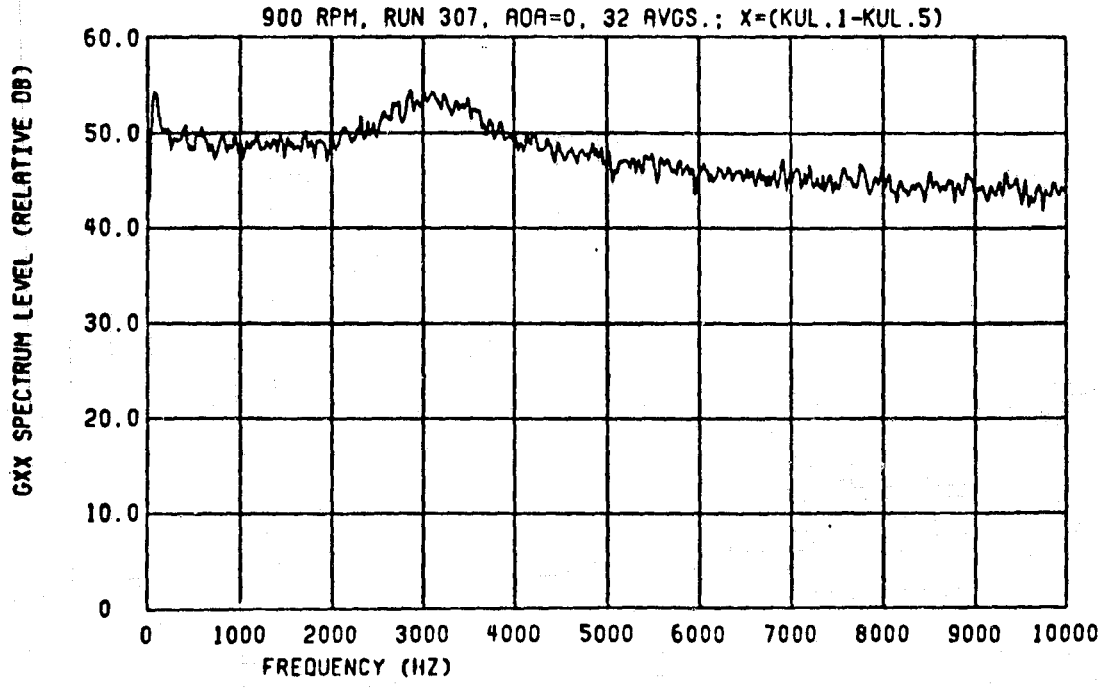

Figure 8.31 Auto-PSD of subtracted signals from TE pair K.1 and K.5

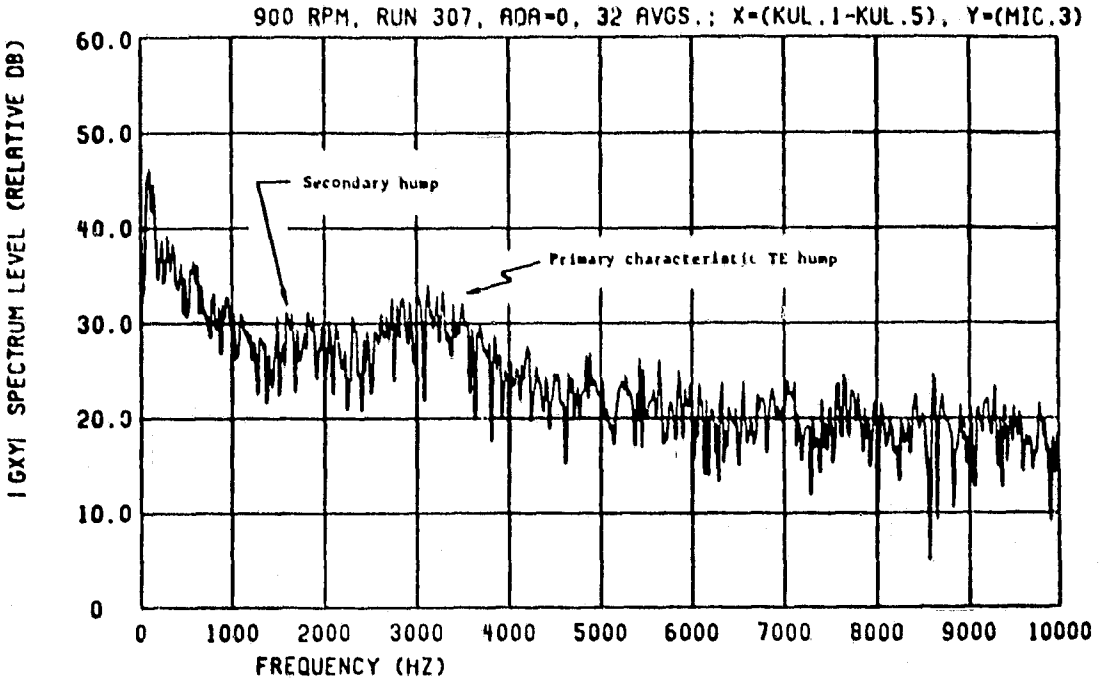

Figure 8.32 Cross-PSD between signals from the subtracted near-field TE pair K.1 and K.5 and far-field M.3

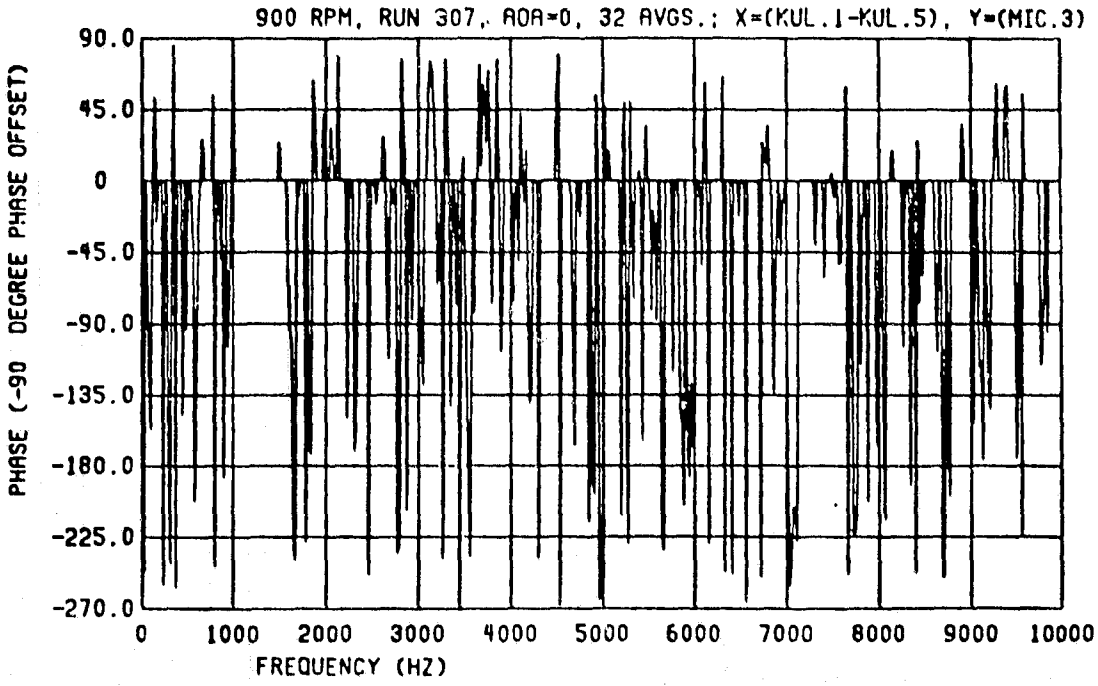

Figure 8.33 Averaged phase between signals from the subtracted near-field TE pair K.1 and K.5 and far-field M.3

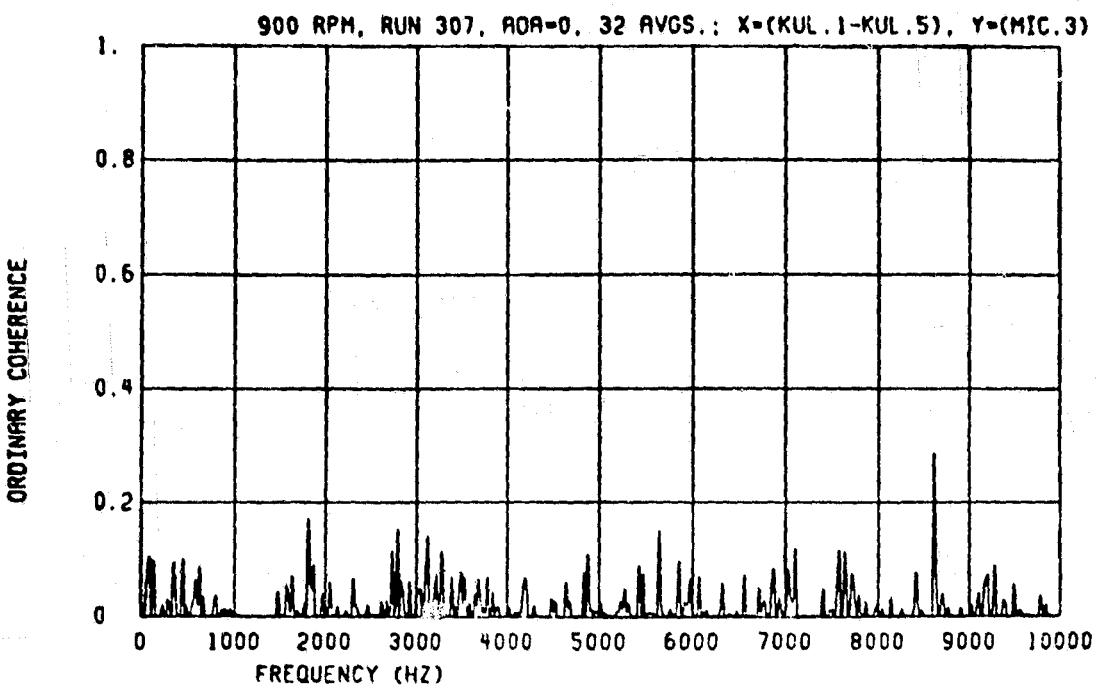

Figure 8.34 Coherence between signals from the subtracted near-field TE pair K.1 and K.5 and far-field M.3

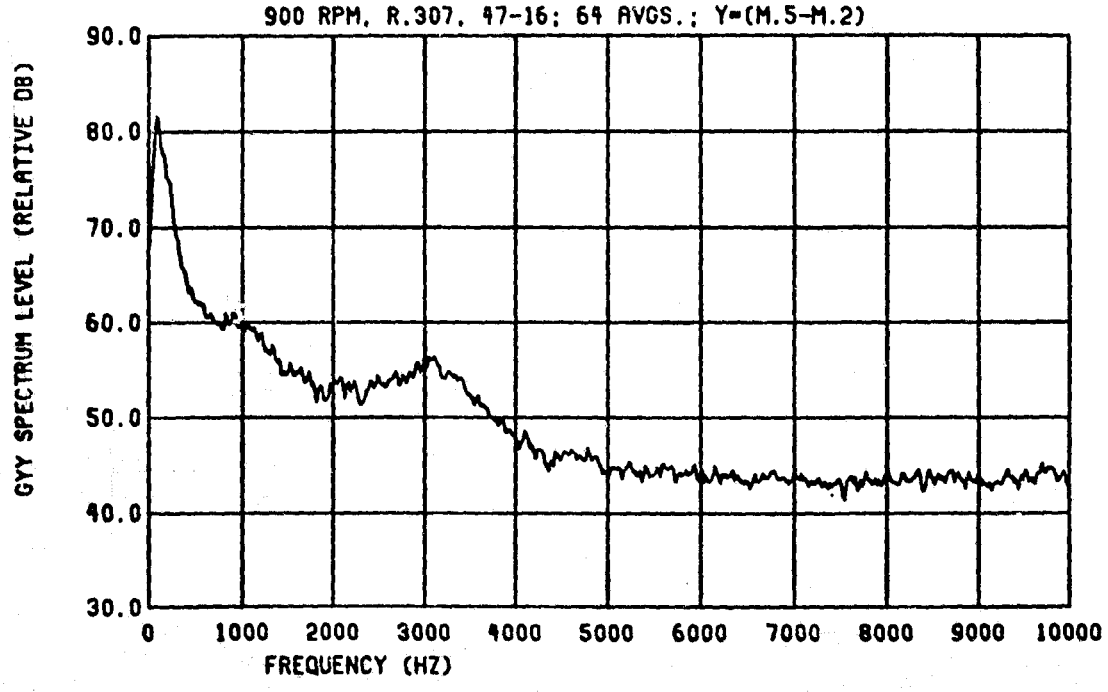

Figure 8.35 Auto-PSD of subtracted signals from far-field pair M.5 and M.2

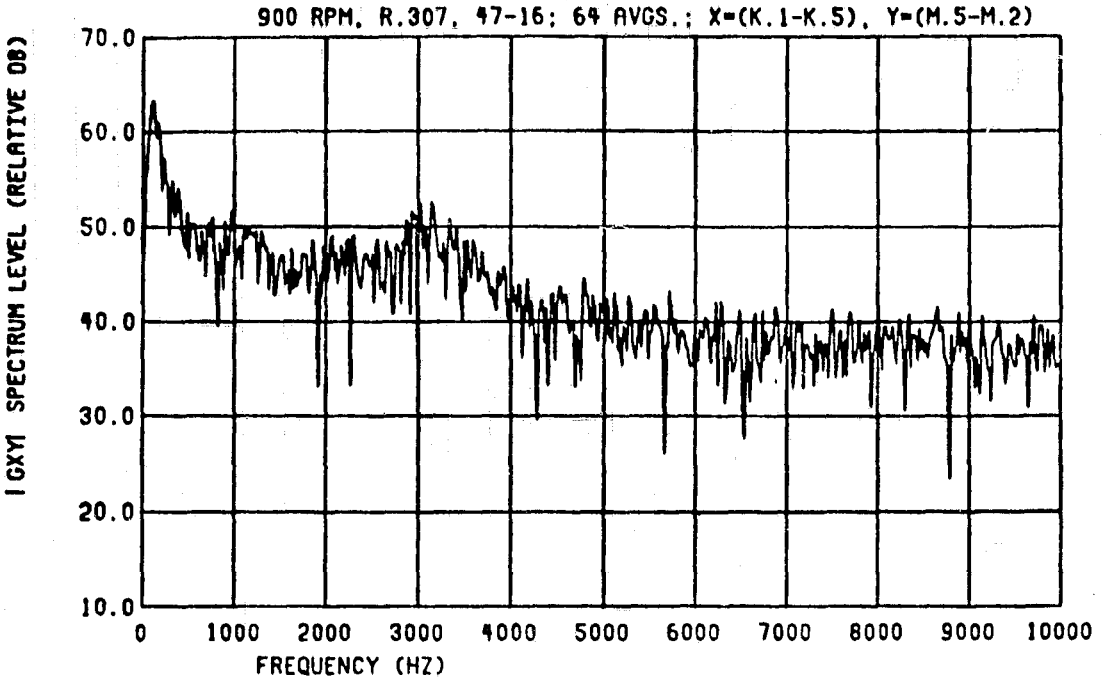

Figure 8.36 Cross-PSD between signals from the subtracted near-field TE pair K.1 and K.5 and the subtracted far-field pair M.5 and M.2

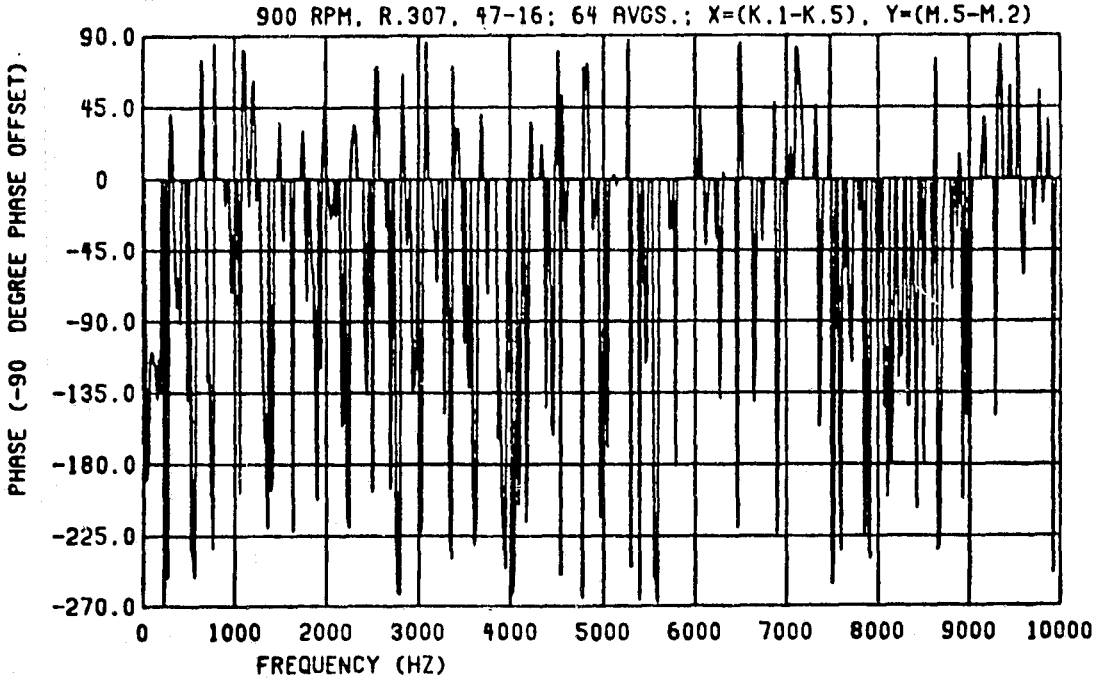

Figure 8.37 Averaged phase between signals from the subtracted near-field TE pair K.1 and K.5 and the subtracted far-field pair M.5 and M.2

Kulite auto-PSD appears the same as Figure 8.31. The primary hump as seen in the auto-PSD of the subtracted far-field microphones (Figure 8.25) is markedly improved over that of 12-foot M.3 (Figure 8.7). Also the smaller secondary hump is more clearly extablished, due in part to the better smoothing that results from the greater number of ensemble averages.

The cross-PSD, phase and coherence (Figures 8.36 - 8.38) do not show evidence of improvement over any previous results.

As a check to verify that the subtraction scheme was indeed enhancing any of the dipole-like phenomena occurring and that the amplitude scaling procedure used was proper, the identical information as in Figures 8.35 - 8.38 was again analyzed. This time, however, the time data series of symmetrically opposite transducers were added point-by-point. The lack of any humps in either auto-PSD or in the cross-PSD (Figures 8.39 - 8.41) is proof that the method used was proper. There was no significant coherence and the phase again was entirely random.

8.8 Detection of Near-Field/Far-Field Relationships via Partial Coherence

The second scheme aimed at establishing some dependence of far-field sound on the pressure in the near-field involved the use of the partial coherence function as described in Section 4.8.

It was believed on the basis of the span-wise TE cross-spectral measurements that the overall far-field sound due to the TE phenomena (i.e., the hump) was the result of emissions from many independent stream-wise "strips" of turbulent activity near the TE (Figure 8.42).

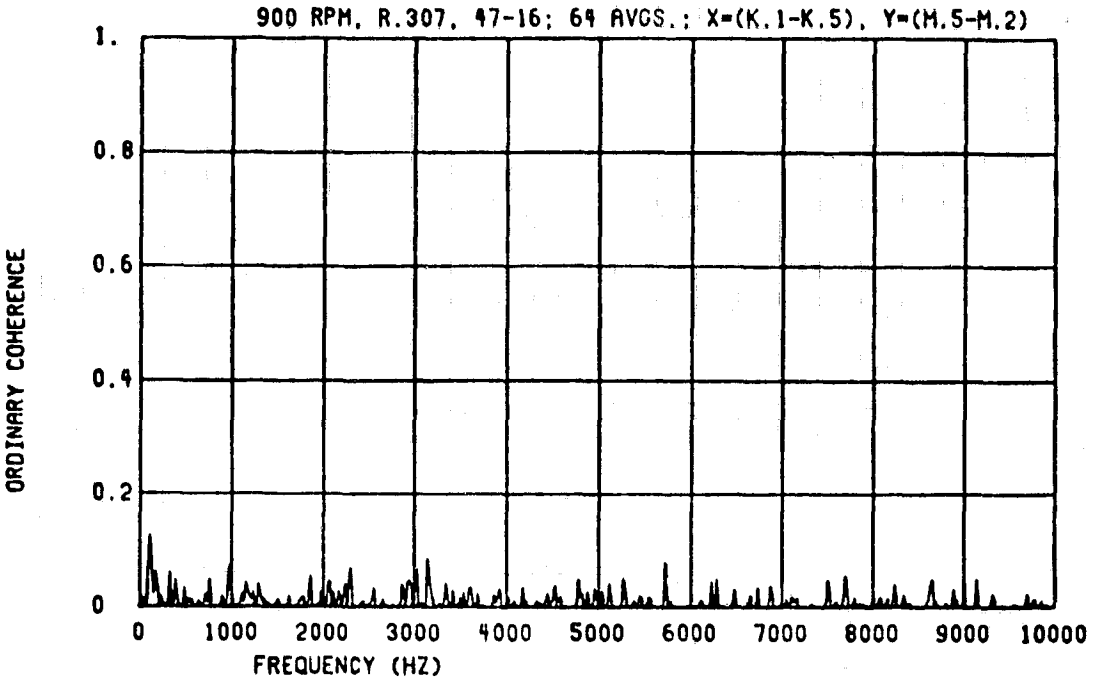

Figure 8.38 Coherence between signals from the subtracted near-field TE pair K.1 and K.5 and the subtracted far-field pair M.5 and M.2

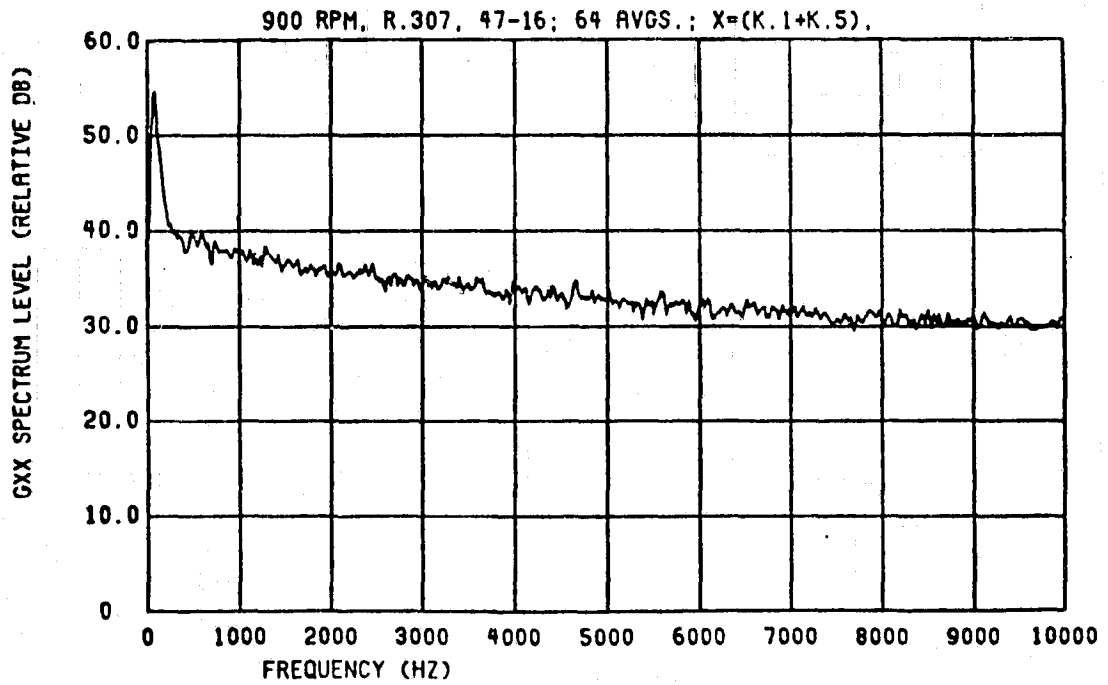

Figure 8.39 Auto-PSD of summed signals from near-field TE pair K.1 and K.5

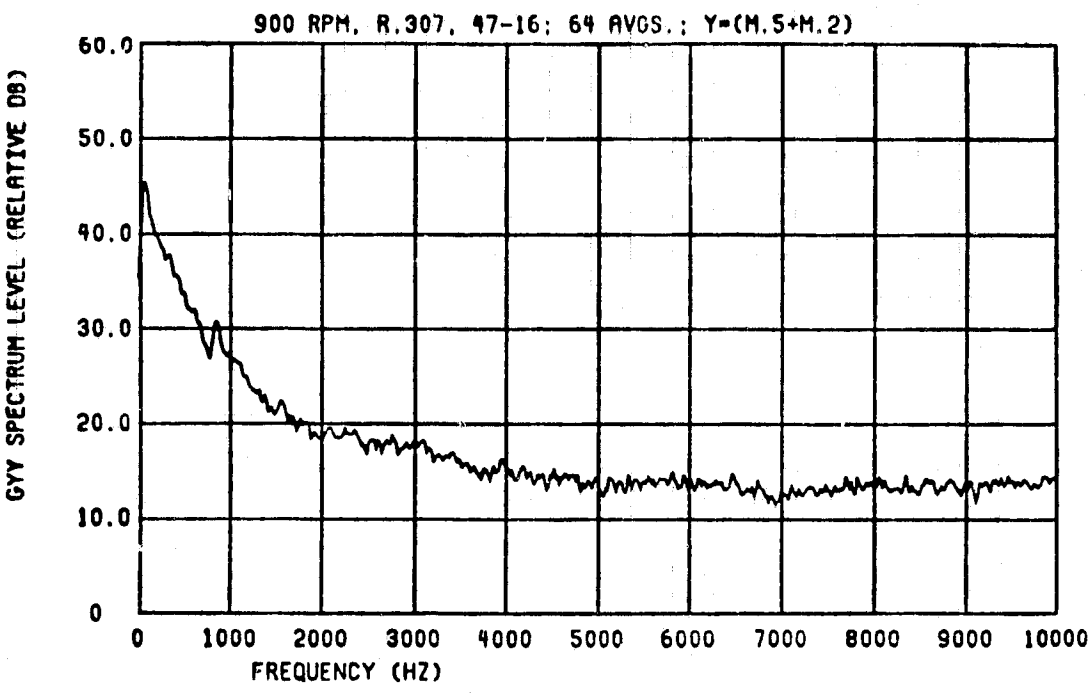

Figure 8.40 Auto-PSD of summed signals from far-field pair M.5 and M.2

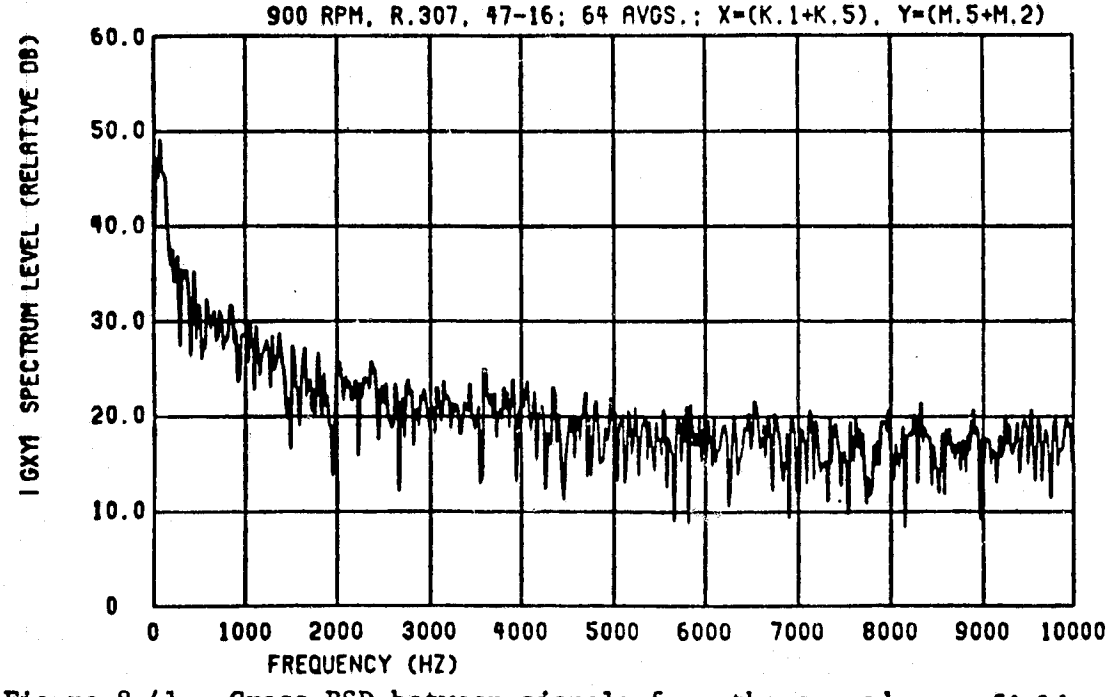

Figure 8.41 Cross-PSD between signals from the summed near-field TE pair K.1 and K.5 and the summed far-field pair M.5 and M.2

By taking into account more of these independent sources through the use of the partial coherence function, it was hoped that some near/far pressure-field connection would at last be established.

In summary, the three-input/one-output program PARTIAL failed to show any improvement over the single-input/single-output results as computed by the program COHERENC. The results for K.1, K.2 and K.3 as inputs with M.5 as the output are shown in Figures 8.43 - 8.45. Apparently not enough of the "strips" of acoustic emission as depicted in Figure 8.42 can be accounted for, even when using the multi-input program PARTIAL.

8.9 Verification of the Fifth-Power Hypothesis

A fundamental precept of the theories of Howe and many others mentioned in the introduction is that the overall sound level in the acoustic far-field increases as the fifth power of the flow velocity [27], i.e.:

$$\hat{p}^2 \simeq k\rho_o^2 \hat{u}_f^2 u_c^2 M[\frac{L\ell}{r^2}]$$

$$\simeq k\,\rho_o^2 \hat{u}_f^2 u_c^2 (\frac{u_\infty}{c})[\frac{L\ell}{r^2}] \qquad (8.8)$$

where:

- k = a factor dependent upon the "flyover" angle (constant for the case of the airfoil and microphone configuration used in this study),
- ρ_o = the mean air density,
- $\hat{u}_f$ = the mean turbulent fluctuation velocity of a turbulent volume or eddy near the TE,
- u_c = the convection velocity,

Regions of turbulence which are:

a) coherent streamwise

b) much less coherent spanwise

⟹ semi-independent "strips" of turbulence generating many separate TE noise emissions

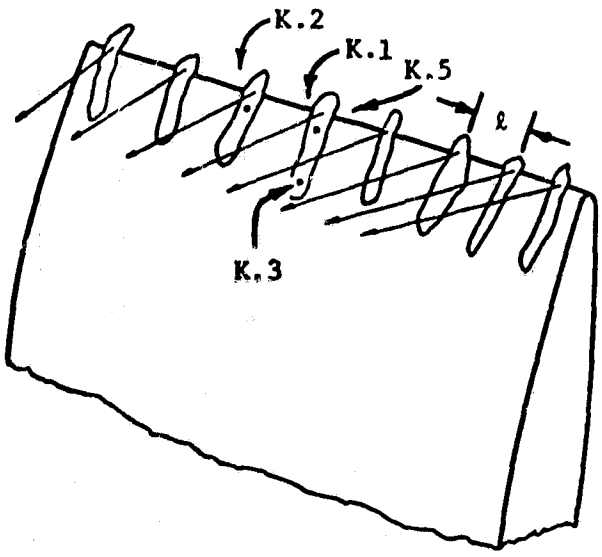

Figure 8.42 Depicting the overall far-field dynamic pressure field to be the result of TE noise emissions from many semi-independent strips of coherent turbulent flow

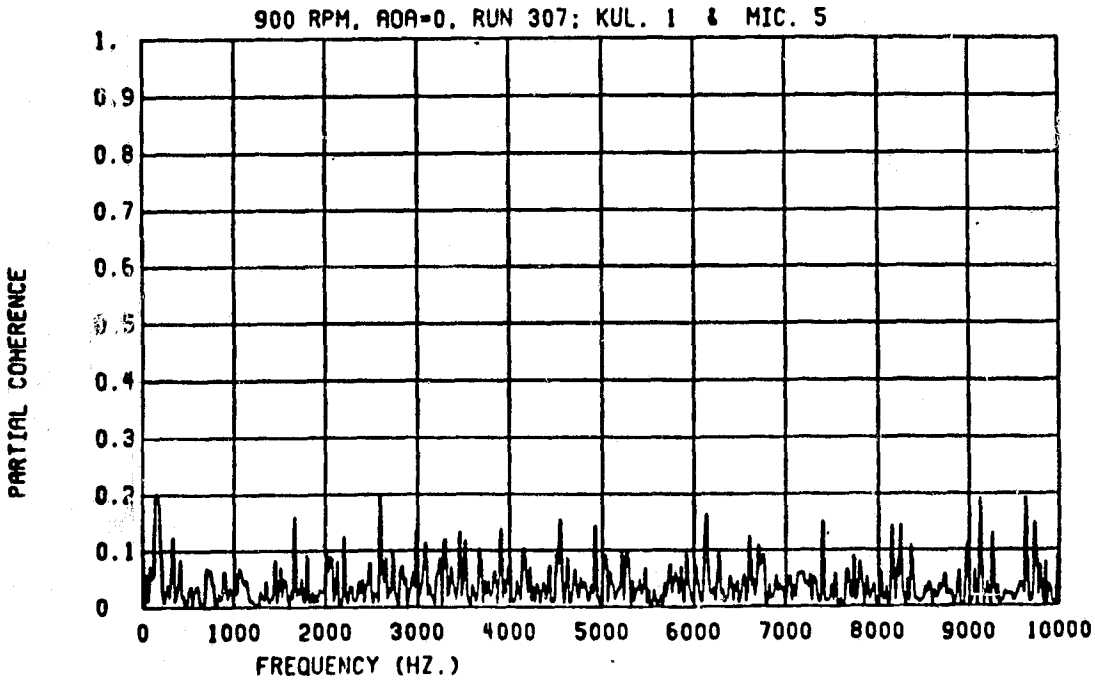

Figure 8.43 Partial coherence between signals from near-field K.1 and far-field M.5 with the phase-coherent effects of K.2 and K.3 removed

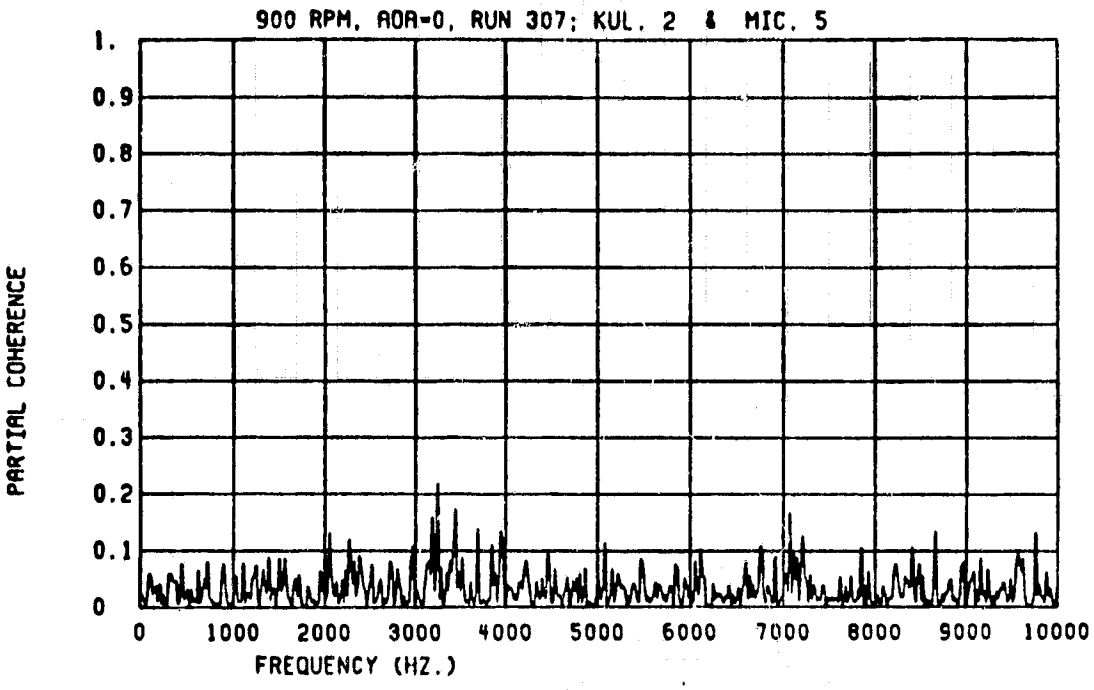

Figure 8.44 Partial coherence between signals from near-field K.2 and far-field M.5 with the phase-coherent effects of K.1 and K.3 removed

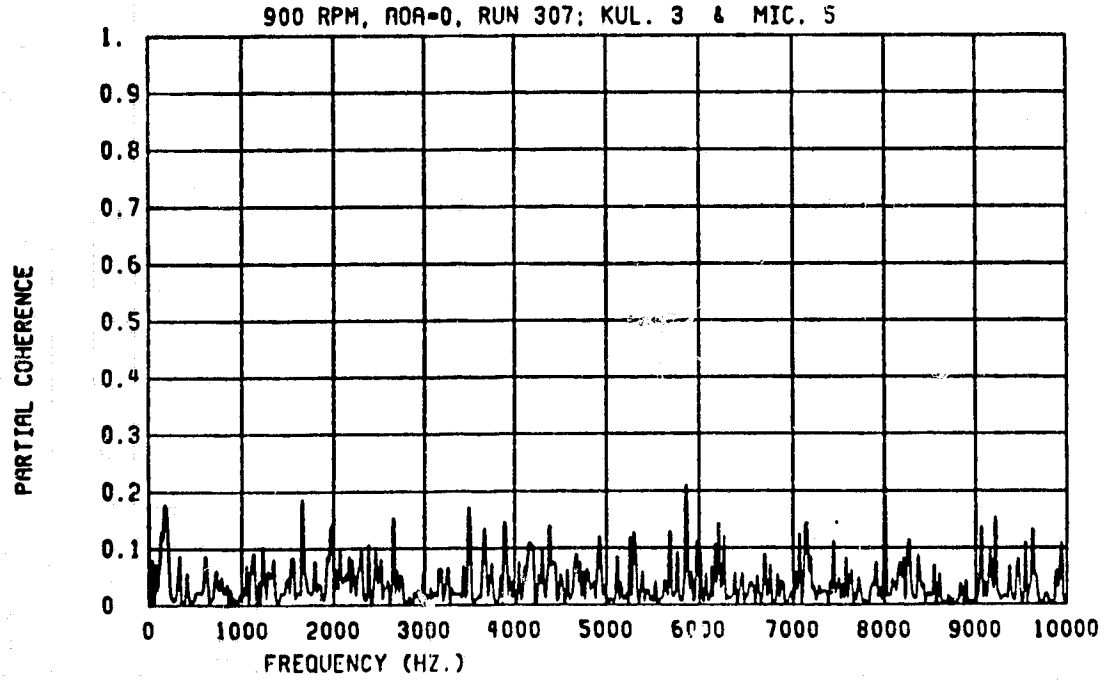

Figure 8.45 Partial coherence between signals from near-field K.3 and far-field M.5 with the phase-coherent effects of K.1 and K.2 removed

M = the Mach number = u_∞/c,

u_∞ = the freestream velocity,

c = the speed of cound,

L = the span of the airfoil TE which is "wetted" by the turbulent eddies,

ℓ = the characteristic turbulence correlation scale (depicted in Figure 8.42),

r = the distance from the TE to the observer position in the far-field.

Since both $\hat{u}_f$ and u_c are approximately linearly proportional to u_∞, Equation (8.8) becomes:

$$\hat{p}^2 \simeq k\rho_o^2 u^5 \left[\frac{L\ell}{r^2}\right] \tag{8.9}$$

where k now has absorbed many other parameters.

To verify this hypothesis, a series of far-field M.3 auto-spectra was computed as the freestream velocity was increased from 123 to 225 feet per second. The spectrum curves were obtained for the test setup with airfoil and without airfoil. After proper amplitude scaling to insure equally pressure sensitive microphone recordings, the line-by-line difference was calculated between the auto-spectrums. This resulted in spectrum values for the hump alone without background noise from which the overall SPL of the hump was computed (Figure 8.46).

The log of both the squared pressure and the velocity was taken and the values plotted (Figure 8.47). The slope of the line, β, was computed from the data points using the method of least squares.

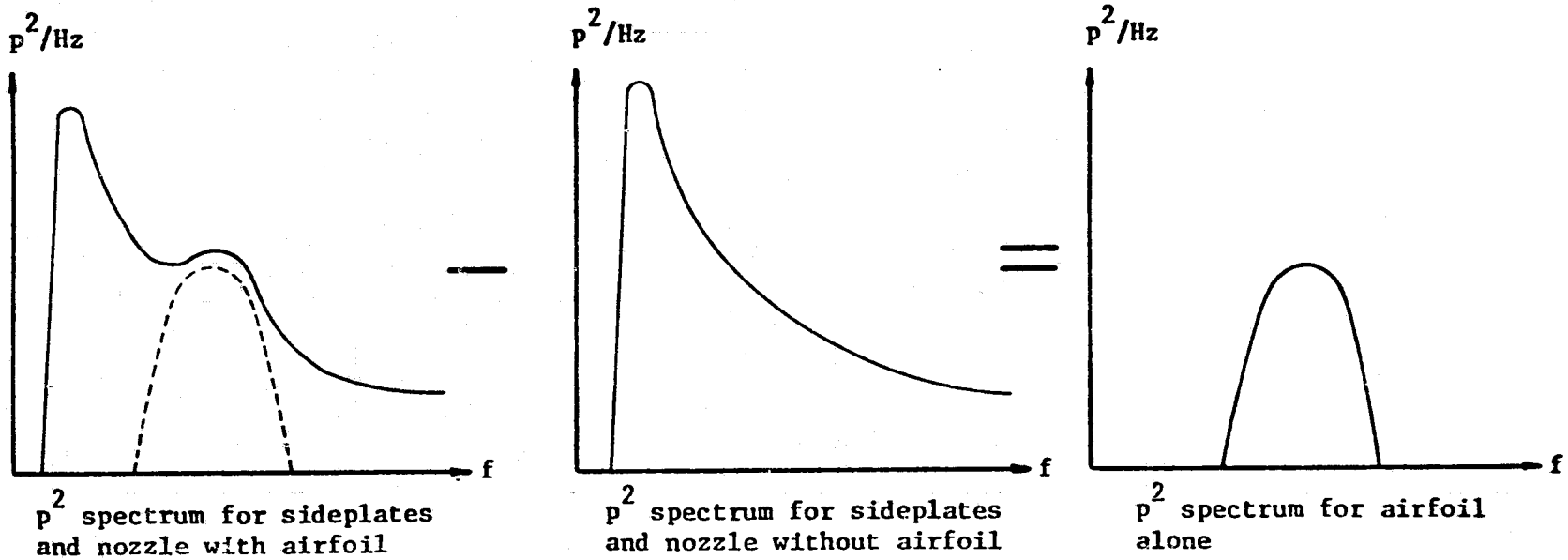

Figure 8.46 Recovery of the characteristic hump far-field pressure spectrum

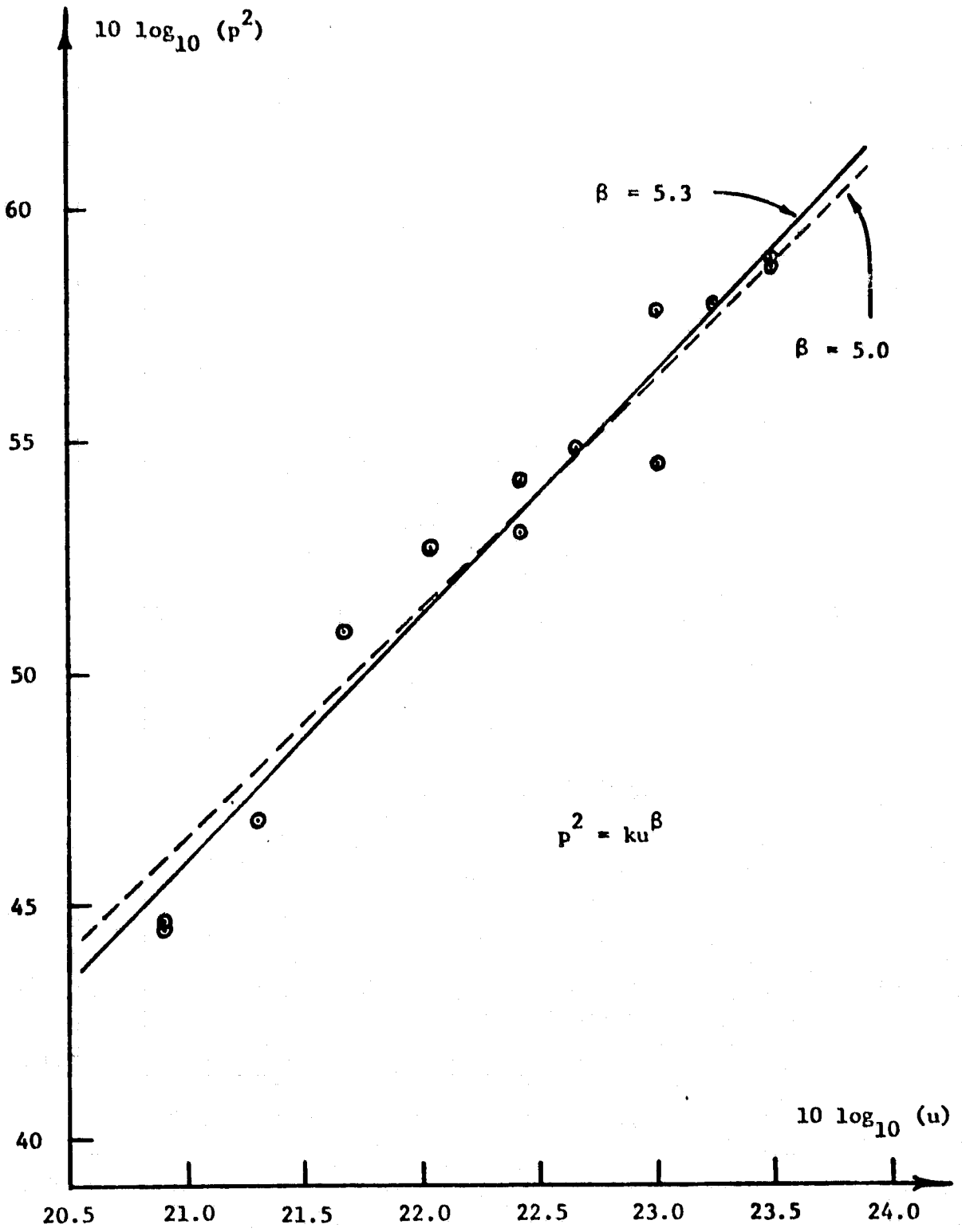

Figure 8.47 Determination of the power β to which the far-field SPL scales

The far-field sound level was found to scale on the freestream velocity raised to a power of $\beta = 5.3$. This is tending towards u^6 which indicates why the dipole-like nature of the hump is observed. However, it is in fair agreement with the predicted power of 5.0. Hence, the trailing edge noise phenomena cannot be called purely dipole-like as the Strouhal relationship might suggest.

8.10 Measurement Difficulties and Their Relationships to Theory

It is evident from Equation (8.9) that the acoustic power radiating from the TE falls off as $(1/r^2)$ as for a spherically diverging sound wave from a "compact" source. By "compact" it is meant that the size of the source is much smaller than the wavelength of sound it radiates. Compactness, then, was verified by both the correlation scale and coherence measurements in the streamwise and spanwise directions as covered in the previous pages and as depicted in Figure 8.42.

Based on the low spanwise coherence measurement (Figure 8.24) the spanwise correlation scale of the turbulence "ℓ" must be equal to or less than the 0.135 inch spacing of the spanwise transducers K.1 and K.2. Therefore, more than $(L/\ell) = (18/0.135) = 133$ sources may have existed along the "wetted" span of the TE. This serves to explain why none of the cross-spectral functions used in this study could successfully establish a near-field/far-field relationship between a single "source" and the sound in the far-field. When any single source region is monitored and compared against the overall far-field sound, all other sources are regarded as uncorrelated signal by the

analysis programs. Hence the great number of uncorrelated signals simply "swamps out" the noise emission from the single source and prevents the analysis programs from detecting any fixed-phase dependence. Thus, the lack of any definite near-field/far-field coherence indirectly verifies the existence of many independent, compact sources.

Another factor which made the detection of TE noise difficult in the ANRL facility was the small size of the test airfoil relative to the dimensions of a full-scale aircraft wing. As an example, consider the wings of a Boeing 747 jumbo jet which have approximately 110 feet of wetted trailing edge per wing and a 30-foot chord. Since all flow and boundary layer characteristics of the test airfoil were approximately the same as that for a full-sized during landing approach conditions, the factor $(L\ell/r^2)$ of Equation (8.9) implies that there are far fewer independent sources for the test airfoil than for the full-scale wing.

If the far-field sound is dependent upon wetted span alone and not upon surface area, the sound power level difference may be expected to be on the order of $10 \log_{10}(1.5/220) \approx -22$ dB. Hence, there is much less sound radiated from the test trailing edge as from the full-scale trailing edge. Noise from the open jet and sideplates is able to effectively mask the radiated TE noise (Figure 8.46) except at higher flow velocities causing the detection schemes to fail.

9. SUMMARY OF RESULTS AND CONCLUSIONS

1. A miniature strain-gauge pressure transducer ("Kulite") was designed and manufactured with outer dimensions of 0.375" L x 0.125" W x 0.045" D and a pinhole opening of 0.0135" diameter. The resonant Helmholtz frequency of the pinhole and internal cavity was approximately 63 kHz. Flat frequency response and phase shift of less than 1.0° were achieved to well beyond the 10.0 kHz frequency limit of data analysis. The nominal sensitivity of the Kulite was 25 mV/psi. Several such Kulites were mounted flush with the airfoil surface near the TE where they satisfactorily detected the local dynamic pressure due to the TE noise phenomena.

2. A companion two-stage amplifier and strain-gauge power supply for the Kulite was designed and constructed that met the operational requirements of the microphone. The final version as used at the NASA ANRL facility employed an Analog Device 521K operational amplifier and an Ithaco model 455 active filter for the respective first and second gain stages. The gain of the first stage was fixed at 50 V/V, while the gain of the second stage was allowed to vary according to signal level and recording requirements. A balanced direct-coupled input from the Kulite to the first stage and ac coupling between the first and second stages simultaneously provided for the rejection of electrical interference and prevented small dc current imbalances in the strain-gauge bridge from overloading the final stage output. Flat frequency response to beyond 100 kHz was achieved with this design.

3. A pressure coupler was constructed which provided for the calibration and performance verification of the Kulite pressure transducers. It utilized a Brüel and Kjaer type 4134 one-half inch condenser microphone as a source and a Brüel and Kjaer type 4138 one-eighth inch condenser microphone as a reference. Interunit phase and amplitude matching of the Kulites was performed using the pressure coupler.

4. Error analysis showed that because of the wide-band random nature of the signals analyzed, the bias error of the spectral density functions was of no concern. The normalized standard error was within ±0.7 dB for the number of spectrum ensemble averages used. The errors associated with the refraction of the sound passing through the open jet shear layer were insignificant. The method used for the bias correction of the ordinary coherence was shown. The error due to the time delay between trailing edge and far-field microphones was shown to give a constant negative bias of -2.03 dB for the worst case 12-foot microphone auto-PSD.

5. All microphone data were assumed to be stationary and suitable for analysis based on their widebanded random but steady nature as verified by visual inspection of the collected data sample records.

6. Auto-PSD results from trailing-edge Kulites and far-field microphones exhibited a single characteristic 3-5 dB "hump" in the 2.0 - 4.0 kHz band.

7. The frequency spectrum of the upstream Kulite exhibited no such hump as described in (6) above. It did, however, exhibit the same flat random noise spectrum as did the TE Kulites.

8. The slope of the far-field background noise floor spectrum was seen to vary as $f^{-1.125}$.

9. Streamwise communication of the turbulent pressure field over a distance of 0.275 inches was quite significant as indicated by the coherence, phase, and correlation computations. A peak coherence of 0.55 at 1.3 kHz was obtained.

10. Rather than use the cross-correlation coefficient, the slope of the phase between the streamwise Kulites was used to clearly establish the turbulent boundary layer convection velocity at 122 feet per second for a freestream velocity of 225 feet per second.

11. The coherence between the streamwise Kulites indicated that the coherent energy/Hz per unit volume decreases with increasing frequency for a given streamwise separation distance.

12. The "notch" in the coherence at 3.1 kHz between streamwise Kulites coincided with the peak of the characteristic trailing edge hump and seems to indicate that the trailing edge noise mechanism selectively extracts energy in the "hump frequencies" out of the boundary layer turbulence for use in the generation of sound.

13. Spanwise communication of the turbulent pressure field over a distance of 0.135 inches across the trailing edge appeared very slight as indicated by coherence and cross-correlation measurements.

14. There existed a 2:1 ratio of the negative slopes between the primary and secondary humps as seen in the cross-PSD plots for either pair of symmetrically opposing microphones (K.1 and K.5 or M.2 and M.5).

15. The peak values of the coherence for both the near-field symmetrically opposing TE Kulites (K.1 and K.5) and the far-field

symmetrically opposing 4-foot-distant microphones (M.2 and M.5) coincided with the 3.1 kHz peak of the characteristic hump seen in the far-field microphone and near-field TE Kulite auto-PSD curves. Peak values for the coherence were approximately 0.59 for the far-field pair and 0.32 for the near-field pair.

16. Symmetrically opposing microphones in both the near-field and the far-field indicate that, on the average, the upper and lower pressure fields were in-phase in the frequencies below the primary characteristic hump, out-of-phase in the hump frequencies, and generally of random phase above the hump frequencies.

17. A computer method for amplitude scaling of the stored digital data was devised that allowed the computer to subtract the time series of symmetrically opposing transducer pairs to better detect the out-of-phase information contained within them.

18. The Strouhal relationship was successfully used with the characteristic turbulent boundary layer convection speed of u_c = 122 feet per second and characteristic trailing edge thickness of 0.10 inches to closely approximate the center frequency of the characteristic hump. A calculated value of 2.9 kHz was obtained versus the observed 3.1 kHz value.

19. The pressure-field that existed in the vicinity of the trailing edge appears to be comprised of streamwise strips of coherent turbulence which were independent of one another in the span-wise direction. Item (13) indicates that the maximum width of such a strip is 0.135 inches. Therefore, greater than (18/0.135) = 133 such "sources" may have existed across the 18-inch span of the airfoil.

20. No spectral relationships or acoustic contributions could be established between the pressure fields at the near-field and far-field microphone positions, nor could the actual source-coherent area of location at or near the trailing edge be determined.

21. The great number of "sources" which may have existed serves to explain why cross-spectral functions could not establish any relationship between a single "source" and the sound in the far field. In such a situation, the emissions from the other independent "sources" would be regarded as noise by the analysis program and their sheer number would prevent the program from resolving any fixed-phase dependence.

22. On the basis of the ordinary and partial coherence results, it may never be practical to attempt the implementation of a partial coherence function with a sufficient number of inputs to adequately represent every "source" along the trailing edge.

23. Much less TE noise is predicted to radiate from the 1.5-foot wetted span of the test airfoil as compared with that which radiates from the wetted TE span of a full-sized aircraft. For the similar flow conditions which exist during landing approach for a Boeing 747 jumbo jet, the difference in sound power level may be on the order of 22 dB.

24. The overall far-field sound pressure level of the hump characteristic alone with background noise flor removed was seen to vary as $u^{5.3}$.

10. LIST OF REFERENCES

1. Amiet, R. K. 1978. Refraction of sound by a shear layer. Journal of Sound and Vibration 58(4):467-482.

2. Beauchamp, K. G. 1973. Signal Processing Using Analog and Digital Techniques. Holstead Press, New York, New York.

3. Bendat, J. S. 1976. Solutions for the multiple input/output problem. Journal of Sound and Vibration 44(3):311-325.

4. Bendat, J. S. 1976. System identification from multiple input/output data. Journal of Sound and Vibration 49(3):293-308.

5. Bendat, J. S. 1978. Statistical errors in measurement of coherence functions and input/output quantities. Journal of Sound and Vibration 59(3):405-421.

6. Bendat, J. S., and G. Piersol. 1971. Random Data: Analysis and Measurement Procedures. Wiley-Interscience, New York, New York.

7. Beranek, L. L. 1971. Noise and Vibration Control. McGraw-Hill, Inc., New York, New York, p. 436.

8. Blomquist, D. S., and E. B. Magrab. 1971. The Measurement of Time-Varying Phenomena. Wiley-Interscience, New York, New York, pp. 246-248.

9. Broch, J. T. 1972. Mechanical Vibration and Shock Measurements. Brüel and Kjaer, Naerum, Denmark, pp. 37, 38.

10. Bull, M. K., and A. S. W. Thomas. 1976. High frequency wall-pressure fluctuations in turbulent boundary layers. The Physics of Fluids 19(4):597-599.

11. Cooke, J. A. 1979. The development of methodology for the application of digital signal processing and coherence functions for noise source identification on textile machinery. M.S. thesis, Center for Acoustical Studies, Department of Mechanical and Aerospace Engineering, North Carolina State University, Raleigh, North Carolina.

12. Cooley, J. W., and J. W. Tukey. 1965. An algorithm for the machine calculation of complex Fourier series. Mathematics of Computation 19:297-301.

13. Couvalt, C. 1976. Langley presses noise reduction efforts. Aviation Week 105(24):63-68.

14. Crighton, D. G. 1972. Radiation from vortex filament motion near a half-plane. Journal of Fluid Mechanics 51:357-362.

15. Curle, N. 1955. The influence of solid boundaries on aerodynamic sound. Proceedings of the Royal Society, Series A, 231:505-514.

16. Dodds, C. J., and J. D. Robson. 1975. Partial coherence in multivariate random processes. Journal of Sound and Vibration 42(2):243-249.

17. Eberhardt, A. C. 1975. Digital signal analysis with application to truck tire sound and vibration. M.S. thesis, Center for Acoustical Studies, Department of Mechanical and Aerospace Engineering, North Carolina State University, Raleigh, North Carolina.

18. Federal Aviation Administration. 1974. Noise standards: Aircraft type and airworthiness certification. Federal Aviation Regulations DOT and FAA, Part 36, Government Printing Offices, Washington, D. C., p. 75.

19. Federal Scientific Corporation. 1972. An Introduction to Correlation. Federal Scientific Corporation, Monograph No. 1, pp. 6, 7.

20. Ffowcs-Williams, J. R., and L. H. Hall. 1970. Aerodynamic sound generation by turbulent flow in the vicinity of a scattering half-plane. Journal of Fluid Mechanics 40, Pt. 4, pp. 657-670.

21. Fink, M. R. 1975. Experimental evaluation of theories for trailing edge and incident fluctuation noise. AIAA Journal 13(11):1472-1477.

22. Hahn, Mansop. 1976. Turbulent boundary-layer surface-pressure fluctuation near an airfoil trailing edge. AIAA Paper No. 76-335. NASA Langley, Hampton, Virginia.

23. Halvorsen, W. G., and J. S. Bendat. 1975. Noise Source Identification using coherent output power spectra. Sound and Vibration 9(8):15-22.

24. Hardin, J. C. 1976. Airframe self-noise--four years of research. AGARD-VKI Lecture Series No. 80 of Aerodynamic Noise. NASA Langley, Hampton, Virginia.

25. Harris, C. M., and C. E. Crede. 1976. Shock and Vibration Handbook. McGraw-Hill, Inc., New York, New York, chapt. 29, pp. 33, 34.

26. Healy, G. J. 1974. Measurement and analysis of aircraft far-field aerodynamic noise. NASA Contractor Report No. 2377. NASA Langley, Hampton, Virginia.

27. Howe, M. S. 1977. A review of the theory of trailing edge noise. NASA Contractor Report No. NAS1 - 14611 - 10. NASA Langley, Hampton, Virginia.

28. Jenkins, G. M., and D. G. Watts. 1968. Spectral Analysis and Its Applications. Holden-Day, Inc., San Francisco, California.

29. Kinsler, L. E., and A. R. Frey. 1962. Fundamentals of Acoustics. John Wiley and Sons, Inc., New York, New York, pp. 186-194.

30. Lighthill, M. J. 1952. On sound generated aerodynamically; Pt. I, General theory. Proceedings of the Royal Society, Series A, 211:564-587.

31. Lighthill, M. J. 1954. On sound generated aerodynamically; Pt. II, Turbulence as a source of sound. Proceedings of the Royal Society, Series A, 222:1-32.

32. Otnes, R. K., and L. Enochsen. 1972. Digital Time Series Analysis. John Wiley and Sons, Inc., New York, New York.

33. Powell, A. 1959. On the aerodynamic noise of a rigid flat plate moving at zero incidence. Journal of the Acoustical Society of America 31(12):1649-1653.

34. Putnam, T. W., P. L. Lasagna and K. C. White. 1975. Measurements and analysis of aircraft airframe noise. AIAA Paper No. 75-510. NASA Langley, Hampton, Virginia.

35. Randall, R. B. 1977. Application of B & K Equipment to Frequency Analysis. Brüel and Kjaer, Naerum, Denmark.

36. Seybert, A. F., and J. F. Hamilton. 1977. Time delay bias errors in estimating frequency response and coherence functions. Journal of Sound and Vibration 60(1):1-9.

37. Siddon, T. E. 1973. Noise source diagnostics using causality correlations. AGARD-CP-131, Paper No. 7. NASA Langley, Hampton, Virginia.

38. Singleton, R. C. 1969. An algorithm for computing the mixed radii fast Fourier transform. IEEE Transactions on Audio and Electroacoustics AU-17(2):93-103.

39. Wylie, C. R. 1975. Advanced Engineering Mathematics. McGraw-Hill, Inc., New York, New York.

40. Yu, J. C., and C. K. W. Tam. 1977. An experimental investigation of the trailing edge noise mechanism. AIAA Paper No. 77-1291. NASA Langley, Hampton, Virginia.

11. APPENDICES

11.1 List of Symbols

a	= linear separation distance
ac, AC	= alternating current
ADC	= analog-to-digital converter
AOA	= angle of attack
b	= standard deviation coefficient for the coherence function confidence interval
B_e	= effective bandwidth = WT^{-1}
BL	= boundary layer
BNF	= background noise floor
BW	= bandwidth = T^{-1}
c	= speed of sound ≈ 1125 feet per second
CMRR	= common mode rejection ratio
d	= linear separation distance
dc, DC	= direct current
er	= normalized standard error
f	= frequency
f_n	= discrete frequency line = n/(Nh)
f_N	= Nyquist frequency; highest frequency of interest analyzed $\leq \frac{1}{2} f_s$
f_s	= sampling frequency or rate
f_o	= resonant peak frequency
f_1	= lower half-power (-3 dB) frequency
f_2	= upper half-power (-3 dB) frequency
$\Delta f_{-3\ dB}$	= half-power (-3 dB) bandwidth
FFT	= fast Fourier transform

FT	= Fourier transform
G_{xx}, G_{yy} or G_{11}, G_{22}	= real, one-sided auto-PSD
G_{xy}, or G_{12}	= complex, one-sided cross-PSD
h	= time interval between consecutive data samples $= f_s^{-1}$; height
H	= transfer function
i	= an index
j	= imaginary unit = $\sqrt{-1}$
k	= a constant
log	= base ten logarithm
K	= wavelength constant = ω/c
K.# or Kul.#	= miniature strain-gauge pressure transducer ("Kulite" microphone) located in the acoustic near-field position # as per Figures 2.4 and 3.9
ℓ	= length; characteristic turbulence correlation scale
L	= wetted span of the airfoil trailing edge
m	= number of averages or ensembles
M	= Mach number = u/c
M.# or Mic.#	= one-half inch B & K type 4133 condenser microphone located in the acoustic far-field at position # as per Figure 2.4
n	= an index
N	= total number of consecutively sampled data points in any single sample record
PSD	= power spectral density function
Q	= quality factor or sharpness of resonance
r	= maximum time-lag number; radius; distance from the TE to the far-field observer position

rms	= root-mean-square
rpm	= revolutions per minute
R	= Reynolds number
R_{xx}, R_{yy}	= real, even auto-correlation function coefficients of x(t), y(t)
R_{xy}	= real cross-correlation function coefficient of x(t) and y(t)
s	= standard deviation
s(t)	= piece-wise smooth continuous function of time
S	= Strouhal number
S/N	= signal-to-noise ratio
SPL	= sound pressure level
t	= time
T	= period of time; single sample record duration
T_t	= total period of data sampling = mT
TE	= trailing edge
u	= flow velocity (general)
u_c	= convection velocity
$\hat{u}_f$	= mean turbulent fluctuation velocity
u_τ	= friction velocity
u_∞	= freestream velocity
V	= volume; voltage
W	= sample record weighting-function bandwidth factor (relative to the bandwidth of a rectangular weighting function)
x(t), y(t), z(t)	= piece-wise smooth (continuous) functions of time
X, Y	= complex-valued two-sided spectral density functions
z	= transformation for the distribution of sample coherence function; a general variable

z_a	= one-sided 100α percentage point of the normal distribution of the data
α	= angle of attack; level of significance
β	= power constant; slope
δ	= boundary layer thickness
δ_1	= displacement thickness
γ_o^2	= uncorrected, biased coherence estimate
γ_{xy}^2, γ_{12}^2	= ordinary coherence function
$\gamma_{24\cdot 13}^2$	= partial coherence function
ν	= kinematic viscosity
θ	= geometric angle; momentum thickness
π	= 3.14159
ρ_{xy}	= normalized cross-correlation coefficient
ρ_o	= mean air density
τ	= lag or delay time; fluid shear stress
ϕ	= phase angle; momentum thickness
ω	= radian frequency = $2\pi f$
$[\ \hat{}\ ]$	= averaged quantity
$[\quad]^*$	= complex conjugate of [ ]
$[\ \underset{\sim}{\ }\ ]$	= complex quantity

11.2 COHERENC

The two-channel program "COHERENC":

1) can delay one time series sample record relative to another, one data point at a time (with the possible sacrifice of frequency resolution as points are deleted).

2) can be used to find an amplitude scale factor.

3) using the scale factor, can amplitude match and then subtract or add two time series on a point-by-point basis to yield a composite signal. A second composite signal obtained in the same manner from two more time series then makes up the pair needed for cross-spectral analysis.

4) removes the overall mean from each of the two time series and amplitude weights each time series with a Hanning ($\sin^2$) function.

5) computes the spectral values for G_{xx}, G_{yy}, G_{xy}, H_{xy}, and ϕ_{xy} via the FFT.

6) averages the above quantities by repeating steps 1, 3, 4 and 5.

7) computes and bias corrects the ordinary coherence.

8) computes the ordinary coherence and confidence interval.

9) computes the coherent power output spectrum, $\hat{\gamma}^2_{xy}\, G_{yy}$.

10) can then scale the PSD quantities against a reference standard to obtain calibrated values if a reference and calibration level are supplied.

11) computes the overall averaged $\hat{G}_{xx}$, $\hat{G}_{yy}$, $\hat{G}_{xy}$, $\hat{\phi}_{xy}$, $\hat{\gamma}^2_{xy}$, $\hat{G}_{yy}$ in chosen frequency bands (method used for finding item 2 above).

12) outputs all above-mentioned averaged quantities on a printout.

13) automatically will scale the plot axes and then plot the $\hat{G}_{xx}$, $\hat{G}_{yy}$, $\hat{G}_{xy}$, $\hat{\phi}_{xy}$, $\hat{\gamma}^2_{xy}$.

```
      INTEGER*2 INFIL,JUNK
      COMPLEX FFT1,FFT2,GXY,HXY
      DIMENSION XOBS(1,515),YOBS(1,515),XDUMMY(1,515),YDUMMY(1,515)
      DIMENSION XLABEL(20),TITLE(20),KIND(5),YLABL1(20),YLABL2(20)
      DIMENSION YLABL3(20),YLABL4(20),YLABL5(20)
      COMMON N,IAVGS,IDAY,ILAG1,ILAG2,KADR,IWT
      COMMON KONFI,NOTOK,REC,REP,PS,PSTOP,PSBASE
      COMMON SPLRT,SMEAR1,SMEAR2,RF1,RF2,RF3,HXYREF
      COMMON INFIL(4096),JUNK(20),INIT(256)
      COMMON GXX(515),GYY(515),GXYAB(515),HXYAB(515),HXYORD(515)
      COMMON PHAZE(515),COHE(515),COSPEC(515),CILWE(515),CIUPR(515)
      COMMON CH1(2048),CH2(2048),XFREQ(515)
      COMMON FFT1(515),FFT2(515),GXY(515),HXY(515)
      COMMON NPAS,NNIH(10),NLOW(10)
      COMMON IDATA,CAL1,CAL2,CAL3,CAL4,CALX,CALY,CALXY
C
   50 FORMAT (20A4)
  500 FORMAT ('1',////,40X,20A4)
C
CCCCCCCCCCCCCCCCCCCCCCCCCCCCCCCCCCCCCCCCCCCCCCCCCCCCCCCCCCCCCCCCCCCCCC
C                                                                     C
C     'IDATA' = 1  ==>  1 OF 2 CHANNEL CAL. RUN, NO PLOTS, 1 AVG./DUMP.C
C             = 2  ==>  NORMAL 2-CHANNEL MODE OF OPERATION.           C
C             = 4  ==>  4-CHANNEL MODE OF OPERATION, PRESENTLY SET UP C
C     AS:  (CH2-CH3) VS. (CH4); 1 AVG./DUMP.                          C
C                                                                     C
C     'IPLOTA' = 1 PLOTS THE AUTO-SPECTRUMS GXX & GYY, THE CROSS-     C
C     SPECTRUM GXY, AND THE PHASE BETWEEN CHANNELS 1 & 2; = 0 DOES NOT.C
C                                                                     C
C     'IPLOTH' = 1 PLOTS THE ORDINARY COHERENCE BETWEEN CHANNELS      C
C     1 & 2; = 0 DOES NOT.                                            C
C                                                                     C
C     'REC' IS THE DATA RECORDING SPEED IN IN/SEC OR CM/SEC.          C
C     'REP' IS THE DATA REPRODUCING SPEED IN IN/SEC OR CM/SEC.        C
C     IF NOT APPLICABLE, SET REC=REP=1.0                              C
C                                                                     C
CCCCCCCCCCCCCCCCCCCCCCCCCCCCCCCCCCCCCCCCCCCCCCCCCCCCCCCCCCCCCCCCCCCCCC
C
      IDATA=2
      IPLOTA=1
      IPLOTH=1
C
      REC=60.0
      REP=15.0
C
CCCCCCCCCCCCCCCCCCCCCCCCCCCCCCCCCCCCCCCCCCCCCCCCCCCCCCCCCCCCCCCCCCCCCC
C                                                                     C
C     'N' = ONE-HALF THE NUMBER OF DATA POINTS PER TIME RECORD;  I.E., C
C     N = THE NUMBER OF SPECTRAL LINES, PRESENTLY LIMITED TO 512 OF   C
C     POSSIBLE 1024.  THIS LEAVES ROOM FOR SHIFTING POINTS (TIME      C
C     DELAYS).                                                        C
C                                                                     C
C     'IAVGS' IS THE NUMBER OF AVERAGES PER FREQUENCY LINE.           C
C                                                                     C
C     'SPLRT' IS THE SAMPLING RATE IN HZ.                             C
C                                                                     C
```

```
C      'PS' = PHASE SHIFT OR OFFSET IN DEGREES.                          C
C                                                                        C
CCCCCCCCCCCCCCCCCCCCCCCCCCCCCCCCCCCCCCCCCCCCCCCCCCCCCCCCCCCCCCCCCCCCCCCC
C
      N=512
      IAVGS=64
      SPLFT=5000.0
      PS=-90.0
C
CCCCCCCCCCCCCCCCCCCCCCCCCCCCCCCCCCCCCCCCCCCCCCCCCCCCCCCCCCCCCCCCCCCCCCCC
C                                                                        C
C     'REF1', 'REF2', 'REF3', AND 'HXYREF' ARE THE REFERENCE VALUES.     C
C                                                                        C
C     'IWT' = 1 SPECIFIES COSINE**2 WEIGHTING; = 0 GIVES BOXCAR.         C
C                                                                        C
C     'KONFI' = 1 CALCULATES THE CONFIDENCE INTERVAL; = 0 DOES NOT.      C
C                                                                        C
C     'IDLAY' DELAYS BOTH CHANNELS BY THE GIVEN NUMBER OF POINTS.        C
C     'ILAG1' DELAYS CHANNEL 1;  'ILAG2' DELAYS CHANNEL 2.               C
C                                                                        C
C     'SMEAR1' IS THE SLIDING DELAY FOR 'ILAG1' IN MSEC.                 C
C     'SMEAR2' IS THE SLIDING DELAY FOR 'ILAG2' IN MSEC.                 C
C                                                                        C
C     'KAPP' = THE NUMBER OF AVERAGES PER BIOMATION DUMP.  THERE ARE     C
C     4096 10-BIT WORDS OR DATA POINTS PER CHANNEL.  WHEN EACH DUMP      C
C     IS DIVIDED IN HALF, IT YIELDS 2048 DATA POINTS AVAILABLE PER       C
C     CHANNEL.  FROM THIS, ONE AVERAGE PER DUMP (WITH 2048 POINTS PER    C
C     CHANNEL) MAY BE REALIZED, OR TWO AVERAGES PER DUMP (WITH 1024      C
C     POINTS PER CHANNEL) MAY BE REALIZED, ETC.      KAPP = (1024/N)     C
C                                                                        C
CCCCCCCCCCCCCCCCCCCCCCCCCCCCCCCCCCCCCCCCCCCCCCCCCCCCCCCCCCCCCCCCCCCCCCCC
C
      REF1=1.0
      REF2=1.0
      REF3=SQRT(REF1*REF2)
      HXYREF=SQRT(REF2/REF1)
C
      IWT=1
      KONFI=1
C
      IDLAY=0
      ILAG1=0
      ILAG2=0
C
      SMEAR1=0.0
      SMEAR2=0.0
C
      KAPP=1024/N
C
CCCCCCCCCCCCCCCCCCCCCCCCCCCCCCCCCCCCCCCCCCCCCCCCCCCCCCCCCCCCCCCCCCCCCCCC
C                                                                        C
C     'CAL#A' = SPL OF THE MIC. CAL. SOURCE EXPRESSED IN DB RE           C
C     CH1 & CH2 (AND 3 & 4 WHEN APPLICABLE; OTHERWISE CAL#A=0.0).        C
C                                                                        C
C     'CAL#B' = DB READING OFF THIS PROGRAM IN THE FREQUENCY BANDS OF    C
C     THE CAL. SOURCE WHEN 'IDATA' = 1.                                  C
```

```
C                                                                       C
C     'GAIN#' = NET DIFFERENCE IN GAIN OF (ACTUAL DATA RUN KNOB         C
C     SETTINGS)-(CAL. RUN KNOB SETTINGS) EXPRESSED IN DB.               C
C                                                                       C
C     'NDAS' = 1 CALCULATES THE OVERALL COHERENCE AND SPECTRUM LEVELS    C
C     IN UP TO 10 CHOSEN FILTERED BANDS; = 0 DOES NOT.                  C
C                                                                       C
C     THE NLOW AND NHIH FILTER CARDS GO HERE; EXAMPLE: NLOW=2 NHIH=50   C
C                                                                       C
CCCCCCCCCCCCCCCCCCCCCCCCCCCCCCCCCCCCCCCCCCCCCCCCCCCCCCCCCCCCCCCCCCCCCCCC
C
      CAL1A=0.0
      CAL1A=0.0
      CAL2A=0.0
      CAL3A=0.0
      CAL4A=0.0
C
      CAL1B=0.0
      CAL2B=0.0
      CAL3B=0.0
      CAL4B=0.0
C
      GAIN1=0.0
      GAIN2=0.0
      GAIN3=0.0
      GAIN4=0.0
C
      CAL1=10.0**((CAL1A-CAL1B-GAIN1)/20.0)
      CAL2=10.0**((CAL2A-CAL2B-GAIN2)/20.0)
      CAL3=10.0**((CAL3A-CAL3B-GAIN3)/20.0)
      CAL4=10.0**((CAL4A-CAL4B-GAIN4)/20.0)
C
      NDAS=4
C
      NLOW(1)=42
      NHIH(1)=104
      NLOW(2)=104
      NHIH(2)=206
      NLOW(3)=309
      NHIH(3)=512
      NLOW(4)=22
      NHIH(4)=512
      NLOW(5)=157
      NHIH(5)=487
C
C     THE FOLLOWING CARDS ARE NOT CHANGED; THEY ARE FOR
C     CALIBRATION AND 4-CHANNEL OPERATION.-------------------------------
C
      IF (IDATA.NE.1) GO TO 10
      IPLOTA=0
      IPLOTB=0
      N=512
      DS=0.1
      IDLAY=0
      ILAG1=0
      ILAG2=0
```

```
      SMEAR1=0.0
      SMEAR2=0.0
      CAL1=0.0
      CAL2=0.0
      CAL3=0.0
      CAL4=0.0
      KADD=1
      NPAS=2
      NLOW(1)=12
      NHIH(1)=16
      NLOW(2)=50
      NHIH(2)=54
      GO TO 20
C
   10 CONTINUE
      IF (IDATA.NE.4) GO TO 20
      N=512
      IDLAY=0
      ILAG1=0
      ILAG2=0
      SMEAR1=0.0
      SMEAR2=0.0
      KADD=1
   20 CONTINUE
C
C
      CALL TRANS2
C
C
      READ (1,50) (TITLE(I),I=1,20)
      WRITE (3,500) (TITLE(I),I=1,20)
C
C
      CALL XPOW
C
C
CCCCCCCCCCCCCCCCCCCCCCCCCCCCCCCCCCCCCCCCCCCCCCCCCCCCCCCCCCCCCCCCCCCCCCCCCCC
C                                                                         C
C     PLOTTER ROUTINE FOR POWER                                           C
C                                                                         C
CCCCCCCCCCCCCCCCCCCCCCCCCCCCCCCCCCCCCCCCCCCCCCCCCCCCCCCCCCCCCCCCCCCCCCCCCCC
C
      IF (IPLOTA.EQ.0.AND.IPLOTB.EQ.0) GO TO 9999
C
      XLNGTH=9.0
      XLEFT=0.0
      XRIGHT=(SPLFT/2.0)*(RFC/PSP)
      XINC=XRIGHT/10.0
      YLNGTH=5.0
      YINC=10.0
      NDECY=1
      MAXPTS=N
      NPTS1=N
      KIND(1)=-1
      LINES=0
C
```

```
      DATA XLABEL/'FREQ','UENC','Y (H','Z)  '/
      DATA YLABL1/'GXX ','SPEC','TRUM',' LEV','EL (','EELA','TIVE',
     &' DB)',' '/
      DATA YLABL2/'GYY ','SPEC','TRUM',' LEV','EL (','RELA','TIVE',
     &' DB)',' '/
      DATA YLABL3/'|GXY','| SP','ECTR','UM L','EVEL',' (RE','LATI',
     &'VE D','B)  '/
      DATA YLABL4/'PHAS','E (-','90  ','DEGR','EE P','HASE',' DEF',
     &'SET)',' '/
      DATA YLABL5/'DEDI','NARY',' COH','EREN','CE  '/
C
      DATA NDECX/0/,NSINGV/1/,MAXCVS/1/,NCURVS/1/,NPTS2/0/,NPTS3/0/
      DATA NPTS4/0/,NPTS5/0/
      IF (IPLOTA.EQ.0) GO TO 30
C
C-----------------------------------------------------------------------
C
C     PLOT CARDS FOR CHANNEL 1 FOLLOW THIS CARD:
C
      YBASE=0.0
      YTOP=20.0
C
      DO 110 I=1,N
      XORD(1,I)=XFREQ(I)
      YORD(1,I)=GXX(I)
  120 CONTINUE
      IF (YORD(1,I).LE.(YTOP-5.0)) GO TO 110
      YTOP=YTOP+10.0
      GO TO 120
  110 CONTINUE
      YBASE=YTOP-60.0
      IF (YORD(1,I).LT.YBASE) YORD(1,I)=YBASE
  130 CONTINUE
C
      CALL PICSIZ(14.0,7.0)
C
      CALL GRAFF(XLNGTH,XLSET,XRIGHT,XINC,NDECX,XLABEL,XORD,XDUMMY,
     &YLNGTH,YBASE,YTOP,YINC,NDECY,YLABL1,YORD,YDUMMY,NSINGV,MAXCVS,
     &NCURVS,MAXPTS,NPTS1,NPTS2,NPTS3,NPTS4,NPTS5,KIND,LINES,TITLE)
C
C-----------------------------------------------------------------------
C
C     PLOT CARDS FOR CHANNEL 2 FOLLOW THIS CARD:
C
      YBASE=0.0
      YTOP=20.0
C
      DO 200 I=1,N
      XORD(1,I)=XFREQ(I)
      YORD(1,I)=GYY(I)
  220 CONTINUE
      IF (YORD(1,I).LE.(YTOP-5.0)) GO TO 210
      YTOP=YTOP+10.0
      GO TO 220
  210 CONTINUE
      YBASE=YTOP-60.0
```

```
      IF (YORD(1,I).LT.YBASE) YORD(1,I)=YBASE
  230 CONTINUE
C
      CALL PICSIZ(14.0,7.0)
C
      CALL GRAFF(XLNGTH,XLEFT,XRIGHT,XINC,NDECX,XLABEL,XORD,XDUMMY,
     &YLNGTH,YBASE,YTOP,YINC,NDECY,YLABL2,YORD,YDUMMY,NSINGV,MAXCVS,
     &NCURVS,MAXPTS,NPTS1,NPTS2,NPTS3,NPTS4,NPTS5,KIND,LINES,TITLE)
C
C-----------------------------------------------------------------------
C
C     PLOT CARDS FOR |GXY| FOLLOW THIS CARD:
C
      YBASE=0.0
      YTOP=20.0
C
      DO 300 I=1,N
      XORD(1,I)=XFREQ(I)
      YORD(1,I)=GXYAB(I)
  320 CONTINUE
      IF (YORD(1,I).LE.(YTOP-5.)) GO TO 310
      YTOP=YTOP+10.0
      GO TO 320
  310 CONTINUE
      YBASE=YTOP-60.0
      IF (YORD(1,I).LT.YBASE) YORD(1,I)=YBASE
  300 CONTINUE
C
      CALL PICSIZ(14.0,7.0)
C
      CALL GRAFF(XLNGTH,XLEFT,XRIGHT,XINC,NDECX,XLABEL,XORD,XDUMMY,
     &YLNGTH,YBASE,YTOP,YINC,NDECY,YLABL3,YORD,YDUMMY,NSINGV,MAXCVS,
     &NCURVS,MAXPTS,NPTS1,NPTS2,NPTS3,NPTS4,NPTS5,KIND,LINES,TITLE)
C
C-----------------------------------------------------------------------
C
C     PLOT CARDS FOR PHASE FOLLOW THIS CARD:
C
      YBASE=PSBASE
      YTOP=PSTOP
      YINC=45.0
C
      DO 7330 I=1,N
      XORD(1,I)=XFREQ(I)
      YORD(1,I)=PHAZE(I)
      IF (YORD(1,I).GT.YTOP) YORD(1,I)=YTOP
      IF (YORD(1,I).LT.YBASE) YORD(1,I)=YBASE
 7330 CONTINUE
C
      CALL PICSIZ(14.0,7.0)
C
      CALL GRAFF(XLNGTH,XLEFT,XRIGHT,XINC,NDECX,XLABEL,XORD,XDUMMY,
     &YLNGTH,YBASE,YTOP,YINC,NDECY,YLABL4,YORD,YDUMMY,NSINGV,MAXCVS,
     &NCURVS,MAXPTS,NPTS1,NPTS2,NPTS3,NPTS4,NPTS5,KIND,LINES,TITLE)
C
C-----------------------------------------------------------------------
```

```
C
   10 CONTINUE
      IF (IPLOTH.EQ.0) GO TO 40
C
C     PLOT CARDS FOR CONFIGURATION FOLLOW THIS CARD:
C
      YBASE=0.0
      YTOP=1.0
      YINC=0.2
C
      DO 7040 I=1,N
      XORD(1,I)=XREC0(I)
      YORD(1,I)=COORD(I)
      IF (YORD(1,I).GT.YTOP) YORD(1,I)=YTOP
      IF (YORD(1,I).LT.YBASE) YORD(1,I)=YBASE
 7040 CONTINUE
C
      CALL PICSIZ(14.0,7.0)
C
      CALL GRAFF(XLNGTH,XLEFT,XRIGHT,XINC,NDECX,XLABEL,XORD,XDUMMY,
     &YLNGTH,YBASE,YTOP,YINC,NDECY,YLABLS,YORD,YDUMMY,NSINGV,MAXCVS,
     &NCURVS,MAXPTS,NPTS1,NPTS2,NPTS3,NPTS4,NPTS5,KIND,LINES,TITLE)
C
   40 CONTINUE
C
C-----------------------------------------------------------------------
C
      CALL PICSIZ(0.0,0.0)
C
C-----------------------------------------------------------------------
C
 9999 STOP
      END
```

```
      SUBROUTINE TRANS2
      INTEGER*2 INFIL,JUNK
      COMPLEX FFT1,FFT2,GXY,HXY,GXYP2
      DIMENSION A(1033),B(1033)
      DIMENSION GXXP2(515),GYYP2(515),GXYP2(515)
      COMMON N,IAVGS,IDLAY,ILAG1,ILAG2,KADD,IWT
      COMMON KONFI,NOTCK,FCC,PSD,PS,FSTOP,PSBASE
      COMMON SPLRT,SMEAR1,SMEAR2,REF1,REF2,REF3,HXYREF
      COMMON INFIL(4096),JUNK(20),INIT(256)
      COMMON GXX(515),GYY(515),GXYAD(515),HXYAD(515),HXYGPD(515)
      COMMON PHAZE(515),COH2(515),COSPEC(515),CTLWR(515),CTUPR(515)
      COMMON CH1(2049),CH2(2049),XFRCO(515)
      COMMON FFT1(515),FFT2(515),GXY(515),HXY(515)
      COMMON NPAS,NHIGH(10),NLOW(10)
      COMMON IDATA,CAL1,CAL2,CAL3,CAL4,CALX,CALY,CALXY
C
  100 FORMAT(40A2)
  152 FORMAT(///,' DUMP NO.',I4,' OMITTED.  NEW IAVGS=',I4)
  155 FORMAT('0POINT NUMBER',I6,' HAS A VALUE OF',I12,' ON BIOMATION DUM
     &P NO.',I4)
 4300 FORMAT ('1',////,8X,'I',7X,'GXX',8X,'GYY',6X,'GXY(REAL)',3X,
     &'GXY(IMAG)',8X,'I',7X,'GXX',8X,'GYY',6X,'GXY(REAL)',3X,
     &'GXY(IMAG)',///,(2(I10,4F12.1)))
C
      PI=3.1415927
      JAV=0
      IDUMP=0
      NOTOK=0
      INI=0
C
      DO 70 I=1,N
      GXX(I)=0.0
      GYY(I)=0.0
      GXY(I)=CMPLX(0.0,0.0)
   70 CONTINUE
C
      DO 80 I=1,KADD
      INIT(I)=INI
      INI=INI+N+N
   80 CONTINUE
C
C     THE NUMBER OF DATA POINTS SHIFTED (TIME DELAYS) IS CALCULATED ----
C
   20 IDUMP=IDUMP+1
C
      LAG1=SMEAR1/FLOAT(IAVGS)*SPLRT/1000.0*FLOAT(JAV)
      LAG2=SMEAR2/FLOAT(IAVGS)*SPLRT/1000.0*FLOAT(JAV)
C
      ILT1=ILAG1+LAG1
      ILT2=ILAG2+LAG2
C
C     THE DATA IS READ (A 4K BIOMATION DUMP) AND CHECKED FOR ERRORS ----
C
      READ (4,100) (INFIL(I),I=1,4096)
C
      DO 150 I=1,4096
```

```
      IF (INFIL(I).LT.1024.AND.INFIL(I).GE.0) GO TO 150
      NOTOK=1
      WRITE (3,155) I,INFIL(I),IDUMP
  150 CONTINUE
C
      IF (NOTOK.EQ.1) GO TO 220
      IAVGS=IAVGS+KADR
      WRITE (3,152) IDUMP,IAVGS
      NOTOK=0
C
      GO TO 90
C
  220 CONTINUE
C
C     THE FIRST 2K IS ASSIGNED TO CHANNEL 1; THE SECOND TO CHANNEL 2 ---
C
      IF (IDATA.EQ.4) GO TO 235
C
      DO 230 I=1,2048
      CH1(I)=INFIL(I)
      CH2(I)=INFIL(I+2048)
  230 CONTINUE
      CALX=CAL1
      CALY=CAL2
      CALXY=SQRT(CAL1*CAL2)
      GO TO 245
C
C     THE FOLLOWING SPECIAL CARDS ARE FOR 4-CHANNEL DATA----------------
C
  235 CONTINUE
      DO 240 I=1,1024
      CH1(I)=100.0*(INFIL(I)*CAL1-INFIL(I+1024)*CAL2)/CAL2
      CH2(I)=100.0*(INFIL(I+2048)*CAL3-INFIL(I+3072)*CAL4)/CAL4
  240 CONTINUE
      CALX=CAL2
      CALY=CAL4
      CALXY=SQRT(CALX*CALY)
C
C     IF NECESSARY, THE DATA POINTS ARE SHIFTED TO PROVIDE TIME DELAYS -
C
  245 CONTINUE
      K=0
C
 1225 CONTINUE
      NIX=1
      EVAL=0.0
      K=K+1
      JAV=JAVG(K)
      JMOV=INIT(K)+IDLAY
C
      DO 1230 I=1,N
      A(I)=CH1(I+I-1+JMOV+ILT1)
      B(I)=CH1(I+I+JMOV+ILT1)
      EVAL=EVAL+A(I)+B(I)
 1230 CONTINUE
C
```

```
C     CHANNEL 1 MEAN VALUE CORRECTION AND HANNING ----------------------
C
      EVAL=EVAL/(N*N)
C
      DO 1231 I=1,N
      A(I)=(A(I)-EVAL)
      B(I)=(B(I)-EVAL)
      IF (IWT.NE.1) GO TO 1231
      A(I)=A(I)*2.0*(SIN((I-1)*PI/(FLOAT(N))))**2
      B(I)=B(I)*2.0*(SIN((I)*PI/(FLOAT(N))))**2
 1231 CONTINUE
C
      GO TO 1275
C
 1250 EVAL=0.0
C
      DO 1255 I=1,N
      A(I)=CH2(I+I-1+JMOV+ILT2)
      B(I)=CH2(I+I+JMOV+ILT2)
      EVAL=EVAL+A(I)+B(I)
 1255 CONTINUE
C
C     CHANNEL 2 MEAN VALUE CORRECTION AND HANNING ----------------------
C
      EVAL=EVAL/(N*N)
C
      DO 1256 I=1,N
      A(I)=(A(I)-EVAL)
      B(I)=(B(I)-EVAL)
      IF (IWT.NE.1) GO TO 1256
      A(I)=A(I)*2.0*(SIN((I-1)*PI/(FLOAT(N))))**2
      B(I)=B(I)*2.0*(SIN((I)*PI/(FLOAT(N))))**2
 1256 CONTINUE
C
C-----------------------------------------------------------------------
C
 1275 CALL FFT(A,B,N,N,N,1)
      CALL REALTR(A,B,N,1)
C
C-----------------------------------------------------------------------
C
      IF (NIX.EQ.2) GO TO 1400
C
C     GXX, GYY, AND GXY ARE COMPUTED AND AVERAGED ----------------------
C
      DO 2001 I=1,N
      FFT1(I)=CMPLX(A(I),B(I))
      GXX(I)=GXX(I)+REAL(CONJG(FFT1(I))*FFT1(I))
 2001 CONTINUE
C
      NIX=2
      GO TO 1250
C
 1400 DO 2002 I=1,N
      FFT2(I)=CMPLX(A(I),B(I))
      GYY(I)=GYY(I)+REAL(CONJG(FFT2(I))*FFT2(I))
```

```
      GXY(I)=GXY(I)+CONJG(FFT2(I))*FFT1(I)
 2222 CONTINUE
C
C     IF ALL THE REQUESTED AVERAGES ('IAVGS') HAVE BEEN TAKEN, STOP
C     READING DATA FROM THE DATA SOURCE ------------------------------
      IF (JAV.GE.IAVGS) GO TO 4000
C
C     IF ALL THE POSSIBLE AVERAGES ('KADP') ARE USED IN A SINGLE 4K
C     DIGITATION DUMP, GO GET ANOTHER DUMP'S WORTH OF DATA -----------
      IF (K.GE.KADP) GO TO 33
C
      GO TO 1225
C
C     END OF AVERAGING.  AUTO AND CROSS-SPECTRUM VALUES ARE CORRECTED
C     WITH FFT PROGRAM FACTORS.---------------------------------------
C
 4000 CONTINUE
      DNORM=4*N*N*IAVGS
      DO 4100 I=1,N
      GXX(I)=GXX(I)/DNORM
      GYY(I)=GYY(I)/DNORM
      GXY(I)=GXY(I)/DNORM
      GXXP2(I)=GXX(I)*(CALX**2)
      GYYP2(I)=GYY(I)*(CALY**2)
      GXYP2(I)=GXY(I)*(CALXY**2)
 4100 CONTINUE
C
      WRITE (3,4310) (I,GXXP2(I),GYYP2(I),GXYP2(I),I=1,N)
C
 9999 RETURN
      END
```

```
      SUBROUTINE XPLOW
      INTEGER*2 INFIL,JUNK
      COMPLEX FFT1,FFT2,GXY,HXY
      COMMON N,NAVGS,IDLAY,ILAG1,ILAG2,KADR,IWT
      COMMON KONFI,NOTOK,FEC,FF2,DS,FSTOP,DSBASE
      COMMON SPLRT,SMEAR1,SMEAR2,FF1,FF2,FF3,HXYFFF
      COMMON INFIL(4096),JUNK(23),INIT(256)
      COMMON GXX(515),GYY(515),GXYAB(515),HXYAB(515),HXYOBD(515)
      COMMON PHAZE(515),COHR(515),COSPEC(515),CILWR(515),CIUPR(515)
      COMMON CH1(2048),CH2(2048),XFREQ(515)
      COMMON FFT1(515),FFT2(515),GXY(515),HXY(515)
      COMMON NPAS,NUTH(10),NLOW(10)
      COMMON IDATA,CAL1,CAL2,CAL3,CAL4,CALX,CALY,CALXY
C
 3461 FORMAT('0',///,' IN THE FREQUENCY BAND FROM',F8.1,' HZ TO',F8.1,
     &' HZ THE OVERALL LEVELS ARE AS FOLLOWS:',//,
     &' GXX:',E7.1,' OR, RE:',F9.6,//,
     &' GYY:',E7.1,' OR, RE:',F9.6,//,
     &' GXY:',E7.1,' OR, RE:',F9.6,//,
     &' COHERENCE:',E7.3,//,
     &' COHERENT SPECTRUM LEVEL:',E7.2,' OR, RE:',F9.6)
 3622 FORMAT ('0',///,7X,'I      FREQ      GXX       GYY     |GXY|    |HXY|
     & HXYOBD    PHASE-HXY    COHERENCE    CIUPR    CILWR    CO-SPECTRUM',
     &/////)
 3700 FORMAT (5X,I4,F9.1,3F8.1,F11.1,F14.4,F10.4,F9.4,F9.1)
C
      PS1=PF1**2
      PS2=PF2**2
      PS3=PF3**2
      HXYPS0=HXYFFF**2
C
      GXXT=0.0
      GYYT=0.0
      GXYT=0.0
C
      DO 2000 I=1,N
C
CC    THE COHERENCE, CO-SPECTRUM AND PHASE BETWEEN X & Y ARE COMPUTED --
C
      PMIN=(1.0/N)**2
      PROD=GXX(I)*GYY(I)
      IF(ABS(PROD).LT.PMIN) PROD=PMIN
C
      COHR(I)=REAL(GXY(I)*CONJG(GXY(I)))/PROD
      HXY(I)=GXY(I)/GXX(I)
C
CC    SET COHERENCE TO ZERO IF EITHER GXX OR GYY ARE LESS THAN 'CUTOFF'.
CC    THIS IS A LOWER LIMIT (DETERMINED BY THE NUMBER OF A/D BITS AND
C     FREQ LINES) SET TO PREVENT COMPUTER ERRORS FROM BECOMING TOO
C     GREAT.  THE RANGE OF THE MAGNITUDE OF THE DATA AT THIS POINT
C     LIES BETWEEN 0**2 AND 512**2 (FOR 10-BIT WORDS). ----------------
C
      CUTOFF=1.0/N
      IF (GXX(I).LT.CUTOFF.OR.GYY(I).LT.CUTOFF) COHR(I)=0.0
C
C     APPLY BIAS CORRECTION TO COHERENCE ESTIMATE ----------------------
```

```
C
      W=1.0
      IF (IWT.EQ.1) W=1.5
      COHP(I)=COHP(I)-(1.0-COHR(I))/(2.0*W*FLOAT(IAVGS))
      IF (COHP(I).LE.0.0) GO TO 1500
C
      TANUP=AIMAG(HXY(I))
      RCHK=REAL(HXY(I))
      IF (ABS(RCHK).LT.EMIN) RCHK=EMIN
C
      PHAZE(I)=57.296*ATAN2(TANUP,RCHK)
C
C     THE PHASE OFFSET FOR PLOTTING THE PHASE IS INTRODUCED ------------
C
      PSTOP=PS+180.0
      PSPASE=PS-180.0
C
      IF (PHAZE(I).GT.PSTOP) PHAZE(I)=PHAZE(I)-360.0
      IF (PHAZE(I).LT.PSPASE) PHAZE(I)=PHAZE(I)+360.0
C
      GO TO 1501
C
 1500 COHR(I)=0.0
      PHAZE(I)=0.0
      IF (I.EQ.1) GO TO 1501
      PHAZE(I)=PHAZE(I-1)
C
 1501 CONTINUE
      CIUPR(I)=0.0
      CILWR(I)=0.0
      IF (KONFI.EQ.0) GO TO 2000
C
C     DETERMINE THE COHERENCE 95% CONFIDENCE INTERVAL ------------------
C
      ZA=1.96
      AVGS=IAVGS
      D=0.5/(AVGS-1.0)
      COHC=COHR(I)
      COH=SQRT(COHC)
      VARI=SQRT(D)*(1.0-0.334**(1.6*COHC+0.22))
      Z=0.5*ALOG((1.0+COH)/(1.0-COH))
      CMIN=TANH(Z-D-ZA*VARI)
      IF(CMIN.LT.0.0) CMIN=0.0
      CMIN=CMIN*CMIN
      CMAX=(TANH(Z-D+ZA*VARI))**2
      CIUPR(I)=CMAX
      CILWR(I)=CMIN
C
C     THE TRANSFER FUNCTION, NET CROSS SPECTRUM AND X & Y CHANNEL
C     SPECTRUMS, AND OTHER VALUES ARE COMPUTED -------------------------
C
      GXY(I)=GXX(I)*(CALX**2)
      GYY(I)=GYY(I)*(CALY**2)
      GXY(I)=GYY(I)*(CALXY**2)
      HXY(I)=HXY(I)*(CALY/CALX)
C
```

```
      CORSPEC(I)=GYY(I)*COHF(I)
      HYY(IFR(I))=GYY(I)/GXX(I)
      GXYAB(I)=CABS(GXY(I))
      HYYAB(I)=CABS(HXY(I))
      GXXT=GXXT+GXX(I)
      GYYT=GYYT+GYY(I)
      GXYT=GXYT+GXYAB(I)
C
C     THE CORRESPONDING BAND CENTER FREQUENCIES ARE COMPUTED ----------
C
      XI=I-1
      XFREQ(I)=(XI*SPLIT*FFC)/(2.0*N*FFR)
C
 2000 CONTINUE
C
      IF (NPAS.LE.0) GO TO 2400
C
C     THE OVERALL COHERENCE, ETC., FOR CHOSEN BANDS IS COMPUTED --------
C
      DO 2500 I=1,NPAS
C
      GXXTB=0.0
      GYYTB=0.0
      GXYTB=0.0
C
      KL=NLOW(I)
      KH=NHIH(I)
C
      DO 2600 J=KL,KH
      GXXTB=GXXTB+GXX(J)
      GYYTB=GYYTB+GYY(J)
      GXYTB=GXYTB+GXYAB(J)
 2600 CONTINUE
C
      COTOTB=(GXYTB*GXYTB)/(GXXTB*GYYTB)
      CORSDB=COTOTB*GYYTB
C
      GXXTB=10.0*ALOG10(GXXTB/RS1)
      GYYTB=10.0*ALOG10(GYYTB/RS2)
      GXYTB=10.0*ALOG10(GXYTB/RS3)
      CORSDB=10.0*ALOG10(CORSDB/RS2)
C
      WRITE (3,3400) XFREQ(KL),XFREQ(KH),GXXTB,RE1,GYYTB,RE2,GXYTB,RE3,
     &COTOTB,CORSDB,RE2
C
 2500 CONTINUE
C
 2400 CONTINUE
C
      COTOT=(GXYT*GXYT)/(GXXT*GYYT)
      CORSD=COTOT*GYYT
C
      GXXT=10.0*ALOG10(GXXT/RS1)
      GYYT=10.0*ALOG10(GYYT/RS2)
      GXYT=10.0*ALOG10(GXYT/RS3)
      CORSD=10.0*ALOG10(CORSD/RS2)
```

```
C
C       THE COHERENCE AND OTHER VALUES FOR EACH BAND IS COMPUTED ---------
C
        CUTX=CUTOFF*CALX**2
        CUTY=CUTOFF*CALY**2
        CUTXY=CUTOFF*CALXY**2
C
        DO 3400 I=1,N
C
        IF (GXX(I).LT.CUTX) GXX(I)=CUTX
        IF (GYY(I).LT.CUTY) GYY(I)=CUTY
        IF (GXYAB(I).LT.CUTXY) GXYAB(I)=CUTXY
        IF (COSPEC(I).LT.CUTY*(COHR(I)+0.001)) COSPEC(I)=
     &CUTY*(COHR(I)+0.001)
        IF (HXYAB(I).LT.SQRT(CUTY/CUTX)) HXYAB(I)=SQRT(CUTY/CUTX)
        IF (HXYORD(I).LT.(CUTY/CUTX)) HXYORD(I)=(CUTY/CUTX)
C
        GXX(I)=10.0*ALOG10(GXX(I)/RS1)
        GYY(I)=10.0*ALOG10(GYY(I)/RS2)
        GXYAB(I)=10.0*ALOG10(GXYAB(I)/RS3)
        COSPEC(I)=10.0*ALOG10(COSPEC(I)/RS2)
        HXYAB(I)=10.0*ALOG10(HXYAB(I)/HXYFS0)
        HXYORD(I)=ALOG10(HXYORD(I)/(HXYFS0**2))
C
 3400 CONTINUE
C
C
        HXYAB(1)=0.0
        HXYORD(1)=0.0
        PHAZE(1)=0.0
C
        WRITE (3,3460) XFREQ(1),XFREQ(N),GXXT,RF1,GYYT,RF2,GXYT,PE3,
     &COTOT,CUPSD,RF2
        WRITE (3,3600)
        WRITE (3,3700) (I,XFREQ(I),GXX(I),GYY(I),GXYAB(I),HXYAB(I),
     &HXYORD(I),PHAZE(I),COHR(I),CIUPP(I),CILWR(I),COSPEC(I),I=1,N)
C
 9999 RETURN
        END
```

11.3 PARTIAL

The four-channel program "PARTIAL":

1) removes the overall mean from each of the four time series sample records and amplitude weights each time series with a Hanning ($\sin^2$) function.

2) computes the spectral values for G_{11}, G_{22}, G_{33}, G_{yy}, G_{y1}, G_{y2}, G_{y3}, G_{12}, G_{13}, and G_{23}, via the FFT.

3) averages the above quantities by repeating steps 1 and 2.

4) computes the ordinary coherences.

5) computes the partial coherences.

6) can then scale the PSD quantities against a reference standard to obtain calibrated values if a reference and calibration level are supplied typically from the output of COHERENC, step 11).

7) outputs all above-mentioned averaged quantities on a printout.

8) automatically will scale the plot axes and then plot the $\hat{G}_{y1}$, $\hat{G}_{y2}$, $\hat{G}_{y3}$, $\hat{\gamma}^2_{12}$, $\hat{\gamma}^2_{13}$, $\hat{\gamma}^2_{23}$, $\hat{\gamma}^2_{1y\cdot 23}$, $\hat{\gamma}^2_{2y\cdot 13}$, $\hat{\gamma}^2_{3y\cdot 12}$.

```
      INTEGER*2 INFIL
      COMPLEX FFT1,FFT2,FFT3,FFT4
      COMPLEX SYY,SYP,SPY,SPP,SYNP,SYNPY,GXYP,PCOH,GXYD
      COMPLEX GYY,G11,G22,G33,GY1,GY2,GY3,G12,G13,G23,GAG
      DIMENSION INFIL(40),FREQ(515)
      DIMENSION CH1(1024),CH2(1024),CH3(1024),CH4(1024)
      DIMENSION GYY(515),G11(515),G22(515),G33(515),GY1(515),GY2(515)
      DIMENSION GY3(515),G12(515),G13(515),G23(515),GAG(1),SYY(4)
      DIMENSION FFT1(515),FFT2(515),FFT3(515),FFT4(515)
      DIMENSION SYP(4),SPY(4),SPP(4),SYNP(4),SYNPY(4),A(515),B(515)
      DIMENSION GXYP(4),PCOH(3,515)
      DIMENSION XDBD(1,515),YDBD(1,515),XDUMMY(1,515),YDUMMY(1,515)
      DIMENSION YLABE2(20),YLABE3(20)
      DIMENSION KIND(5),XLABEL(20),YLABEL(20),TITL1(20),TITL2(20)
      DIMENSION TITL3(20),TITL4(20),TITL5(20),TITL6(20)
C
  152 FORMAT(///,' DUMP NO.',I4,' OMITTED.  NEW IAVGS=',I4)
  155 FORMAT('0POINT NUMBER',I6,' HAS A VALUE OF',I12,' ON RIOMATION DUM
     1P NO.',I4)
  200 FORMAT (20A4)
 1101 FORMAT(40A2)
 1210 FORMAT ('1',////,8X,'I',15X,'GYY',15X,'G11',19X,'G22',19X,
     &'G33',19X,'GY1',//,17X,'REAL',7X,'IMAG',7X,'REAL',7X,'IMAG',7X,
     &'REAL',7X,'IMAG',7X,'REAL',7X,'IMAG',7X,'REAL',7X,'IMAG',//)
 1211 FORMAT ('1',////,8X,'I',15X,'GY2',19X,'GY3',19X,'G12',19X,
     &'G13',19X,'G23',//,17X,'REAL',7X,'IMAG',7X,'REAL',7X,'IMAG',7X,
     &'REAL',7X,'IMAG',7X,'REAL',7X,'IMAG',7X,'REAL',7X,'IMAG',//)
 1276 FORMAT (21X,I4,2E20.2)
 2460 FORMAT(///,' CMINV FAILED AT FREQ. COMP.',I4,' OF CHANNEL',I2,'
     &D1=',E8.1,'  D2=',E8.1,//)
 4041 FORMAT ('1',////,8X,'MAGNITUDE OF CROSS-SPECTRUM BETWEEN CHANNEL 1
     & AND THE OUTPUT CHANNEL 4:',//,8X,20A4,///,23X,'I',13X,'FREQUENCY'
     &,14X,'X-SPEC',//)
 4041 FORMAT ('1',////,8X,'MAGNITUDE OF CROSS-SPECTRUM BETWEEN CHANNEL 2
     & AND THE OUTPUT CHANNEL 4:',//,8X,20A4,///,23X,'I',13X,'FREQUENCY'
     &,14X,'X-SPEC',//)
 4042 FORMAT ('1',////,8X,'MAGNITUDE OF CROSS-SPECTRUM BETWEEN CHANNEL 3
     & AND THE OUTPUT CHANNEL 4:',//,8X,20A4,///,23X,'I',13X,'FREQUENCY'
     &,14X,'X-SPEC',//)
 4050 FORMAT ('1',////,8X,'ORDINARY COHERENCE BETWEEN CHANNELS 1 AND 2:'
     &,//,8X,20A4,///,23X,'I',13X,'FREQUENCY',12X,'COHERENCE',//)
 4051 FORMAT ('1',////,8X,'ORDINARY COHERENCE BETWEEN CHANNELS 1 AND 3:'
     &,//,8X,20A4,///,23X,'I',13X,'FREQUENCY',12X,'COHERENCE',//)
 4052 FORMAT ('1',////,8X,'ORDINARY COHERENCE BETWEEN CHANNELS 2 AND 3:'
     &,//,8X,20A4,///,23X,'I',13X,'FREQUENCY',12X,'COHERENCE',//)
 4060 FORMAT ('1',////,8X,'PARTIAL COHERENCE BETWEEN CHANNEL 1 AND THE O
     &UTPUT CHANNEL 4:',//,8X,20A4,///,23X,'I',13X,'FREQUENCY',
     &12X,'COHERENCE',//)
 4061 FORMAT ('1',////,8X,'PARTIAL COHERENCE BETWEEN CHANNEL 2 AND THE O
     &UTPUT CHANNEL 4:',//,8X,20A4,///,23X,'I',13X,'FREQUENCY',
     &12X,'COHERENCE',//)
 4062 FORMAT ('1',////,8X,'PARTIAL COHERENCE BETWEEN CHANNEL 3 AND THE O
     &UTPUT CHANNEL 4:',//,8X,20A4,///,23X,'I',13X,'FREQUENCY',
     &12X,'COHERENCE',//)
 4221 FORMAT (6X,I4,10F11.1)
C
```

```
C
C     'IPLOTA' = 1 PLOTS THE MAGNITUDE OF THE CROSS-SPECTRUM BETWEEN
C     INPUT CHANNELS 1,2, & 3 V.S. THE OUTPUT CHANNEL 4; = 0 DOES NOT.
C
C     'IPLOTB' = 1 PLOTS THE ORDINARY COHERENCE BETWEEN INPUT CHANNELS
C     1 & 2, 1 & 3, AND 2 & 3; = 0 DOES NOT.
C
C     'IPLOTC' = 1 PLOTS THE PARTIAL COHERENCE BETWEEN INPUT CHANNELS
C     1,2, & 3 V.S. THE OUTPUT CHANNEL 4; = 0 DOES NOT.
C
C     'REC' IS THE DATA RECORDING SPEED IN IN/SEC OR CM/SEC.
C     'REP' IS THE DATA REPRODUCING SPEED IN IN/SEC OR CM/SEC.
C     IF NOT APPLICABLE, SET REC=REP=1.0
C
C
      IPLOTA=1
      IPLOTB=1
      IPLOTC=1
C
      REC=60.0
      REP=15.0
C
C
C     'N' = ONE-HALF THE NUMBER OF DATA POINTS PER TIME RECORD;  I.E.,
C     N = THE NUMBER OF SPECTRAL LINES.
C
C     'IAVGS' IS THE NUMBER OF AVERAGES PER FREQUENCY LINE.
C
C     'SPLRT' IS THE SAMPLING RATE IN HZ.
C
C     'REF' IS THE REFERENCE VALUE FOR THE DECIBEL SCALE.
C
C     'KADP' = THE NUMBER OF AVERAGES PER BIOMATION DUMP.  THERE ARE
C     4096 10-BIT WORDS OF DATA POINTS PER CHANNEL.  WHEN EACH DUMP
C     IS DIVIDED INTO FOURTHS, IT YIELDS 1024 DATA POINTS AVAILABLE PER
C     CHANNEL.  FROM THIS, ONE AVERAGE PER DUMP (WITH 1024 POINTS PER
C     CHANNEL) MAY BE REALIZED, OR TWO AVERAGES PER DUMP (WITH 512
C     POINTS PER CHANNEL) MAY BE REALIZED, ETC.     KADP = ((512/N)
C
C
      N=512
      IAVGS=32
      SPLRT=5000.0
      REF=1.0
C
      KADP=512/N
C
C
C     'CAL#A' = SPL OF THE MIC. CAL. SOURCE EXPRESSED IN DB FOR
C     CHANNELS 1,2,3, & 4.
C
```

```
C      'CAL#B' = DB READING OFF THE CALIBRATION PROGRAM IN THE           C
C      FREQUENCY BANDS OF THE CAL. SOURCE WHEN 'ICATA' = 1.              C
C                                                                        C
C      'GAIN#' = NET DIFFERENCE IN GAIN OF (ACTUAL DATA RUN KNOB         C
C      SETTINGS)-(CAL. RUN KNOB SETTINGS) EXPRESSED IN DB.               C
C                                                                        C
CCCCCCCCCCCCCCCCCCCCCCCCCCCCCCCCCCCCCCCCCCCCCCCCCCCCCCCCCCCCCCCCCCCCCCCCC
C
      CAL1A=0.0
      CAL2A=112.5
      CAL3A=112.5
      CAL4A=124.0
C
      CAL1B=0.0
      CAL2B=47.8
      CAL3B=50.0
      CAL4B=46.8
C
      GAIN1=0.0
      GAIN2=35.0
      GAIN3=35.0
      GAIN4=35.0
C
      CAL1=10.0**((CAL1A-CAL1B-GAIN1)/20.0)
      CAL2=10.0**((CAL2A-CAL2B-GAIN2)/20.0)
      CAL3=10.0**((CAL3A-CAL3B-GAIN3)/20.0)
      CAL4=10.0**((CAL4A-CAL4B-GAIN4)/20.0)
C
      DO 1200 I=1,N
      GVV(I)=CMPLX(0.0,0.0)
      G11(I)=CMPLX(0.0,0.0)
      G22(I)=CMPLX(0.0,0.0)
      G33(I)=CMPLX(0.0,0.0)
      GV1(I)=CMPLX(0.0,0.0)
      GV2(I)=CMPLX(0.0,0.0)
      GV3(I)=CMPLX(0.0,0.0)
      G12(I)=CMPLX(0.0,0.0)
      G13(I)=CMPLX(0.0,0.0)
      G23(I)=CMPLX(0.0,0.0)
 1200 CONTINUE
C
      PI=3.1415927
      IDUMP=0
      NOTOK=0
 1515 IDUMP=IDUMP+1
      K=0
C
C     THE DATA IS READ (A 4K BIOMATION DUMP) AND CHECKED FOR ERRORS.-----
C
      READ (4,1100) (INFIL(I),I=1,4096)
C
      DO 150 I=1,4096
      IF (INFIL(I).LT.1024.AND.INFIL(I).GE.0) GO TO 150
      NOTOK=1
      WRITE (3,155) I,INFIL(I),IDUMP
  150 CONTINUE
```

```
C
      IF (NOTOK.EQ.0) GO TO 123
      IAVGS=IAVGS-1
      IDUMP=IDUMP-1
      WRITE (3,152) IDUMP,IAVGS
      NOTOK=0
C
      GO TO 1515
C
  123 CONTINUE
      JMOV=0
 1616 CONTINUE
      K=K+1
C
C     THE FIRST 1K IS ASSIGNED TO CH1, THE SECOND TO CH2, ETC.----------
C
      DO 11 I=1,1024
      CH1(I)=INFIL(I)*CAL1
      CH2(I)=INFIL(I+1024)*CAL2
      CH3(I)=INFIL(I+2048)*CAL3
      CH4(I)=INFIL(I+3072)*CAL4
   11 CONTINUE
C
C
      EVAL=0.0
C
      DO 22 I=1,N
      A(I)=CH1(I+I+JMOV-1)
      B(I)=CH1(I+I+JMOV)
      EVAL=EVAL+A(I)+B(I)
   22 CONTINUE
C
      EVAL=EVAL/FLOAT(N+N)
C
      DO 33 I=1,N
      A(I)=(A(I)-EVAL)*2.0*(SIN((I-1)*PI/(FLOAT(N))))**2
      B(I)=(B(I)-EVAL)*2.0*(SIN((I*PI)/(FLOAT(N))))**2
   33 CONTINUE
C
      CALL FFT(A,B,N,N,N,1)
      CALL REALTP(A,B,N,1)
C
      DO 44 I=1,N
      FFT1(I)=CMPLX(A(I),B(I))
      G11(I)=G11(I)+CONJG(FFT1(I))*FFT1(I)
   44 CONTINUE
C
C
      EVAL=0.0
C
      DO 55 I=1,N
      A(I)=CH2(I+I+JMOV-1)
      B(I)=CH2(I+I+JMOV)
      EVAL=EVAL+A(I)+B(I)
   55 CONTINUE
C
```

```
      EVAL=EVAL/FLOAT(N+N)
C
      DO 66 I=1,N
      A(I)=(A(I)-EVAL)*2.0*(SIN((I-1)*PI/(FLOAT(N))))**2
      B(I)=(B(I)-EVAL)*2.0*(SIN((I*PI)/(FLOAT(N))))**2
   66 CONTINUE
C
      CALL FFT(A,B,N,N,N,1)
      CALL REALTR(A,B,N,1)
C
      DO 77 I=1,N
      FFT2(I)=CMPLX(A(I),B(I))
      G22(I)=G22(I)+CONJG(FFT2(I))*FFT2(I)
   77 CONTINUE
C
C
      EVAL=0.0
C
      DO 88 I=1,N
      A(I)=CH3(I+I+JMOV-1)
      B(I)=CH3(I+I+JMOV)
      EVAL=EVAL+A(I)+B(I)
   88 CONTINUE
C
      EVAL=EVAL/FLOAT(N+N)
C
      DO 99 I=1,N
      A(I)=(A(I)-EVAL)*2.0*(SIN((I-1)*PI/(FLOAT(N))))**2
      B(I)=(B(I)-EVAL)*2.0*(SIN((I*PI)/(FLOAT(N))))**2
   99 CONTINUE
C
      CALL FFT(A,B,N,N,N,1)
      CALL REALTR(A,B,N,1)
C
      DO 1010 I=1,N
      FFT3(I)=CMPLX(A(I),B(I))
      G33(I)=G33(I)+CONJG(FFT3(I))*FFT3(I)
 1010 CONTINUE
C
C
      EVAL=0.0
C
      DO 1111 I=1,N
      A(I)=CH4(I+I+JMOV-1)
      B(I)=CH4(I+I+JMOV)
      EVAL=EVAL+A(I)+B(I)
 1111 CONTINUE
C
      EVAL=EVAL/FLOAT(N+N)
C
      DO 1212 I=1,N
      A(I)=(A(I)-EVAL)*2.0*(SIN((I-1)*PI/(FLOAT(N))))**2
      B(I)=(B(I)-EVAL)*2.0*(SIN((I*PI)/(FLOAT(N))))**2
 1212 CONTINUE
C
      CALL FFT(A,B,N,N,N,1)
```

```
      CALL REALTR(A,B,N,1)
C
      DO 1313 I=1,N
      FFT4(I)=CMPLX(A(I),B(I))
      GYY(I)=GYY(I)+CONJG(FFT4(I))*FFT4(I)
 1313 CONTINUE
C
C
      DO 1414 I=1,N
      GY1(I)=GY1(I)+FFT1(I)*CONJG(FFT4(I))
      GY2(I)=GY2(I)+FFT2(I)*CONJG(FFT4(I))
      GY3(I)=GY3(I)+FFT3(I)*CONJG(FFT4(I))
      G12(I)=G12(I)+FFT2(I)*CONJG(FFT1(I))
      G13(I)=G13(I)+FFT3(I)*CONJG(FFT1(I))
      G23(I)=G23(I)+FFT3(I)*CONJG(FFT2(I))
 1414 CONTINUE
C
C
      IF (IDUMO.EQ.IAVGS) GO TO 1717
      IF (K.EQ.KADD) GO TO 1515
      JMOV=JMOV+N+N
      GO TO 1616
C
 1717 CONTINUE
C
C
C     END OF AVERAGING.  AUTO AND CROSS-SPECTRUM VALUES ARE CORRECTED
C     WITH FFT PROGRAM FACTORS.-----------------------------------------
C
 4000 DNORM=4.*N*IAVGS*N
C
      DO 4100 I=1,N
      GYY(I)=GYY(I)/DNORM
      G11(I)=G11(I)/DNORM
      G22(I)=G22(I)/DNORM
      G33(I)=G33(I)/DNORM
      GY1(I)=GY1(I)/DNORM
      GY2(I)=GY2(I)/DNORM
      GY3(I)=GY3(I)/DNORM
      G12(I)=G12(I)/DNORM
      G13(I)=G13(I)/DNORM
      G23(I)=G23(I)/DNORM
 4100 CONTINUE
C
      WRITE (3,1216)
      WRITE (3,4201) (I,GYY(I),G11(I),G22(I),G33(I),GY1(I),I=1,N)
      WRITE (3,1217)
      WRITE (3,4201) (I,GY2(I),GY3(I),G12(I),G13(I),G23(I),I=1,N)
C
C     PARAMETERS FOR PLOTTING ARE INPUTED-------------------------------
C
      READ (1,200) (TITL1(I),I=1,20)
      READ (1,200) (TITL2(I),I=1,20)
      READ (1,200) (TITL3(I),I=1,20)
      READ (1,200) (TITL4(I),I=1,20)
      READ (1,200) (TITL5(I),I=1,20)
```

```
      READ (1,200) (TITLS(I),I=1,20)
C
      XLNGTH=8.0
      XLEFT=0.0
      XRIGHT=(SPLPT/2.0)*(REC/REP)
      XINC=XRIGHT/10.0
      YLNGTH=5.0
      YINC=10.
      NDECY=1
      MAXPTS=N
      NPTS1=N
      KIND(1)=1
      LINES=0
C
      DATA XLABEL/'FREQ','UENC','Y (H','Z.) '/
      DATA YLABEL/'POWE','R SP','ECTR','AL D','ENSI','TY  ','(DB)','_'/
      DATA YLABE2/'PART','IAL ','COHE','RENC','E_'/
      DATA YLABE3/'ORDI','NATE','  OH','EREN','CE_'/
C
      DATA NDECX/0/,NSINGV/1/,MAXCVS/1/,NCURVS/1/,NPTS2/0/,NPTS3/0/
      DATA NPTS4/0/,NPTS5/0/
C
C-----------------------------------------------------------------------
C
C     PLOT CARDS FOR |GY1| FOLLOW THIS CARD:
C
      YBASE=0.0
      YTOP=20.0
C
      DO 111 I=1,N
      XI=I-1
      FREQ(I)=(SPLPT*REC*XI)/(2.0*REP*FLOAT(N))
      XORD(1,I)=FREQ(I)
      YORD(1,I)=SQRT(REAL(CONJG(GY1(I))*GY1(I)))
      YORD(1,I)=10.*ALOG10(YORD(1,I)/REF)
  120 CONTINUE
      IF (YORD(1,I).LE.(YTOP-5.0)) GO TO 110
      YTOP=YTOP+10.0
      GO TO 120
  110 CONTINUE
      YBASE=YTOP-60.0
      IF (YORD(1,I).LT.YBASE) YORD(1,I)=YBASE
  111 CONTINUE
C
      WRITE (3,4040) (TITL1(I),I=1,20)
      WRITE (3,1976) (1,XORD(1,I),YORD(1,I),I=1,N)
C
      IF (IPLOTA.EQ.0) GO TO 10
      CALL PICSIZ (14.0,7.0)
      CALL GRAFF (XLNGTH,XLEFT,XRIGHT,XINC,NDECX,XLABEL,XORD,XDUMMY,YLNG
     ?TH,YBASE,YTOP,YINC,NDECY,YLABEL,YORD,YDUMMY,NSINGV,MAXCVS,NCURVS,M
     ?AXPTS,NPTS1,NPTS2,NPTS3,NPTS4,NPTS5,KIND,LINES,TITL1)
   10 CONTINUE
C
C-----------------------------------------------------------------------
C
```

```
C       PLOT CARDS FOR |GY2| FOLLOW THIS CARD:
C
        YBASE=0.0
        YTOP=20.0
C
        DO 220 I=1,N
        XORD(1,I)=FREQ(I)
        YORD(1,I)=SQRT(REAL(CONJG(GY2(I))*GY2(I)))
        YORD(1,I)=10.*ALOG10(YORD(1,I)/REF)
  220 CONTINUE
        IF (YORD(1,I).LE.(YTOP-5.0)) GO TO 210
        YTOP=YTOP+10.0
        GO TO 220
  210 CONTINUE
        YBASE=YTOP-60.0
        IF (YORD(1,I).LT.YBASE) YORD(1,I)=YBASE
  222 CONTINUE
C
        WRITE (3,4041) (TITL2(I),I=1,20)
        WRITE (3,1976) (I,XORD(1,I),YORD(1,I),I=1,N)
C
        IF (IPLOTA.EQ.0) GO TO 20
        CALL PICSIZ (14.0,7.0)
        CALL GRAFF (XLNGTH,XLEFT,XRIGHT,XINC,NDECX,XLABEL,XORD,XDUMMY,YLNG
       ?TH,YBASE,YTOP,YINC,NDECY,YLABEL,YORD,YDUMMY,NSINGV,MAXCVS,NCURVS,M
       ?AXPTS,NPTS1,NPTS2,NPTS3,NPTS4,NPTS5,KIND,LINES,TITL2)
   20 CONTINUE
C
C-----------------------------------------------------------------------
C
C       PLOT CARDS FOR |GY3| FOLLOW THIS CARD:
C
        YBASE=0.0
        YTOP=20.0
C
        DO 333 I=1,N
        XORD(1,I)=FREQ(I)
        YORD(1,I)=SQRT(REAL(CONJG(GY3(I))*GY3(I)))
        YORD(1,I)=10.*ALOG10(YORD(1,I)/REF)
  320 CONTINUE
        IF (YORD(1,I).LE.(YTOP-5.0)) GO TO 310
        YTOP=YTOP+10.0
        GO TO 320
  310 CONTINUE
        YBASE=YTOP-60.0
        IF (YORD(1,I).LT.YBASE) YORD(1,I)=YBASE
  333 CONTINUE
C
        WRITE (3,4042) (TITL3(I),I=1,20)
        WRITE (3,1976) (I,XORD(1,I),YORD(1,I),I=1,N)
C
        IF (IPLOTA.EQ.0) GO TO 30
        CALL PICSIZ (14.0,7.0)
        CALL GRAFF (XLNGTH,XLEFT,XRIGHT,XINC,NDECX,XLABEL,XORD,XDUMMY,YLNG
       ?TH,YBASE,YTOP,YINC,NDECY,YLABEL,YORD,YDUMMY,NSINGV,MAXCVS,NCURVS,M
       ?AXPTS,NPTS1,NPTS2,NPTS3,NPTS4,NPTS5,KIND,LINES,TITL3)
```

```
   30 CONTINUE
C
C-----------------------------------------------------------------------
C
      DO 300 I=1,N
      PCOH(1,I)=CONJG(G12(I))*G12(I)/(G11(I)*G22(I))
      PCOH(2,I)=CONJG(G13(I))*G13(I)/(G11(I)*G33(I))
      PCOH(3,I)=CONJG(G23(I))*G23(I)/(G22(I)*G33(I))
  300 CONTINUE
C
C-----------------------------------------------------------------------
C
C     PLOT CARDS FOR THE ORDINARY COHERENCE BETWEEN CH1 & CH2
C     FOLLOW THIS CARD:
C
      YBASE=0.0
      YTOP=1.0
      YINC=0.2
C
      DO 1980 I=1,N
      YORD(1,I)=REAL(PCOH(1,I))
      XORD(1,I)=FREQ(I)
 1980 CONTINUE
C
      WRITE (3,4050) (TITL4(I),I=1,20)
      WRITE (3,1976) (I,XORD(1,I),YORD(1,I),I=1,N)
C
      IF (IPLOTR.EQ.0) GO TO 40
      CALL PICSIZ (14.0,7.0)
      CALL GRAFF (XLNGTH,XLEFT,XRIGHT,XINC,NDECX,XLABEL,XORD,XDUMMY,YLNG
     ?TH,YBASE,YTOP,YINC,NDECY,YLABEL,YORD,YDUMMY,NSINGV,MAXCVS,NCURVS,M
     ?AXPTS,NPTS1,NPTS2,NPTS3,NPTS4,NPTS5,KIND,LINES,TITL4)
   40 CONTINUE
C
C-----------------------------------------------------------------------
C
C     PLOT CARDS FOR THE ORDINARY COHERENCE BETWEEN CH1 & CH3
C     FOLLOW THIS CARD:
C
      DO 1981 I=1,N
      YORD(1,I)=REAL(PCOH(2,I))
      XORD(1,I)=FREQ(I)
 1981 CONTINUE
C
      WRITE (3,4051) (TITL5(I),I=1,20)
      WRITE (3,1976) (I,XORD(1,I),YORD(1,I),I=1,N)
C
      IF (IPLOTR.EQ.0) GO TO 50
      CALL PICSIZ (14.0,7.0)
      CALL GRAFF (XLNGTH,XLEFT,XRIGHT,XINC,NDECX,XLABEL,XORD,XDUMMY,YLNG
     ?TH,YBASE,YTOP,YINC,NDECY,YLABEL,YORD,YDUMMY,NSINGV,MAXCVS,NCURVS,M
     ?AXPTS,NPTS1,NPTS2,NPTS3,NPTS4,NPTS5,KIND,LINES,TITL5)
   50 CONTINUE
C
C-----------------------------------------------------------------------
C
```

```
C      PLOT CARDS FOR THE ORDINARY COHERENCE BETWEEN CH2 & CH3
C      FOLLOW THIS CARD:
C
       DO 1982 I=1,N
       YORD(1,I)=REAL(RCOH(3,I))
       XORD(1,I)=FREQ(I)
 1982  CONTINUE
C
       WRITE (3,4052) (TITL6(I),I=1,20)
       WRITE (3,1976) (I,XORD(1,I),YORD(1,I),I=1,N)
C
       IF (IPLOTD.EQ.0) GO TO 60
       CALL PICSIZ (14.0,7.0)
       CALL GRAPH (XLNGTH,XLEFT,XRIGHT,XINC,NDECX,XLABEL,XORD,XDUMMY,YLNG
      ?TH,YBASE,YTOP,YINC,NDECY,YLABEL,YORD,YDUMMY,NSINGV,MAXCVS,NCURVS,M
      ?AXPTS,NPTS1,NPTS2,NPTS3,NPTS4,NPTS5,KIND,LINES,TITL6)
   60  CONTINUE
C
C-----------------------------------------------------------------------
C
C      THE CARDS FOR COMPUTING THE PARTIAL COHERENCES FOLLOW THIS CARD:
C
       IP=-1
C
 2000  DO 7000 J=1,N
C
       IF(IP)2100,2200,2300
C
 2100  GAG(1)=GYY(J)
       GAG(2)=CONJG(GY1(J))
       GAG(3)=CONJG(GY2(J))
       GAG(4)=CONJG(GY3(J))
       GAG(5)=GY1(J)
       GAG(6)=G11(J)
       GAG(7)=CONJG(G12(J))
       GAG(8)=CONJG(G13(J))
       GAG(9)=GY2(J)
       GAG(10)=G12(J)
       GAG(11)=G22(J)
       GAG(12)=CONJG(G23(J))
       GAG(13)=GY3(J)
       GAG(14)=G13(J)
       GAG(15)=G23(J)
       GAG(16)=G33(J)
C
       GO TO 2400
C
 2200  GAG(1)=GYY(J)
       GAG(2)=CONJG(GY2(J))
       GAG(3)=CONJG(GY1(J))
       GAG(4)=CONJG(GY3(J))
       GAG(5)=GY2(J)
       GAG(6)=G22(J)
       GAG(7)=G12(J)
       GAG(8)=CONJG(G23(J))
       GAG(9)=GY1(J)
```

```
      GAG(13)=CONJG(G12(J))
      GAG(11)=G11(J)
      GAG(12)=CONJG(G13(J))
      GAG(13)=GY3(J)
      GAG(14)=G23(J)
      GAG(15)=G13(J)
      GAG(16)=G33(J)
C
      GO TO 2400
C
 2300 GAG(1)=GYY(J)
      GAG(2)=CONJG(GY1(J))
      GAG(3)=CONJG(GY2(J))
      GAG(4)=CONJG(GY1(J))
      GAG(5)=GY3(J)
      GAG(6)=G33(J)
      GAG(7)=G23(J)
      GAG(8)=G13(J)
      GAG(9)=GY2(J)
      GAG(10)=CONJG(G23(J))
      GAG(11)=G22(J)
      GAG(12)=G12(J)
      GAG(13)=GY1(J)
      GAG(14)=CONJG(G13(J))
      GAG(15)=CONJG(G12(J))
      GAG(16)=G11(J)
C
      GO TO 2400
C
 2400 SYY(1)=GAG(1)
      SYY(2)=GAG(2)
      SYY(3)=GAG(5)
      SYY(4)=GAG(6)
      SDY(1)=GAG(3)
      SDY(2)=GAG(4)
      SDY(3)=GAG(7)
      SDY(4)=GAG(8)
      SYD(1)=GAG(9)
      SYD(2)=GAG(10)
      SYD(3)=GAG(13)
      SYD(4)=GAG(14)
      SDD(1)=GAG(11)
      SDD(2)=GAG(12)
      SDD(3)=GAG(15)
      SDD(4)=GAG(16)
C
      IPC=IPC+2
C
      CALL CMINV(SDD,2,D1,D2)
C
      IF(D1.NE.0.0.AND.D2.NE.0.0) GO TO 2470
      WRITE(3,2460)J,IPC,D1,D2
C
      PCON(IPC,J)=CMPLX(0.0,0.0)
      GO TO 2550
C
```

```
 2470 CALL CMPRD(SYY,SPD,SYNP,2)
      CALL CMPRD(SYNP,SPY,SYNPY,2)
C
      DO 2500 I=1,4
      GXYP(I)=SYY(I)-SYNPY(I)
 2500 CONTINUE
C
 2550 CONTINUE
      GXYD=GXYP(1)*GXYP(4)
      GXYR=CABS(GXYD)
C
      REFSQ=REF*REF
      REFOR=REFSQ*REFSQ
C
      IF(GXYR.LT.REFOR) GO TO 2900
C
      PCOH(IPC,J)=(REAL(GXYP(3))**2+AIMAG(GXYP(3))**2)/GXYD
      GO TO 2950
C
 2900 PCOH(IPC,J)=CMPLX(0.0,0.0)
C
 2950 CONTINUE
 3000 CONTINUE
C
      IP=IP+1
      IF(IP.GE.2) GO TO 3100
C
      GO TO 2000
C
 3100 CONTINUE
C
C-----------------------------------------------------------------------
C
C     PLOT CARDS FOR THE PARTIAL COHERENCE BETWEEN CH1 & THE OUTPUT
C     CHANNEL FOLLOW THIS CARD:
C
      DO 1993 I=1,N
      YORD(1,I)=REAL(PCOH(1,I))
      XORD(1,I)=FREQ(I)
 1993 CONTINUE
C
      WRITE (3,4060) (TITL1(I),I=1,20)
      WRITE (3,1976) (I,XORD(1,I),YORD(1,I),I=1,N)
C
      IF (IPLOTC.EQ.0) GO TO 70
      CALL PICSIZ (14.0,7.0)
      CALL GRAFF (XLNGTH,XLEFT,XRIGHT,XINC,NDECX,XLABEL,XORD,XDUMMY,YLNG
     ?TH,YBASE,YTOP,YINC,NDECY,YLABEL,YCRD,YDUMMY,NSINGV,MAXCVS,NCURVS,M
     ?AXPTS,NPTS1,NPTS2,NPTS3,NPTS4,NPTS5,KIND,LINES,TITLE)
   70 CONTINUE
C
C-----------------------------------------------------------------------
C
C     PLOT CARDS FOR THE PARTIAL COHERENCE BETWEEN CH2 & THE OUTPUT
C     CHANNEL FOLLOW THIS CARD:
C
```

```
C
      DO 1984 I=1,N
      YORD(1,I)=REAL(PCOH(2,I))
      XORD(1,I)=FREQ(I)
 1984 CONTINUE
C
      WRITE (3,4061) (TITL2(I),I=1,20)
      WRITE (3,1976) (I,XORD(1,I),YORD(1,I),I=1,N)
C
      IF (IPLOTC.EQ.0) GO TO 90
      CALL PICSIZ (14.0,7.0)
      CALL GRAFF (XLNGTH,XLEFT,XRIGHT,XINC,NDECX,XLABEL,XORD,XDUMMY,YLNG
     ?TH,YBASE,YTOP,YINC,NDECY,YLABF2,YORD,YDUMMY,NSINGV,MAXCVS,NCURVS,M
     ?AXPTS,NPTS1,NPTS2,NPTS3,NPTS4,NPTS5,KIND,LINES,TITL2)
   90 CONTINUE
C
C-----------------------------------------------------------------------
C
C     PLOT CARDS FOR THE PARTIAL COHERENCE BETWEEN CH3 & THE OUTPUT
C     CHANNEL. FOLLOW THIS CARD:
C
      DO 1985 I=1,N
      YORD(1,I)=REAL(PCOH(3,I))
      XORD(1,I)=FREQ(I)
 1985 CONTINUE
C
      WRITE (3,4062) (TITL3(I),I=1,20)
      WRITE (3,1976) (I,XORD(1,I),YORD(1,I),I=1,N)
C
      IF (IPLOTC.EQ.0) GO TO 90
      CALL PICSIZ (14.0,7.0)
      CALL GRAFF (XLNGTH,XLEFT,XRIGHT,XINC,NDECX,XLABEL,XORD,XDUMMY,YLNG
     ?TH,YBASE,YTOP,YINC,NDECY,YLABF2,YORD,YDUMMY,NSINGV,MAXCVS,NCURVS,M
     ?AXPTS,NPTS1,NPTS2,NPTS3,NPTS4,NPTS5,KIND,LINES,TITL3)
   90 CONTINUE
C
C-----------------------------------------------------------------------
C
      IF (IPLOTA.EQ.0.AND.IPLOTB.EQ.0.AND.IPLOTC.EQ.0) GO TO 9999
      CALL PICSIZ(0.0,0.0)
C
C-----------------------------------------------------------------------
C
 9999 STOP
      END
```

```
      SUBROUTINE CMINV(SPP,N,D1,D2)
      DIMENSION SPP(4),A(4),B(4),E(4),F(4),G(4)
      COMPLEX SPP
      DO 10 I=1,4
      A(I)=REAL(SPP(I))
      B(I)=AIMAG(SPP(I))
      E(I)=A(I)
   10 CONTINUE
      CALL MINV(E,N,D)
      D1=D
      CALL MPROD(B,E,F,N)
      CALL MPROD(F,B,G,N)
      DO 20 I=1,4
      A(I)=A(I)+G(I)
   20 CONTINUE
      CALL MINV(A,N,D)
      D2=D
      CALL MPROD(A,F,B,N)
      DO 30 I=1,4
      SPP(I)=CMPLX(A(I),-B(I))
   30 CONTINUE
      RETURN
      END
```

```
      SUBROUTINE MINV(A,N,D)
      DIMENSION A(4),L(4),M(4)
      D=1.0
      NK=-N
      DO 80 K=1,N
      NK=NK+N
      L(K)=K
      M(K)=K
      KK=NK+K
      BIGA=A(KK)
      DO 20 J=K,N
      IZ=N*(J-1)
      DO 20 I=K,N
      IJ=IZ+I
   10 IF( ABS(BIGA)- ABS(A(IJ))) 15,20,20
   15 BIGA=A(IJ)
      L(K)=I
      M(K)=J
   20 CONTINUE
      J=L(K)
      IF(J-K) 35,35,25
   25 KI=K-N
      DO 30 I=1,N
      KI=KI+N
      HOLD=-A(KI)
      JI=KI-K+J
      A(KI)=A(JI)
   30 A(JI) =HOLD
   35 I=M(K)
      IF(I-K) 45,45,38
   38 JP=N*(I-1)
      DO 40 J=1,N
      JK=NK+J
      JI=JP+J
      HOLD=-A(JK)
      A(JK)=A(JI)
   40 A(JI) =HOLD
   45 IF(BIGA) 48,46,48
   46 D=0.0
      RETURN
   48 DO 55 I=1,N
      IF(I-K) 50,55,50
   50 IK=NK+I
      A(IK)=A(IK)/(-BIGA)
   55 CONTINUE
      DO 65 I=1,N
      IK=NK+I
      HOLD=A(IK)
      IJ=I-N
      DO 65 J=1,N
      IJ=IJ+N
      IF(I-K) 60,65,60
   60 IF(J-K) 62,65,62
   62 KJ=IJ-I+K
      A(IJ)=HOLD*A(KJ)+A(IJ)
   65 CONTINUE
```

```
      KJ=K-N
      DO 75 J=1,N
      KJ=KJ+N
      IF(J-K) 70,75,70
   70 A(KJ)=A(KJ)/BIGA
   75 CONTINUE
      D=D*BIGA
      A(KK)=1.0/BIGA
   80 CONTINUE
      K=N
  100 K=(K-1)
      IF(K) 150,150,105
  105 I=L(K)
      IF(I-K) 120,120,108
  108 JQ=N*(K-1)
      JR=N*(I-1)
      DO 110 J=1,N
      JK=JQ+J
      HOLD=A(JK)
      JI=JR+J
      A(JK)=-A(JI)
  110 A(JI) =HOLD
  120 J=M(K)
      IF(J-K) 100,100,125
  125 KI=K-N
      DO 130 I=1,N
      KI=KI+N
      HOLD=A(KI)
      JI=KI-K+J
      A(KI)=-A(JI)
  130 A(JI) =HOLD
      GO TO 100
  150 RETURN
      END
```

```
      SUBROUTINE CMPFD(A,B,F,N)
      DIMENSION A(4),B(4),F(4)
      COMPLEX A,B,F
      IF=0
      IK=-N
      DO 10 K=1,N
      IK=IK+N
      DO 10 J=1,N
      IF=IF+1
      JI=J-N
      IB=IK
      F(IF)=0
      DO 10 I=1,N
      JI=JI+N
      IB=IB+1
   10 F(IF)=F(IF)+A(JI)*B(IB)
      RETURN
      END
```

```
      SUBROUTINE MPFD(A,B,F,N)
      DIMENSION A(4),B(4),F(4)
      IF=0
      IK=-N
      DO 10 K=1,N
      IK=IK+N
      DO 10 J=1,N
      IF=IF+1
      JI=J-N
      IB=IK
      F(IF)=0
      DO 10 I=1,N
      JI=JI+N
      IB=IB+1
   10 F(IF)=F(IF)+A(JI)*B(IB)
      RETURN
      END
```

11.4 CIRCXCOR

The two-channel program "CIRCXCOR":

1) removes the overall mean from each of the two time series sample records and amplitude weights each time series with a Hanning ($\sin^2$) function.

2) computes the spectral values for the two-sided spectra G_{xx}, G_{yy}, G_{xy} via the FFT.

3) averages the above quantities by repeating steps 1 and 2.

4) "edits" the spectral values in chosen frequency bands (digital filtering).

5) computes the frequency-filtered values for $\hat{R}_{xx}$, $\hat{R}_{yy}$, and $\hat{R}_{xy}$ via the inverse FFT and the convolution theorem [3, 4]; i.e., circular cross-correlation.

6) computes the correlation coefficient, $\hat{\rho}_{xy}$.

7) outputs all above-mentioned averaged quantities on a printout.

8) automatically will scale the plot axes and then plot $\hat{\rho}_{xy}$.

```
      INTEGER*2 INFIL,JUNK
      REAL*4 MSDAT,MSCUR
      COMPLEX FFT1,FFT2,GXY,RXYCX
      DIMENSION JUNK(20)
      DIMENSION MSDAT(20),MSCUR(20),DEL(99),SNFIL(2048)
      DIMENSION XORD(1,1201),YORD(1,1201),XDUMMY(1,1201),YDUMMY(1,1201)
      DIMENSION XLABEL(20),YLABEL(20),TITLE(20),KIND(5)
      DIMENSION RXX(2048),RYY(2048),PXY(2048),GXY(2048),XFREQ(2048)
      DIMENSION TAU(2048),INFIL(4096),CH1(2048),CH2(2048),INIT(100)
      DIMENSION A(2048),B(2048),FFT1(2048),FFT2(2048)
      DIMENSION NLOW(10),NHIH(10),GXX(2048),GYY(2048),RXYCX(2048)
C
   50 FORMAT ('1',////,40X,20A4)
  100 FORMAT(40A2)
  155 FORMAT('0POINT NUMBER',I6,' HAS A VALUE OF',I12)
  500 FORMAT (20A4)
 1058 FORMAT('1',///,' CHANNEL',I3,' ZERO-MEAN INPUT:',//,(10F12.1))
 3000 FORMAT(' ITERATION NUMBER',I3,' EXPONENT OF',F6.2,' DEL=',F9.1,//)
 3311 FORMAT('1',///,' CHANNEL',I3,' DATA AFTER DECAY CORRECTION:',//,
     1(10F12.1))
 4300 FORMAT('1IBAND, FREQUENCY, GXX, GYY, GXY (COMPLEX)',//,
     1(2(III,F9.1,4F10.1)))
 4345 FORMAT(' ',//,' ON FILTER PASS',I3,' THE AVERAGE X-SPECTRAL VALUE,
     1 GXYAVE, IS',F8.2,' UNITS, OF',I5,' FILTERED',/,' SPECTRAL LINES,'
     2,I5,' WERE ABOVE THE DXYTST VALUE OF',F8.2,' AND WERE ADJUSTED.',/,
     3' THE POST-WHITENED X-SPECTRUM IS AS FOLLOWS:',//,' IBAND FREQUENC
     4Y, GXY (COMPLEX)',//)
 4346 FORMAT(2(I25,F9.1,2F10.1))
 5100 FORMAT(' MSDAT(',I2,') =',F14.1)
 5200 FORMAT(' THE MSV OF ALL DATA =',F9.1,///)
 5500 FORMAT(' MSCUR(',I2,') =',F14.5)
 5600 FORMAT(' THE MSV OF THE EXP CURVE =',F8.5,'   THE REQUIRED GAIN IS
     1 THUS',F8.1)
 6000 FORMAT('0',//,' FILTER PASS',I3,F8.1,' HZ TO',F8.1,' HZ',//,
     2I6,' INITIAL POINTS ARE OMITTED FROM EACH CHANNEL.',//)
 6010 FORMAT('0I, TAU(I)-(CH1 LEAD IN MSEC), RXY(I), RXX(I), AND RYY(I),
     2 I=1 TO 2*N',//,(2(III,F10.2,3F13.4)))
C
CCCCCCCCCCCCCCCCCCCCCCCCCCCCCCCCCCCCCCCCCCCCCCCCCCCCCCCCCCCCCCCCCCCCCCCCC
C                                                                       C
C     XDELAY SPECIFIES THE POS. & NEG. DELAY (IN MSEC) FOR THE PLOT.    C
C                                                                       C
C     IF JFLAG = 0 , NON-ESSENTIAL PRINT OUT IS DELETED IE. GXX,GYY...  C
C                                                                       C
C     IDMPSK SPECIFIES DUMP TO BE SKIPPED DUE TO FILE ERROR.            C
C                                                                       C
C     NOMIT INITIAL POINTS ARE OMITTED FROM EACH CHANNEL.               C
C                                                                       C
C     IF INDOW = 0, FILTERS WILL BE ABRUPT TRUNCATION.                  C
C                                                                       C
C     NLOW(JPAS) AND NHIH(JPAS) SET BAND-PASS FILTER CUT-OFF            C
C     FREQUENCIES; NLOW(JPAS)=1 AND NHIH(JPAS)=N FOR NO FILTERING.      C
C                                                                       C
C     SPECTRA ARE POST-WHITENED UNLESS  IWHITE=0.                       C
C                                                                       C
C     DECAY CORRECTION:  SPECIFY IDECAY=1                               C
```

```
C                                                                       C
CCCCCCCCCCCCCCCCCCCCCCCCCCCCCCCCCCCCCCCCCCCCCCCCCCCCCCCCCCCCCCCCCCCCCCCC
C
      XDFLAY=1.0
      JFLAG=0
      N=512
      IAVGS=64
      IDMPSK=0
      NOWIT=0
      INDOW=0
      SPLRT=20000.0
      PI=3.1415927
C
      NPAS=2
      NLOW(1)=1
      NHIH(1)=N
      NLOW(2)=104
      NHIH(2)=206
C
      IWHITE=0
      IDECAY=0
      NPTSBL=128
      NBLOKS=8
      DELXPO=1.0
C
      N2H=N+N
      KADP=1024/N
C
C     DATA LABEL CARDS GO HERE:
C
      DATA XLABEL/'TAU ','- CH','ANNE','L 1 ','LEAD',' (MS','EC)_'/
      DATA YLABEL/'CORR','FLAT','ION ','COEF','FICI','ENT_'/
C
      READ (1,500) (TITLE(I),I=1,20)
C
      DTAU=1000./SPLRT
      JAV=0
      IDUMP=0
C
      DO 70 I=1,N2H
      GXX(I)=0.0
      GYY(I)=0.0
      GXY(I)=CMPLX(0.0,0.0)
   70 CONTINUE
C
      INI=0
      DO 80 I=1,KADP
      INIT(I)=INI
      INI=INI+N+N
   80 CONTINUE
C
   90 READ (4,100) (INFIL(I),I=1,4096)
C
      NOTOK=0
      DO 148 I=1,4096
      IF(INFIL(I).LT.1024.AND.INFIL(I).GE.0) GO TO 148
```

```
      NOTOK=1
      WRITE(3,155)I,INFIL(I)
  148 CONTINUE
C
C     IF(NOTOK.EQ.1) GO TO 9999
C
  220 IDUMP=IDUMP+1
      IF(IDUMP.EQ.IDMPSK) GO TO 90
C
      K=0
      IEND=2048-NOMIT
C
      DO 240 I=1,IEND
      CH1(I)=INFIL(I+NOMIT)
      CH2(I)=INFIL(I+2048+NOMIT)
  240 CONTINUE
C
      IF(IDECAY.EQ.0) GO TO 1225
C
C     SET ZERO-MEAN AND DECAY CORRECT:
C
      RMV1=0.0
      RMV2=0.0
      DO 1221 I=1,IEND
      RMV1=RMV1+CH1(I)
      RMV2=RMV2+CH2(I)
 1221 CONTINUE
      RMV1=RMV1/IEND
      RMV2=RMV2/IEND
      DO 1222 I=1,IEND
      CH1(I)=CH1(I)-RMV1
      CH2(I)=CH2(I)-RMV2
 1222 CONTINUE
C
      IDCH=1
      NPOIT=IEND
C
      DO 1056 I=1,NPOIT
      SNFIL(I)=CH1(I)
 1056 CONTINUE
C
 1057 SUMM1=0.0
C
      WRITE(3,1058)IDCH,(SNFIL(I),I=1,NPOIT)
C
      DO 1110 J=1,NBLOKS
C
      SUM=0.0
      DO 1010 I=1,NPTSBL
      JRUN=NPTSBL*(J-1)+I
      SUM=SUM+(SNFIL(JRUN))**2
 1010 CONTINUE
C
      MSDAT(J)=SUM/NPTSBL
C
      WRITE(3,5100) J,MSDAT(J)
```

```
C
      SUMM1=SUMM1+MSDAT(J)/NBLOKS
C
 1110 CONTINUE
C
      WRITE(3,5200)SUMM1
C
      XPO=0.0
      ITNO=1
 1150 SUMM2=0.0
C
      DO 1310 J=1,NBLOKS
      MSCUR(J)=1.0/EXP(2.0*XPO*(NPTSBL*(J-1)+NPTSBL/2)/SPLRT)
C
      WRITE(3,5500)J,MSCUR(J)
C
      SUMM2=SUMM2+MSCUR(J)/NBLOKS
 1310 CONTINUE
      GAIN=SUMM1/SUMM2
C
      WRITE(3,5600)SUMM2,GAIN
C
      DEL(ITNO)=0.0
C
      DO 2000 I=1,NBLOKS
      DEL(ITNO)=DEL(ITNO)+ABS(MSDAT(I)-GAIN*MSCUR(I))
 2000 CONTINUE
C
      WRITE(3,3000)ITNO,XPO,DEL(ITNO)
C
      IF(ITNO.EQ.1) GO TO 3100
      IF(ITNO.GE.99) GO TO 9999
C
      CKDEL=1.001*DEL(ITNO-1)
      IF(DEL(ITNO).GT.CKDEL) GO TO 3111
C
 3100 ITNO=ITNO+1
      XPO=XPO+DELXPO
      GO TO 1150
C
 3111 XPO=XPO-DELXPO
C
      DO 3211 I=1,NPOIT
      SNFIL(I)=SNFIL(I)*EXP(XPO*I/SPLRT)
 3211 CONTINUE
C
      WRITE(3,3311)IDCH,(SNFIL(I),I=1,NPOIT)
C
      IF(IDCH.EQ.2) GO TO 6103
C
      DO 6102 I=1,NPOIT
      SNFIL(I)=CH2(I)
 6102 CONTINUE
C
      IDCH=2
      GO TO 1057
```

```
C
 6103 CONTINUE
C
C       END DECAY CORRECTION.
C
 1225 JAV=JAV+1
      K=K+1
      NIX=1
      EVAL=0.0
C
      DO 1230 I=1,N
      A(I)=CH1(I)
      B(I)=0.0
      EVAL=EVAL+A(I)
 1230 CONTINUE
C
      EVAL=EVAL/N
C
C       CHANNEL 1 MEAN VALUE CORRECTION
C
      DO 1231 I=1,N
      A(I)=(A(I)-EVAL)
 1231 CONTINUE
C
      DO 1232 I=1,N
      I2H=I+N
      A(I2H)=0.0
      B(I2H)=0.0
 1232 CONTINUE
C
      GO TO 1275
C
 1250 EVAL=0.0
C
      DO 1255 I=1,N
      A(I)=0.0
      B(I)=0.0
 1255 CONTINUE
C
      DO 1257 I=1,N
      I2H=I+N
      A(I2H)=CH2(I)
      B(I2H)=0.0
      EVAL=EVAL+A(I2H)
 1257 CONTINUE
C
      EVAL=EVAL/N
C
C       CHANNEL 2 MEAN VALUE CORRECTION
C
      DO 1256 I=1,N
      I2H=I+N
      A(I2H)=A(I2H)-EVAL
 1256 CONTINUE
C
 1275 CALL FFT(A,B,N2H,N2H,N2H,1)
```

```
C
      IF(NIX.EQ.2) GO TO 1400
C
      DO 2001 I=1,N2H
      FFT1(I)=CMPLX(A(I),B(I))
      GXX(I)=GXX(I)+REAL(CONJG(FFT1(I))*FFT1(I))
 2001 CONTINUE
C
      NIX=2
      GO TO 1250
C
 1400 DO 2002 I=1,N2H
      FFT2(I)=CMPLX(A(I),B(I))
      GYY(I)=GYY(I)+REAL(CONJG(FFT2(I))*FFT2(I))
      GXY(I)=CONJG(FFT1(I))*FFT2(I)+GXY(I)
 2002 CONTINUE
C
      IF(JAV.EQ.IAVGS) GO TO 4000
      IF(K.GE.KADP) GO TO 90
      GO TO 1225
C
 4000 CONTINUE
C
C     END AVERAGING
C
      DNORM=4*N*N*IAVGS
      DO 4100 I=1,N2H
      GXX(I)=GXX(I)/DNORM
      GYY(I)=GYY(I)/DNORM
      GXY(I)=GXY(I)/DNORM
      XFREQ(I)=(I-1)*SPLRT/(N+N)
 4100 CONTINUE
C
C     AUTO AND CROSS SPECTRA ARE COMPUTED.  PUNCH OR STORE OUTPUT.
C
      IF(JFLAG.EQ.0) GO TO 4304
C
      WRITE(3,4300)(I,XFREQ(I),GXX(I),GYY(I),GXY(I),I=1,N2H)
C
C     BANDPASS FILTER THE TWO-SIDED SPECTRA...
C
 4304 CONTINUE
      JPAS=0
 4305 CONTINUE
      JPAS=JPAS+1
C
      DO 4310 I=1,N2H
      RXX(I)=0.0
      RYY(I)=0.0
      RXYCX(I)=CMPLX(0.0,0.0)
 4310 CONTINUE
C
      ILOW=NLOW(JPAS)
      IHIH=NHIH(JPAS)
C
      DO 4320 I=ILOW,IHIH
```

```
C
      N2I=N2H+2-I
      RXX(I)=GXX(I)
      RXX(N2I)=GXX(N2I)
      RYY(I)=GYY(I)
      RYY(N2I)=GYY(N2I)
      RXYCX(I)=GXY(I)
      RXYCX(N2I)=GXY(N2I)
C
      IF(NLOW(JPAS).NE.1) GO TO 4320
C
      NA1=N+1
      RXX(NA1)=GXX(NA1)
      RYY(NA1)=GYY(NA1)
      RXYCX(NA1)=GXY(NA1)
 4320 CONTINUE
C
C     POST-WHITEN THE BAND-LIMITED DATA...
C
      IF(IWHITE.EQ.0) GO TO 4350
C
      NGAINS=0
      GXYAVE=0.0
C
      DO 4335 I=1,N2H
      GXYAVE=GXYAVE+CABS(RXYCX(I))
 4335 CONTINUE
C
      IDNM=2*(IHIH-ILOW+1)
      GXYAVE=GXYAVE/IDNM
      DXYTST=GXYAVE*10.0
C
      DO 4340 I=1,N
      N2I=N2H+2-I
      CHECK=0.5*(CABS(RXYCX(I))+CABS(RXYCX(N2I)))
C
      IF(CHECK.LT.DXYTST) GO TO 4340
C
      NGAINS=NGAINS+1
      GAIN=DXYTST/CHECK
C
      RXX(I)=RXX(I)*GAIN
      RXX(N2I)=RXX(N2I)*GAIN
      RYY(I)=RYY(I)*GAIN
      RYY(N2I)=RYY(N2I)*GAIN
      RXYCX(I)=RXYCX(I)*GAIN
      RXYCX(N2I)=RXYCX(N2I)*GAIN
 4340 CONTINUE
C
      IDNM=IDNM/2
C
      WRITE(3,4345) JPAS,GXYAVE,IDNM,NGAINS,DXYTST
      WRITE(3,4346)(I,XFRFQ(I),RXYCX(I),I=1,N2H)
C
C     END POST-WHITEN.
C
```

```
 4350 IF(INDOW.EQ.0) GO TO 4360
C
C       TAPER THE FILTER WINDOWS.
C
        ILOW=NLOW(JPAS)
        IHIH=NHIH(JPAS)
        DELF=IHIH-ILOW
C
        DO 4355 I=ILOW,IHIH
        TAPER=SIN(PI*(I-ILOW)/DELF)
        N2I=N2H+2-I
        RXX(I)=RXX(I)*TAPER
        RXX(N2I)=RXX(N2I)*TAPER
        RYY(I)=RYY(I)*TAPER
        RYY(N2I)=RYY(N2I)*TAPER
        RXYCX(I)=RXYCX(I)*TAPER
        RXYCX(N2I)=RXYCX(N2I)*TAPER
 4355 CONTINUE
C
C       END TAPER.
C
 4360 DO 4400 I=1,N2H
        A(I)=REAL(RXYCX(I))
        B(I)=-AIMAG(RXYCX(I))
 4400 CONTINUE
C
        CALL FFT(A,B,N2H,N2H,N2H,+1)
C
        DO 4410 I=1,N2H
        RXY(I)=A(I)
 4410 CONTINUE
C
        DO 4600 I=1,N2H
        A(I)=RYY(I)
        B(I)=0.0
 4600 CONTINUE
C
        CALL FFT(A,B,N2H,N2H,N2H,-1)
C
        DO 4710 I=1,N2H
        RYY(I)=A(I)
 4710 CONTINUE
C
        DO 4800 I=1,N2H
        A(I)=RXX(I)
        B(I)=0.0
 4800 CONTINUE
C
        CALL FFT(A,B,N2H,N2H,N2H,-1)
C
        DO 4910 I=1,N2H
        RXX(I)=A(I)
 4910 CONTINUE
C
        DN1=RXX(1)
        DN2=RYY(1)
```

```
      DN3=SQRT(DN1*DN2)
C
      DO 5000 I=1,N
      RXX(I)=RXX(I)/DN1*FLOAT(N)/(N+1-I)
      RYY(I)=RYY(I)/DN2*FLOAT(N)/(N+1-I)
      RXY(I)=RXY(I)/DN3*FLOAT(N)/I
      TAU(I)=(I-N-1)*DTAU
 5000 CONTINUE
C
      N1=N+1
      DO 5010 I=N1,N2M
      RXX(I)=RXX(I)/DN1*FLOAT(N)/(I-N)
      RYY(I)=RYY(I)/DN2*FLOAT(N)/(I-N)
      RXY(I)=RXY(I)/DN3*FLOAT(N)/(N+N+1-I)
      TAU(I)=(I-N-1)*DTAU
 5010 CONTINUE
C
      WRITE (3,50) (TITLE(L),L=1,20)
      WRITE(3,6000)(JPAS,XFREQ(NLOW(JPAS)),XFREQ(NHIH(JPAS)),NOMIT)
      WRITE(3,6010)(I,TAU(I),RXY(I),RXX(I),RYY(I),I=1,N2M)
C
      IF (JPAS.LT.NPAS) GO TO 4305
C
C     PLOTTER ROUTINE FOR CIRCXCOR.
C
      MAXPTS=1201
      XINC=XDELAY/4.0
      XLEFT=-XDELAY
      XRIGHT=XDELAY
      YTOP=0.0
      YBASE=0.0
C
C     'M' = THE # OF POINTS PLOTTED
C
      M2=XDELAY*(11.0/12.0)*(SPLRT/1000.0)
      INEG=N-M2
      IPOS=N+M2
      M=2*M2+1
      J=0
C
      DO 6050 I=INEG,IPOS
      J=J+1
      YORD(1,J)=RXY(I)
      XORD(1,J)=TAU(I)
C
      IF (YORD(1,J).GE.1.0) YORD(1,J)=1.0
      IF (YORD(1,J).LE.-1.0) YORD(1,J)=-1.0
C
 6020 CONTINUE
      IF (YORD(1,J).LE.YTOP) GO TO 6030
      YTOP=YTOP+0.25
      GO TO 6020
C
 6030 CONTINUE
      IF (YORD(1,J).GE.YBASE) GO TO 6040
      YBASE=YBASE-0.25
```

```
      GO TO 6030
C
 6040 CONTINUE
 6050 CONTINUE
C
      IF (-YBASE.GT.YTOP) YTOP=-YBASE
      IF (YTOP.GT.-YBASE) YBASE=-YTOP
C
      YINC=YTOP/5.0
      KIND(1)=-1
C
      CALL PICSIZ(15.0,9.0)
C
      CALL GRAFF (9.0,XLEFT,XRIGHT,XINC,3,XLABEL,XORD,XDUMMY,
     15.0,YBASE,YTOP,YINC,2,YLABEL,YORD,YDUMMY,
     21,1,1,MAXPTS,M,0.0,0.0,0.0,KIND,0,TITLE)
C
      CALL PICSIZ(0.0,0.0)
C
 9999 STOP
      END
```

11.5 Fast Fourier Transform (FFT)

```
      SUBROUTINE FFT (A, B, NTOT, N, NSPAN, ISN)
C     USING MIXED-RADIX FAST FOURIER TRANSFORM ALGORITHM.
C     MULTIVARIATE COMPLEX FOURIER TRANSFORM, COMPUTED IN PLACE
C     BY R. C. SINGLETON, STANFORD RESEARCH INSTITUTE, OCT. 1968
C     ARRAYS A AND B ORIGINALLY HOLD THE REAL AND IMAGINARY
C     COMPONENTS OF THE DATA, AND RETURN THE REAL AND
C     IMAGINARY COMPONENTS OF THE RESULTING FOURIER COEFFICIENTS.
C     MULTIVARIATE DATA IS INDEXED ACCORDING TO THE FORTRAN
C     ARRAY ELEMENT SUCCESSOR FUNCTION, WITHOUT LIMIT
C     ON THE NUMBER OF IMPLIED MULTIPLE SUBSCRIPTS.
C     THE SUBROUTINE IS CALLED ONCE FOR EACH VARIATE.
C     THE CALLS FOR A MULTIVARIATE TRANSFORM MAY BE IN ANY ORDER.
C     NTOT IS THE TOTAL NUMBER OF COMPLEX DATA VALUES.
C     N IS THE DIMENSION OF THE CURRENT VARIABLE.
C     NSPAN/N IS THE SPACING OF CONSECUTIVE DATA VALUES
C     WHILE INDEXING THE CURRENT VARIABLE.
C     THE SIGN OF ISN DETERMINES THE SIGN OF THE COMPLEX
C     EXPONENTIAL, AND THE MAGNITUDE OF ISN IS NORMALLY ONE.
      DIMENSION A(1), B(1)
C     A TRI-VARIATE TRANSFORM WITH A(N1,N2,N3), B(N1,N2,N3)
C     IS COMPUTED BY
C       CALL FFT(A,B,N1*N2*N3,N1,N1,1)
C       CALL FFT(A,B,N1*N2*N3,N2,N1*N2,1)
C       CALL FFT(A,B,N1*N2*N3,N3,N1*N2*N3,1)
C     FOR A SINGLE-VARIATE TRANSFORM,
C     NTOT = N = NSPAN = (NUMBER OF COMPLEX DATA VALUES), E.G.
C     CALL FFT(A,B,N,N,N,1)
C     THE DATA MAY ALTERNATIVELY BE STORED IN A SINGLE COMPLEX
C     ARRAY A, THEN THE MAGNITUDE OF ISN CHANGED TO TWO TO
C     GIVE THE CORRECT INDEXING INCREMENT AND A(2) USED TO
C     PASS THE INITIAL ADDRESS FOR THE SEQUENCE OF IMAGINARY
C     VALUES, E.G.
C       CALL FFT(A,A(2),NTOT,N,NSPAN,2)
C     ARRAYS AT(MAXF), CK(MAXF), BT(MAXF), SK(MAXF), AND NP(MAXP)
C     ARE USED FOR TEMPORARY STORAGE.  IF THE AVAILABLE STORAGE
C     IS INSUFFICIENT, THE PROGRAM IS TERMINATED BY A STOP.
C     MAXF MUST BE .GE. THE MAXIMUM PRIME FACTOR OF N.
C     MAXP MUST BE .GT. THE NUMBER OF PRIME FACTORS OF N.
C     IN ADDITION, IF THE SQUARE-FREE PORTION K OF N HAS TWO OR
C     MORE PRIME FACTORS, THEN MAXP MUST BE .GE. K-1.
C     ARRAY STORAGE IN NFAC FOR A MAXIMUM OF 11 FACTORS OF N.
C     IF N HAS MORE THAN ONE SQUARE-FREE FACTOR, THE PRODUCT OF THE
C     SQUARE-FREE FACTORS MUST BE .LE. 1501
      DIMENSION NFAC(21),NP(1500)
C     ARRAY STORAGE FOR MAXIMUM PRIME FACTOR OF 373
      DIMENSION AT(373),CK(373),BT(373),SK(373)
      EQUIVALENCE (I,II)
C     THE FOLLOWING TWO CONSTANTS SHOULD AGREE WITH THE ARRAY DIMENSIONS.
      MAXF=373
      MAXP=1500
      IF(N .LT. 2) RETURN
      INC=ISN
      RAD=8.0*ATAN(1.0)
      S72=RAD/5.0
      C72=COS(S72)
      S72=SIN(S72)
```

```
      S120=SQRT(0.75)
      IF(ISN .GE. 0) GO TO 10
      S72=-S72
      S120=-S120
      RAD=-RAD
      INC=-INC
10    NT=INC*NTOT
      KS=INC*NSPAN
      KSPAN=KS
      NN=NT-INC
      JC=KS/N
      RADF=RAD*FLOAT(JC)*0.5
      I=0
      JF=0
C     DETERMINE THE FACTORS OF N
      M=0
      K=N
      GO TO 20
15    M=M+1
      NFAC(M)=4
      K=K/16
20    IF(K-(K/16)*16 .EQ. 0) GO TO 15
      J=3
      JJ=9
      GO TO 30
25    M=M+1
      NFAC(M)=J
      K=K/JJ
30    IF(MOD(K,JJ) .EQ. 0) GO TO 25
      J=J+2
      JJ=J**2
      IF(JJ .LE. K) GO TO 30
      IF(K .GT. 4) GO TO 40
      KT=M
      NFAC(M+1)=K
      IF(K .NE. 1) M=M+1
      GO TO 80
40    IF(K-(K/4)*4 .NE. 0) GO TO 50
      M=M+1
      NFAC(M)=2
      K=K/4
50    KT=M
      J=2
60    IF(MOD(K,J) .NE. 0) GO TO 70
      M=M+1
      NFAC(M)=J
      K=K/J
70    J=((J+1)/2)*2+1
      IF(J .LE. K) GO TO 60
80    IF(KT .EQ. 0) GO TO 100
      J=KT
90    M=M+1
      NFAC(M)=NFAC(J)
      J=J-1
      IF(J .NE. 0) GO TO 90
C     COMPUTE FOURIER TRANSFORM
```

```
100   SD=RADF/FLOAT(KSPAN)
      CD=2.0*SIN(SD)**2
      SD=SIN(SD+SD)
      KK=1
      I=I+1
      IF(NFAC(I) .NE. 2) GO TO 400
C     TRANSFORM FOR FACTOR OF 2 (INCLUDING ROTATION FACTOR)
      KSPAN=KSPAN/2
      K1=KSPAN+2
210   K2=KK+KSPAN
      AK=A(K2)
      BK=B(K2)
      A(K2)=A(KK)-AK
      B(K2)=B(KK)-BK
      A(KK)=A(KK)+AK
      B(KK)=B(KK)+BK
      KK=K2+KSPAN
      IF(KK .LT. NN) GO TO 210
      KK=KK-NN
      IF(KK .LE. JC) GO TO 210
      IF(KK .GT. KSPAN) GO TO 800
220   C1=1.0-CD
      S1=SD
230   K2=KK+KSPAN
      AK=A(KK)-A(K2)
      BK=B(KK)-B(K2)
      A(KK)=A(KK)+A(K2)
      B(KK)=B(KK)+B(K2)
      A(K2)=C1*AK-S1*BK
      B(K2)=S1*AK+C1*BK
      KK=K2+KSPAN
      IF(KK .LT. NT) GO TO 230
      K2=KK-NT
      C1=-C1
      KK=K1-K2
      IF(KK .GT. K2) GO TO 230
      AK=C1-(CD*C1+SD*S1)
      S1=(SD*C1-CD*S1)+S1
C     THE FOLLOWING THREE STATEMENTS COMPENSATE FOR TRUNCATION
C     ERROR.  IF ROUNDED ARITHMETIC IS USED, SUBSTITUTE
C     C1=AK
      C1=0.5/(AK**2+S1**2)+0.5
      S1=C1*S1
      C1=C1*AK
      KK=KK+JC
      IF(KK .LT. K2) GO TO 230
      K1=K1+INC+INC
      KK=(K1-KSPAN)/2+JC
      IF(KK .LE. JC+JC) GO TO 220
      GO TO 100
C     TRANSFORM FOR FACTOR OF 3 (OPTIONAL CODE)
320   K1=KK+KSPAN
      K2=K1+KSPAN
      AK=A(KK)
      BK=B(KK)
      AJ=A(K1)+A(K2)
```

```
      BJ=B(K1)+B(K2)
      A(KK)=AK+AJ
      B(KK)=BK+BJ
      AK=-0.5*AJ+AK
      BK=-0.5*BJ+BK
      AJ=(A(K1)-A(K2))*S120
      BJ=(B(K1)-B(K2))*S120
      A(K1)=AK-BJ
      B(K1)=BK+AJ
      A(K2)=AK+BJ
      B(K2)=BK-AJ
      KK=K2+KSPAN
      IF(KK .LT. NN) GO TO 320
      KK=KK-NN
      IF(KK .LE. KSPAN) GO TO 320
      GO TO 700
C     TRANSFORM FOR FACTOR OF 4
400   IF(NFAC(I) .NE. 4) GO TO 600
      KSPNN=KSPAN
      KSPAN=KSPAN/4
410   C1=1.0
      S1=0
420   K1=KK+KSPAN
      K2=K1+KSPAN
      K3=K2+KSPAN
      AKP=A(KK)+A(K2)
      AKM=A(KK)-A(K2)
      AJP=A(K1)+A(K3)
      AJM=A(K1)-A(K3)
      A(KK)=AKP+AJP
      AJP=AKP-AJP
      BKP=B(KK)+B(K2)
      BKM=B(KK)-B(K2)
      BJP=B(K1)+B(K3)
      BJM=B(K1)-B(K3)
      B(KK)=BKP+BJP
      BJP=BKP-BJP
      IF(ISN .LT. 0) GO TO 450
      AKP=AKM-BJM
      AKM=AKM+BJM
      BKP=BKM+AJM
      BKM=BKM-AJM
      IF(S1 .EQ. 0.0) GO TO 460
430   A(K1)=AKP*C1-BKP*S1
      B(K1)=AKP*S1+BKP*C1
      A(K2)=AJP*C2-BJP*S2
      B(K2)=AJP*S2+BJP*C2
      B(K3)=AKM*S3+BKM*C3
      A(K3)=AKM*C3-BKM*S3
      KK=K3+KSPAN
      IF(KK .LE. NT) GO TO 420
440   C2=C1-(CD*C1+SD*S1)
      S1=(SD*C1-CD*S1)+S1
C     THE FOLLOWING THREE STATEMENTS COMPENSATE FOR TRUNCATION
C     ERROR.  IF ROUNDED ARITHMETIC IS USED, SUBSTITUTE
C     C1=C2
```

```
      C1=0.5/(C2**2+S1**2)**0.5
      S1=C1*S1
      C1=C1*C2
      C2=C1**2-S1**2
      S2=2.0*C1*S1
      C3=C2*C1-S2*S1
      S3=C2*S1+S2*C1
      KK=KK-NT+JC
      IF(KK .LE. KSPAN) GO TO 420
      KK=KK-KSPAN+INC
      IF(KK .LE. JC) GO TO 410
      IF(KSPAN .EQ. JC) GO TO 800
      GO TO 100
  450 AKP=AKM+BJM
      AKM=AKM-BJM
      BKP=BKM-AJM
      BKM=BKM+AJM
      IF(S1 .NE. 0.0) GO TO 430
  460 A(K1)=AKP
      B(K1)=BKP
      A(K2)=AJP
      B(K2)=BJP
      A(K3)=AKM
      B(K3)=BKM
      KK=K3+KSPAN
      IF(KK .LE. NT) GO TO 420
      GO TO 440
C     TRANSFORM FOR FACTOR OF 5 (OPTIONAL CODE)
  510 C2=C72**2-S72**2
      S2=2.0*C72*S72
  520 K1=KK+KSPAN
      K2=K1+KSPAN
      K3=K2+KSPAN
      K4=K3+KSPAN
      AKP=A(K1)+A(K4)
      AKM=A(K1)-A(K4)
      BKP=B(K1)+B(K4)
      BKM=B(K1)-B(K4)
      AJP=A(K2)+A(K3)
      AJM=A(K2)-A(K3)
      BJP=B(K2)+B(K3)
      BJM=B(K2)-B(K3)
      AA=A(KK)
      BB=B(KK)
      A(KK)=AA+AKP+AJP
      B(KK)=BB+BKP+BJP
      AK=AKP*C72+AJP*C2+AA
      BK=BKP*C72+BJP*C2+BB
      AJ=AKM*S72+AJM*S2
      BJ=BKM*S72+BJM*S2
      A(K1)=AK-BJ
      A(K4)=AK+BJ
      B(K1)=BK+AJ
      B(K4)=BK-AJ
      AK=AKP*C2+AJP*C72+AA
      BK=BKP*C2+BJP*C72+BB
```

```
      AJ=AKM*S2-AJM*S72
      BJ=BKM*S2-BJM*S72
      A(K2)=AK-BJ
      A(K3)=AK+BJ
      B(K2)=BK+AJ
      B(K3)=BK-AJ
      KK=K4+KSPAN
      IF(KK .LT. NN) GO TO 520
      KK=KK-NN
      IF(KK .LE. KSPAN) GO TO 520
      GO TO 700
C     TRANSFORM FOR ODD FACTORS
600   K=NFAC(I)
      KSPNN=KSPAN
      KSPAN=KSPAN/K
      IF(K .EQ. 3) GO TO 320
      IF(K .EQ. 5) GO TO 510
      IF(K .EQ. JF) GO TO 640
      JF=K
      S1=RAD/FLOAT(K)
      C1=COS(S1)
      S1=SIN(S1)
      IF(JF .GT. MAXF) GO TO 998
      CK(JF)=1.0
      SK(JF)=0.0
      J=1
630   CK(J)=CK(K)*C1+SK(K)*S1
      SK(J)=CK(K)*S1-SK(K)*C1
      K=K-1
      CK(K)=CK(J)
      SK(K)=-SK(J)
      J=J+1
      IF(J .LT. K) GO TO 630
640   K1=KK
      K2=KK+KSPNN
      AA=A(KK)
      BB=B(KK)
      AK=AA
      BK=BB
      J=1
      K1=K1+KSPAN
650   K2=K2-KSPAN
      J=J+1
      AT(J)=A(K1)+A(K2)
      AK=AT(J)+AK
      BT(J)=B(K1)+B(K2)
      BK=BT(J)+BK
      J=J+1
      AT(J)=A(K1)-A(K2)
      BT(J)=B(K1)-B(K2)
      K1=K1+KSPAN
      IF(K1 .LT. K2) GO TO 650
      A(KK)=AK
      B(KK)=BK
      K1=KK
      K2=KK+KSPNN
```

```
      J=1
660   K1=K1+KSPAN
      K2=K2-KSPAN
      JJ=J
      AK=AA
      BK=BB
      AJ=0.0
      BJ=0.0
      K=1
670   K=K+1
      AK=AT(K)*CK(JJ)+AK
      BK=BT(K)*CK(JJ)+BK
      K=K+1
      AJ=AT(K)*SK(JJ)+AJ
      BJ=BT(K)*SK(JJ)+BJ
      JJ=JJ+J
      IF(JJ .GT. JF) JJ=JJ-JF
      IF(K .LT. JF) GO TO 670
      K=JF-J
      A(K1)=AK-BJ
      B(K1)=BK+AJ
      A(K2)=AK+BJ
      B(K2)=BK-AJ
      J=J+1
      IF(J .LT. K) GO TO 660
      KK=KK+KSPNN
      IF(KK .LE. NN) GO TO 640
      KK=KK-NN
      IF(KK .LE. KSPAN) GO TO 640
C     MULTIPLY BY ROTATION FACTOR (EXCEPT FOR FACTORS OF 2 AND 4)
700   IF(I .EQ. M) GO TO 800
      KK=JC+1
710   C2=1.0-CD
      S1=SD
720   C1=C2
      S2=S1
      KK=KK+KSPAN
730   AK=A(KK)
      A(KK)=C2*AK-S2*B(KK)
      B(KK)=S2*AK+C2*B(KK)
      KK=KK+KSPNN
      IF(KK .LE. NT) GO TO 730
      AK=S1*S2
      S2=S1*C2+C1*S2
      C2=C1*C2-AK
      KK=KK-NT+KSPAN
      IF(KK .LE. KSPNN) GO TO 730
      C2=C1-(CD*C1+SD*S1)
      S1=S1+(SD*C1-CD*S1)
C     THE FOLLOWING THREE STATEMENTS COMPENSATE FOR TRUNCATION
C     ERROR.  IF ROUNDED ARITHMETIC IS USED, THEY MAY
C     BE DELETED.
      C1=0.5/(C2**2+S1**2)+0.5
      S1=C1*S1
      C2=C1*C2
      KK=KK-KSPNN+JC
```

```
      IF(KK .LE. KSPAN) GO TO 720
      KK=KK-KSPAN+JC+INC
      IF(KK .LE. JC+JC) GO TO 710
      GO TO 100
C     PERMUTE THE RESULTS TO NORMAL ORDER---DONE IN TWO STAGES
C     PERMUTATION FOR SQUARE FACTORS OF N
800   NP(1)=KS
      IF(KT .EQ. 0) GO TO 890
      K=KT+KT+1
      IF(M .LT. K) K=K-1
      J=1
      NP(K+1)=JC
810   NP(J+1)=NP(J)/NFAC(J)
      NP(K)=NP(K+1)*NFAC(J)
      J=J+1
      K=K-1
      IF(J .LT. K) GO TO 810
      K3=NP(K+1)
      KSPAN=NP(2)
      KK=JC+1
      K2=KSPAN+1
      J=1
      IF(N .NE. NTOT) GO TO 850
C     PERMUTATION FOR SINGLE-VARIATE TRANSFORM (OPTIONAL CODE)
820   AK=A(KK)
      A(KK)=A(K2)
      A(K2)=AK
      BK=B(KK)
      B(KK)=B(K2)
      B(K2)=BK
      KK=KK+INC
      K2=KSPAN+K2
      IF(K2 .LT. KS) GO TO 820
830   K2=K2-NP(J)
      J=J+1
      K2=NP(J+1)+K2
      IF(K2 .GT. NP(J)) GO TO 830
      J=1
840   IF(KK .LT. K2) GO TO 820
      KK=KK+INC
      K2=KSPAN+K2
      IF(K2 .LT. KS) GO TO 840
      IF(KK .LT. KS) GO TO 830
      JC=K3
      GO TO 890
C     PERMUTATION FOR MULTIVARIATE TRANSFORM
850   K2=KK+JC
860   AK=A(KK)
      A(KK)=A(K2)
      A(K2)=AK
      BK=B(KK)
      B(KK)=B(K2)
      B(K2)=BK
      KK=KK+INC
      K2=K2+INC
      IF(KK .LT. K) GO TO 860
```


C-3

```
      KK=KK+KS-JC
      K2=K2+KS-JC
      IF(KK .LT. NT) GO TO 850
      K2=K2-NT+KSPAN
      KK=KK-NT+JC
      IF(K2 .LT. KS) GO TO 850
870   K2=K2-NP(J)
      J=J+1
      K2=NP(J+1)+K2
      IF(K2 .GT. NP(J)) GO TO 870
      J=1
880   IF(KK .LT. K2) GO TO 850
      KK=KK+JC
      K2=KSPAN+K2
      IF(K2 .LT. KS) GO TO 880
      IF(KK .LT. KS) GO TO 870
      JC=K3
890   IF(2*KT+1 .GE. M) RETURN
      KSPNN=NP(KT+1)
C     PERMUTATION FOR SQUARE-FREE FACTORS OF N
      J=M-KT
      NFAC(J+1)=1
900   NFAC(J)=NFAC(J)*NFAC(J+1)
      J=J-1
      IF(J .NE. KT) GO TO 900
      KT=KT+1
      NN=NFAC(KT)-1
      IF(NN .GT. MAXP) GO TO 998
      JJ=0
      J=0
      GO TO 906
902   JJ=JJ-K2
      K2=KK
      K=K+1
      KK=NFAC(K)
904   JJ=KK+JJ
      IF(JJ .GE. K2) GO TO 902
      NP(J)=JJ
906   K2=NFAC(KT)
      K=KT+1
      KK=NFAC(K)
      J=J+1
      IF(J .LE. NN) GO TO 904
C     DETERMINE THE PERMUTATION CYCLES OF LENGTH GREATER THAN 1
      J=0
      GO TO 914
910   K=KK
      KK=NP(K)
      NP(K)=-KK
      IF(KK .NE. J) GO TO 910
      K3=KK
914   J=J+1
      KK=NP(J)
      IF(KK .LT. 0) GO TO 914
      IF(KK .NE. J) GO TO 910
      NP(J)=-J
```

```
      IF(J .NE. NN) GO TO 914
      MAXF=INC*MAXF
C     REORDER A AND B, FOLLOWING THE PERMUTATION CYCLES
      GO TO 950
924   J=J-1
      IF(NP(J) .LT. 0) GO TO 924
      JJ=JC
926   KSPAN=JJ
      IF(JJ .GT. MAXF) KSPAN=MAXF
      JJ=JJ-KSPAN
      K=NP(J)
      KK=JC*K+II+JJ
      K1=KK+KSPAN
      K2=0
928   K2=K2+1
      AT(K2)=A(K1)
      BT(K2)=B(K1)
      K1=K1-INC
      IF(K1 .NE. KK) GO TO 928
932   K1=KK+KSPAN
      K2=K1-JC*(K+NP(K))
      K=-NP(K)
936   A(K1)=A(K2)
      B(K1)=B(K2)
      K1=K1-INC
      K2=K2-INC
      IF(K1 .NE. KK) GO TO 936
      KK=K2
      IF(K .NE. J) GO TO 932
      K1=KK+KSPAN
      K2=0
940   K2=K2+1
      A(K1)=AT(K2)
      B(K1)=BT(K2)
      K1=K1-INC
      IF(K1 .NE. KK) GO TO 940
      IF(JJ .NE. 0) GO TO 926
      IF(J .NE. 1) GO TO 924
950   J=K3+1
      NT=NT-KSPNN
      II=NT-INC+1
      IF(NT .GE. 0) GO TO 924
      RETURN
C     ERROR FINISH, INSUFFICIENT ARRAY STORAGE
998   ISN=0
C     PRINT 999
999   FORMAT(44HOARRAY BOUNDS EXCEEDED WITHIN SUBROUTINE FFT)
      RETURN
      END
```

```
      SUBROUTINE REALTR(A,B,N,ISN)
      DIMENSION A(1),B(1)
      REAL IM
      INC=IABS(ISN)
      NK=N*INC+2
      NH=NK/2
      SD=2.0*ATAN(1.0)/FLOAT(N)
      CD=2.0*SIN(SD)**2
      SD=SIN(SD+SD)
      SN=0.0
      CN=1.0
      A(NK-1)=A(1)
      B(NK-1)=B(1)
   10 DO 20 J=1,NH,INC
      K=NK-J
      AA=A(J)+A(K)
      AB=A(J)-A(K)
      BA=B(J)+B(K)
      BB=B(J)-B(K)
      RE=CN*BA+SN*AB
      IM=SN*BA-CN*AB
      B(K)=IM-BB
      B(J)=IM+BB
      A(K)=AA-RE
      A(J)=AA+RE
      AA=CN-(CD*CN+SD*SN)
      SN=(SD*CN-CD*SN)+SN
C     THE FOLLOWING THREE STATEMENTS COMPENSATE FOR TRUNCATION
      CN=0.5/(AA**2+SN**2)+0.5
      SN=CN*SN
   20 CN=CN*AA
      RETURN
      END
```

SPECIAL ACKNOWLEDGEMENTS

All drawings by Kathy Bond and Mark Manley.

Typing by Selma McEntire.